Università degli Studi di Padova

Head Office: Università degli Studi di Padova

Department of Mathematics "Tullio Levi-Civita"

Ph.D. Course in Mathematical Sciences

Curriculum Mathematics

XXXVIII Cycle

Schrödinger-Poisson and Beyond: Dynamical Models for Dark Matter

Coordinator:
Prof. Giovanni Colombo

Supervisor:
Prof. Antonio Ponno

Co-Supervisor:
Dr. Lorenzo Zanelli

Ph.D. Candidate:
Gaia Marangon

Abstract

This Ph.D. thesis investigates the Schrödinger-Poisson system as a model for dark matter dynamics, conceived as an aggregate of self-gravitating particles. The dark matter density distribution is represented by the squared modulus of a matter field, while the self-interactions are described by a gravitational field. The two components evolve in a coupled manner: the matter field according to a Schrödinger equation, and the gravitational potential according to Poisson dynamics. The model is applied to dark matter halos in galaxies, describing both their dynamics and equilibrium configurations. It also provides predictions for rotation curves, which represent the most significant observational data in this context.

Specifically, this thesis explores the connection between the Schrödinger-Poisson system and established physical theories, showing how it can equivalently emerge from different foundational assumptions. A heuristic approach to the problem is presented, illustrating how general physical hypotheses about the nature of dark matter naturally lead to the identification of the mathematical structure of the problem, suggesting characteristic parameters and rescalings needed to express the system in dimensionless form.

Through numerical calculations, the structure of spherically symmetric stationary states of the system is systematically analyzed, and a set of heuristic laws is identified that describe how their fundamental features depend on the excitation index. The same analysis is extended to the rotation curves predicted from the stationary states. The relevance of these heuristic laws for model applications is demonstrated through the construction of fits to experimental rotation curves. In particular, it is shown how the presence of these laws facilitates the fitting process by significantly reducing the required computational effort.

A possible relativistic extension of the model, the Klein-Gordon–Wave system, is then addressed. The typical regimes of this system are described, and it is shown how in the low-energy limit and weak field limit it reduces to the previously described Schrödinger-Poisson system. The connection between the two models is formalized through perturbative techniques typical of Hamiltonian systems, showing how the Schrödinger-Poisson system emerges from the first-order truncation of the Hamiltonian normal form of the Klein-Gordon–Wave problem.

Finally, the thesis concludes with some observations on the stability of the Schrödinger-Poisson and Klein-Gordon–Wave systems. The challenges arising from nonlinearity are highlighted, and the linearized version of the perturbed Klein-Gordon–Wave system is examined both analytically and numerically, showing that its stationary states exhibit spectral instability.

Contents

Chapter 1

Introduction

The underlying problem that motivates this thesis is one of the most compelling in modern astrophysics: dark matter. This type of matter interacts gravitationally but remains inert with respect to electromagnetic interactions, making direct observation through telescopes impossible. The information we possess regarding its presence and the aggregates it forms is therefore entirely indirect: we measure the effects of gravitational attraction that it exerts on ordinary matter and draw inferences based on these observations. Starting from this limited set of information, heuristic models are hypothesized to describe the dynamics of dark matter: how it distributes in space, under which regimes it forms aggregates, and which of these configurations are stable. These models must simultaneously be consistent with fundamental physics principles by finding their place within recognized theories, while providing plausible predictions of experimental physical data. The result is often models with clear physical interpretation and good predictive power, but whose mathematical properties are only partially known. This opens extensive avenues for research, often complicated by the nonlinearities typical of the problem and therefore developed in parallel using both analytical and numerical techniques.

In this thesis, we focus on a particular class of dark matter aggregates, those identified on galactic scale, and on a specific mathematical model used to describe them, the Schrödinger-Poisson model. The research we propose develops around this system, interweaving its physical and mathematical aspects and employing different approaches, both numerical and analytical. Rather than focusing on a single aspect of the problem, our contribution develops on multiple fronts, proposing a series of advances that can serve as a foundation for more targeted and specific future developments.

In this introduction, we provide a general overview of the problem, highlighting the open questions that characterize it and that have guided our research. We hope to clarify the holistic mindset with which we have approached the problem, based on a broad, interdisciplinary vision that respects the various lines of research currently active on this topic. Given the profound connection between the Schrödinger-Poisson model and the physical application we primarily refer to, we begin with a brief presentation of the physical context, whose specificities justify the choice of the system under examination as the base model and allow us to understand its interpretation and structure. We then move to a more accurate description of the Schrödinger-Poisson system, illustrating its mathematical structure, the Lagrangian and Hamiltonian formulations, and the symmetries that characterize it. Finally, we provide a brief overview of the research, illustrating the structure of this thesis, and highlighting the open questions it addresses and its main results.

1.1 Physical Context: Rotation Curves

The fundamental scenario we consider is that of spiral galaxies. Spiral galaxies, such as the Milky Way, consist of a flat disk of stars, often endowed with a small central spherical bulge and embedded with a cloud of interstellar gas and dust. This whole cluster of matter rotates around its center, causing the flat distribution to form characteristic spiral arms. The rotational velocity of the aggregate can be measured through telescopic observations: starting from the center and progressing outward, one can probe the visible galaxy up to beyond its dimension and measure, for each radial position, the rotational velocity of a test object in orbit, such as a star or a portion of gas. By plotting these rotational velocities at different radial positions, we obtain the so-called rotation curves, which are a key experimental measurement in galactic studies.

Given the low velocities involved, predictions for this type of curve are provided by classical

Newtonian physics: the test object is maintained in orbit by a centripetal force, which is given by the gravitational attraction exerted on the test object by galactic matter:

$$V(R) = \sqrt{\frac{G\,4\pi \int_0^R P(S)S^2\,\mathrm{d}S}{R}}\,. \tag{1.1}$$

where R is the position of the test object, G is the gravitational constant, and the integral $M(R) = 4\pi \int_0^R P(S)S^2\,\mathrm{d}S$ is the mass contained in a sphere of radius R, expressed in terms of the spherically symmetric matter density distribution $P(S)$. The latter is understood as an effective density, averaged over angular components to maintain a purely radial dependence. Note that the relationship between velocity and mass distribution would be more correctly expressed in terms of time averages, which describe well the physical state of a virialized system. However, in the case of quasi-circular orbits it is possible to remove the averages and write the relationship as in (1.1).

Thus, according to this description, the velocity of a test object is completely predictable given the density distribution $P(S)$ of matter content in the galaxy. The latter can be estimated experimentally by collecting luminosity measurements through telescopic observations and converting them, up to proportionality constants, into measurements of the amount of visible mass in the galaxy. Using these estimates, one can therefore provide a prediction for the rotation curve of each galaxy. In the case of spiral galaxies, on which we focus, the measured densities have a finite central density and a finite extent, mathematically represented by $P(0) < \infty$ and by a long-range decay for $P(R)$ faster than R^{-3}. This results in a predicted velocity that is approximately linear in the short range, and with a Keplerian decay $V(R) \sim R^{-1/2}$ beyond the finite extent of the matter distribution.

Curiously, in all observed galaxies the rotation curve predicted from luminosity data is strongly incongruent with the experimental curve, which extends to much larger radial positions before showing the Keplerian decline, often not even reached by the measurements. See Figure 1.1 for an example, taken from Salucci [128]. The most natural explanation for this incongruence is the presence of a large quantity of mass not detected by luminosity observations because it lacks electromagnetic interactions: dark matter.

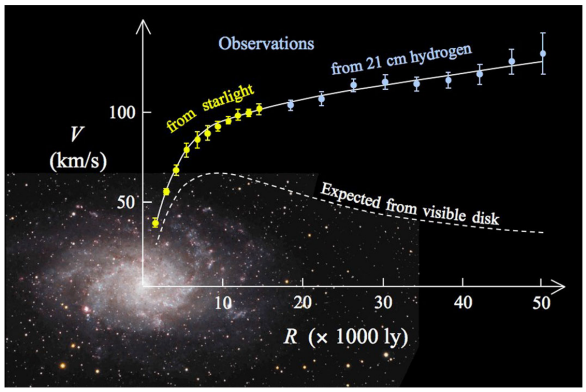

Figure 1.1: Observed rotation curve (yellow and blue data) compared to physical prediction (dashed line). Figure from Salucci [128].

The systematic measurement of these rotation curves has provided the first heuristic observations on its nature, exposed in the brilliant pioneering work of Burstein and Rubin [33]. First, "*The dark matter is clumped around galaxies and is not just an extension of the background matter of the universe*" [33]. This suggests that it is reasonable to restrict ourselves to the galactic scale and study a localized model, centered around the visible matter. Second, "*The dark matter is less centrally concentrated than the luminous matter*" [33], suggesting that in the central zone of the galaxy the luminous matter is relevant in determining the profile of the curves, while dark matter becomes dominant for larger radial positions. With the exception of the central region, it therefore becomes reasonable to neglect the contribution of visible matter as a first approximation and study a model for dark matter alone. Third, "*Rotation curve forms are similar for spirals of very different morphologies, from which we infer that the distribution of the dark matter is independent of galaxy type*" [33]. It follows that the model describing it must be unique for all galaxies, and that dark matter aggregates on galactic scale have a universal character.

These observations have guided the identification of the fundamental characteristics of the system under examination: an aggregate of non-visible particles, inert with respect to electromagnetic forces,

which aggregate by gravity and form galactic-scale structures, incorporating visible matter at the center and having a universal structure independent of the specific galaxy under analysis.

Based on these assumptions, a wide variety of models have been defined to describe the dynamics of dark matter, trading off between a connection with established physical theories and the need to obtain consistent predictions for rotation curves. In the broad landscape of theories that emerged in this context, in this thesis we focus on one of the most successful, the Scalar Field Dark Matter model, according to which dark matter consists of ultralight bosonic particles with masses of the order of 10^{-24} eV (10^{-57} g), clustered in the same fundamental state at minimum energy in a so-called Bose-Einstein condensate. The mathematical description of this system involves a scalar matter field, whose squared modulus represents the density distribution of dark matter particles, and a coupled gravitational potential field, which acts on the particles and whose dynamics is influenced by the distribution of particles itself. In the limit of low energies and in the non-relativistic regime, this model reduces to the celebrated Schrödinger-Poisson system, which will be the main object of study of this thesis.

1.2 Schrödinger-Poisson Model

The Schrödinger-Poisson model describes the dynamics of a particle density distribution $|\psi|^2(t,x)$ under self-gravity. Formally, it defines the evolution of the complex-valued scalar matter field $\psi(t,x)$ via the Schrödinger equation, subjected to the real-valued scalar gravitational potential $\phi(t,x)$. The gravitational potential, in turn, satisfies the Poisson equation, with $|\psi|^2(t,x)$ as the source term, realizing the coupling. Additional external sources $\rho(x)$ may optionally be considered, in view of physical applications. In non-dimensional units, and assuming $x \in \mathbb{R}^3$ for physical reasons, the Schrödinger-Poisson model reads:

$$\begin{cases} i\partial_t\psi = -\frac{\Delta}{2}\psi + \phi\psi \\ \Delta\phi = |\psi|^2 + \rho \end{cases} . \tag{1.2}$$

To avoid handling numerical factors in the denominator, we can consider an alternative formulation of system (1.2), equivalent and widely used, which is obtained by rescaling the time $t \to 2t$. This yields:

$$\begin{cases} i\partial_t\psi(t,x) = (-\Delta + 2\phi(t,x))\psi(t,x) \\ \Delta\phi(t,x) = |\psi|^2(t,x) + \rho(x) \end{cases} . \tag{1.3}$$

We will use the first formulation (1.2) in the study of the Lagrangian and Hamiltonian structure of the system, while in the work on stationary states we will refer to formulation (1.3).

Lagrangian Formulation

This system admits a Lagrangian formulation. Let $\psi_t \equiv \partial_t\psi$ and $\psi_{x_j} \equiv \partial_{x_j}\psi$ for $j = 1,2,3$ denote the partial derivatives with respect to the time t and space coordinates $x \equiv (x_1,x_2,x_3) \in \mathbb{R}^3$. The appropriate Lagrangian density is the following functional of the fields ψ, ψ^*, ϕ and their partial derivatives:

$$\mathscr{L} \equiv \frac{i}{2}(\psi^*\psi_t - \psi\psi_t^*) - \frac{1}{2}|\nabla\psi|^2 - \frac{1}{2}|\nabla\phi|^2 - \phi|\psi|^2 - \rho\phi\,. \tag{1.4}$$

The associated action functional is $S = \int \mathscr{L}\, d^3x\, dt$. To derive the equations of motion, we apply the principle of stationary action $\delta S = 0$, namely we look for the functions ψ, ϕ that let the differential of the action δS vanish for any increment $\delta\psi$ and $\delta\phi$. These critical points of the action are characterized as the solutions of the following Euler-Lagrange equations:

$$\frac{\partial\mathscr{L}}{\partial\psi^*} - \sum_{j=1}^{3}\frac{\partial}{\partial x_j}\frac{\partial\mathscr{L}}{\partial\psi^*_{x_j}} - \frac{\partial}{\partial t}\frac{\partial\mathscr{L}}{\partial\psi^*_t} = 0\,,$$

$$\frac{\partial\mathscr{L}}{\partial\phi} - \sum_{j=1}^{3}\frac{\partial}{\partial x_j}\frac{\partial\mathscr{L}}{\partial\phi_{x_j}} - \frac{\partial}{\partial t}\frac{\partial\mathscr{L}}{\partial\phi_t} = 0\,,$$

which, assuming that ϕ depends on time only through ψ, coincide exactly with the Schrödinger-Poisson system (1.2).

Symmetries and Conserved Quantities

The Schrödinger-Poisson system (1.2) exhibits four fundamental symmetries. Its Lagrangian density (1.4) is invariant under three transformations involving space and time coordinates: time translation $t \to t + s$, for any $s \in \mathbb{R}$; space translation $x \to x + y$ for any $y \in \mathbb{R}^3$; and space rotation $x \to Ax$, for any $A \in SO(3)$. The problem is also invariant under the gauge transformation of the field: $\psi \to e^{i\alpha}\psi$ for any $\alpha \in \mathbb{R}$.

According to Noether's theorem, each symmetry corresponds to a conservation law. The Schrödinger-Poisson dynamics thus preserves the following quantities: the energy functional, associated with time translation

$$H = \int \left[\frac{|\nabla\psi|^2}{2} + \frac{|\nabla\phi|^2}{2} + |\psi|^2\phi + \rho\phi \right] \mathrm{d}^3x \,, \tag{1.5}$$

the total momentum, associated with space translation

$$\mathbf{P} = \int \frac{i}{2} \left(\psi^* \nabla\psi - \psi \nabla\psi^* \right) \mathrm{d}^3x \,,$$

the angular momentum, associated with space rotation

$$\mathbf{L} = \int x \wedge \frac{i}{2} \left(\psi^* \nabla\psi - \psi \nabla\psi^* \right) \mathrm{d}^3x \,,$$

and finally the particle number, associated with the gauge symmetry:

$$N = \int |\psi|^2 \, \mathrm{d}^3x \,.$$

In addition, as first noted by Lieb [100], the Schrödinger-Poisson system (1.2) is invariant under scaling:

$$\tilde{x} = N^{-1}x \,, \qquad \tilde{t} = N^{-1}t \,, \qquad \tilde{\psi} = N^2\psi \,, \qquad \tilde{\phi} = N^2\phi \,. \tag{1.6}$$

This scaling preserves the equations (1.2), while modifying the Lagrangian, so that the transformed functions $\tilde{\psi}, \tilde{\phi}$ still solve the Schrödinger-Poisson problem but with different values of the constants of motion. For example, the number of particles in the transformed variables is scaled by a factor N:

$$\int_{\mathbb{R}^3} |\tilde{\psi}|^2(t, \tilde{x}) \, \mathrm{d}^3\tilde{x} = N \int_{\mathbb{R}^3} |\psi|^2(t, x) \, \mathrm{d}^3x \,. \tag{1.7}$$

Hamiltonian Formulation

The Schrödinger-Poisson system (1.2) also admits a Hamiltonian formulation. To cast the system in Hamiltonian normal form, let us treat ψ and ψ^* as canonical conjugate variables, with the Poisson bracket:

$$\{F, G\} = \frac{1}{i} \int \left(\frac{\delta F}{\delta\psi} \frac{\delta G}{\delta\psi^*} - \frac{\delta F}{\delta\psi^*} \frac{\delta G}{\delta\psi} \right) \mathrm{d}^3x \,.$$

The Hamiltonian functional $H = \int \mathscr{H} d^3x$ coincides with the conserved energy (1.5) derived from time translation symmetry, expressed as a function of the conjugate variables ψ and ψ^* and of the field ϕ. The resulting Hamilton equations, $\partial_t\psi = \{\psi, H\}$ and its complex conjugate, yield the Schrödinger equation in (1.2). For the real-valued potential ϕ, we consider it as a Lagrange multiplier imposing a constraint. Letting the functional derivative with respect to ϕ vanish precisely results in the Poisson equation in (1.2).

Stationary States

Among the fundamental characteristics of a dynamical system we find its stationary states, namely solutions that do not depend explicitly on time. In the case of the Schrödinger-Poisson system (1.2), the invariance with respect to the gauge transformation $\psi \to e^{i\alpha}\psi$ suggests that a solution is defined up to a phase. It is therefore useful to extend the definition of stationary state by admitting the possibility of an oscillating phase in time, that is, considering steady state solutions of the form $(e^{i\varepsilon t} f(x), \phi(x))$, with ε an energy parameter and $f(x)$ a real-valued field. This choice is typical of problems subject to gauge invariance, particularly those of Schrödinger type. In this case, even though

the field oscillates in time, the matter density $|\psi|^2$ is independent of it, thus resulting in a stationary quantity. Solutions in this form solve the following stationary Schrödinger-Poisson problem, obtained from formulation (1.3):

$$\begin{cases} \Delta f = (\varepsilon + 2\phi) f \\ \Delta \phi = f^2 \\ \int_{\mathbb{R}^3} f^2(x)\, \mathrm{d}^3 x = 1 \end{cases} . \tag{1.8}$$

In the definition we have included a choice for the $L^2(\mathbb{R}^3)$ norm of the matter field f, necessary to uniquely identify a specific stationary state. Indeed, due to invariance under transformations (1.6), for every stationary state solving (1.8) with a unitary norm of the matter field there exists an infinite family of solutions, obtained through transformations (1.6), which solve the same problem with norm N, thus introducing the need to declare the norm to avoid ambiguity.

Solving the Poisson equation in problem (1.8) and substituting in the equation for $f(x)$ results in the so-called Choquard equation:

$$\begin{cases} \Delta f + \dfrac{1}{2\pi} \left(\displaystyle\int_{\mathbb{R}^3} \frac{f^2(y)}{|x-y|}\, \mathrm{d}^3 y \right) f = \varepsilon f & \text{(1.9a)} \\ \phi = -\dfrac{1}{4\pi} \displaystyle\int_{\mathbb{R}^3} \frac{f^2(y)}{|x-y|}\, \mathrm{d}^3 y & \text{(1.9b)} \\ \displaystyle\int_{\mathbb{R}^3} f^2(x)\, \mathrm{d}^3 x = 1 & \text{(1.9c)} \end{cases} .$$

The Choquard equation (1.9a) is a nonlinear eigenvalue problem, with ε representing the eigenvalue, $f(x)$ the eigenfunction, and where the nonlinearity is due to coupling with the Poisson equation. The associated potential $\phi(x)$, defined by (1.9b), will be referred to as the eigenpotential. Most works in the literature on the stationary Schrödinger-Poisson problem focus on spherical stationary states, for which an infinite discrete family of solutions exists [100, 101]: $\{\varepsilon_n,\, f_n(r),\, \phi_n(r)\}_{n=0}^{\infty}$ with $n \in \mathbb{N}$. Given their strong analogy with the radial eigenfunctions of the hydrogen atom problem [136], these solutions are often termed "excited", with n representing the excitation index and $n = 0$ the "ground" solution. Even though the nonlinearity of problem (1.9) prevents a spectral decomposition, making this terminology slightly inappropriate, we follow a common approach (see e.g. [58, 71, 73]) and use it freely in the thesis.

Stability

Once the stationary states have been identified, it is fundamental to study their stability to understand which configurations are preserved by the dynamics and from which instead the system moves away. In the case of the Schrödinger-Poisson system, the problem of stability of stationary states is particularly difficult to treat. The main issue stems from the nonlinearity of the problem, caused by the coupling between the matter field and the gravitational field. It makes the application of the main analytical strategies for stability studies rather difficult, and most works on this topic are therefore developed with numerical techniques. These studies, repeated with increasingly refined techniques and extended also to non-spherically symmetric cases, suggest that the excited eigenstates of the Schrödinger-Poisson system are unstable and tend to expel mass until falling back to the ground state, which is instead considered stable. This phenomenon is known as gravitational cooling [66].

1.3 Outline of the Research

In this section, we summarize the main content of the thesis, focused on the study of the Schrödinger-Poisson system. This presentation aims to guide the reader through the work, exposing the main open problems that have guided our research and reporting the main results obtained. As already mentioned, the work develops on several fronts, deepening novel aspects and laying the foundations for future developments.

Schrödinger-Poisson: physical foundations

The mathematical study of the Schrödinger-Poisson system can develop completely independently of its physical interpretation. However, we believe that it is important to have a complete understanding

of the underlying physical problem, for a dual motivation. On the one hand, the interest of the scientific community for this system has always been strongly linked to its physical applications, which go well beyond its use in the context of dark matter. It follows that an understanding of the main physical arguments associated with this system facilitates its study, allowing one to fully grasp the most relevant works that have historically laid its foundations. On the other hand, the interest of the physics community for this system is still strong, making it a current problem not only in the context of dark matter but also on other fronts, such as the investigation of quantum theory foundations [43, 120, 119] or studies of optomechanics [60, 21], Bose-Einstein condensates [55, 108], non-linear optics [113] and much more [117]. This vivid interest guides the need to deepen some aspects of the problem, including mathematical ones. Mathematical research can therefore serve these demands, clarifying key aspects and providing broader and more solid knowledge to support a deep understanding of the physical world.

It is for these reasons that we dedicate Chapter 2 of this thesis to clarifying the physical foundation of the Schrödinger-Poisson system. As a description of quantum matter interacting through gravity, the model is strictly related to the two main established physical theories – general relativity and quantum physics – and is affected by the deep discussions concerning their irreconcilability. Briefly reporting the necessary basic notions, we clarify how the system connects to these two theories, and how it emerges invariably, in the limit of low energies and weak gravitational field, starting from very different points of view – both with a quantum gravity approach and with a semiclassical gravity one. Despite obtaining the same system (1.2), the underlying physical interpretation and the relationship with the fundamental systems of which the Schrödinger-Poisson is the effective approximation changes notably with the adopted approach.

Illustrating this complex landscape allows one to understand more deeply the model for galactic dark matter we study in this thesis – the Scalar Field Dark Matter model, reducing in specific limits to the Schrödinger-Poisson system. In particular, in Chapter 2 we show how few reasonable and rather general physical assumptions – dark matter particles are quantum bosons in a virialized, completely condensed cluster – allow us to derive the typical quantities of the problem, obtaining directly the non-dimensional version of the problem and deriving the fundamental parameters that govern its regime. In particular, in the case of the many-body Schrödinger-Poisson problem our approach rigorously justifies the standard scaling of the interaction term by the total number of particles, demonstrating that such scaling arises naturally from the underlying physical principles. Moreover, a governing parameter μ^2 is identified, which ensures that the system's energy is compatible with the non-relativistic regime. This parameter will have an important role in Chapter 5, where we study a relativistic extension of the Schrödinger-Poisson system. Our analysis, which we propose with a personal point of view, shows the strong connection between physical assumptions and mathematical structure, allowing one to grasp the deeper motivations that underlie the definition of the model.

Schrödinger-Poisson: numerical characterization of excited eigenstates

A central part of this research, reported in Chapter 3 and in two companion papers Marangon et al. [104, 103], is dedicated to the analysis of excited spherically symmetric eigenstates $\{\varepsilon_n, f_n(r), \phi_n(r)\}_{n=0}^{\infty}$ of the Schrödinger-Poisson system. The state of the art is advanced by providing them with a comprehensive numerical characterization: through numerical computation of highly excited eigenstates, novel heuristic laws are proposed, which describe how their fundamental features scale with the excitation index n. Key characteristics of the eigenfunctions include: the effective support, which exhibits a parabolic dependence on the excitation index; the distances between adjacent nodes, whose pattern varies regularly with n; and the oscillation amplitude, which follows a power law with an exponent approaching -1 for large n. Similar laws are also provided for the eigenpotential. Based on eigenfunctions, eigenvelocities are conveniently defined, which represent the numerical counterpart of the experimental rotation curves. They exhibit a mid-range oscillatory region with an average linear trend, whose slope approaches zero in the large n limit; and they are characterized by heuristic scaling relationships with the excitation index n, revealing an intrinsic universal behavior. The model is then extended to account for the presence of external sources. Numerical computations are performed, selecting different external density profiles – exponential, hard-sphere and truncated Plummer – and letting their parameters vary to observe their effect on the computed eigenstates.

Schrödinger-Poisson: fit of excited eigenstates to SPARC data

In Chapter 4, we address an important aspect for the study of any physical model: its validation against experimental data. In the case of the Schrödinger-Poisson model, and particularly regarding

its excited eigenstates, validation against experimental rotation curves is a rather delicate matter. Indeed, given the numerical evidence of their instability, the direct use of excited eigenstates to describe galactic dark matter configurations is currently disfavored, while more complex combinations that include, for example, multimodal states or rotational or temperature effects are preferred.

Without delving into the various modifications proposed by the scientific community, whose study would merit dedicated work that goes beyond our mathematical objectives, we maintain our focus on the excited eigenstates of Schrödinger-Poisson and adopt a slightly different point of view. Rather than aiming to obtain reliable information on the physical parameters involved, which is difficult in our case for the reasons outlined above, we perform a model fit to the experimental data with the purpose of demonstrating the role of the mathematical structure of eigenstates in a fitting procedure.

The scaling laws derived in Chapter 3, in fact, play a fundamental role in model fitting procedures, significantly optimizing parameter space exploration and thereby enhancing computational efficiency. The main problem they solve is that of testing different combinations of free parameters in an implicit model, where calculating a prediction requires the numerical solution of a system rather than the simple evaluation of an expression. The detailed knowledge that these laws provide allows for an advance estimation of some of the free parameters, based only on appropriate experimental references and considerably limiting the parameter space to be tested, which results in a largely reduced computational effort.

The methodology is successfully implemented in the fitting process of two sample rotation curves from the SPARC database [94], concerning galaxies with and without bulge and accounting for the presence of external sources. This process demonstrates how knowledge of the mathematical structure underlying a problem considerably facilitates comparison with experimental data.

Beyond Schrödinger-Poisson: the Klein-Gordon–Wave model

The Schrödinger-Poisson system, obtained in the weak-field and low-energies limit, is completely non-relativistic. Aiming to generalize the system in a relativistic framework, we introduce a new model that maintains the effective nature and simple mathematical structure of the Schrödinger-Poisson system but is Lorentz invariant, thus being compatible with a special-relativity context.

The system we analyze is a Klein-Gordon–Wave model, in which the matter field $u(t,x)$ satisfies a Klein-Gordon equation while the gravitational field $\phi(t,x)$ solves a wave equation, maintaining a Hamiltonian structure and minimal coupling similar to that of the Schrödinger-Poisson system:

$$\begin{cases} \Box\, u &= (\mu^2 + 2\phi)\, u \\ \Box\, \phi &= u^2 \end{cases} .$$

In Chapter 5, we study this new model in detail, analyzing its fundamental properties in analogy to what was observed for the Schrödinger-Poisson system and identifying the regimes in which it operates. We find that the main parameter μ^2 governing the system dynamics is the same characteristic parameter identified in Chapter 2 for the Schrödinger-Poisson system, associated with the system's energy and depending on the mass and number of particles in the cluster. In the case of small clusters with massive particles, a relativistic regime is observed, potentially leading to the formation of stationary states. This regime is compatible with the characteristic scales of primordial black holes, a prominent candidate for dark matter.

Conversely, for large clusters with ultralight particles at typical galactic scales, the Klein-Gordon–Wave model reduces approximately to a Schrödinger-Wave system, exhibiting dynamics similar to the Schrödinger-Poisson model and sharing the same stationary states. This similarity is formalized using perturbative Hamiltonian techniques, which show that a Schrödinger-Wave Hamiltonian can be obtained as the first-order truncation of the Klein-Gordon–Wave Hamiltonian, with the square inverse $\varepsilon \equiv \mu^{-2}$ of the governing parameter μ^2 as the perturbation parameter. The Schrödinger-Poisson system is further obtained in the $\varepsilon \to 0$ limit. This result is non-trivial, since it extends the standard Normal Form procedure to a case where the unperturbed Hamiltonian has a component with unbounded flow. This particular condition is handled by adapting the definition of normal form and the averaging principle procedure used to obtain it.

The study we propose therefore has dual significance: on the one hand, it extends the class of problems that can be studied with normal form techniques, proposing a new constructive approach; on the other hand, it offers a new point of view on how the Schrödinger-Poisson system and the Klein-Gordon–Wave system relate to each other, clarifying how Lorentz covariance is gradually lost and a conservation law is gained in the approximation process. These results, illustrated in Chapter 5, are also presented in the paper Marangon et al. [102].

Considerations on stability

The final topic of this research, addressed in Chapter 6, concerns the stability of stationary states. In the Schrödinger-Poisson case, this problem has been extensively studied, predominantly through numerical investigations that have long indicated instability for all excited stationary states, with only the ground state appearing to be stable. In this work, we focus on the Klein-Gordon–Wave case, for whose stationary states – to the best of our knowledge – no numerical or analytical stability analysis exists.

Addressing the complete nonlinear stability problem analytically presents considerable challenges. To illustrate how these difficulties manifest, we provide some preliminary analytical considerations that demonstrate why a standard approach based on level sets of first integrals for confining the dynamics fails in our case, thus necessitating less conventional strategies.

Given the difficulty of treating the complete problem, we restrict our investigation by studying the linearized evolution of perturbations to stationary states, focusing on spectral stability. An analytical approach suggests that the spectrum of the linearized perturbation problem associated with each eigenstate – including the ground state – contains at least one unstable eigenmode. We then further narrow our scope to the radial case to test this result numerically. The negative part of the spectrum of the radial linear perturbation problem for the n-th eigenstate is computed for several excitation indices n. Our calculations reveal that it includes $n + 1$ unstable eigenmodes, and we visualize both the eigenvalues and the profiles of the corresponding eigenfunctions. This numerical study confirms our analytical intuition that linear perturbations to all stationary states, including the ground state, exhibit unstable modes.

Chapter 2

Physical Background

2.1 Introduction

The profound uncertainty about dark matter's nature and origin makes it extremely difficult to define its fundamental characteristics and to identify the physical theories needed to describe it. The main difficulty stems from its link with two main established physical theories: General Relativity, which is necessarily involved in describing particles interacting mainly through gravity; and Quantum Mechanics, which is considered the fundamental description of every form of matter. Indeed, the currently unresolved dichotomy between these two theories is particularly pressing when investigating the nature of dark matter, and the attempts to reconcile different aspects result in a variety of models, differing in the underlying approach and involving a vast physical background.

On one hand, General Relativity provides the most complete, fundamental description of the gravitational interactions which dominate dark matter dynamics. Based on a characterizing geometrical formalism, it models classical dark matter as a massive field coupled to an evolving spacetime metric, with a dynamics ruled by the Einstein-Klein-Gordon (EKG) equations. In the non-relativistic limit, which provides a good approximation for dark matter's current behavior, the EKG equations reduce to the Schrödinger-Poisson system, thus suggesting a first possible justification for the adoption of this simpler system.

On the other hand, dark matter's quantum character must also be addressed. By analogy with ordinary matter, dark matter's fundamental constituents are assumed to be particles, of still unknown nature, that aggregate according to quantum mechanical laws. They are therefore fundamentally described by quantum field theory, with a formalism based on operator-valued distributions and states of the Fock space. Once we define the fundamental theory that describes the phenomenon exactly, we still seek effective theories that describe the system's average behavior through simpler models, and even in this case the Schrödinger-Poisson system is naturally derived in the low-energy and weak field limit.

While we do not propose an exhaustive description of these wide and complex topics, in this chapter we collect some fundamental notions of General Relativity and quantum field theory to facilitate understanding of the relevant literature on dark matter, with a specific focus on galactic-scale applications. We pay particular attention to the Schrödinger-Poisson system, the main object of study in this thesis. This system emerges recurrently despite different underlying assumptions: it stems from purely classical General Relativity, from a quantum gravity approach, or from a semiclassical gravity approach. In each case, the mathematical form of the final system is identical, but the different origins provide profoundly different interpretations, sometimes even changing the meaning of the quantities involved. Although mathematical works on this topic have transversal validity, it is important to understand the physical framework behind them to track the possible implications of the results and guide research in directions useful for potential applications.

In Section 2.2 we present useful elements of General Relativity. Starting from the differential geometry notions that constitute its basis, we define Einstein's field equation and its coupling with classical matter, then restrict ourselves to the specific case of linearized gravity, deriving the Schrödinger-Poisson system in the Newtonian limit of weak gravitational fields.

In Section 2.3 we describe the mathematical structure underlying quantum field theory. By defining the function space typical of this theory and the fundamental operators that characterize it, we build the foundations for scalar field quantization – the procedure that allows us to rewrite classical matter dynamics in terms typical of quantum field theory.

Finally, we conclude the general overview of these two theories with Section 2.4, which presents the most common approaches to incorporate them and write coupled dynamics for a quantum matter field and the geometric structure incorporating gravity. We highlight the difference between a quantum gravity approach, in which gravity is fundamentally quantum, and a semi-classical gravity approach, in which it remains fundamentally classical. We show how both result, in the appropriate limits, in a Schrödinger-Poisson system, albeit with profound interpretative differences.

The last Section 2.5 deals more specifically with dark matter, showing how the theories described above converge in a particularly promising model: the Scalar Field Dark Matter model. After a general presentation of the theory, aimed at showing how the approaches described above apply to dark matter on galactic scales, we propose a heuristic analysis of the model. Through our own personal revisitation, we retrace the fundamental heuristic hypotheses that lead to the definition of Scalar Field Dark Matter theory. This analysis highlights how the model's characteristic parameters and its dimensionless description derive directly from these hypotheses, creating a clear, elegant and intuitive bridge between the physical theory and the model's mathematical structure.

2.2 Notes on General Relativity

We start by summarizing some notions of General Relativity, with the aim of facilitating the understanding of those works in the literature on dark matter that involve this theory. We focus in particular on the underlying mathematical structure, gradually defining the objects necessary to write the main physical equation of relativity, the Einstein's field equation. We then briefly present its coupling with a matter field in a classical context, recovering the famous Einstein-Klein-Gordon system, and we derive its Newtonian limit, showing how the Schrödinger-Poisson system studied in this thesis emerges naturally.

2.2.1 The geometric setting

Lorentzian manifold

In General Relativity, motions occur along a 4-dimensional differentiable manifold $\mathcal{M}$ named the spacetime, which represents the space and time dimensions needed to describe the dynamics. Such manifolds are described by differential geometry, which provides a whole set of mathematical concepts to formalize the intuitive idea of motions along a curved space. A full description of these notions can be found, for example, in the reference textbook by Misner et al. [110], (see also the excellent lecture notes by Tong [138]), while in the following we just recall the concepts that are more strictly related to the Einstein-Klein-Gordon equations.

In General Relativity, manifolds are equipped with a metric g. It represents the core concept of the whole theory, bridging between physics and geometry. Indeed, in Einstein's theory the gravitational force is mediated precisely by the metric, which is an evolving quantity: massive objects generate gravitational attraction by modifying the metric g of the spacetime; in turn, variations of the metric g affect the spacetime geometry and thus the trajectories of massive objects. Unlike that of the other fundamental forces, the action of the gravitational force is thus modeled as a modification of the underlying geometry, rather than as an interaction with an external field. In this Section we define the physical rules governing the metric evolution, giving a precise mathematical description of the involved quantities.

The first assumption we introduce is that of a Lorentzian metric g, that is a metric with exactly one negative entry. Observe that this definition is independent of the choice of coordinates, as guaranteed by Sylverster's law of inertia [138]. A manifold $\mathcal{M}$ equipped with such a metric g is called a Lorentzian manifold $(\mathcal{M}, g)$. The simplest example of a Lorentzian manifold is the Minkowski space $(\mathbb{R}^4, \eta)$ consisting of the Euclidean space $\mathcal{M} = \mathbb{R}^4$ with a diagonal metric:

$$\eta = -\,\mathrm{d}x^0 \otimes \mathrm{d}x^0 + \mathrm{d}x^1 \otimes \mathrm{d}x^1 + \mathrm{d}x^2 \otimes \mathrm{d}x^2 + \mathrm{d}x^3 \otimes \mathrm{d}x^3\,,$$

where x^μ denotes the coordinates, $\mu = 0$ representing the time and $\mu = 1, 2, 3$ the space, while $\eta_{00} = -1$, $\eta_{11} = \eta_{22} = \eta_{33} = +1$ are the non-vanishing components of the metric η. The Minkowski space represents a *flat* spacetime and is characteristic of special relativity. In General Relativity, instead, more general Lorentzian manifolds $(\mathcal{M}, g)$ are allowed, introducing the possibility of a *curved* spacetime.

Connections and covariant derivatives

Once a metric is selected for a given manifold, it defines a natural connection on it. Recall that a connection represents a natural way to differentiate tensor fields on curved manifolds, generalizing the notion of partial derivatives from flat space. Formally, a connection is a map $\nabla : \mathfrak{X}(\mathcal{M}) \times \mathfrak{X}(\mathcal{M}) \to \mathfrak{X}(\mathcal{M})$, where $\mathfrak{X}(\mathcal{M})$ denotes the space of vector fields on $\mathcal{M}$. Its action, denoted by $\nabla(X, Y) = \nabla_X Y$, must satisfy the following properties for all vector fields X, Y, and Z, and all smooth functions f and g:

$$\begin{aligned}\nabla_X(Y + Z) &= \nabla_X Y + \nabla_X Z,\\ \nabla_{fX+gY} Z &= f\nabla_X Z + g\nabla_Y Z,\\ \nabla_X(fY) &= f\nabla_X Y + (\nabla_X f)Y,\end{aligned}$$

where $\nabla_X f = X(f)$ represents the directional derivative of the function f along X. For a fixed vector field X, the operator ∇_X is called the covariant derivative with respect to X and intuitively reflects the concept of partial derivative on a curved manifold. Given a coordinate basis $\{e_\mu\}$, the connection can be expressed in components $\Gamma^\mu{}_{\rho\nu}$ by writing the associated covariant derivatives along the basis vectors $\nabla_\mu \equiv \nabla_{e_\mu}$:

$$\nabla_\rho e_\nu \equiv \nabla_{e_\rho} e_\nu = \Gamma^\mu{}_{\rho\nu} e_\mu,$$

The covariant derivative of a vector field Y along the basis vector e_ν can also be expressed in components:

$$(\nabla_\nu Y)^\mu = \partial_\nu Y^\mu + \Gamma^\mu{}_{\nu\rho} Y^\rho,$$

where ∂_ν denotes the ordinary partial derivative with respect to the coordinate x^ν. In this description, covariant differentiation is often denoted by semicolons $\nabla_\nu Y^\mu = Y^\mu_{;\nu}$, while commas denote partial differentiation: $\partial_\nu Y^\mu = Y^\mu_{,\mu}$.

From any connection, we can construct two fundamental tensors that characterize its geometric properties. The torsion tensor T is a rank $(1, 2)$ tensor defined by its action on vector fields X and Y and one-forms ω:

$$T(\omega; X, Y) = \omega(\nabla_X Y - \nabla_Y X - [X, Y]),$$

where $[X, Y]$ denotes the Lie bracket of the vector fields, $[X, Y](f) = X(Y(f)) - Y(X(f))$. A connection with vanishing torsion $T = 0$ is called torsion-free.

The curvature tensor, also known as the Riemann tensor, is a rank $(1, 3)$ tensor R defined by

$$R(\omega; X, Y, Z) = \omega(\nabla_X \nabla_Y Z - \nabla_Y \nabla_X Z - \nabla_{[X,Y]} Z).$$

The Riemann tensor satisfies the fundamental Bianchi identity. Denoting by $R^\rho{}_{\sigma\mu\nu}$ the Riemann tensor components, this identity reads:

$$\nabla_\lambda R^\sigma{}_{\rho\mu\nu} + \nabla_\sigma R^\sigma{}_{\rho\lambda\nu} + \nabla_\rho R^\sigma{}_{\lambda\sigma\nu} = 0. \tag{2.1}$$

The Levi-Civita connection and Einstein's tensor

The definition of a connection on a manifold is not unique – infinitely many connections can be defined on any given manifold. However, when the manifold is equipped with a metric tensor $g_{\mu\nu}$, there exists a natural and canonical choice. The fundamental theorem of Riemannian geometry (which also holds for Lorentzian geometries) states that there exists a unique torsion-free connection that is compatible with the metric, where metric compatibility means that the covariant derivative of the metric tensor vanishes for all vector fields X:

$$\nabla_X g = 0\,.$$

This unique connection is called the Levi-Civita connection, and its components $\Gamma^\mu{}_{\rho\nu}$, called the Christoffel symbols, can be computed explicitly from the metric tensor:

$$\Gamma^\mu{}_{\rho\nu} = \frac{1}{2} g^{\mu\lambda} \left(\partial_\rho g_{\lambda\nu} + \partial_\nu g_{\lambda\rho} - \partial_\lambda g_{\rho\nu}\right).$$

The Christoffel symbols are symmetric in their lower indices: $\Gamma^{\mu}{}_{\rho\nu} = \Gamma^{\mu}{}_{\nu\rho}$, reflecting the torsion-free property of the Levi-Civita connection.

Once the Levi-Civita connection is established, we can construct two relevant quantities from its associated Riemann tensor. The Ricci tensor $R_{\mu\nu}$ is obtained by contracting the first and third indices of the Riemann tensor:

$$R_{\mu\nu} = R^{\rho}{}_{\mu\rho\nu}\,,$$

while further contraction with the metric tensor yields the Ricci scalar, which represents the trace of the Ricci tensor and provides a measure of the overall curvature of the spacetime manifold at each point:

$$R = g^{\mu\nu} R_{\mu\nu}. \tag{2.2}$$

The Bianchi identity (2.1) has an interesting implication for the Ricci tensor and the Ricci scalar. By appropriately contracting the identity and by using the symmetries of the Riemann tensor, it results in the contracted Bianchi identity:

$$\nabla^{\mu} R_{\mu\nu} = \frac{1}{2} \nabla_{\nu} R.$$

This identity suggests the natural definition of the so-called Einstein tensor:

$$G_{\mu\nu} = R_{\mu\nu} - \frac{1}{2} R g_{\mu\nu},$$

which, due to the contracted Bianchi identity, is automatically covariantly constant, or divergence-free:

$$\nabla^{\mu} G_{\mu\nu} = 0.$$

This property will be fundamentally important in the construction of Einstein's field equations, ensuring their consistency with the conservation of energy and momentum. Indeed, the Einstein tensor encodes the information about the metric that is relevant for Einstein's field equations, providing the geometric side of the fundamental relationship between matter and spacetime geometry.

2.2.2 Einstein's field equations

The vacuum Einstein's field equations

Up to now we have defined the notion of spacetime as a Lorentzian manifold, analyzing the main geometric quantities that the metric induces on it. We now incorporate physics into this geometric framework, defining the fundamental laws governing the evolution of the metric on a Lorentzian manifold. The transition from pure geometry to physical dynamics is accomplished through the action principle, which provides the most elegant and powerful framework for describing classical field theories. This principle consists of formulating the dynamics through action minimization: a functional S, named action, is defined as the integral over the manifold of a Lagrangian density, which depends on the fields of interest and their derivatives; then, this functional is required to be stationary under variations of the fields. This condition results in the Euler-Lagrange equations of motion, which describe the dynamical evolution of the field of interest.

To construct an action functional, we must integrate a scalar quantity over the manifold $\mathcal{M}$. This requires the specification of a volume form among the infinitely many that can be defined on a manifold. However, selecting a metric g induces a canonical volume form for integration:

$$v = \sqrt{-\det g_{\mu\nu}}\, \mathrm{d}x^0 \wedge \mathrm{d}x^1 \wedge \mathrm{d}x^2 \wedge \mathrm{d}x^3\,,$$

with the minus sign accounting for the negative determinant of a Lorentzian metric. This volume form is intrinsic to the metric itself and remains invariant under coordinate transformations, ensuring that physical quantities computed through integration do not depend on our choice of coordinates. The factor $\sqrt{-g} \equiv \sqrt{-\det g_{\mu\nu}}$ provides a natural measure that weights different regions of the manifold according to their geometric properties. Intuitively, the regions where the metric is "stretched" contribute more heavily to integrals, while the regions where it is "compressed" contribute less.

Once the volume form is established, the construction of an action reduces to selecting an appropriate scalar function to integrate. For gravitational dynamics, the simplest non-trivial choice is the Ricci scalar R, which yields the Einstein-Hilbert action:

$$S_{EH} = \frac{c^3}{16\pi G} \int_{\mathcal{M}} R\sqrt{-g}\, d^4x,$$

where the factor $c^3/(16\pi G)$ provides the dimensions of energy by time required for an action, c being the speed of light and G Newton's gravitational constant. To derive the field equations from the Einstein-Hilbert action, we apply the variational principle by introducing small variations in the metric – $g_{\mu\nu}(x) \to g_{\mu\nu}(x) + \delta g_{\mu\nu}(x)$ – and by computing the corresponding change δS in the action:

$$\delta S_{EH} = \frac{c^3}{16\pi G} \int d^4x \left[(\delta\sqrt{-g}) g^{\mu\nu} R_{\mu\nu} + \sqrt{-g}(\delta g^{\mu\nu}) R_{\mu\nu} + \sqrt{-g} g^{\mu\nu} \delta R_{\mu\nu} \right].$$

We omit the lengthy but straightforward calculations of the terms, which can be found, for example, in [138]. Under appropriate boundary conditions and using the inverse metric variation $\delta g^{\mu\nu} = -g^{\mu\alpha} g^{\nu\beta} \delta g_{\alpha\beta}$ rather than the direct variation $\delta g_{\mu\nu}$, the variation of the action reads:

$$\delta S_{EH} = \frac{c^3}{16\pi G} \int d^4x \sqrt{-g} \left(R_{\mu\nu} - \frac{1}{2} R g_{\mu\nu} \right) \delta g^{\mu\nu}.$$

Demanding that the action be stationary, $\delta S = 0$, for arbitrary variations $\delta g^{\mu\nu}$ yields the vacuum Einstein field equations:

$$G_{\mu\nu} \equiv R_{\mu\nu} - \frac{1}{2} R g_{\mu\nu} = 0, \tag{2.3}$$

where $G_{\mu\nu}$ is the Einstein tensor. Contracting with $g^{\mu\nu}$ gives $R - 2R = 0$, which implies $R = 0$. Substituting back into the field equations, we find that the vacuum Einstein equations are equivalent to the requirement that spacetime be Ricci flat:

$$R_{\mu\nu} = 0.$$

Among the simplest solutions of the vacuum Einstein equations (2.3) we have the Minkowski metric:

$$\mathrm{d}s^2 = -\,\mathrm{d}t^2 + \mathrm{d}x^2 + \mathrm{d}y^2 + \mathrm{d}z^2$$

and the Schwarzschild metric:

$$\mathrm{d}s^2 = -\left(1 - \frac{2GM}{r}\right) \mathrm{d}t^2 + \left(1 - \frac{2GM}{r}\right)^{-1} \mathrm{d}r^2 + r^2\, \mathrm{d}\theta^2 + r^2 \sin^2\theta\, \mathrm{d}\phi^2.$$

Observe that, just like most other actions considered in physics, the Einstein-Hilbert action is second-order in derivatives of the metric – loosely speaking, $R_{\mu\nu} \sim \partial\Gamma + \Gamma\Gamma$, while the Levi-Civita connection itself is $\Gamma^\lambda_{\mu\nu} \sim \partial g$. In principle, it is possible to include higher-order derivatives in the action, and careful combinations of them would still result in equations of motion of the second order (Lovelock's theorem, see [138]). However, including such additional higher derivative terms becomes relevant only for fast-varying fields, while they are generally neglected for standard purposes in General Relativity, in favor of the simpler vacuum Einstein equations (2.3).

Another more interesting alternative option in the definition of the gravitational action consists in including an additional constant value:

$$S_{EH} = \frac{c^3}{16\pi G} \int_{\mathcal{M}} (R - 2\Lambda)\sqrt{-g}\, d^4x, \tag{2.4}$$

This modification was originally motivated by Einstein's desire to find static cosmological solutions, thus justifying the name of cosmological constant for Λ. Variation of this modified action yields the Einstein field equations with cosmological constant:

$$R_{\mu\nu} - \frac{1}{2} R g_{\mu\nu} = -\Lambda g_{\mu\nu}\,, \tag{2.5}$$

or, in the rephrased version:

$$R_{\mu\nu} = \Lambda g_{\mu\nu}.$$

Thus, in the presence of a cosmological constant, spacetime is no longer Ricci flat but instead has a Ricci tensor proportional to the metric. Physics does not suggest a clear value for the cosmological constant Λ and the solutions of Einstein equations (2.5) can take a very different form depending on its sign. For $\Lambda = 0$ we recover the equations (2.3), with solutions such as the Minkowski metric or the Schwarzschild metric. For $\Lambda > 0$, a common solution is the de Sitter space:

$$\mathrm{d}s^2 = -\left(1 - \frac{r^2}{R^2}\right)\mathrm{d}t^2 + \left(1 - \frac{r^2}{R^2}\right)^{-1}\mathrm{d}r^2 + r^2\,\mathrm{d}\theta^2 + r^2\sin^2\theta\,\mathrm{d}\phi^2,$$

while for $\Lambda < 0$ we have the anti-de Sitter space:

$$\mathrm{d}s^2 = -\left(1 + \frac{r^2}{R^2}\right)\mathrm{d}t^2 + \left(1 + \frac{r^2}{R^2}\right)^{-1}\mathrm{d}r^2 + r^2\,\mathrm{d}\theta^2 + r^2\sin^2\theta\,\mathrm{d}\phi^2.$$

Matter field equations on a curved space

The vacuum equations (2.5) derived from the Einstein-Hilbert action involve only geometric information, encoded in the Ricci scalar in the action and in the Einstein tensor in the field equations. To describe gravity comprehensively, we must formalize how matter interacts with this geometrical framework, namely, how to characterize their coupling, also called *backreaction*.

We begin by addressing how to describe matter and its evolution on curved spacetime. Within a classical framework, which is common in astrophysics and cosmology, matter is represented as scalar fields whose dynamics is governed by a Lagrangian formulation. This classical description constitutes an approximation, since matter is fundamentally quantum. However, quantum effects typically become negligible due to the macroscopic length scales involved in gravitational phenomena, thereby justifying the classical limit $\hbar \to 0$. We proceed with this classical treatment, while the alternative quantum approach and its implications are examined in Section 2.4.

In analogy to the variational principle employed for metric evolution, the equations of motion for scalar matter fields can be derived through a variational approach. In flat spacetime endowed with the Minkowski metric, the action assumes the form

$$S_M = \int d^4x \left[-\frac{1}{2}\eta^{\mu\nu}\partial_\mu\phi\partial_\nu\phi - V(\phi)\right],$$

where $\eta^{\mu\nu}$ denotes the Minkowski metric, ϕ is the scalar field and $V(\phi)$ its potential energy. Variation of this action yields the standard Klein-Gordon equation of motion of special relativity:

$$\eta^{\mu\nu}\partial_\mu\partial_\nu\phi - \frac{\partial V}{\partial\phi} = 0.$$

In the presence of curved spacetime, this action can be generalized by replacing the Minkowski metric with the general metric $g_{\mu\nu}$, upgrading partial derivatives to covariant derivatives and incorporating the appropriate volume element:

$$S_M = \int d^4x\sqrt{-g}\left[-\frac{1}{2}g^{\mu\nu}\nabla_\mu\phi\nabla_\nu\phi - V(\phi) - \frac{1}{2}\xi R\phi^2\right]. \tag{2.6}$$

Here we have introduced an additional coupling term proportional to the Ricci scalar R, where ξ is a dimensionless constant. This term vanishes in Minkowski spacetime since $R = 0$, thus reducing to the flat space action, while allowing for a broader generalization of the metric metric $g_{\mu\nu} \neq \eta_{\mu\nu}$.

Demanding stationary variations of the action with respect to the field ϕ while keeping the metric fixed, we obtain the equation of motion for a scalar matter field on a curved spacetime:

$$g^{\mu\nu}\nabla_\mu\nabla_\nu\phi - \frac{\partial V}{\partial\phi} - \xi R\phi = 0. \tag{2.7}$$

As a special case, we may consider scalar matter fields ϕ that are free of any self-interactions. In this particular case, the potential is quadratic in the field, $V(\phi) = (m_0^2\phi^2)/2$, with m_0 indicating the rest mass of a field particle. In addition, we may consider the case $\xi = 0$. By defining $\Box \equiv g^{\mu\nu}\nabla_\mu\nabla_\nu$, we recognize in the above equation of motion the familiar Klein-Gordon equation on curved spacetime:

$$(\Box - m_0^2)\phi = 0. \tag{2.8}$$

The Einstein field equations with matter

The scalar field action (2.6) governs the evolution of matter fields in curved spacetime. To complete the gravitational theory, we must allow matter to serve as a source in the evolution of the metric itself. Since the scalar field action (2.6) already couples both the matter field and the metric, we combine it with the Einstein-Hilbert action (2.4) to obtain the total action:

$$S = S_{EH} + S_M = \frac{1}{16\pi G}\int d^4x\sqrt{-g}(R-2\Lambda) + \int d^4x\sqrt{-g}\left[-\frac{1}{2}g^{\mu\nu}\nabla_\mu\phi\nabla_\nu\phi - V(\phi) - \frac{1}{2}\xi R\phi^2\right].$$

When computing variations of this combined action with respect to the metric, a new contribution emerges from the matter sector. This contribution can be conveniently characterized by defining the energy-momentum tensor:

$$T_{\mu\nu} \equiv -\frac{2}{\sqrt{-g}}\frac{\delta S_M}{\delta g^{\mu\nu}}.$$

With this definition, variation of the total action yields the following coupled system of equations:

$$\begin{cases} G_{\mu\nu} + \Lambda g_{\mu\nu} = 8\pi G T_{\mu\nu}, \\ g^{\mu\nu}\nabla_\mu\nabla_\nu\phi - \frac{\partial V}{\partial\phi} - \xi R\phi = 0 \end{cases} . \tag{2.9}$$

The second equation represents precisely the evolution of the matter field on curved spacetime described previously. The first equation constitutes the Einstein field equations in the presence of matter, where the energy-momentum tensor acts as the source term and realizes the coupling – or backreaction – between matter and geometry. This backreaction represents the fundamental principle that matter tells spacetime how to curve, while curved spacetime tells matter how to move.

The cosmological constant term can be absorbed into the energy-momentum tensor by defining an effective energy-momentum tensor that includes the vacuum contribution:

$$T^{\text{eff}}_{\mu\nu} = T_{\mu\nu} - \frac{\Lambda}{8\pi G}g_{\mu\nu}.$$

With this redefinition, the Einstein field equations assume their most commonly encountered form:

$$G_{\mu\nu} = 8\pi G T^{\text{eff}}_{\mu\nu}. \tag{2.10}$$

An alternative formulation, known as trace-reversed form, consists in taking the trace of equation (2.10), i.e. contracting it with $g^{\mu\nu}$, and substituting this back in (2.10) to express it in terms of the Ricci tensor, with $T \equiv g^{\mu\nu}T_{\mu\nu}$:

$$R_{\mu\nu} = 8\pi G\left(T_{\mu\nu} - \frac{1}{2}T g_{\mu\nu}\right)$$

2.2.3 Linearized gravity and Newtonian limit

Linearized gravity

In astrophysical and cosmological applications, situations frequently arise in which spacetime is approximately flat. In these cases, the Einstein field equations can be safely approximated by letting the metric deviate only slightly from the Minkowski background. For simplicity, we assume $\Lambda = 0$ and write the metric $g_{\mu\nu}$ as a small perturbation of the Minkowski metric $\eta_{\mu\nu} = \text{diag}(-1,+1,+1,+1)$:

$$g_{\mu\nu} = \eta_{\mu\nu} + h_{\mu\nu},$$

where the perturbative components $h_{\mu\nu}$ satisfy the smallness condition $|h_{\mu\nu}| \ll 1$.

In this regime, the Einstein equations can be systematically expanded to linear order in the small perturbation $h_{\mu\nu}$ [110]. This linearization procedure is significantly simplified by imposing an appropriate gauge condition, the de Donder gauge, defined in analogy with the Lorentz gauge in electromagnetism:

$$\partial^\mu h_{\mu\nu} - \frac{1}{2}\partial_\nu h = 0,$$

where $h = \eta^{\mu\nu}h_{\mu\nu}$ denotes the trace of the perturbation. This gauge choice can always be achieved through an appropriate coordinate transformation and leads to substantial simplifications in the Einstein field equations, which assume the form:

$$\Box h_{\mu\nu} - \frac{1}{2}\Box h\eta_{\mu\nu} = -16\pi G T_{\mu\nu}.$$

These equations can be further simplified by introducing the trace-reversed perturbation: $\bar{h}_{\mu\nu} = h_{\mu\nu} - \frac{1}{2}h\eta_{\mu\nu}$, which satisfies $\bar{h} = \eta^{\mu\nu}\bar{h}_{\mu\nu} = -h$. In terms of this new variable, the linearized Einstein equations reduce to a set of decoupled wave equations:

$$\Box\bar{h}_{\mu\nu} = -16\pi G T_{\mu\nu}, \tag{2.11}$$

where $\Box = \eta^{\mu\nu}\partial_\mu\partial_\nu$ represents the d'Alembertian operator. Equivalently, we could maintain the variable $h_{\mu\nu}$ and rewrite the equation in trace-reversed form:

$$\Box h_{\mu\nu} = -16\pi G\left(T_{\mu\nu} - \frac{1}{2}T\eta_{\mu\nu}\right). \tag{2.12}$$

In both cases, the equations can be solved explicitly [110]. The expression for the trace-reversed perturbation $\bar{h}_{\mu\nu}$ reads:

$$\bar{h}_{\mu\nu}(t,x) = \int \frac{4T_{\mu\nu}(t-|x-y|,y)}{|x-y|}\,\mathrm{d}^3y\,. \tag{2.13}$$

It consists of a retarded integral, in which the value of the perturbation $\bar{h}_{\mu\nu}$ at a given time t depends on the value of the energy-momentum tensor $T_{\mu\nu}$ throughout the whole past history of the system.

Simultaneously, the Klein-Gordon equation for scalar matter fields (2.7) is simplified in the linearized regime. We do not report the explicit expression here, as we perform computations directly in the Newtonian limit case, where the result is more meaningful.

Newtonian Limit

When matter exhibits low density and fields evolve slowly compared to the speed of light, an additional approximation can be implemented, reducing the linearized equations of General Relativity to the familiar framework of Newtonian gravity [110]. Under these conditions, the energy-momentum tensor is dominated by the rest mass density $\rho(x)$, while the off-diagonal and spatial components become negligible:

$$T_{00} = \rho(x), \quad T_{0i} = T_{ij} = 0\,. \tag{2.14}$$

Due to the slow evolution of the fields, the temporal retardation in (2.13) characterizing the trace-reversed metric perturbation $\bar{h}_{\mu\nu}(t,x)$ can be neglected. The wave operator in Einstein field equations (2.11) is formally replaced by the three-dimensional Laplacian: $\Box \to \Delta$, and they simplify considerably:

$$\Delta\bar{h}_{00} = -16\pi G\rho(x), \quad \Delta\bar{h}_{0i} = \Delta\bar{h}_{ij} = 0.$$

With appropriate boundary conditions requiring the perturbations to vanish at spatial infinity, the solutions are:

$$\bar{h}_{00} = -4\Phi(x), \quad \bar{h}_{0i} = \bar{h}_{ij} = 0, \tag{2.15}$$

where $\Phi(x)$ is the Newtonian gravitational potential satisfying Poisson's equation:

$$\Delta\Phi = 4\pi G\rho(x). \tag{2.16}$$

Thus, in the Newtonian limit, the only non-vanishing component $\bar{h}_{00}$ of the trace-reversed perturbation $\bar{h}_{\mu\nu}$ coincides with the standard Newtonian gravitational potential up to a scaling factor of -4.

Consider now the Klein-Gordon equation (2.7) for the massive field ϕ [62]. For simplicity, assume $\xi = 0$, neglecting the term proportional to R, and assume the massive field to be free, $V(\phi) = (m_0^2\phi^2)/2$. In the linearized gravity case $g_{\mu\nu} = \eta_{\mu\nu} + h_{\mu\nu}$, combined with the Newtonian limit where only $h_{00} = -4\Phi$ is non-vanishing, the metric assumes a much simpler form:

$$\mathrm{d}s^2 = -(1+2\Phi)\,\mathrm{d}t^2 + (1-2\Phi)(\mathrm{d}x^2 + \mathrm{d}y^2 + \mathrm{d}z^2)$$

and the Klein-Gordon equation (2.7) becomes

$$-(1-2\Phi)\partial_t^2\phi + (1+2\Phi)\Delta\phi - m_0^2\phi = 0\,.$$

With no loss of generality, we write a WKB-type ansatz for the matter field:

$$\phi(t,x) = \psi(t,x)e^{-imt}\,,$$

we plug it into the Klein-Gordon equation, compute the derivatives, drop the exponential, and divide by $m^2\psi$:

$$-2\Phi + 2i(1-2\Phi)\frac{\partial_t\psi}{m_0\psi} + (1-2\Phi)\frac{\partial_t^2\psi}{m_0^2\psi} + (1+2\Phi)\frac{\Delta\psi}{m_0^2\psi} = 0\,.$$

We finally recall the weak potential assumption and the low-density, slowly varying fields hypothesis:

$$\Phi \sim \mathcal{O}(\varepsilon)\,, \qquad \left|\frac{\partial_t\psi}{m_0\psi}\right| \sim \mathcal{O}(\varepsilon)\,, \qquad \left|\frac{\partial_t^2\psi}{m_0^2\psi}\right| \sim \mathcal{O}(\varepsilon^2)\,, \qquad \left|\frac{\Delta\psi}{m_0^2\psi}\right| \sim \mathcal{O}(\varepsilon)\,.$$

With these orders, and dropping the ε^2 terms, the matter field equation reduces to the Poisson equation

$$i\partial_t\psi = -\frac{\Delta\psi}{2m_0} + m_0\Phi\psi\,.$$

Thus, in the Newtonian limit, the Einstein-Klein-Gordon equations (2.9) reduce to the Schrödinger-Poisson problem (1.2).

2.3 Notes on Quantum Field Theory

According to our current understanding, matter is fundamentally quantum in nature. While classical descriptions of matter provide adequate models for macroscopic phenomena, they fail to capture essential physics at the microscopic scale, where quantum behaviors emerge as dominant features. Quantum mechanics provides the correct mathematical formalism to describe these behaviors. In standard quantum mechanics, classical degrees of freedom are promoted to operators that act on elements of a Hilbert space, called wave functions, which describe the state of the system by representing particles as wave-like rather than point-like objects.

Although quantum mechanics appropriately describes a wide range of physical phenomena, this framework becomes less effective for modeling processes at even smaller scales, where the number of particles is not conserved. Below a characteristic length threshold, known as the Compton wavelength $\lambda_C = h(mc)^{-1}$ (where h is Planck's constant, m is the particle mass and c is the speed of light), particle-antiparticle pairs may spontaneously appear from the vacuum or be annihilated, and the concept of a single point-like particle breaks down completely.

To describe such phenomena, the appropriate theoretical framework is Quantum Field Theory, which models particles as excitations of underlying quantum fields that permeate all of spacetime. In this picture, the annihilation and creation of particles is understood as the emergence and disappearance of excitations in a unified field, and their common origin explains why quantum particles of the same type are fundamentally indistinguishable.

In this Section, we recall some fundamental concepts of Quantum Field Theory, which serve as a preliminary basis for understanding several relevant works on dark matter. A more thorough description can be found in the textbooks by Combescure and Robert [40] (chapter 10) and Berezin and Shubin [23] (chapter 5), while a concise but effective presentation is given in the excellent lecture notes by Tong [137] and in the work by Alcubierre et al. [2].

2.3.1 The Fock Space

The quantum field formalism is specifically designed to model systems with a varying number of particles. Instead of working with a single one-particle Hilbert space, the fundamental state space is a Fock space, which, loosely speaking, consists of infinitely many stacked n-particle Hilbert spaces. In this way, as the number of particles varies, the state of the system remains described by an element of the same comprehensive Hilbert space.

Formally, a Fock space is defined by the following hierarchical construction. Let $\mathfrak{h}$ denote a one-particle Hilbert space with orthonormal basis $\{e_i\}_{i=1}^{\infty}$ and with inner product $\langle\psi,\phi\rangle_{\mathfrak{h}}$ for any $\psi,\phi\in\mathfrak{h}$. Elements in this space represent the state of a single particle.

An n-particle Hilbert space is constructed as the n-fold tensor product of $\mathfrak{h}$ with itself:

$$\mathfrak{h}^{\otimes n} \equiv \mathfrak{h}\otimes\ldots\otimes\mathfrak{h} \quad (n \text{ times})\,,$$

with basis elements in the form $\{e_{i_1} \otimes \cdots \otimes e_{i_n}\}_{i_1,\dots,i_n=1}^{\infty}$. The single basis elements represent all possible configurations in which n particles can be placed in the infinitely many one-particle basis states $\{e_i\}_{i=1}^{\infty}$. Loosely speaking, the element $e_{i_1} \otimes \cdots \otimes e_{i_n}$ represents a state where the first particle is the state e_{i_1}, the second is the state e_{i_2}, up to the n-th particle which is the state e_{i_n}, each one-particle state $e_{i_1}, \dots, e_{i_n}$ belonging to the basis of one-particle space $\hbar$. Elements of the n-particle space are defined as linear combinations of the basis elements and are denoted as

$$\Psi^{(n)} = \sum_{i_1,\dots,i_n=1}^{\infty} c_{i_1 \dots i_n} e_{i_1} \otimes \cdots \otimes e_{i_n},$$

while the inner product is induced from the one-particle Hilbert space:

$$\langle e_{i_1} \otimes \cdots \otimes e_{i_n}, e_{j_1} \otimes \cdots \otimes e_{j_n} \rangle_{\hbar^{\otimes n}} \equiv \langle e_{i_1} \otimes e_{j_1} \rangle_{\hbar} \dots \langle e_{i_n} \otimes e_{j_n} \rangle_{\hbar},$$

and is then generalized by linearity to any $\Psi^{(n)}, \Phi^{(n)} \in \hbar^{\otimes n}$. This n-particle space $\hbar^{\otimes n}$ represents the n-particle sector of a Fock space.

As a last step, the Fock space $\mathcal{F}(\hbar)$ is defined as the direct sum of infinitely many n-particle sectors

$$\mathcal{F}(\hbar) = \oplus_{n \geq 0} \hbar^{\otimes n},$$

where $\hbar^{\otimes 0} = \mathbb{C}$ represents the zero-particles vacuum space. This introduces the possibility of collecting in a unique state configurations with different number of particles and grants the opportunity of switching between n-particle sectors while remaining in the same Hilbert space. Elements in the Fock space $\mathcal{F}(\hbar)$ take the form

$$\Psi = (\Psi^{(0)}, \Psi^{(1)}, \dots, \Psi^{(n)}, \dots),$$

with basis elements $(0, \dots, 0, e_{i_1} \otimes \cdots \otimes e_{i_n}, 0, \dots)$, with indices $i_1, \dots, i_n$ spanning the basis of each n-th sector. The natural inner product is induced from that of the n-sector:

$$\langle \Psi, \Phi, \rangle_{\mathcal{F}} = \sum_{n \geq 0} \langle \Psi^{(n)}, \Phi^{(n)} \rangle_{\hbar^{\otimes n}}.$$

Bosonic Fock space

In quantum mechanics, particles are classified into two fundamental families: bosons and fermions, distinguished by their statistical behavior and specifically by the sign change (or lack thereof) in the system's state when two particles are exchanged. To account for these two distinct natures, specialized Fock spaces are constructed in which states follow the prescribed sign behavior under particle permutation. We focus here on the bosonic case, which is particularly relevant in our work.

Bosonic particles preserve the state sign under particle exchange. Thus, a bosonic Fock space must account for the symmetry with respect to all permutations of particles. This is realized by considering a symmetrization operator S_n that acts on $\Psi^{(n)} \equiv \Psi_1^{(n)} \otimes \cdots \otimes \Psi_n^{(n)} \in \hbar^{\otimes n}$ by combining all possible permutations:

$$S_n(\Psi_1^{(n)} \otimes \cdots \otimes \Psi_n^n) = \frac{1}{n!} \sum_{\sigma \in \mathfrak{S}_n} \Psi_{\sigma(1)}^{(n)} \otimes \cdots \otimes \Psi_{\sigma(n)}^n,$$

where $\mathfrak{S}_n$ is the set of all permutations of n objects. This symmetrization operator defines a modified n-particle sector in the form $\hbar_B^{\otimes n} \equiv S_n \hbar^{\otimes n}$, which is invariant under permutation of the one-particle constituents $\Psi_1^{(n)}, \dots, \Psi_n^{(n)}$ of each state.

The basis of the bosonic n-particle sector $\hbar_B^{\otimes n}$ is in the form: $\{e_{i_1} \vee \cdots \vee e_{i_n}\}_{i_1,\dots,i_n=1}^{\infty}$, with $\vee$ denoting the normalized symmetric tensor product:

$$e_{i_1} \vee \cdots \vee e_{i_n} = \sqrt{\frac{n!}{i_1! \dots i_n!}} S_n(e_{i_1} \otimes \cdots \otimes e_{i_n}).$$

Given the symmetry characterizing bosons, each element $e_{i_1} \vee \cdots \vee e_{i_n}$ can be rearranged, listing all one-particle basis elements and raising them by an index denoting the number of particles in that state: $e_1^{\alpha_1} \vee e_2^{\alpha_2} \vee \cdots \vee e_k^{\alpha_k} \vee \dots$, where α_k is the number of particles in the k-th one-particle state e_k and $\sum_{k=1}^{\infty} \alpha_k = n$ is the total number of particles. Multi-indices $\alpha \equiv (\alpha_1 \alpha_2 \dots \alpha_k \dots)$ collect

the so called occupancy numbers, and basis elements in this form are also denoted by the so-called occupancy number notation:

$$|\alpha_1\alpha_2\dots\alpha_k\dots\rangle \equiv e_1^{\alpha_1} \vee e_2^{\alpha_2} \vee \dots \vee e_k^{\alpha_k} \vee \dots . \tag{2.17}$$

Given the bosonic n-sector, the construction of the complete bosonic Fock space $\mathcal{F}_B(\mathcal{H})$ proceeds analogously to the general case, maintaining the direct sum structure over all particle number sectors.

2.3.2 Annihilation and Creation Operators

A Fock space can be populated by defining a vacuum vector representing a state with no particles and by letting two special operators act on it – the so-called annihilation and creation operators, which model the vanishing and emerging of a particle in a specific state. The iterated application of these operators to the vacuum vector allows us to progressively define a complete basis of the Fock space, thus providing a description of every state in the Fock space.

Formally, an annihilation operator and a creation operator can be defined for any function $f \in \mathcal{H}$ in the one-particle space, and they are denoted $a(f)$ and $a^\dagger(f)$, respectively. Their definition can be given for the basis elements $\{e_j\}_{j=1}^\infty$ of $\mathcal{H}$, simplifying the notation to $a_j^\dagger \equiv a^\dagger(e_j)$ and $a_j \equiv a(e_j)$, and then it can be extended to any function $f \in \mathcal{H}$ by anti-linearity for the annihilation operator $a(f)$ and by linearity for the creation operator $a^\dagger(f)$. Each couple of operators $a_j^\dagger$ and a_j is defined on the Fock space and returns an element of the Fock space, $a_j^\dagger, a_j : \mathcal{F}(\mathcal{H}) \mapsto \mathcal{F}(\mathcal{H})$. Their action on the element $\Psi = (\Psi^{(0)}, \Psi^{(1)}, \dots, \Psi^{(n)}, \dots)$ can be described component-wise, defining how they transform an element $\Psi^{(n)}$ of the n-th sector. To this aim, it is sufficient to describe how they act on each basis function $e_{i_1} \otimes \dots \otimes e_{i_n}$ of the n-th sector and to extend the definition by linearity. The action of the annihilation and creation operators $a_j^\dagger$ and a_j on each basis function $e_{i_1} \otimes \dots \otimes e_{i_n}$, denoted by the same symbols with abuse of notation, is expressed through the following conditions:

$$\begin{aligned} a_j\Psi^{(0)} = 0, \quad a_j^\dagger\Psi^{(0)} = e_j, \\ a_j(e_{i_1} \otimes \dots \otimes e_{i_n}) = \sqrt{n+1}\langle e_j, e_{i_1}\rangle_{\mathcal{H}} e_{i_2} \otimes \dots \otimes e_{i_n} \\ a_j^\dagger(e_{i_1} \otimes \dots \otimes e_{i_n}) = \frac{1}{\sqrt{n}} e_j \otimes e_{i_1} \otimes \dots \otimes e_{i_n} \end{aligned} \tag{2.18}$$

where $\Psi^{(0)}$ is the normalized basis element of the 0-particle space $\mathcal{H}^{\otimes 0}$, also called the vacuum state.

Loosely speaking, the annihilation operator a_j takes a state with n particles and annihilates a particle in the state e_j, resulting in a space of $n-1$ particles; while the creation operator $a_j^\dagger$ takes a state with n particles and creates a particle in the state e_j, resulting in a space of $n+1$ particles. Indeed, the action of the operators a_j, $a_j^\dagger$ varies the number of particles in a state, providing a way to move across different n-sectors of the Fock space. Their definition is intrinsically based on the hierarchical structure of the whole Fock space, and their action, while leaving the Fock space invariant, is fundamentally non-trivial, since it cannot be restricted to a single n-sector.

In the case of bosonic Fock spaces, the above definition (2.18) can be adapted to ensure that the operators are well defined on $\mathcal{F}_B(\mathcal{H})$, preserving the space. This is performed using the usual symmetrization operator S_n, which is conveniently promoted to act on the entire Fock space. The component-wise action of the modified operators reads:

$$(a_B)_j = a_j S_n\,, \qquad (a_B)_j^\dagger = a_j^\dagger S_n\,.$$

For Bosonic Fock spaces, the definitions (2.18) ensure that the operators $(a_B)_j$, $(a_B)_j^\dagger$ satisfy the commutation relations:

$$[(a_B)_j, (a_B)_k^\dagger] = \langle e_j, e_k\rangle \mathbb{1}\,, \tag{2.19a}$$

$$[(a_B)_j, (a_B)_k] = [(a_B)_j^\dagger, (a_B)_k^\dagger] = 0 \tag{2.19b}$$

where $[A, B] \equiv AB - BA$ denotes the commutator. Together with the property $(a_B)_j\Psi^{(0)} = 0$ that the vacuum vector is annihilated by all annihilation operators $(a_B)_j$, these relations provide a characterization of the two sets of operators $\{(a_B)_j\}_{j=1}^\infty$ and $\{(a_B)_j^\dagger\}_{j=1}^\infty$.

In the following, we will focus on bosonic spaces, omitting subscripts B for a simpler notation when no ambiguity arises.

Based on the definitions (2.18), adapted to the bosonic case, the iterated application of the creation operators $\{a_j^\dagger\}_{j=1}^\infty$ can be used to construct a whole basis of each n-particle sector:

$$|\alpha_1\alpha_2\dots\rangle \equiv \frac{(a_1^\dagger)^{\alpha_1}}{\sqrt{\alpha_1!}}\frac{(a_2^\dagger)^{\alpha_2}}{\sqrt{\alpha_2!}}\dots\Psi^{(0)}\,. \tag{2.20}$$

We recognize here the standard basis of the n-sector of the Fock space in the occupancy number notation (2.17), with each α_j representing the number of particles in the one-particle state e_j and with $\sum_{j=1}^\infty \alpha_j = n$ the total number of particles. The commutation relations (2.19) ensure that the basis functions $|\alpha_1\alpha_2\dots\rangle$ are normalized and mutually orthogonal.

This constructive approach provides a complete characterization of Fock spaces. Indeed, a Fock space can be abstractly described as a Hilbert space $\mathcal{F}$ equipped with operators $\{a_j\}_{j=1}^\infty$ and $\{a_j^\dagger\}_{j=1}^\infty$ satisfying the canonical commutation relations (2.19), together with a normalized vector $\Psi^{(0)}$ that is annihilated by all a_i and such that the vectors constructed as in (2.20) form a complete orthonormal basis. If these conditions are satisfied, the Hilbert space is called a Fock space, with $\Psi^{(0)}$ representing the vacuum vector and $\{a_i, a_i^\dagger\}_{i=1}^\infty$ the annihilation and creation operators.

In addition, there exists a unique unitary isomorphism between any two such spaces, which identifies the vacuum vectors and the corresponding operators $\{a_j\}_{j=1}^\infty$ and $\{a_j^\dagger\}_{j=1}^\infty$. Thus, we can identify different Fock spaces, regarding them as different realizations of the same abstract Fock space.

2.3.3 Quantization of a scalar field

A standard way to define a quantum field system consists in starting from a classical problem and promoting it to the quantum field formalism. This is performed through canonical rules known as second quantization, in contrast to the first quantization rules that allow to write classical problems in terms of standard quantum mechanics.

In view of creating a connection with the Einstein-Klein-Gordon equations, we present here the case of a classical massive scalar field ϕ satisfying the free Klein-Gordon equation, as derived in Section 2.2.2:

$$(\Box - m_0^2)\phi = 0\,, \tag{2.21}$$

where $\Box \equiv g^{\mu\nu}\nabla_\mu\nabla_\nu$ is the curved D'Alembertian operator and m_0 is the inverse Compton length of the field, playing the role of particle rest mass in the field theory.

To construct the quantum field analogue of this problem [2], we first consider the space of real solutions to the equation (2.21) and extend it to complex solutions. This space, denoted by $\mathcal{X}$, can be equipped with an inner product. Given two complex-valued solutions $\phi_1, \phi_2 \in \mathcal{X}$, we can define the map $(\cdot,\cdot)$:

$$(\phi_1, \phi_2) \equiv -i\int_{\Sigma_t} [\phi_1\partial_t\phi_2^* - (\partial_t\phi_1)\phi_2^*]\sqrt{\det(\gamma_{ij})}d^3x \tag{2.22}$$

where $\phi_1^*(x)$ denotes the complex conjugate of $\phi_1(x)$, Σ_t is a Cauchy hypersurface at time t (a fixed-time leaf of a foliation of the spacetime manifold), ∂_t denotes the time derivative, and $\sqrt{\det(\gamma_{ij})}d^3x$ is the volume element on the hypersurface. For solutions of equation (2.21) that decay sufficiently fast at spatial infinity, the quantity (ϕ_1, ϕ_2) does not depend on the choice of the Cauchy hypersurface.

The map $(\cdot,\cdot)$ defined by (2.22) and acting on $\mathcal{X}$ does not yet represent an inner product, since the quantity $(\phi,\phi) = 2\mathrm{Im}\int_{\Sigma_t}\phi\partial_t\phi^*\sqrt{\det(\gamma_{ij})}d^3x$ may fail to be positive definite. To ensure that this expression truly defines an inner product, we assume that the space $\mathcal{X}$ can be decomposed as

$$\mathcal{X} = \mathcal{X}_+ \oplus \mathcal{X}_+^*\,,$$

where $\mathcal{X}_+$ consists of solutions with positive norm and its complex conjugate space $\mathcal{X}_+^*$ is orthogonal to it, such that $(f, g^*) = 0$ for all $f, g \in \mathcal{X}_+$. This decomposition ensures that the restriction of the map $(\cdot,\cdot)$ defined by (2.22) to the space $\mathcal{X}_+$ is indeed positive definite and defines a proper inner product. Although this assumption is quite strong, the existence of a preferred decomposition ensuring the proper definition of an inner product is valid for a wide variety of spacetime manifolds, particularly static or stationary ones, as discussed by Ashtekar et al. [7].

The space $\hbar \equiv \mathcal{X}_+$ equipped with the inner product (2.22) defines a one-particle Hilbert space. It can be used to construct the Fock space $\mathcal{F}(\hbar)$ as described in Section 2.3: given an orthonormal basis

$\{e_j\}_{j=1}^{\infty}$ of the one-particle Hilbert space $\hbar$, we can define for each basis function the annihilation and creation operators $\{a_j\}_{j=1}^{\infty}$ and $\{a_j^\dagger\}_{j=1}^{\infty}$ as in (2.18), and these operators in turn populate the Fock space by constructing the basis functions (2.20).

The *field operator* $\hat{\phi}$ is then defined as

$$\hat{\phi}(x) = \sum_{j=1}^{\infty} [a_j e_j(x) + a_j^\dagger e_j^*(x)] \tag{2.23}$$

and in the bosonic case it inherits the commutation relations:

$$[\hat{\phi}(x), \hat{\phi}^\dagger(y)] = \sum_{j=1}^{\infty} e_j(x) e_j^*(y) = \delta(x-y)\,, \qquad [\hat{\phi}(x), \hat{\phi}(y)] = [\hat{\phi}^\dagger(x), \hat{\phi}^\dagger(y)] = 0\,.$$

With definition (2.23), the field operator $\hat{\phi}$ is an operator-valued distribution parametrized by points x in spacetime, each $\hat{\phi}(x)$ at fixed x representing an operator on the Fock space $\mathcal{F}(\hbar)$. The dependence on the spacetime coordinate that determines the field nature of $\hat{\phi}$ is encoded in the coefficients $e_j(x)$ and $e_j^*(x)$, while the operator-valued nature of $\hat{\phi}$ is given by the operators a_j and $a_j^\dagger$, which are independent of space and time. The field operator encodes the fundamental quantum processes of particle creation and annihilation, localizing them at each point x of spacetime. When $\hat{\phi}(x)$ acts on a quantum state, it can modify the particle content through the action of the creation and annihilation operators, while the spacetime functions $e_j(x)$ and $e_j^*(x)$ determine how these processes are distributed across different spatial and temporal locations. Observe furthermore that the field operator (2.23) is self-adjoint, $\hat{\phi}^\dagger = \hat{\phi}$, for $\{e_j\}_{j=1}^{\infty}$ real functions.

Given this definition, the action of the annihilation and creation operators on a generic function $f = \sum_j c_j e_j \in \hbar$ can be equivalently described in terms of the field operator, by integrating out the dependence on the spacetime coordinates through the inner product $(\cdot,\cdot)$ defined in (2.22):

$$\begin{aligned}
(\hat{\phi}, f) = \quad \sum_{j=1}^{\infty} a_j (e_j, f) \quad &= \quad \sum_{j=1}^{\infty} c_j a_j = \quad a\left(\sum_{j=1}^{\infty} c_j e_j\right) = a(f)\,, \\
-(\hat{\phi}, f^*) = -\sum_{j=1}^{\infty} a_j^\dagger (e_j^*, f^*) = -\sum_{j=1}^{\infty} c_j a_j^\dagger &= a^\dagger\left(\sum_{j=1}^{\infty} c_j e_j\right) = a^\dagger(f)\,,
\end{aligned}$$

where we used the orthogonality of the basis functions and the decomposition property $(f, g^*) = 0$ for all $f, g \in \mathcal{X}_+$, together with the linearity of $a(f)$ and the anti-linearity of $a^\dagger(f)$. This relationship demonstrates how the field operator collects and organizes all the annihilation and creation operators, providing a unified description of particle creation and annihilation processes throughout spacetime.

To better clarify the creation and annihilation components in the field operator $\hat{\Phi}$ (2.23), they are often denoted with specific symbols:

$$\hat{\Phi}(x) = \hat{\Psi}(x) + \hat{\Psi}^\dagger(x)\,, \qquad \hat{\Psi}(x) \equiv \sum_{j=1}^{\infty} a_j e_j(x)\,, \quad \hat{\Psi}^\dagger(x) \equiv \sum_{j=1}^{\infty} a_j^\dagger e_j(x)\,. \tag{2.24}$$

For bosonic fields, they satisfy the commutation relations:

$$[\hat{\Psi}(x), \hat{\Psi}^\dagger(y)] = \sum_{j=1}^{\infty} e_j(x) e_j^*(y) = \delta(x-y)\,, \qquad [\hat{\Psi}(x), \hat{\Psi}(y)] = [\hat{\Psi}^\dagger(x), \hat{\Psi}^\dagger(y)] = 0 \tag{2.25}$$

It is important to note that the definition of the field operator is not unique, since it depends on the choice of the orthonormal basis functions $\{e_j\}$. However, different choices of basis lead to field operators that are related through unitary transformations. Specifically, if $\{g_k\}$ is another orthonormal basis related to $\{e_j\}$ by a unitary transformation $g_k = \sum_j U_{kj} e_j$, then the corresponding creation and annihilation operators are related by $b_k = \sum_j U_{kj} a_j$, where the matrix U is unitary. The resulting field operators represent the same physical field and are connected by an isomorphism between the corresponding Fock spaces. In this sense, while the mathematical expression of the field operator depends on the chosen basis, the physical field it represents is unique and well-defined.

Once the field operator $\hat{\phi}(x)$ is defined from the classical problem (2.21), the dynamics of the physical system can be described in the Heisenberg perspective by letting the field operator evolve. Since

the dependence of $\hat{\phi}$ on the spacetime coordinates is encoded in the coefficients $\{e_j(x), e_j^*(x)\}_{j=1^\infty}$ that solve the classical problem (2.21) by construction, the field operator $\hat{\phi}(x)$ will in turn satisfy the free Klein-Gordon equation in the second quantization formalism:

$$(\Box - m_0^2)\hat{\phi}(x) = 0 \tag{2.26}$$

Thus, there is a profound relationship between the dynamics of the field operator and the corresponding classical dynamics. In particular, although the quantum description is the valid one at the fundamental level, under specific conditions it is legitimate to reduce to classical dynamics. This occurs, for example, in the case of stationary spacetimes with energies below a certain threshold. Under these conditions, the number of particles is conserved, and one can reasonably restrict oneself to a fixed n-sector of the Fock space, where the dynamics describes the evolution of the coefficients $\{e_j(x), e_j^*(x)\}_{j=1}^{\infty}$ and is governed by the classical problem (2.21) This reduction therefore justifies the use of classical equations in a fundamentally quantum context – the classical equations hold and describe the evolution of the coefficients $\{e_j(x), e_j^*(x)\}_{j=1}^{\infty}$ of the underlying quantum field $\hat{\phi}(x)$ given by (2.23).

The Schrödinger picture

The second quantization procedure we just described is constructed in the so-called Heisenberg picture, in which the dynamics lets the operators evolve while the states are considered fixed. In our case, in fact, the dynamics is defined on the matter field $\hat{\Phi}$, which is an operator-valued distribution that depends explicitly on time and does not concern the states of the Fock space. The alternative approach, which is completely equivalent for the purpose of describing experimental phenomena, is the so-called Schrödinger picture, in which the operators are fixed while the states are evolved through a Schrödinger equation.

In this case, the prescription for the second quantization consists in considering the Hamiltonian description of the classical problem and in promoting it to the Quantum Field Theory formalism. In our problem, this is performed by expressing the classical Klein-Gordon equation as the Hamilton equation of a given Hamiltonian:

$$H = \int d^3x \left[\frac{1}{2}\pi^2(x,t) + \frac{1}{2}(\nabla\phi(x,t))^2 + \frac{1}{2}m^2\phi^2(x,t)\right]$$

where $\phi(x,t)$ is the classical scalar field and $\pi(x,t) = \partial_t\phi(x,t)$ is the associated canonical momentum. These quantities represent the fundamental degrees of freedom of the problem in the classical Hamiltonian description, whose inherent structure is characterized by the Poisson brackets:

$$\{\phi(x,t), \pi(y,t)\} = \delta^3(x-y)\,, \qquad \{\phi(x,t), \phi(y,t)\} = \{\pi(x,t), \pi(y,t)\} = 0\,.$$

The fundamental assumption in constructing the quantum dynamics is that the whole Hamiltonian structure should be preserved in the Quantum Field Theory formalism: the fundamental degrees of freedom $\phi(x,t)$ and $\pi(x,t)$ are promoted to self-adjoint operators $\hat{\Phi}(x,t)$ and $\hat{\Pi}(x,t)$, while the Poisson brackets result in the canonical commutation relations:

$$[\hat{\Phi}(x,t), \hat{\Pi}(y,t)] = i\hbar\delta^3(x-y)\,, \qquad [\hat{\Phi}(x,t), \hat{\Phi}(y,t)] = [\hat{\Pi}(x,t), \hat{\Pi}(y,t)] = 0\,.$$

The Hamiltonian is then expressed in operator terms:

$$\hat{H} = \int d^3x \left[\frac{1}{2}\hat{\Pi}^2(x,t) + \frac{1}{2}(\nabla\hat{\Phi}(x,t))^2 + \frac{1}{2}m^2\hat{\Phi}^2(x,t)\right] \tag{2.27}$$

and, in analogy with the classical rule $\frac{df}{dt} = \{f, H\}$, each generic operator $\hat{O}$ would evolve according to the Heisenberg equation:

$$\frac{d\hat{O}}{dt} = \frac{i}{\hbar}[\hat{H}, \hat{O}]\,. \tag{2.28}$$

Finally, in the Schrödinger picture, the evolution is transferred from the operators to the states. This is based on the assumption that the only observable quantities are the averages of the operators on the states, $\langle\psi|\hat{O}|\psi\rangle$, and the evolution of these averages can be equivalently described either by letting the operators evolve while fixing the states or by letting the states evolve while fixing the operators. Formally, the evolution of the average in the Schrödinger picture is written as

$$\frac{d}{dt}\langle\psi(t)|\hat{O}|\psi(t)\rangle = \left\langle \frac{d\psi(t)}{dt}\middle|\hat{O}\middle|\psi(t)\right\rangle + \left\langle \psi(t)\middle|\hat{O}\middle|\frac{d\psi(t)}{dt}\right\rangle$$

By imposing that it is equivalent to its Heisenberg picture analogue:

$$\frac{d}{dt}\langle\psi|\hat{O}(t)|\psi\rangle = \left\langle\psi\middle|\frac{d\hat{O}}{dt}\middle|\psi\right\rangle = \frac{i}{\hbar}\langle\psi|[\hat{H},\hat{O}]|\psi\rangle$$

for all operators $\hat{O}$, it results in the Schrödinger equation:

$$i\hbar\frac{\partial}{\partial t}\psi(t) = \hat{H}\psi(t)\,. \tag{2.29}$$

This equation is thus simply a consequence of promoting the Hamiltonian structure to the Quantum Field Theory formalism and of writing the dynamics on the states rather than on the operators. This description is completely equivalent to the previous construction in the Heisenberg picture, and the underlying Fock space structure still holds, as described above. The only difference concerns the dynamics, which now affects only the states while keeping the matter field operators $\hat{\Phi}$ time-independent.

Restriction to the n-sector

In certain regimes, such as when the energies are sufficiently low, particle creation and annihilation processes do not occur, and the number of particles is conserved along the motion. This implies that n-sectors are invariant and the dynamics on the Fock space reduces to dynamics on each fixed n-sector. The latter can be expressed in the familiar form of first quantization – that is, in the Schrödinger picture, as dynamics on the n-particle wave function $\psi^{(n)}(r_1,\dots,r_n)$.

The relation between the n-particle state $|\Psi^{(n)}\rangle$ in the Fock space and the n-particle wave function $\psi^{(n)}(r_1,\dots,r_n)$ in first quantization is expressed as in [9] by

$$|\Psi^{(n)}\rangle = \frac{1}{\sqrt{n!}}\int\prod_{i=1}^{n} d^3r_i\,\psi^{(n)}(r_1,\dots,r_n)\hat{\Psi}^\dagger(r_1)\cdots\hat{\Psi}^\dagger(r_n)|0\rangle \tag{2.30}$$

At this point, the action of a Fock space operator on the state $|\Psi^{(n)}\rangle$ can be explicitly calculated and expressed in terms of the wave function $\psi^{(n)}(r_1,\dots,r_n)$. We report the example of the operator $\hat{\Psi}(x)$, namely the destructive part of the field operator $\hat{\Phi}(x)$ defined in (2.24). The calculation is performed by recalling the commutation relations (2.25), and the property of the operator $\hat{\Psi}(x)$ to annihilate the vacuum vector: $\hat{\Psi}(x)|0\rangle = 0$. With these notions, one can proceed in the calculation recursively, gradually moving the operator $\hat{\Psi}(x)$ to the right using the commutation rules until it acts against the vacuum operator. At each commutation between $\hat{\Psi}(x)$ and the j-th operator $\hat{\Psi}^\dagger(r_j)$, the commutation rules produce two terms:

$$\hat{\Psi}(x)\hat{\Psi}^\dagger(r_j) = \delta^3(x-r_j) + \hat{\Psi}^\dagger(r_j)\hat{\Psi}(x)$$

In the term $\delta(x-r_j)$, the operator $\hat{\Psi}(x)$ no longer appears, and the contribution is in its final form, which does not require further elaboration; in the term $\hat{\Psi}^\dagger(r_j)\hat{\Psi}(x)$, the operator $\hat{\Psi}(x)$ is shifted one step to the right, and the calculation proceeds recursively. At the $(n-1)$-th final commutation, the operator $\hat{\Psi}(x)$ acts against the vacuum vector and the contribution vanishes. Overall, therefore, the contributions consist of each j-th term with $\delta(x-r_j)$. The explicit calculation takes the form:

$$\begin{aligned}
\hat{\Psi}(x)|\Psi^{(n)}\rangle &= \hat{\Psi}(x)\frac{1}{\sqrt{n!}}\int\prod_{i=1}^{n} d^3x_i\,\psi^{(n)}(r_1,\dots,r_n)\hat{\Psi}^\dagger(r_1)\cdots\hat{\Psi}^\dagger(r_n)|0\rangle \\
&= \frac{1}{\sqrt{n!}}\int\prod_{i=1}^{n} d^3x_i\,\psi^{(n)}(r_1,\dots,r_n)\hat{\Psi}(x)\hat{\Psi}^\dagger(r_1)\cdots\hat{\Psi}^\dagger(r_n)|0\rangle \\
&= \frac{1}{\sqrt{n!}}\int\prod_{i=1}^{n} d^3x_i\,\psi^{(n)}(r_1,\dots,r_n)\delta^3(x-r_1)\hat{\Psi}^\dagger(r_2)\cdots\hat{\Psi}^\dagger(r_n)|0\rangle \\
&\quad + \frac{1}{\sqrt{n!}}\int\prod_{i=1}^{n} d^3x_i\,\psi^{(n)}(r_1,\dots,r_n)\hat{\Psi}^\dagger(r_1)\hat{\Psi}(x)\hat{\Psi}^\dagger(r_2)\cdots\hat{\Psi}^\dagger(r_n)|0\rangle \\
&= \frac{1}{\sqrt{n!}}\sum_{j=1}^{n}\int\prod_{i\neq j} d^3x_i\,\psi^{(n)}(r_1,\dots,x_{j-1},x,x_{j+1},\dots,r_n) \\
&\quad\times\hat{\Psi}^\dagger(r_1)\cdots\hat{\Psi}^\dagger(x_{j-1})\hat{\Psi}^\dagger(x_{j+1})\cdots\hat{\Psi}^\dagger(r_n)|0\rangle\,.
\end{aligned} \tag{2.31}$$

2.4 Quantum and semiclassical gravity

The two theories we have just briefly presented – General Relativity (GR) and Quantum Field Theory (QFT) – are fundamentally different in their mathematical structure and approach to physics. Both are extremely elegant in form and predict experimental results with remarkable precision, making it extremely difficult to question their validity. Yet when attempts are made to combine them, profound and extremely challenging difficulties arise that have so far thwarted efforts to formulate a unified theory of everything.

On one hand, General Relativity provides an excellent description of gravity, formulating gravitational interaction in geometric terms and placing the dynamics of matter, assumed to be classical, in a fundamentally curved spacetime that evolves in response to matter. On the other hand, Quantum Field Theory provides an accurate description of physics at the microscopic level, assigning matter a fundamentally quantum nature and describing its interaction with fundamental forces in terms of a restricted number of particle families, classified by an extremely elegant framework - the Standard Model. Although QFT has been successfully combined with the formalism of special relativity, which reasons in terms of spacetime but does not consider it curved and evolving, the combination with GR gives rise to much more significant difficulties.

The most logical step to address this division would be to find an alternative formulation for the descriptive elements of GR, such as spacetime and the metric, expressing them in terms of new concepts more compatible with the Hilbert space formalism typical of QFT. Attempts of this kind fall under the name of Quantum Gravity and represent a research field that remains among the most studied, although it has not yet led to generally accepted formulations. Examples in this sphere include string theory, supersymmetry, and loop quantum gravity. While a thorough discussion of this topic is out of the scope of this work, in Section 2.4.4 we show how the Schrödinger-Poisson system may emerge from a quantum gravity approach, in the Newtonian limit and in an effective many-body sense.

Faced with the enormous formal difficulties that emerged with this approach, researchers have questioned whether it is truly necessary to quantize gravity, or whether gravity might instead be fundamentally classical. In this second scenario, known as semiclassical gravity, it is assumed that gravity has a fundamentally different nature compared to other fundamental forces: while these are essentially mediated by particles of quantum fields, gravity is purely classical and therefore it makes no sense to force its formalism into terms different from those already proposed by General Relativity.

In the case of semiclassical gravity, the choice to keep gravity classical while describing matter in terms of field theory forces a revision of how their coupling is formulated. The reference equations for the dynamics of a system of gravitating particles would be the Einstein's field equation (2.10), originally expressed for classical matter:

$$G_{\mu\nu} = 8\pi G T_{\mu\nu}$$

and the Klein-Gordon equation, formulated in the Heisenberg picture in terms of field theory (2.26):

$$(\Box - m_0^2)\hat{\phi}(x) = 0\,.$$

Regarding the matter field equation, the coupling with Einstein's equation consists of transitioning from a d'Alembertian operator $\Box = \eta^{\mu\nu}\partial_\mu\partial_\nu$ written in terms of the Minkowski metric $\eta_{\mu\nu}$ to a d'Alembertian operator $\Box = g^{\mu\nu}\nabla_\mu\nabla_\nu$ referred to a more general curved metric $g^{\mu\nu}$. Analogously, in a Schrödinger picture in which the states evolve according to the Schrödinger equation (2.29) the coupling is encoded in the Hamiltonian, which is written in terms of the curved metric $g^{\mu\nu}$ (here, the interpretation of the time derivative in the Schrödinger equation requires particular caution, and has to be referred to a specific spacetime foliation). Even with a fixed metric – that is, neglecting the backreaction of Einstein's equation that would cause the metric to evolve in a coupled manner – the study of QFT on curved space is inherently challenging and defines a research line known as Quantum Field Theory in Curved Spacetime (QFTCS), which we briefly discuss in Section 2.4.1.

Once we understand how to treat QFT on curved spacetime, the problem of formalizing the coupling arises: while the classical Einstein equation involves the classical energy-momentum tensor $T_{\mu\nu}$ as a source, in the case of matter described by quantum fields the tensor would be promoted to an operator $\hat{T}_{\mu\nu}$. This different mathematical structure prevents its direct use in Einstein's equation, introducing the need for new assumptions about how to define the source. The predominantly used approach consists of using as a source the expectation value over a certain state $\Psi \in \mathcal{F}(\hbar)$ of the energy-momentum operator: $\langle\hat{T}_{\mu\nu}\rangle_\Psi \equiv \langle\Psi|\hat{T}_{\mu\nu}|\Psi\rangle$. In this way, the evolution of the metric will depend on the *state* of matter, and the matter state will in turn be affected due to the involvement

of the metric in the Klein-Gordon equation. We will treat this approach in depth in Section 2.4.2.

The semiclassical approach has formal and interpretative consequences that are profoundly different from the quantum gravity approach. As we show in Sections 2.4.3 and 2.4.4, the fundamental distinction lies in how non-linearity emerges in the dynamics: while in the quantum gravity case it results from effective approximation of an underlying linear theory, in the semiclassical approach the dynamics is non-linear at a fundamental level.

This difference had interesting consequences for the wave function collapse problem – a fundamental behavior in quantum theory whose origin remains widely debated. Since this phenomenon is necessarily non-linear, the semiclassical Schrödinger-Poisson system has been a prominent candidate in explaining this mechanism, although it finally proved insufficient for the purpose, still requiring the support of collapse theories to model the stochastic part of the process, and presenting considerable difficulties in managing potential superluminal effects. For a thorough discussion, see Bahrami et al. [9] and the references cited therein.

In addition, the two approaches have profound differences on the interpretative level, particularly regarding the meaning to be assigned to the wave function: while the standard quantum mechanical approach gives a probabilistic interpretation to the square of the wave function, reading it as a probability distribution for observing the particle, the semiclassical approach naturally suggests a more literal interpretation, in which the square of the wave function represents the matter distribution of the particle, which is spatially organized in a wave packet rather than being concentrated in a point-like object. This motivates the considerable caution with which the results on the Schrödinger-Poisson systems presented in this thesis should be addressed: even though the same mathematical structure emerges from different approaches, its physical interpretation could be profoundly different based on the underlying assumptions.

Given the conspicuous distance between these two approaches, semiclassical gravity has been strongly criticized and often judged inconsistent, although no unanimous agreement has been reached on the validity of these criticisms, ultimately leaving the final judgment to comparison with experimental data [9].

2.4.1 Schrödinger-Poisson from Quantum Field Theory on Curved Spacetime

As suggested by its name, Quantum Field Theory on Curved Spacetime (QFTCS) is concerned with studying the properties of QFT on curved space with a fixed metric, ignoring the backreaction in Einstein's equation that would cause the curvature of spacetime to evolve. In this framework, matter represents a kind of test system for probing the gravitational field. This is typical, for example, of quantum optical experiments, where optical setups are used to simulate the effects of a fixed curved spacetime in the laboratory [60, 21]. Studies of this kind, edging between the Newtonian and the relativistic descriptions of gravity, allow for experimental and theoretical investigation of the so-called post-Newtonian effects of gravity on quantum systems, that is, those phenomena that are explainable as corrections to successive orders of Newtonian gravity.

To understand the typical context of this kind of research, consider the case of stationary spacetimes with limited energy levels, where the particle number is conserved and one can restrict to classical (or first-quantized) dynamics on a fixed n-sector. In the Newtonian limit where all relativistic effects are neglected, the dynamics would be governed by the Schrödinger equation subject to a background Newtonian gravitational potential:

$$i\hbar\partial_t\Psi = \left(-\frac{\hbar^2}{2m}\Delta + m\Phi\right)\Psi\,.$$

When relativistic effects begin to manifest, corrections should be made to this equation by including new couplings to obtain a still approximate but more accurate description that takes into account first-order relativistic effects. While these modifications can be introduced through heuristic approaches, more systematic studies are necessary to guarantee the completeness and independence of the new information, i.e. to ensure that no relevant corrections are lost and that no redundant ones are written. QFTCS therefore deals with deriving these effective post-Newtonian corrections starting from fundamental laws, providing a solid theoretical foundation for the heuristic descriptions. Once appropriately justified, these approximate models are then used in practical situations, such as the above-mentioned quantum optical experiments, to simplify the complicated quantum field formalism without losing the post-Newtonian corrections.

In this regard, see the interesting works [57, 56] by Giulini and collaborators, who start from classical relativistic quantum equations and formally expand them through a WKB-inspired approach, deriving a Schrödinger equation with post-Newtonian corrections.

2.4.2 The semiclassical approach

The most delicate point in formulating a theory of semiclassical gravity consists in defining the coupling, or backreaction, between the spacetime metric, assumed to be fundamentally classical, and matter, described by a quantum field. Formally, the difficulty lies in writing the source in Einstein's field equation, finding an appropriate substitute for the classical energy-momentum tensor $T_{\mu\nu}$ when this, in the context of a quantum matter field, is promoted to an operator $\hat{T}_{\mu\nu}$.

In the quantum formalism, the energy-momentum operator is expressed as:

$$\hat{T}_{\mu\nu} = (\nabla_\mu \hat{\Phi})(\nabla_\nu \hat{\Phi}) - \frac{1}{2} g_{\mu\nu}[(\nabla_\alpha \hat{\Phi})(\nabla^\alpha \hat{\Phi}) + m_0^2 \hat{\Phi}^2]$$

following a form analogous to the classical energy-momentum tensor $T_{\mu\nu}$ and promoting the classical field ϕ to the self-adjoint operator $\hat{\Phi}$. The mathematical definition of this operator is delicate due to the presence of quadratic terms like ϕ^2, whose promotion to operator products $\hat{\Phi}\hat{\Phi}$ is not well-posed. In this work, we do not include a complete discussion of this problem, for which we refer to Alcubierre et al. [2] and the references cited therein. We just follow the standard prescription – namely, the Wick normal ordering – according to which all creation operators are moved to the left of all annihilation operators. With this assumption, and using the field operator definition (2.23), the energy-momentum operator becomes:

$$\hat{T}_{\mu\nu} = \frac{1}{2} \sum_{j,k} \Big[(a_j^\dagger a_k + a_k^\dagger a_j) T_{\mu\nu}(e_j, e_k) + \text{H.c.} \Big]$$

where H.c. stands for Hermitian conjugation and $T_{\mu\nu}(e_j, e_k)$ represents the classical energy-momentum tensor for complex scalar fields $e_j(x)$ and $e_k(x)$:

$$T_{\mu\nu}(e_j, e_k) \equiv (\nabla_\mu e_j)(\nabla_\nu e_k) + (\nabla_\nu e_j)(\nabla_\mu e_k) - g_{\mu\nu}[(\nabla_\alpha e_j)(\nabla^\alpha e_k) + m_0^2 e_j e_k] \,.$$

The critical step consists of deriving from this operator an effective source for Einstein's field equation, of a form compatible with its classical structure. The most common choice consists of using as the source the expectation value calculated over a certain state $\Psi \in \mathcal{F}(\mathcal{H})$ of the energy-momentum operator: $\langle \hat{T}_{\mu\nu} \rangle_\Psi \equiv \langle \Psi | \hat{T}_{\mu\nu} | \Psi \rangle$. Einstein's field equation for semiclassical gravity is thus written as:

$$G_{\mu\nu} = 8\pi G \langle \hat{T}_{\mu\nu} \rangle_\Psi$$

When this is coupled to an equation for the matter field, as in the case of the Einstein-Klein-Gordon system, the expectation value that serves as the source evolves according to the equation for the matter field, either because the state Ψ is the current-time solution of the dynamics (Schrödinger picture), or because the operator $\hat{T}_{\mu\nu}$ is constructed from the field operator $\hat{\Phi}$ that solves the dynamical equation at the current time (Heisenberg picture). The system is therefore completely coupled, according to a scheme that represents the physical situation well but is technically difficult to study. For this reason, a standard procedure consists in writing the state Ψ as a linear combination of an appropriate basis of the Fock space. If the choice of basis is well designed with respect to the form of the energy-momentum operator, the backreaction can be approximated in a convenient way, for example, through controlled truncations that maintain the dominant terms while neglecting higher-order ones.

Among the possible choices of bases, we cite two that are particularly used: the standard basis in occupancy number notation and coherent states. The basis in occupancy number notation (2.17) describes states in which the number of particles in each single-particle state is known. In this case, the contributions to the expectation value $\langle \alpha | \hat{T}_{\mu\nu} | \alpha \rangle$ calculated on a single element $|\alpha\rangle \equiv |\alpha_1 \alpha_2 \dots \rangle$ of the basis are of types $\langle \alpha | a_j^\dagger a_k | \alpha \rangle = \alpha_j \delta_{jk}$ and $\langle \alpha | a_j a_k | \alpha \rangle = 0$, so that the expectation value of the energy-momentum tensor reduces to:

$$\langle \alpha | \hat{T}_{\mu\nu} | \alpha \rangle = \sum_j \alpha_j T_{\mu\nu}(e_j, e_j)$$

where $T_{\mu\nu}(e_j, e_j)$ represents the classical energy-momentum tensor calculated for the j-th mode function. The expectation value $\langle \hat{T}_{\mu\nu} \rangle_{|\alpha\rangle}$ of the operator $\hat{T}_{\mu\nu}$ on an element $|\alpha\rangle$ of the occupancy number

basis (2.17) is therefore given by a sum, weighted by the occupation numbers, of the classical energy-momentum tensors $T_{\mu\nu}(e_j, e_j)$ calculated for each basis function e_j. In this sense, it is as if $n = \sum_j \alpha_j$ independent complex classical fields contributed to the source of Einstein's field equation. According to this analogy, it is natural to interpret the mode functions e_j as the wave functions of quantum particles, and the semiclassical equations are equivalent to the classical Einstein-Klein-Gordon system for a family of non-interacting, complex, free, minimally coupled scalar fields, which form an orthonormal set of basis functions of the subspace $\mathcal{X}_+$ of positive norm solutions of the Klein-Gordon equation.

Another basis that is particularly used for expanding the state Ψ in the expectation value is that given by coherent states. Coherent states, denoted here with the same symbol $|\alpha\rangle$, are defined as the eigenstates of the annihilation operators:

$$a_j|\alpha\rangle = \alpha_j|\alpha\rangle$$

and play a very important role in the framework of Fock spaces. See the excellent review by Zhang et al. [147] for a clear and thorough description. Coherent states are characterized as the states with minimum uncertainty relationship:

$$\langle\alpha|(\hat{q} - \langle\hat{q}\rangle)^2|\alpha\rangle \ \langle\alpha|(\hat{p} - \langle\hat{p}\rangle)^2|\alpha\rangle = \left(\frac{1}{2}\right)^2$$

where $\hat{q} \equiv (a + a^\dagger)/\sqrt{2}$ and $\hat{p} \equiv (a - a^\dagger)/(i\sqrt{2})$ are the coordinate and momentum operators and $\langle\hat{f}\rangle \equiv \langle\alpha|\hat{f}|\alpha\rangle$ denotes the expectation value of an operator $\hat{f}$ on the state. In this sense, by saturating the quantum uncertainty principle, they behave as close as possible to classical field excitations. When calculating the expectation value of the energy-momentum operator on a coherent state, the relevant contributions take the form $\langle\alpha|a_j^\dagger a_k|\alpha\rangle = \alpha_j^* \alpha_k$ and $\langle\alpha|a_j a_k|\alpha\rangle = \alpha_j \alpha_k$, resulting in:

$$\langle\alpha|\hat{T}_{\mu\nu}|\alpha\rangle = \frac{1}{2} T_{\mu\nu}(\phi_{\rm cl}, \phi_{\rm cl}) \tag{2.32}$$

where $\phi_{\rm cl} = \sum_j [\alpha_j e_j(x) + \alpha_j^* e_j^*(x)]$ represents the classical analogue of the quantum field operator. In this way, the expectation value of the energy-momentum operator on a coherent state coincides, up to a factor of 1/2, with the classical energy-momentum tensor calculated for the classical matter field $\phi_{\rm cl}$. Therefore, it is as if the latter were solely responsible for generating the source in Einstein's field equation, and the semiclassical system is identical to the classical Einstein-Klein-Gordon system for the single, real, free, minimally coupled scalar field $\phi_{\rm cl}$.

Thus, through the choice of convenient basis functions, the semiclassical EKG system – which still describes matter as fundamentally quantum – can be equivalently written as the corresponding classical problem, where the role of the classical matter field is played by different objects depending on the choice of the basis – for example, by a set of independent complex fields in the case of the occupancy number basis, or a single real field in the case of the coherent states.

2.4.3 Schrödinger-Poisson from Semiclassical Gravity

In Section 2.2.3 we showed that in standard General Relativity, where matter is treated as classical, the Schrödinger-Poisson equations emerge as the Newtonian limit of the Einstein-Klein-Gordon equations. In this Section, we extend the same approach to the semiclassical case, in which gravity remains fundamentally classic, while matter is described in a second quantization formalism. Even in this case, the Schrödinger-Poisson equations emerge in the same limit, under the assumption of low energies resulting in a constant number of particles. The presentation follows the excellent work of Bahrami et al. [9].

We consider the case of an approximately flat spacetime, in which the metric is described by a perturbation of the Minkowski metric, $g_{\mu\nu} = \eta_{\mu\nu} + h_{\mu\nu}$, and in which linearized gravity provides a good approximation. In the semiclassical framework, we write the classical Einstein field equations for linearized gravity in trace-reversed form as in (2.12), using as the source term the expectation value of the energy-momentum operator in a given state, $\langle\Psi|\hat{T}_{\mu\nu}|\Psi\rangle$, where $\hat{T}_{\mu\nu}$ is an operator. We obtain:

$$\Box h_{\mu\nu} = -\frac{16\pi G}{c^4}\langle\Psi|\hat{T}_{\mu\nu}|\Psi\rangle - \frac{1}{2}\eta_{\mu\nu}\langle\Psi|\eta^{\rho\sigma}\hat{T}_{\rho\sigma}|\Psi\rangle\,.$$

In the Newtonian limit of a low-density slowly-evolving matter field, the Poisson equation can be obtained in complete analogy to the classical case (2.16):

$$\Delta V = \frac{4\pi G}{c^2}\langle\Psi|\hat{T}_{00}|\Psi\rangle\,,$$

where the potential V is related to the dominant component of the metric perturbation by $V \equiv -\frac{c^2}{2}h_{00}$. Note that, due to the semiclassical assumption, the potential has a classical form and depends on the state $|\Psi\rangle$, which appears in the expectation value.

In the semiclassical framework, the equations of motion for the matter field are expressed in the second quantization formalism. Following Bahrami et al. [9], we work in the Schrödinger picture, where the evolution of the Fock state $|\Psi\rangle \in \mathcal{F}(\mathcal{H})$ is governed by the Schrödinger equation. The Hamiltonian in the second quantization formalism is obtained by promoting the classical Hamiltonian to operator form, as in Section 2.3.3, and by including the interaction term $\hat{H}_{\rm int}$. In the Newtonian approximation, the latter involves the dominant component of the metric perturbation h_{00} and of the energy-momentum operator $\hat{T}_{00} \equiv mc^2\hat{\Psi}^\dagger\hat{\Psi}$. Given that the former is related to the solution of the Poisson equation, the interaction term reads:

$$\hat{H}_{\rm int} = -\frac{1}{2}\int d^3x\, h_{00}\hat{T}_{00} = -Gm^2\int d^3x \int d^3x' \frac{\langle\Psi|\hat{\Psi}^\dagger(\mathbf{x}')\hat{\Psi}(\mathbf{x}')|\Psi\rangle}{|\mathbf{x}-\mathbf{x}'|}\hat{\Psi}^\dagger(\mathbf{x})\hat{\Psi}(\mathbf{x})\,,$$

so that the equation of motion for the matter quantum state is expressed as:

$$\begin{aligned} i\hbar\frac{\partial}{\partial t}|\Psi\rangle = \Bigg[\int d^3x\hat{\Psi}^\dagger(\mathbf{x})\left(-\frac{\hbar^2}{2m}\Delta\right)\hat{\Psi}(\mathbf{x}) + \\ -Gm^2\int d^3x\int d^3x'\frac{\langle\Psi|\hat{\Psi}^\dagger(\mathbf{x}')\hat{\Psi}(\mathbf{x}')|\Psi\rangle}{|\mathbf{x}-\mathbf{x}'|}\hat{\Psi}^\dagger(\mathbf{x})\hat{\Psi}(\mathbf{x})\Bigg]|\Psi\rangle\,. \end{aligned}$$

Observe that due to the involvement of the state $|\Psi\rangle$ in the Poisson equation, the Schrödinger equation for the state $|\Psi\rangle$ in the Fock space is fundamentally nonlinear.

At this point, we impose the additional assumption that the energy is low enough to prevent variations in the number of particles. We can then restrict the full dynamics on the Fock space to the dynamics within a fixed N-particle sector, as described in Section 2.3.3. By substituting the expression (2.30) for the N-particle state $|\Psi^{(N)}\rangle$ of the Fock space, the expectation value in the interaction term becomes:

$$\langle\Psi^{(N)}|\hat{\Psi}^\dagger(\mathbf{x})\hat{\Psi}(\mathbf{x})|\Psi^{(N)}\rangle = \sum_{j=1}^{N}\int\prod_{i\neq j}d^3x_i\left|\psi^{(N)}(\mathbf{x}_1,\ldots,\mathbf{x}_{j-1},\mathbf{x},\mathbf{x}_{j+1},\ldots,\mathbf{x}_N)\right|^2$$

Using the same expression (2.30), the dynamics of $|\Psi^{(N)}\rangle$ reduces to that of the N-particle wave function $\psi^{(N)}(\mathbf{x}_1,\ldots,\mathbf{x}_N)$, and results in the N-body Schrödinger-Poisson equation:

$$i\hbar\frac{\partial}{\partial t}\psi^{(N)}(\mathbf{x}_1,\ldots,\mathbf{x}_N) = \left[-\sum_{j=1}^{N}\frac{\hbar^2}{2m}\Delta_j - Gm^2\sum_{j<k}^{N}\int\prod_{l=1}^{N}d^3x_l'\frac{|\psi^{(N)}(\mathbf{x}_1',\ldots,\mathbf{x}_N')|^2}{|\mathbf{x}_j-\mathbf{x}_k|}\right]\psi^{(N)}(\mathbf{x}_1,\ldots,\mathbf{x}_N)$$

In the one-particle case, the Schrödinger-Poisson equation we are studying in this thesis follows immediately.

2.4.4 Schrödinger-Poisson system from Quantum Gravity

Given that the Schrödinger-Poisson emerges as the Newtonian limit of the EKG equations both in the classical General Relativity and in Semiclassical Gravity, it is natural to wonder if the same occurs in the Quantum Gravity case. In this Section we investigate this topic, applying the same approaches and highlighting the differences with respect to the semiclassical case. The presentation follows the excellent work of Bahrami et al. [9].

As in the previous Section, we consider the case of an approximately flat spacetime, in which the metric is described by a perturbation of the Minkowski metric, $g_{\mu\nu} = \eta_{\mu\nu} + h_{\mu\nu}$, and in which linearized gravity holds in good approximation. Assuming that gravity is fundamentally described by a quantum theory, both the energy-momentum tensor $T_{\mu\nu}$ and the metric perturbation $h_{\mu\nu}$ are promoted to operators, $\hat{T}_{\mu\nu}$ and $\hat{h}_{\mu\nu}$. The classical Einstein field equations for linearized gravity, expressed in trace-reversed form as in (2.12), become:

$$\Box\hat{h}_{\mu\nu} = -16\pi G\left(\hat{T}_{\mu\nu} - \frac{1}{2}\eta_{\mu\nu}\hat{T}\right),$$

where $\hat{T} \equiv \eta^{\rho\sigma}\hat{T}_{\rho\sigma}$, and $\hat{h}_{\mu\nu}$ is now a linear quantum operator. In the Newtonian limit of a low-density slowly-evolving matter field, the Poisson equation can be obtained in complete analogy to the classical case (2.16):

$$\Delta\hat{V} = \frac{4\pi G}{c^2}\hat{\Psi}^\dagger\hat{\Psi}, \tag{2.33}$$

where the gravitational potential $\hat{V}$ is an operator, as well. Observe that, in contrast to the semiclassical case, the Poisson equation involves the creation and annihilation parts $\hat{\Psi}^\dagger$, $\hat{\Psi}$ of the matter field rather than the state $|\Psi\rangle$ of the system. This difference captures the core distinction between the semiclassical and the quantum approach, the former introducing an expectation value computed on the current state and the latter concerning solely the matter field components $\hat{\Psi}^\dagger$, $\hat{\Psi}$.

The equations of motion of the matter field are also expressed in the second quantization formalism. In the Schrödinger picture, the evolution of the Fock state $|\Psi\rangle \in \mathcal{F}(\mathcal{H})$ is still ruled by the Schrödinger equation, as in the semiclassical case. In this case, the interaction term $\hat{H}_{\text{int}}$ involves the dominant component of the metric in operator form $\hat{h}_{00}$, which is still related to the potential $\hat{V}$ solving the Poisson equation:

$$\hat{H}_{\text{int}} = -\frac{1}{2}\int d^3x\, \hat{h}_{00}\hat{T}_{00} = -Gm^2\int d^3x \int d^3x' \frac{\hat{\Psi}^\dagger(\mathbf{x}')\hat{\Psi}(\mathbf{x}')\hat{\Psi}^\dagger(\mathbf{x})\hat{\Psi}(\mathbf{x})}{|\mathbf{x}-\mathbf{x}'|}\,.$$

The equation of motion for the matter quantum state thus read:

$$i\hbar\frac{\partial}{\partial t}|\Psi\rangle = \left[\int d^3\mathbf{x}\,\hat{\Psi}^\dagger(\mathbf{x})\left(-\frac{\hbar^2}{2m}\Delta\right)\hat{\Psi}(\mathbf{x}) - Gm^2\int d^3\mathbf{x}\,d^3\mathbf{x}'\frac{\hat{\Psi}^\dagger(\mathbf{x}')\hat{\Psi}(\mathbf{x}')\hat{\Psi}^\dagger(\mathbf{x})\hat{\Psi}(\mathbf{x})}{|\mathbf{x}-\mathbf{x}'|}\right]|\Psi\rangle\,.$$

Observe that due to the absence of the state $|\Psi\rangle$ in the Poisson equation, the Schrödinger problem ruling the evolution of $|\Psi\rangle$ in the Fock state is fundamentally linear. In this, the Newtonian limit of the EKG equations in Quantum Gravity is profoundly different from its Semiclassical Gravity analogue, in which the non-linearity already appeared at this stage.

As in the semiclassical case, we proceed by assuming that the energy is sufficiently low to prevent variations of the number of particles. We can then restrict the full dynamics on the Fock space to the dynamics of a fixed N-particle sector, as we did in the previous Section. In this case, however, the different structure we have derived results in a different N-body Schrödinger equation:

$$i\hbar\frac{\partial}{\partial t}\psi^{(N)}(\mathbf{x}_1,\dots,\mathbf{x}_N) = \left[-\sum_{j=1}^{N}\frac{\hbar^2}{2m_j}\Delta_j - Gm^2\sum_{i<j}\frac{1}{|\hat{\mathbf{x}}_i-\hat{\mathbf{x}}_j|}\right]\psi^{(N)}(\mathbf{x}_1,\dots,\mathbf{x}_N), \tag{2.34}$$

The interaction term in the N-body problem is strongly different from that derived in the semiclassical equation: while there the N-particle density $\int d^3\mathbf{x}_1\dots d^3\mathbf{x}_N\,|\psi^N(\mathbf{x}_1,\dots,\mathbf{x}_N)|^2$ is included, involving the N-particle wave function $\psi^{(N)}(\mathbf{x}_1,\dots,\mathbf{x}_N)$ and thus making the equation non-linear, the interaction term in the quantum gravity case involves only the reciprocal distances between the particles, thus preventing self-interactions of the state $\psi^{(N)}(\mathbf{x}_1,\dots,\mathbf{x}_N)$. Thus, the N-body Schrödinger-Poisson problem in the Quantum Gravity scenario is still linear.

Since the dynamics can be observed on a fixed N-sector of the Fock space, we can work in a many-body perspective. This approach is very common, and paves the way for condensed matter approaches to the study of gravitational systems [20, 45, 109, 97].

Following this approach, we can consider the case of a large number of particles $N \to \infty$, all having the same mass m. As described by Bardos et al. [20] (see also [45, 109]), we can compute the mean-field limit of the N-body Schrödinger equation and obtain the non-linear Hartree equation:

$$i\hbar\frac{\partial}{\partial t}\psi(t,\mathbf{x}) = \left(-\frac{\hbar^2}{2m}\Delta - Gm^2\int d^3\mathbf{x}'\frac{|\psi(t,(\mathbf{x}'))|^2}{|\mathbf{x}-\mathbf{x}'|}\right)\psi(t,r), \tag{2.35}$$

which in the gravitational case is exactly the Schrödinger-Poisson equation.

In contrast to the semiclassical case, this derivation required taking a mean-field limit, so that the Schrödinger-Poisson equation in quantum gravity represents only an *effective* description of the system. Only at this point do the equations involve a non-linearity.

This observation represents a key point for supporters of the semiclassical gravity approach, and in particular for those studies that seek to explain wavefunction collapse through gravity, for which the emergence of non-linearity is necessary at a fundamental level and not only as an approximation of a fundamentally linear theory [9].

2.5 Scalar Field Dark Matter

Among the theories currently used to describe dark matter, one of the most widespread and promising is Scalar Field Dark Matter (SFDM) [73]. According to the SFDM model, dark matter consists of ultralight particles with masses in the range 10^{-24}–10^{-22} eV (10^{-57}–10^{-55} g), with zero spin and thus mathematically represented by a scalar field. This characteristic classifies them as bosons, and ensures that they can all be arranged in the same fundamental state at minimum energy, forming a Bose-Einstein condensate (BEC).

The characteristic scales of this theory are consistent with the formation of aggregates, whose structure is strongly linked to their quantum nature but whose dimensions are comparable with astrophysical scales. The ultralight nature of these particles, in fact, endows them with an enormous Compton wavelength [132], $\lambda_C \equiv h(mc)^{-1} \sim 10$ pc (with h the Planck constant, c the speed of light and m the particle mass)[1]. At the same time, their number density is estimated to be very high, resulting in a much shorter interparticle distance, of the order 10^{-13} cm [132]. Their wave functions therefore overlap heavily, allowing the formation of a condensed state in which they move collectively and form a coherent wave, with a de Broglie wavelength comparable to the galactic scale, $\lambda_B \sim 1$ kpc. The resulting single entity is rather heavy, so that the system is often assumed to be non-relativistic.

The SFDM model has aroused strong interest and has been developed simultaneously in multiple directions and with different variants. It is therefore known under various names, each highlighting slightly different aspects of the theory: ultralight DM, BEC DM, superfluid DM, fuzzy DM, quintessential DM, ultra-light axion (ULA), and wave/ψ-DM, among others [88, 105]. A complete treatment of the SFDM model can be found in excellent reviews, such as Ureña-López [141], Ferreira [49], Lee [88], Matos et al. [105] and Salucci [128].

In this work, we focus only on some key aspects of this theory, exploring the hypotheses from which it emerges and the consequences for the mathematical structure of the problem. In the remainder of this section, in Section 2.5.1 we briefly present the main features of scalar field models in astrophysics and cosmology, highlighting their connection with the theories of General Relativity and quantum field theory presented previously and showing the main elements that can vary within the model. Then we focus on their application to the galactic dark matter case, completing the overview. In Section 2.5.2, we address the heuristic description of the SFDM model: proceeding with our own personal reconstruction, we illustrate how a series of simple physical hypotheses lead to deducing the orders of magnitude of the fundamental scales of the system, naturally suggesting the parameters that govern its regime. In addition to recovering the scales of magnitude reported in the literature, we derive a characteristic length that allows writing the model in dimensionless form and gives a direct and elegant justification of the mathematical structure commonly used in many-body theories. A second parameter is derived, which incorporates information about the energetic regime of the system and which will play a key role in Chapter 5, in the definition of a relativistic extension of the SP model.

2.5.1 Scalar Field Models

The study of SFDM is based on a series of early works that since the 1960s have investigated the characteristics of scalar fields in astrophysical and cosmological contexts, not necessarily with reference to dark matter.

The foundations of this research were laid by Ruffini and Bonazzola [126], who first conducted a systematic study of systems of self-gravitating particles in the ground state, establishing the formal basis and studying their equilibrium configurations. In this work, the authors consider two possible scenarios: in the case of bosonic particles with spin 0, the matter field is of scalar type and satisfies a Klein-Gordon equation; while in the case of fermionic particles with spin 1/2 (which we do not treat in this thesis), the field is of spinorial type and satisfies a Dirac equation. In both cases, the dynamics is described according to a semiclassical approach, as described in Section 2.4: the matter field is described by a second-quantized free field, while the self-gravitating character is given by coupling

[1] 1pc $\sim$ 3.26 light-years is approximately the distance between the Sun and the nearest star, Proxima Centauri. Galaxy diameters typically range from 1 to 100 kpc.

with Einstein's field equation, with a source term given by the mean value of the energy-momentum tensor operator constructed from the matter field. The system is described by the coupled Einstein-Klein-Gordon equations in the bosonic case, and by Einstein-Dirac equations in the fermionic case.

The study by Ruffini and Bonazzola [126], and particularly the bosonic case, opened the way to a series of works that investigate the behavior of scalar fields in astrophysical and cosmological contexts. As well explained in Guzmán and Ureña López [66], there are two possible scenarios for aggregates of this type: real scalar fields, used for neutral particles, and complex scalar fields, which generalize to potentially charged particles. As already in Ruffini and Bonazzola [126], the fundamental equations are those of Einstein-Klein-Gordon, with an energy-momentum tensor that accounts for the real or complex nature of the field.

In both cases, spherically symmetric equilibrium configurations are studied, namely the nontrivial solutions of the spherically symmetric EKG system that are regular everywhere, asymptotically flat, and for which the scalar field is confined to a finite region. In the case of complex fields, these solutions are known as boson stars. Expressed in the form $\phi(r,t) = \psi(r)e^{-i\omega t}$, with $\psi(r)$ a real function and ω the fundamental frequency of the boson star, they result in metric functions that are time independent. Under appropriate assumptions of regularity and boundary conditions, they solve an eigenvalue problem, generally studied numerically. This is a much-studied model, including the non-spherically symmetric case. See Schunck and Mielke [131] for a comprehensive review and [98, 2, 123] for some more recent works.

In the case of real fields, it is not possible to construct stationary and regular solutions that make the metric time independent. The easiest alternative is therefore to Fourier expand the field and the metric and transfer the dynamics to the coefficients of this expansion. To avoid a system of infinite equations, a cut-off is generally introduced, neglecting modes that exceed a certain threshold. Solutions of this type, studied numerically under appropriate regularity and boundary conditions, are known as oscillatons. They are very similar in form to those obtained for complex fields, so the two cases show very similar properties [66].

The study of both types of scalar field can be specialized to the case of weak field, applying the Newtonian limit as described in 2.2.3. In this case, the solutions described above take the name of Newtonian boson stars and Newtonian oscillatons. Both are derived with a similar procedure, of post-Newtonian type. The only difference lies in the number of variables involved, which is greater in the case of oscillatons to account for the real nature of the field. In both cases, however, the fundamental dynamics is described by a Schrödinger-Poisson system, so that the properties of the two types of aggregate remain very similar even in the Newtonian limit.

Another variable element in the study of scalar fields is the type of potential assumed for the matter field [105]. As seen in Section 2.2.2, in addition to the gravitational potential that emerges from coupling with Einstein's equation, matter is generally subject to its own potential $V(\phi)$, which determines the type of self-interaction between particles. In the simplest case of a non-interacting field, it is of type $V(\phi) = \frac{1}{2}m^2\phi^2$. In more general cases, it could have other forms, which can be suggested by the physical theory assumed as the origin for the scalar field. In the case of dark matter, for which proposals on the origin span widely, we find, for example, the potential $V(\phi) = f\sin(b\phi)$ proposed for QCD axions, or $V(\phi) = A[\cosh(b\phi)-1]$ derived from superstring theory [105]. In general, it is physically reasonable to assume that the potential has a minimum around which it oscillates. In this case, the potential expanded around the minimum takes the form

$$V(\phi) = V_0 + \frac{1}{2}m^2\phi^2 + \frac{\lambda}{4}\phi^4 + \mathcal{O}(\phi^6)\,,$$

where the quadratic term is the contribution of the non-interacting field and $(\lambda/4)\phi^4$ is the first correction for a weakly interacting field. A potential of this type is the simplest solution for studying a self-interacting field, a type of system of wide interest [89, 67, 31, 36].

Scalar Fields: a Cosmological Point of View

The effective equations derived for Newtonian scalar fields are appropriate on astrophysical scales (up to about ~ 10 Mpc) in which isolated clusters of matter are studied. However, on cosmological scales (beyond ~ 100 Mpc), matter is typically seen as a single aggregate described by a homogeneous and isotropic fluid, an assumption known as Cosmological Principle. In this fluid, small almost-Gaussian initial perturbations grow through merging to create complex structures, originating all the objects seen in the Universe. As shown in Schaller et al. [129], the fluid is typically described by a phase space density distribution $f(x,v,t)$, representing how matter is distributed in space, velocity and time. The spatial density is obtained by integrating over velocity, $\rho(x,t) = \int f(x,v,t)\,\mathrm{d}^3v$, and perturbations

are defined by subtracting from it the average density, $\delta\rho(x,t) = \rho(x,t) - \bar{\rho}(t)$. Following the Liouville theorem and assuming that the only relevant force is the gravitational potential $\phi(x)$, the appropriate dynamics for the fluid is given by the Vlasov-Poisson system:

$$\begin{cases} \frac{\partial f}{\partial \tau} + \frac{v}{a(\tau)}\frac{\partial f}{\partial x} - a(\tau)\nabla\phi\frac{\partial f}{\partial v} = 0 \\ \Delta\phi = 4\pi G a^2(\tau)\delta\rho \end{cases},$$

where G is the gravitational constant, x, v are comoving coordinates and velocities, τ is the conformal time and $a(\tau)$ is the cosmic scale factor that encodes the mean expansion of the Universe and is subject to the Friedmann equation [121, 129].

Exact solutions to the Vlasov-Poisson system are extremely difficult to compute, mainly because of the high dimensionality of the phase space, involving both space and velocity. To handle this problem, the standard strategy consists in defining a parallelism with quantum dynamics, in which a single wave function $\psi(x,t)$, independent of velocity, collects all the information [129, 145]. This parallelism is set through the Wigner distribution function

$$f(x,v) \simeq \int e^{i\frac{vy}{\hbar}} \psi^* \left(x + \frac{y}{2}\right) \psi \left(x - \frac{y}{2}\right) \mathrm{d}^3 y \,,$$

which maps the Vlasov-Poisson dynamics in a Schrödinger-Poisson dynamics. To ensure the original complexity of the distribution function is not lost during the transformation, a whole set of wavefunctions $\{\psi_n(x,t)\}_n$ is often used, leading to the many-body Schrödinger-Poisson problem:

$$\begin{cases} i\hbar\partial_\tau\psi_n = -\frac{\hbar}{2a^2(\tau)}\Delta\psi_n + \phi\psi_n \\ \Delta\phi \quad\;\; = 4\pi G\delta\rho \end{cases}.$$

Observe that, in a cosmological context, the parallelism with quantum mechanics is merely intended as a mathematical trick to solve the "true" classical Vlasov-Poisson system. The $\hbar$ constant is intended as a numerical parameter, not related to the Planck constant, while the wavefunction is interpreted in a purely classical manner, as a matter distribution [129].

This numerical approach recovers the Schrödinger-Poisson problem even on cosmological scales. Two relevant differences compared to the astronomical SP problem are worth noting. First, the expansion of the universe is taken into account through the cosmic scale factor $a(\tau)$. Second, only perturbations of the density generate gravitational potential, so that a background term needs to be subtracted from the density on the right-hand side of the Poisson equations [129]. These variations are essential to study large-scale structures (beyond ~ 100 Mpc). However, they can be safely neglected on astrophysical scales (up to about ~ 10 Mpc), which will be the main focus of this thesis.

We conclude the overview on the use of SP in cosmology with one final comment. While the SP system is considered a useful approximation of the Vlasov-Poisson problem, in some situation an alternative formulation is preferred, to remark the fluid-like nature of the system. This fluid description is obtained by applying the Madelung transformation to the SP problem. Setting $\psi \equiv \sqrt{\rho}e^{iS}$ the complex matter field ψ is expressed in terms of the real density field $\rho \equiv |\psi|^2$ and of the real action or phase function S, whose gradient defines the bulk velocity $v \equiv \nabla S$. In terms of the hydrodynamic variables ρ and v, the complex Schrödinger equation corresponds to the real continuity and Euler equations of a quantum hydrodynamic fluid, so that the Schrödinger-Poisson system becomes:

$$\begin{cases} \partial_t\rho + \nabla\cdot(\rho\vec{v}) = 0 \\ \partial_t\vec{v} + (\vec{v}\cdot\nabla)\vec{v} = -\nabla\phi - \frac{1}{2}\nabla\left(\frac{\Delta\sqrt{\rho}}{\sqrt{\rho}}\right) \\ \Delta\phi = \rho \end{cases}.$$

This type of description is widely used for cosmological simulations and structure formation studies [28, 38, 50, 139].

Scalar Field models for Dark Matter

The idea of using scalar fields as a model for dark matter dates back to Baldeschi et al. [11], who first compared models for self-gravitating particle systems, bosonic or fermionic, with galactic scales, deriving an estimate of the single particle mass between 10^{-24} eV and 10 eV in the bosonic case.

Sin [132] first proposed a direct comparison with experimental rotation curves, suggesting the use of excited states of SP rather than the ground state to reproduce the experimentally observed

plateau. The same study was extended to account for the presence of baryonic matter in galaxies [78] and to include the possibility of self-interactions [89], with potential in the form $V(\phi) = \lambda\phi^4/4$. Similar studies were also developed independently by Guzmán and Matos [69].

In the same years, the study of the SP system emerging from the SFDM assumption was also advanced using numerical techniques. Widrow and Kaiser [145] first used the SP model to numerically approximate the Vlasov equation for a collisionless fluid, showing the possible formation of aggregate structures. Later, Guzmán and his collaborators dedicated a series of works [65, 66, 67] to the study of numerical stability of the stationary states of the SP system, in view of their application to the dark matter problem. They found that the ground state or zero-node configuration is intrinsically stable, while the excited states are unstable and tend to collapse to the ground state by emitting scalar matter. The latter process, called gravitational cooling, is so efficient as to allow any initial configuration to decay into a zero-node Newtonian scalar soliton. While for large objects this gravitational cooling is long enough to explain the existence of galaxy clusters, for smaller masses it is too short to explain the shape of galaxies. This result discouraged the use of single excited stationary states as descriptions of galactic dark matter halos and led to modified versions of the SP model, including for example rotational effects or combining the ground and the excited state into multimodal configurations [140, 68, 3]. Other studies also accounted for temperature effects [122] or random potentials [70]. With these modifications, stability is generally improved, providing a more reliable description of galactic halos.

Another important development in dark matter modeling on galactic scales is represented by three-dimensional numerical simulations. Schive et al. [130] first proposed simulations of this type for the SP model, performing them at an unprecedentedly high resolution. These and other subsequent simulations, see [105] and references therein, have clarified the processes of structure formation on galactic scales, showing how matter tends to aggregate into core-tail halos, namely distributions characterized by a flat, oscillating core surrounded by an envelope of highly energetic granular structures, which continuously fluctuate in density and velocity. From these works effective models are built to describe matter density distributions averaged over time or solid angle. Models of this type are often heuristic and include the ground state of SP as the core, combined with density profiles defined on-demand for the halo [80, 19, 24].

2.5.2 Heuristic Analysis of Scalar Field Dark Matter

In this section, we analyze the underlying assumptions of the SFDM model on galactic scales, retracing the heuristic steps that led to its definition [11, 132, 89]. We proceed by gradually imposing a set of physical hypotheses, showing how they naturally define the characteristic dimensions of the model, such as the ultralight mass or the large particle number.

The object of our description is a gas of quantum particles that attract each other gravitationally, forming an aggregate. Let R be the average extension of the aggregate, ℓ the average interparticle distance, N the total number of particles, m the mass of each particle, and p its momentum. In view of giving a rough, order-of-magnitude estimate of the characteristic dimensions of the problem, we can think of the aggregate as a sphere of radius R and the average volume of each particle as a sphere of radius ℓ. The total volume of the particles must coincide with the volume of the aggregate, $N\ell^3 \sim R^3$, namely:

$$\ell \sim \frac{R}{N^{1/3}}\,. \tag{2.36}$$

The first assumption we make is that the gas is virialized, meaning that the kinetic and potential energies are comparable on average over time. This assumption is natural for stable aggregates, in which the dispersive effect of kinetic energy is balanced by the collapse effect due to potential energy, resulting in an object of approximately stable dimensions. For simplicity, in view of an order-of-magnitude argument, we omit temporal averages, assuming that the current state of the system is approximately equal to its mean state. Equating the total kinetic energy Np^2m^{-1} and the potential energy $G(Nm)^2R^{-1}$, we obtain:

$$N\frac{p^2}{m} \sim G\frac{(Nm)^2}{R}\,. \tag{2.37}$$

The second assumption is that the gas is made of quantum particles. Each particle is described by a wave function with characteristic wavelength λ, which is related to the particle's momentum p

through the de Broglie relation:

$$p \sim \frac{\hbar}{\lambda} \,. \tag{2.38}$$

We then assume that the wave functions of individual particles overlap, forming an aggregate state known as Bose-Einstein condensate. This assumption provides the wavelength with a lower bound – it must be greater than the interparticle distance to allow overlap; and an upper bound – in the case of completely overlapping wave functions, their wavelength equals the radius of the aggregate:

$$\ell \lesssim \lambda \lesssim R \,. \tag{2.39}$$

In particular, for a completely condensed gas with $\lambda \sim R$ the above relationships (2.37) and (2.38) can be combined to obtain

$$R \sim \frac{\hbar^2}{m^3 G N} = \frac{\ell_P}{N} \left(\frac{m_P}{m}\right)^3 , \tag{2.40}$$

with $\ell_P \equiv \sqrt{\hbar G c^{-3}}$ and $m_P \equiv \sqrt{\hbar c G^{-1}}$ the Planck length and mass, respectively. Thus, the characteristic radius of a virialized self-gravitating boson gas that forms a complete condensate depends only on the number of particles N and on the mass m of the single gas particle.

In the same spirit, we can compute the kinetic energy for the complete condensate to understand whether it is compatible with a classical regime or requires a relativistic treatment. The relativistic energy of a free particle is computed through the relativistic dispersion relation:

$$K = \sqrt{p^2c^2 + m^2c^4} = mc^2 \left(1 + \frac{1}{2}\frac{p^2}{m^2c^2} + \mathcal{O}\left(\frac{p^4}{m^4c^4}\right)\right) = mc^2 + \frac{1}{2}\frac{p^2}{m} + \mathcal{O}\left(\frac{p^4}{m^3c^2}\right) .$$

where mc^2 is the rest mass – a constant that does not affect the classical theory – while $p^2/(2m)$ is the classical kinetic energy. This expression is derived by expanding the kinetic energy in terms of $\varepsilon \equiv p^2(mc)^{-2}$ assumed small, $\varepsilon \ll 1$. Based again on the hypothesis of complete condensation $\lambda \sim R$ and on the relationships (2.37) and (2.38), this quantity is expressed as:

$$\varepsilon \equiv \frac{p^2}{m^2c^2} \overset{(2.38)}{\sim} \frac{\hbar^2}{R^2m^2c^2} \overset{(2.40)}{\sim} \frac{\hbar^2}{m^2c^2} \left(\frac{m^3GN}{\hbar^2}\right)^2 = N^2 \left(\frac{m}{m_P}\right)^4 \tag{2.41}$$

The parameter ε ruling the energy regime of the condensate – classical for $\varepsilon \ll 1$ and relativistic otherwise – does therefore depend only on the number of particles N and on the mass m of the single gas particle, in a way similar to the characteristic radius R (2.40).

Up to now, the assumptions concern a generic condensate, without specifying the physical problem under consideration. As a final hypothesis, we specialize to the galactic scale, assuming that the aggregate has characteristic dimensions such as to explain the inconsistencies in the rotation curves. Recall that rotation curves are obtained by measuring the velocity v with which a test object orbits around the galaxy at a distance r from its center. We can apply the virial theorem, equating, on temporal average, the kinetic energy of the test object and the potential energy that attracts it toward the center of the galaxy:

$$\langle v^2 \rangle = \left\langle G\,\frac{M(r)}{r} \right\rangle ,$$

where $M(r)$ represents the mass contained in a sphere of radius r, whose gravitational action maintains the test object in orbit. In the case of nearly circular orbits, the time average can be removed, and the relation holds robustly. We finally assume that the dark matter aggregate we are describing is solely responsible for the rotation velocity of the test object, and we neglect, in an order-of-magnitude approach, the effect of baryonic matter. At a distance $r \sim R$, which encompasses the entire mass of the aggregate $M(R) = Nm$, the expression for the velocity $V \equiv v(R)$ reduces to:

$$V^2 \sim G\,\frac{Nm}{R} \,. \tag{2.42}$$

We now combine all the assumptions in the galactic-scale case. They consist of four equations (2.36), (2.37), (2.38) and (2.42) plus the bounds (2.39), and they involve five unknowns ℓ, N, m, p and λ, plus two parameters R, V that can be estimated from experimental rotation curves. We first

elaborate on them to express the bounds (2.39) in terms of the particle mass m, and then specialize to a limiting case to derive explicit estimates of the quantities involved.

The virial relation (2.37) can be combined with the de Broglie relation (2.38) – letting the wavelength λ appear instead of p; and with the assumption on galactic scales (2.42) – letting the rotation curve dimensions V, R appear instead of N. The result is a relation between the condensate parameters λ and m, involving the velocity V as an experimental parameter:

$$\lambda \sim \frac{\hbar}{Vm}\,.$$

Using this relation, the upper bound in (2.39) on λ can be expressed in terms of m:

$$m \gtrsim \frac{\hbar}{VR}\,. \tag{2.43}$$

The lower bound in (2.39) can analogously be expressed in terms of m using the same expression for λ and the geometric consideration (2.36) to eliminate ℓ, combined with the assumption on galactic scales (2.42) to further eliminate N. The result is:

$$m^4 \lesssim \frac{\hbar^3}{GVR^2}\,. \tag{2.44}$$

Recalling that the orders of magnitude of the experimental parameters are $R \sim 10 \div 100$ kpc and $V \sim 100$ km/s, the bounds on the particle mass (2.43) and (2.44) read:

$$10^{-24} \div 10^{-23}\ \mathrm{eV} \lesssim m \lesssim 10 \div 10^{\,\mathrm{eV}}\,.$$

Let us finally specialize to the case – rather common in the literature – of complete condensation, in which the wavelength λ coincides with the extent of the aggregate R. Under this assumption, all characteristic quantities can be estimated, following the relations (2.36), (2.37), (2.38) and (2.42):

$$m \sim \frac{\hbar}{VR} \simeq 10^{-24} \div 10^{-23}\ \mathrm{eV}\ \ (\simeq 10^{-57} \div 10^{-56}\ \mathrm{g})\,, \tag{2.45a}$$

$$N \sim \frac{V^3R^2}{G\hbar} \simeq 10^{100} \div 10^{102}\,, \tag{2.45b}$$

$$\lambda \sim R \simeq 10 \div 100\ \mathrm{kpc}\,, \tag{2.45c}$$

$$p \sim \frac{\hbar}{R} \simeq 10^{-29} \div 10^{-28}\ \mathrm{eV/c}\,, \tag{2.45d}$$

$$\ell \sim \frac{R}{N^{1/3}} \simeq 10^{-11}\ \mathrm{cm}\,, \tag{2.45e}$$

$$\varepsilon \sim N^2 \left(\frac{m}{m_P}\right)^4 \simeq 10^{-4} \tag{2.45f}$$

Observe that the resulting estimate for the total dark matter mass $mN \sim 10^{44} \div 10^{45}$ g has an order of magnitude comparable to and slightly larger than that of the total baryonic matter, which is about $10^9 \div 10^{12} M_\odot \simeq 10^{42} \div 10^{45} g$. This is consistent with the hypothesis that dark matter is the dominant attractor of an orbiting test object, which led to the relation (2.37).

In addition, the parameter ε is actually small, $\varepsilon \sim 10^{-4} \ll 1$, confirming that the complete condensate compatible with the galactic scales has a classical rather than a relativistic behavior.

Heuristic analysis and the N-body problem

In Section 2.4.4 we have shown how dynamics for the matter field in second quantization can be reduced, in the low-energy limit, to dynamics on the N-particle sector. In this space, a generic N-body Hamiltonian dynamics with pairwise interactions is described by a Hamiltonian of the type:

$$H_N = \sum_{j=1}^{N} T_j + \frac{1}{N} \sum_{1 \le k < l \le N} W_{kl}$$

with T_j the kinetic energy of the j-th particle and W_{kl} the potential acting on the pair (k, l) of particles [97]. The $1/N$ parameter is necessary to ensure that the scaling with N of the total kinetic energy is comparable to that of the total potential energy, which would grow as N^2. With the

prefactor $1/N$, the two energies scale with N in the same way, and the dispersive effect of the kinetic energy balances the interaction effect of the potential energy, ensuring that the system can assume, on average, stable configurations. While its presence is formally necessary, its physical meaning is rather counterintuitive, since there is no apparent reason for which the potential energy between two particles should scale as $1/N$.

In the case of the Schrödinger-Poisson problem discussed in this thesis, the presence of this parameter naturally results from rescaling the physical problem to the corresponding non-dimensional problem, using the scaling given by the characteristic dimensions derived from the heuristic analysis.

Consider the Hamiltonian of the N-body Schrödinger-Poisson problem (2.34), expressed in physical units:

$$H_N = \sum_{j=1}^{N} \left(-\frac{\hbar^2 \Delta_{x_j}}{2m} \right) - G \sum_{1 \le k < l \le N} \frac{m^2}{|x_k - x_l|} \, .$$

The associated dynamics is given by the Schrödinger equation $i\hbar \partial_t \psi^{(N)} = H_N \psi^{(N)}$ or, for stationary states of the form $\psi^{(N)} = e^{-iEt/\hbar}\Phi(x)$, by the time-independent Schrödinger equation $H_N \Phi = E\Phi$. Consider the latter case for simplicity, although the procedure holds in both cases.

In order to rescale the problem to non-dimensional form, let us introduce the change of variables $x_j = R y_j$ for all space coordinates $j = 1, \dots, N$, while a rescaling to the non-dimensional field ϕ does not affect the problem by linearity. It results:

$$\left[-\sum_{j=1}^{N} \frac{\hbar^2 \Delta_{y_j}}{2mR^2} - \frac{G}{R} \sum_{1 \le k < l \le N} \frac{m^2}{|y_k - y_j|} \right] \phi = E\phi \, .$$

The kinetic energy is naturally proportional to R^{-2}, while the gravitational energy is a homogeneous function of degree -1 in R, and therefore is proportional to R^{-1}.

Assuming that our system is a virialized and completely condensed boson gas, our heuristic analysis provides a natural estimate of the characteristic length R to be used, that is, equation (2.40). With this scale factor, the non-dimensional problem becomes:

$$\left[-\sum_{j=1}^{N} \frac{\Delta_{y_j}}{2} - \frac{1}{N} \sum_{1 \le k < l \le N} \frac{1}{|y_k - y_j|} \right] \phi = \mathcal{E}\phi \, ,$$

with $\mathcal{E} \equiv EmR^2/\hbar^2$. In this form, the factor $1/N$ emerges naturally, and the problem is written in a familiar non-dimensional form [97]. This occurrence is not accidental, but rather derives from the fact that the characteristic length R (2.40) was obtained precisely by requiring the system to be virialized, that is, the kinetic and potential energies of the system balance on average. In other words, the reasoning simply demonstrates how the idea of energetic equilibrium of a system (in the virial sense) can be incorporated through an appropriate rescaling, which leads straightforwardly to the desired non-dimensional formulation and to the necessary $1/N$ prefactor. This role of the characteristic length R (2.40) highlights its importance in the study of dynamics, as a bridge between the intrinsic mathematical structure of the problem and its physical origin, which is encoded in R in the form of the characteristic parameters N, m.

Complete condensate hypothesis and experimental rotation curves

Estimates (2.45) are derived under the assumption of complete condensation of the aggregated gas and yield a prediction of the mass m of individual particles that depends exclusively on the values R and V. The latter – representing respectively the mean size of the aggregate and the rotation velocity of a test object at distance R from the galactic center – are assumed to be known experimentally. If the dark matter particle has a unique nature and uniformly has mass m, then the prediction in (2.45) should yield approximately the same result across the galaxies, namely the product VR should be nearly constant. This hypothesis could be tested experimentally.

Drawing from a sufficiently large database of rotation curves, one could extract the values R_i and V_i for each i-th curve and create a sample of estimates $\{m_i = \hbar (V_i R_i)^{-1}\}_{i=1}^{N_{\text{gal}}}$, where N_{gal} is the number of galaxies. Expecting a constant value, we could create a histogram with these values and observe whether the resulting distribution is indeed peaked around a mass value consistent with the estimate in (2.45). Alternatively, the hypothesis of a constant product $R_i V_i$ could be tested by

linearly fitting the log-log plot of the values $\{R_i, V_i\}_{i=1}^{N_{\rm gal}}$, checking the agreement with the prediction in (2.45).

Although large databases of rotation curves are available, such as the SPARC database [94], rotation curves are generally incomplete and do not reach the expected Keplerian decline for distances beyond the extension R of the galactic halo. If this part of the curve were visible, one could unambiguously extract the desired values V_i and R_i and construct the aforementioned histogram. In the absence of this information, however, the treatment becomes rather approximate.

We nevertheless report an example histogram, solely as a placeholder pending more accurate experimental data on which to perform the analysis.

To construct an approximate histogram, we consider the rotation curves tabulated in the SPARC database [94]. As described more thoroughly in Chapter 4, these curves exhibit approximately linear behavior at intermediate radii, before a final Keplerian decline – often not reached by the measurements – which should begin precisely at the radius R_i we seek. A linear fit to the experimental data points in an arbitrary region $[0.2R_{{\rm obs},i}, 0.8R_{{\rm obs},i}]$ of the measurement domain $R_{{\rm obs},i}$ provides an approximate estimate of the relationship between the quantities V_i and R_i that we wish to estimate. Once the value R_i is defined, the estimate of V_i is obtained as the corresponding value at R_i in the linear fit.

The problem thus reduces to estimating R_i. Since it is impossible to predict where the Keplerian decline will begin, we can only assume that R_i is proportional to the measurement domain $R_{{\rm obs},i}$, and use the latter as reference data. The resulting histogram is illustrated in Figure 2.1a. A tentative relationship $V_i(R_i)$ across different galaxies is also illustrated in Figure 2.1b. The latter suggests that the constant quantity is not the product V_iR_i, but rather (roughly) the quantity $V_iR_i^{-1/2}$. While far from thorough, such results indicate that further analysis on this topic – combining analytical, heuristic and experimental considerations – might still yield relevant novel information.

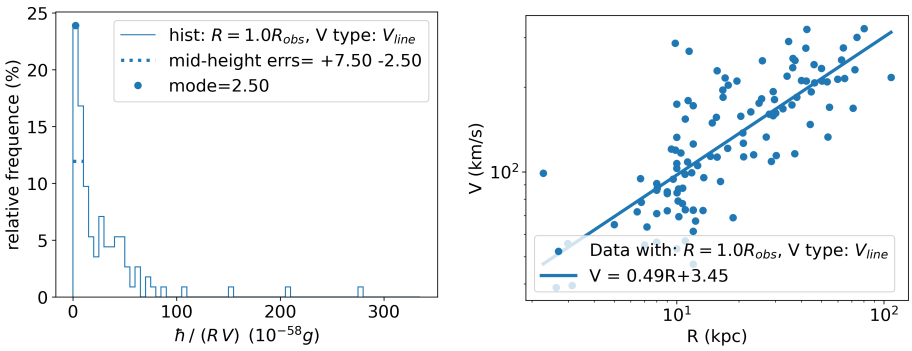

(a) Histogram. (b) $V_i(R_i)$ log-log plot.

Figure 2.1: Histogram of the dataset $\{m_i = \hbar(V_iR_i)^{-1}\}_{i=1}^{N_{\rm gal}}$ (left) and log-log plot of the $V_i(R_i)$ relationship (right). Data are derived from the SPARC database [94].

Chapter 3

Numerical simulation of excited stationary states

3.1 Introduction

Stationary states represent one of the main features characterizing a dynamical system, and analyzing their existence and uniqueness, their stability properties and their behavior is fundamental to gain a complete understanding of the system, particularly in view of physical applications.

In the Schrödinger-Poisson case, the wide popularity of the system led to a conspicuous series of works exploring the analytical and numerical properties of its stationary states. Most of these studies focus on spherically symmetric stationary states, which are known to comprise an infinite, discrete family of solutions ranged by an excitation index n. Although many of their properties have been discussed, as we review in Section 3.1.1, a complete understanding of their mathematical structure has not yet been achieved. Indeed, no analytic expressions currently exist for these stationary states, which are therefore mainly known through numerical simulations and asymptotic estimates. The aim of this chapter is to present a rigorous characterization of their structure, based on numerically derived heuristic laws that describe how their main properties scale with the excitation index n.

In view of the physical application to the problem of galactic dark matter distributions, we extend the analysis of scaling behaviors to the eigenvelocities, namely the theoretical counterparts in the Schrödinger-Poisson model of experimental rotation curves. This characterization provides a more refined understanding of the mathematical structure of the problem and facilitates comparison with physical intuitions and expectations. More specifically, as will be described in Chapter 4, the heuristic laws we provide can then be straightforwardly compared to the observed features they predict, promoting the identification of optimal values for the free parameters of the model.

The connection between the matter field and the potential in the stationary states is further explored through a formal analogy with the WKB approximation, usually applied to linear problems. Although purely numerical, the formal comparison we conduct shows that the WKB approach provides a good approximation of our numerically simulated stationary states, suggesting that further analytical investigations in this direction might be promising.

In order for the study to be more effective in modeling physical problems, we include simulations of the stationary states in presence of external gravitational sources, which in the case of galactic dark matter distributions account for the baryonic mass components.

Observe that, while our analysis is mainly oriented to the application of excited Schrödinger-Poisson stationary states as models for galactic dark matter distributions, their role in this context has been gradually reconsidered, favoring their combination with other more complex features. Although we do not delve into these variations of the model, in Section 3.1.2 we discuss this point, presenting the main concerns on the application of the excited stationary states and their current role in constructing predictive models.

In the remaining part of this preamble, we briefly define the stationary states, revising the relevant literature and summarizing our main results (Section 3.1.1); then, we discuss the motivation supporting excited Schrödinger-Poisson stationary states as models for galactic dark matter distributions, specifying their role in the current literature (Section 3.1.2). In addition to this preamble, this chapter includes four sections: in Section 3.2 we present the numerical implementation of the stationary Schrödinger-Poisson problem, through which we simulated stationary states up to high excitations;

Section **??** collects the heuristic laws characterizing the scaling with the excitation index n of the stationary states; Section 3.3 presents the formal analogy with the WKB approach; while Section **??** explores the excited stationary states behavior in presence of external gravitational sources.

3.1.1 Excited stationary states: structure and literature comparison

The form in which stationary solutions of a dynamical system are expressed depends on the specific features of the problem. As mentioned in Chapter 1, the gauge invariance in the Schrödinger-Poisson equations suggests that the stationary states should include an oscillating phase, so we express them in the form $(e^{i\varepsilon t} f(x), \phi(x))$, with ε representing the associated energy parameter. Without loss of generality, the spatial component $f(x)$ of the matter field can be assumed real. Moreover, we focus on states with a unitary matter field L^2-norm, thus fixing the degree of freedom arising from the scaling invariance (1.6).

The stationary Schrödinger-Poisson problem with unitary norm condition, reported here for ease of reference, reads:

$$\begin{cases} \triangle f(x) = (\varepsilon + 2\phi(x)) f(x) \\ \triangle \phi(x) = f^2(x) \\ \int_{\mathbb{R}^3} f^2(x)\, \mathrm{d}^3x = 1 \end{cases} . \tag{3.1}$$

Solving the Poisson equation and substituting in the equation for $f(x)$ results in:

$$\begin{cases} \triangle f(x) + \dfrac{1}{2\pi} \left(\displaystyle\int_{\mathbb{R}^3} \frac{f^2(y)}{|x-y|}\, \mathrm{d}^3y \right) f(x) = \varepsilon f(x) & \text{(3.2a)} \\ \phi(x) = -\dfrac{1}{4\pi} \displaystyle\int_{\mathbb{R}^3} \frac{f^2(y)}{|x-y|}\, \mathrm{d}^3y & \text{(3.2b)} \\ \displaystyle\int_{\mathbb{R}^3} f^2(x)\, \mathrm{d}^3x = 1 & \text{(3.2c)} \end{cases} .$$

where the Choquard equation (3.2a) is a nonlinear eigenvalue problem, with ε representing the eigenvalue, $f(x)$ the eigenfunction, and where the nonlinearity is due to the coupling with the Poisson equation. The associated potential $\phi(x)$, defined by (3.2c), will be referred to as the eigenpotential.

In this thesis we focus on the spherically symmetric stationary states of the Schrödinger-Poisson problem, for which there exists an infinite discrete family of solutions $\{\varepsilon_n,\, f_n(r),\, \phi_n(r)\}_{n=0}^{\infty}$ with excitation index $n \in \mathbb{N}$ [100, 101]. An example of such eigenstate - including an associated velocity profile $v_n(r)$ to be defined below in a dedicated paragraph - is reported in figure 3.1 for $n = 8$.

Comparison with literature and results - eigenfunctions

Pioneering work on the stationary Schrödinger-Poisson problem (3.2) was conducted by Lieb [100], who established the well-posedness of the ground state, and Lions [101], who first proved that problem (3.2) admits an infinite discrete family of spherically symmetric solutions $\{\varepsilon_n,\, f_n(r),\, \phi_n(r)\}_{n=0}^{\infty}$, with excitation index $n \in \mathbb{N}$. These eigenstates, which represent the main focus of this chapter, have been widely studied in the later literature. Bernstein et al. [25], Moroz et al. [112], Harrison et al. [71] performed valuable numerical investigations of low-excitation states ($n \lesssim 15$), providing significant qualitative insights into the eigenfunction properties. They showed that the eigenfunctions display oscillatory behavior, featuring n nodes and $n+1$ local extrema of alternating sign with diminishing amplitudes, monotonically decaying to zero beyond the last oscillation. An example of simulated eigenstate for $n = 8$ is reported in figure 3.1.

Subsequent work provided partial analytical support for these numerical observations. Tod and Moroz [136] demonstrated the smoothness and boundedness of the eigenfunctions, while Tod [135], focused on the construction of bounds, proving that all eigenvalues are negative[1]. Greiner and Wunner [58] established connections with quantum defect theory and Kiessling [82] investigated the long-range behavior of the eigenfunctions.

However, due to the difficulties in handling the nonlinearity, no exact analytical expression for the eigenfunction has been derived yet. To overcome this issue in the practical application of the model, ad hoc density functions such as $\rho(r) = \sin(r) r^{-1}$ were proposed as alternatives to $|\psi(t,x)|^2$ [105, 29]. While these approximations are widely adopted in physical applications, they are inadequate

[1] We use a different sign convention, so in our presentation all eigenvalues are positive.

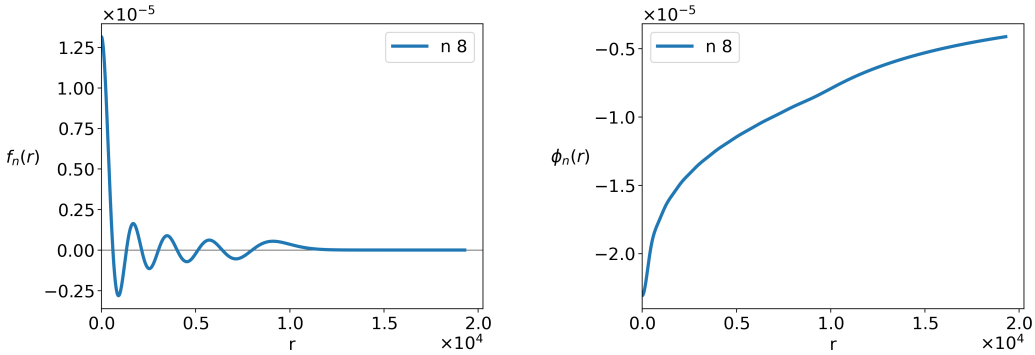

(a) Eigenfunction $f_8(r)$.

(b) Eigenpotential $\phi_8(r)$.

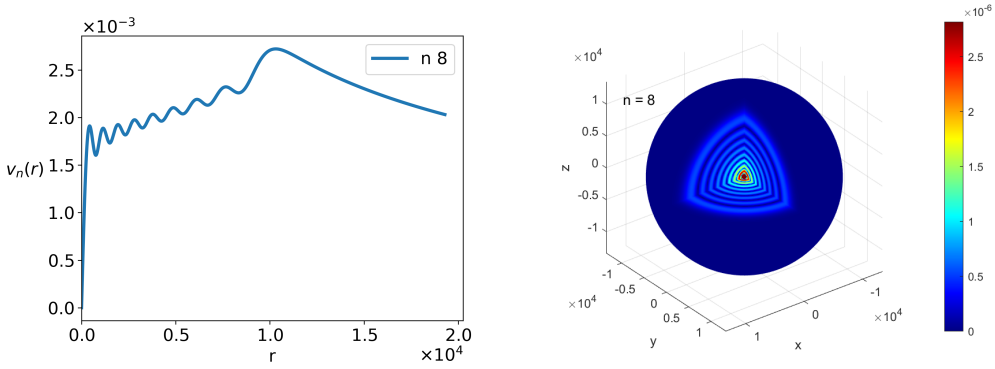

(c) Eigenvelocity $v_8(r)$.

(d) Three-dimensional section of $|f_8(r)|$.

Figure 3.1: Example of spherically symmetric eigenstate $(f_n(r), \phi_n(r), v_n(r))$ for $n = 8$, including: the eigenfunction $f_8(r)$ (top left panel), the eigenpotential $\phi_8(r)$ (top right panel), the eigenvelocity $v_8(r)$ (bottom left panel) and a three-dimensional section of the matter distribution (bottom right panel). For visualization purposes, in the three-dimensional figure the modulus $|f_8|(r)$ is shown rather than the actual predicted matter density $|f_8|^2(r)$. The structure exhibits 9 shells of decreasing density separated by 8 voids (shown in dark blue).

to capture both the irregular nodal spacing and the precise power law decay of the eigenfunctions, highlighting the need for deeper structural understanding. More generally, a comprehensive analysis of how the properties of the eigenstates scale with the excitation index n remains lacking. To address this gap, we propose quantitative heuristic laws derived from numerical simulations of highly excited stationary states ($n \leq 80$), with the aim of providing foundations for future analytical and physical studies. Specifically, we analyze the structure of the eigenfunctions characterizing them as oscillatory functions modulated by a power law. The radial position of the last oscillation, which approximately defines the eigenfunction support, exhibits a clear parabolic dependence on n, characteristic of Keplerian problems like the Bohr model for the hydrogen atom (see e.g. [59]). The spacing between adjacent nodes increases with the radial position, following a consistent pattern across increasing n values – showing modest increases at small radii and more pronounced increases at larger radii. This behavior constitutes a key correction to the $\sin(r)r^{-1}$ approximation, which fails to account for irregular nodal spacing. Finally, the power law governing amplitude modulation is characterized by fitting local extrema at small radial positions, with deviations observed near the last extremum. The power law exponent approaches -1 asymptotically as n increases, recovering the r^{-1} approximation in the large n limit.

Comparison with literature and results - eigenvelocities

Given a predicted matter density distribution $f_n^2(r)$, one can calculate the tangential velocity of a test object in circular orbit at radius r from the distribution's center. This calculation assumes that

velocity is determined by the gravitational force exerted by matter within a sphere of radius r:

$$v_n(r) = \sqrt{\frac{\int_0^r f_n^2(s)s^2 ds}{r}}\,. \tag{3.3}$$

This type of prediction is typical of galactic dark matter models, as in this context it can be compared with experimental rotation curves of spiral galaxies [132, 94, 80, 70, 64, 26], providing both model validation and deeper physical insights into the problem. In this framework, observed rotation curves typically show mid-range oscillatory behavior with an approximately linear trend, forming a plateau. This plateau generally exhibits a near-flat slope, although both positive and negative slopes have also been documented (see e.g. [124, 133, 94]). Moreover, physical intuition suggests that galactic-scale dark matter clusters, which are responsible for these rotation curves, might exhibit some kind of universal behavior [125, 33], possibly in an average sense [3]. Sin [132] first noted that the key features displayed by the eigenvelocities in the Schrödinger-Poisson model align well with these physical observations, especially when taking into account the presence of a baryonic bulge [78].

Building on the work by Sin [132] and Ji and Sin [78], in this chapter we provide numerical simulations for the eigenvelocities (3.3) associated with the Schrödinger-Poisson eigenstates $\{f_n(r), \phi_n(r)\}_{n=0}^{\infty}$. An example for $n = 8$ is reported in figure 3.1. We extend the scaling analysis to the eigenvelocities and show how their key features behave with the excitation index n, providing a comprehensive quantitative description of their structure. These results are particularly relevant in view of physical applications, where they considerably facilitate the process of fitting the model to experimental data by providing optimal estimates for the free parameters (see Chapter 4).

In interpreting our results, we note that the large-n approximation $f_n(r) \sim r^{-1}$ derived from the local extrema fit implies an approximately constant eigenvelocity (3.3), consistent with an expected flat plateau. Our systematic results refine this intuition, showing how the slopes of the mid-range eigenvelocities decay with n according to a power law. In addition, the velocity at the last local oscillation exhibits a clear dependence on its radial position, which itself varies with n. This relationship reveals appropriate scaling laws under which all predicted eigenvelocities converge to a similar shape, independent of n, exhibiting an intrinsic universal behavior that might be useful in modeling configurations with (possibly on average) common features.

The interpretation of our results is to be intended with the due caution. Indeed, the analysis of Schrödinger-Poisson eigenvelocities and their straightforward comparison with experimental data are motivated by the assumption that single Schrödinger-Poisson eigenstates are a valuable model for galactic dark matter distributions, an assumption that has been gradually reconsidered in the literature. A more detailed discussion of this point is reported in the next Section 3.1.2.

3.1.2 Model motivation

The use of excited Schrödinger-Poisson stationary states as models for ultralight galactic dark matter distributions and the approximate behavior of the corresponding rotation curves were explored in a series of works [132, 78, 89], matching some relevant physical expectations [33, 124, 125]. However, their role was reconsidered after the discovery of numerical instability [66] and the development of more detailed three-dimensional simulations of the Schrödinger-Poisson system (1.2) [130]. The latter showed the formation of a flat, oscillating core surrounded by an envelope of highly energetic granular structures, which continuously fluctuate in density and velocity. The solid angle averages and the time averages of the resulting anisotropic time-dependent density configurations provide a universal density profile, whose core is well fitted by the ground state of the Schrödinger-Poisson problem (1.2) and whose halo resembles the Navarro-Frenk-White profile of standard CDM [130, 3]. The subsequent literature aimed to construct on-demand density profiles describing such average behaviors and to study their stability with simulations [3], eventually fitting them to experimental data [94, 80]. The excited Schrödinger-Poisson stationary states are still used in some contemporary descriptions of dark matter density profiles, which assume simultaneous occupation of several states resulting in stable multimodal configurations [140, 68, 3].

Despite the nonlinearity of the problem, which complicates the use of knowledge on excited stationary states to study superposed configurations, a refined understanding of the properties of such states may be of interest. Indeed, even though instability issues may discourage their application as physical models, let us observe that the instability of a stationary state does not imply unobservability. Indeed, as is well known, a dynamical system can spend a large amount of time in the neighborhood of an unstable (hyperbolic) equilibrium before moving away from it. Regarding dark matter, this possibility has often been considered, starting with the early works of Sin [132] and Lee

and Koh [89], then with Guzmán and Ureña López [66], up to more recent works such as Roque et al. [123], who observed that "the shortest living unstable mode for each n (i.e., the one with the largest real part) has a lifetime that increases with n. In this sense, higher excited states are less unstable than lower excited ones". This comment refers to the exponential growth factor $e^{\lambda_n t}$ characterizing instability, with λ_n the positive real part of the stability eigenvalues representing the reciprocal of the characteristic instability time $\tau = \lambda_n^{-1}$. From the numerical simulations reported by Roque et al. [123] (see Figure 4 therein), the value λ_n seems to approach zero for $n \to \infty$, implying that the characteristic instability time $\tau = \lambda_n^{-1}$ may diverge. Based on this, we stress in particular the results we obtain for large-n asymptotic behaviors, for which the instability issue might have a reduced impact. Further discussion on the topic is beyond the scope of this work. We limit ourselves to observing that instability may not be a limitation for physical applications and that our work may still be useful in supporting future analytical and physical developments in different areas.

3.2 Implementation

In this Section we present the numerical implementation of the stationary SP problem (3.1), through which we compute stationary states up to high excitations. The `MATLAB` code used for the simulations is available at `https://github.com/GaiaMarangon/PhD---SP-Eigenstates.git`.

The implementation is based on the work by Bernstein et al. [25], which is briefly reported in Section 3.2.1. Using this procedure, simulations were pushed up to high excitation, with the due caution in tuning the parameters and in checking the robustness of the algorithm, so as to ensure the quality of the simulation. A brief report on the results of the tests we performed on the numerical implementation is reported in section 3.2.2.

3.2.1 Numerical procedure

Based on the reference work [25], we simulate spherically symmetric solutions of the stationary SP problem (3.1). In this Section 3.2 we slightly modify problem (3.1) using the norm scalings (1.6) to set the L^2-norm of the matter field to $N = 4\pi$, a choice that is particularly convenient for implementing the spherically symmetric case. In presenting the results of the simulations in the other sections we will return to the unitary norm $N = 1$, which is the standard choice in more general studies. To simplify the notation, we drop the tilde in the new variables (1.6), so that the reference problem in this section reads:

$$\begin{cases} \triangle f = (\varepsilon + 2\phi) f \\ \triangle \phi = f^2 \\ \int f^2(x)\, \mathrm{d}^3x = 4\pi \end{cases} . \tag{3.4}$$

Observe that this notation is slightly different from the one adopted in Bernstein et al. [25]. For comparison with the original notation $(\varepsilon_B, f_B, \phi_B)$ adopted in that work, it is sufficient to set $\varepsilon = -2\varepsilon_B$, $f = \sqrt{4\pi} f_B$ and $\phi = \phi_B$.

We now focus on the spherically symmetric case. Again, with a slight abuse of notation, we use the same symbols for the radial functions $f(r)$ and $\phi(r)$ as for the general stationary states $f(x)$ and $\phi(x)$. In the spherically symmetric case, the Laplace operator acts as $(\triangle f)(r) = \frac{1}{r}(rf)''$, with $f'(r)$ denoting the derivative with respect to r; while for the potential, we write more conveniently: $(\triangle \phi)(r) = \frac{1}{r^2}(r^2\phi')'$, with the same notation for the first derivative. The system (3.4) thus reads:

$$\begin{cases} (rf)'' = (\varepsilon + 2\phi) rf \\ (r^2\phi')' = (rf)^2 \\ \int f^2(r)\, r^2\, \mathrm{d}r = 1 \end{cases} .$$

The unknown f can be conveniently redefined as:

$$g \equiv rf\,,$$

so that the system reads:

$$\begin{cases} g''(r) = (\varepsilon + 2\phi) g \\ (r^2\phi')' = g^2 \\ \int g^2(r)\, \mathrm{d}r = 1 \end{cases} . \tag{3.5}$$

Regarding the boundary conditions, they are set at $r = 0$ and at $r \to \infty$, similarly to [25]. Specifically, two Dirichlet conditions are set for $g(r)$, which correspond to analogous Dirichlet conditions on the original unknown $f(x)$; whereas a Neumann and a Dirichlet conditions are set on the potential $\phi(r)$:

$$\begin{cases} g(0) = 0 & \text{(equivalenty: } f(0) = f_0\text{)} \\ \lim_{r\to\infty} g(r) = 0 & \text{(equivalenty: } \lim_{r\to\infty} rf(r) = 0\text{)} \\ \phi'(0) = 0 & \\ \lim_{r\to\infty} \phi(r) = 0. & \end{cases} . \tag{3.6}$$

With the given boundary conditions, the equation on $\phi(r)$ can be solved explicitly. Integrating both sides from 0 to r, and using the Neumann boundary condition at $r = 0$, we get:

$$\phi'(r) = \frac{1}{r^2} \int_0^r g^2(s)\,\mathrm{d}s\,.$$

Denote by $I(r) \equiv \int_0^r g^2(s)\,\mathrm{d}s$ the integral on the right-hand side. By performing a second integration from r to ∞ to exploit the Dirichlet condition $\lim_{r\to\infty} \phi(r) = 0$ and by integrating the right-hand side by parts, we obtain:

$$\begin{aligned} \phi(r) &= -\int_r^\infty \frac{1}{s^2} I(s)\,\mathrm{d}s \\ &= -\left[-\frac{1}{s} I(s)\right]_r^\infty + \int_r^\infty \left(-\frac{1}{s}\right) I'(s)\,\mathrm{d}s. \end{aligned}$$

Recall the definition of $I(s)$ and observe that $\lim_{s\to\infty} I(s) = 1$, due to the normalization condition imposed on $g(r)$. Adjust the extremes of integration to start from zero. The resulting expression for the potential is:

$$\begin{aligned} \phi(r) &= -\frac{1}{r} \int_0^r g^2(s)\,\mathrm{d}s - \int_r^\infty \frac{g^2(s)}{s}\,\mathrm{d}s \\ &= -\frac{1}{r} \int_0^r g^2(s)\,\mathrm{d}s - \int_0^\infty \frac{g^2(s)}{s}\,\mathrm{d}s + \int_0^r \frac{g^2(s)}{s}\,\mathrm{d}s\,, \end{aligned}$$

so that the system to be solved numerically is:

$$\begin{cases} g''(r) = (\varepsilon + 2\phi)g \\ \phi(r) = -\frac{1}{r}\int_0^r g^2(s)\,\mathrm{d}s - \int_0^\infty \frac{g^2(s)}{s}\,\mathrm{d}s + \int_0^r \frac{g^2(s)}{s}\,\mathrm{d}s \\ \int g^2(r)\,\mathrm{d}r = 1 \end{cases} . \tag{3.7}$$

The goal is therefore to implement a procedure for solving system (3.7) together with boundary conditions (3.6). We already know that substituting the expression for $\phi(r)$ in the equation for $g(r)$ results in the Choquard equation, which admits an infinite discrete family of eigenstates $\{\varepsilon_n, g_n(r), \phi_n(r)\}_{n=0}^\infty$; and we already know from [100, 101] that the eigenvalues are monotonically decreasing to zero for growing n. We thus structure the numerical solver to find the n-th solution $\{\varepsilon_n, g_n, \phi_n\}$ to system (3.7) according to the order given by the eigenvalues.

Solver implementation

The numerical procedure to solve problem (3.7) with boundary conditions (3.6) consists of two nested iterations. The external one is needed to fix the problem of representing $r \to \infty$ numerically, when imposing the boundary conditions. This problem is handled by iteratively fixing the extent of the domain $[0, R]$, solving the problem with approximate boundary conditions $g(R) = 0$ and $\phi(R) = 0$, and then extending the domain $R \to R + \mathrm{d}R$ for the next iteration. This procedure is iterated until the currently computed eigenvalue $\varepsilon_n^{(j)}$ differs from the previous-iteration value $\varepsilon_n^{(j-1)}$ by less than a certain tolerance tol_{Ext}; at this point the approximation $R \sim \infty$ and the corresponding solution are considered sufficiently accurate and the external iteration is interrupted.

At each external iteration, an internal iterative procedure is used to solve the system (3.7) at fixed domain $[0, R]$. The internal iterations are needed to fix the problem of the coupling of the equations: first, an initial guess $g_n^{(0)}(r)$ is set for the function $g_n(r)$; then, the unknowns are iteratively corrected: at the i-th internal iteration, $g_n^{(i-1)}$ is substituted in the second equation of (3.7), which is solved to

get $\phi_n^{(i)}(r)$; and $\phi_n^{(i)}(r)$ is substituted in the first equation of (3.7), which is solved to get $g_n^{(i)}$. As before, this progressive correction is iterated until the currently computed eigenvalue $\varepsilon_n^{(i)}$ differs from the previous-iteration value $\varepsilon_n^{(i-1)}$ by less than a certain tolerance tol_{Int}; at this point the solutions are considered sufficiently accurate and the internal iteration is interrupted.

Once the iterative procedures are completed and the numerical solution $\{\varepsilon_n, g_n, \phi_n\}$ is found, the original unknown $f_n(r)$ can be recovered by: $f_n(r) = g_n(r)r^{-1}$.

Poisson equation

Within the internal iterative process, we need to compute $\phi_n(r)$ in (3.7) with fixed $g(r) = g_n^{(i-1)}$ and in the approximation $R \sim \infty$. The integrals are performed with the corrected trapezoidal rule:

$$I[u] \equiv \int_a^b u(r)\,\mathrm{d}r \;\sim\; CT_h[u] \equiv \sum_{j=0}^{m-1} \frac{h}{2}(u(r_{j+1}) + u(r_j)) - \frac{h^2}{12}(u'(b) - u'(a))\,.$$

with $\{r_j\}_{j=0}^m$ representing the evenly discretized nodes of the domain and h denoting the stepsize. The first derivatives at the internal points are approximated by the second-order centered formula, whereas at the boundaries $r = 0$, $r = R$ they are approximated by the second-order forward and backward formulas, respectively:

$$\begin{aligned} u'(r_j) &\sim \frac{1}{2h}(u(r_{j+1}) - u(r_{j-1})), \\ u'(0) &\sim \frac{1}{2h}(-3u(0) + 4u(h) - u(2h))), \\ u'(R) &\sim \frac{1}{2h}(3u(R) - 4u(R-h) + u(R-2h)). \end{aligned}$$

In this way, the final algorithm to compute $\phi(r)$ has an error $\mathcal{O}(h^4, R^{-4})$ [25].

Eigenvalue problem

Within the internal iterative process, we need to solve the first equation of (3.7) with fixed $\phi(r) = \phi_n^{(i)}(r)$ and with boundary conditions (3.6). To this aim, the second derivative is discretized via the second-order centered formula:

$$g''(r_j) = \frac{g(r_{j+1}) - 2g(r_j) + g(r_{j-1})}{h^2}\,,$$

with $\{r_j\}_{j=0}^m$ representing the evenly discretized nodes of the domain and h denoting the stepsize. The equation results in a linear eigenvalue problem:

$$A\mathbf{g} = \varepsilon\mathbf{g}\,,$$

with:

$$A = \begin{bmatrix} \ddots & \ddots & & & 0 \\ \ddots & \ddots & \ddots & & \\ & \beta & \alpha & \beta & \\ & & \ddots & \ddots & \ddots \\ 0 & & & \ddots & \ddots \end{bmatrix} \quad \mathbf{g} = \begin{bmatrix} g(r_0) \\ \vdots \\ g(r_m) \end{bmatrix} \quad \text{with} \quad \begin{cases} \alpha_j = -\frac{2}{h^2} - 2\phi_n(r_j) \\ \beta \;\; = \;\; \frac{1}{h^2} \end{cases}$$

The system is solved on internal points, while the boundary conditions (3.6) are naturally satisfied, requiring no further correction. To solve the problem, a dedicated built-in `MATLAB` function is used and the solutions are sorted by descending eigenvalues to select the n-th one. As a last step, before proceeding with the internal iterative process, the eigenfunction $g_n(r)$ is normalized to satisfy the norm requirement in (3.7):

$$g_n \to \frac{g_n}{(\int_0^R g_n(s)^2\,\mathrm{d}s)^{\frac{1}{2}}}$$

where the integral is computed via the corrected trapezoidal rule, as before.

3.2.2 Algorithm Sensitivity

In order to test the reliability of the algorithm, we perform a sensitivity analysis, investigating how variations on the numerical parameters impact the result. We report here the results concerning the mesh size, which is the most influential numerical parameter. The mesh size h, which determines how finely the spatial domain is represented, is tuned specifically for each n-th eigenstate and is gradually reduced to obtain more and more refined discretizations, computing each time the corresponding n-th stationary state $(\varepsilon_n, f_n(r), \phi_n(r), v_n(r))$. For each n-th stationary state we test five values of mesh size $\{h_i\}_{i=1}^5$, and we quantify the variations on the results using the following metrics. First, we compare the eigenvalues $\varepsilon_n(h)$ and compute their difference for successive values of h, relative to the eigenvalue with higher refinement:

$$\Delta\varepsilon_n(h_i) := \frac{\varepsilon_n(h_i) - \varepsilon_n(h_{i-1})}{\varepsilon_n(h_5)}\,, \qquad \text{for } i = 2, \dots, 5\,. \tag{3.8}$$

Then, we focus on the eigenfunctions and check the radial position $r_{Out}(h_i)$ of the outermost local extremum, and the corresponding absolute value of the eigenfunction $f_{Out} := |f_n(r_{Out})|$. Again, we compute the relative difference for successive values of h:

$$\Delta r_{Out}(h_i) := \frac{r_{Out}(h_i) - r_{Out}(h_{i-1})}{r_{Out}(h_5)}\,, \qquad \text{for } i = 2, \dots, 5\,, \tag{3.9a}$$

$$\Delta f_{Out}(h_i) := \frac{f_{Out}(h_i) - f_{Out}(h_{i-1})}{f_{Out}(h_5)}\,, \qquad \text{for } i = 2, \dots, 5\,. \tag{3.9b}$$

The results on the outermost local maximum of the eigenvelocities are quite similar, so we do not report them. Instead, we focus on the innermost local maximum (r_{inn}, v_{inn}) of the eigenvelocity $v_n(r)$, which plays a key role in our fitting procedure. As usual, we compute the relative differences for decreasing values of h:

$$\Delta r_{inn}(h_i) := \frac{r_{inn}(h_i) - r_{inn}(h_{i-1})}{r_{inn}(h_5)}\,, \qquad \text{for } i = 2, \dots, 5\,, \tag{3.10a}$$

$$\Delta v_{inn}(h_i) := \frac{v_{inn}(h_i) - v_{inn}(h_{i-1})}{v_{inn}(h_5)}\,, \qquad \text{for } i = 2, \dots, 5\,. \tag{3.10b}$$

In table 3.1, we report the results for two different stationary states, one with a low excitation index $n = 5$ and one with higher excitation index $n = 80$.

Table 3.1: Results of the sensitivity test, collecting the relative differences of some reference quantities for variation of the mesh size parameter h. Reference quantities include: eigenvalues ε_n, outermost local extremum of the eigenfunction (r_{Out}, f_{Out}), innermost local maximum of the eigenvelocity (r_{inn}, v_{inn}). Relative differences are computed as in equations (3.8), (3.9) and (3.10). Consistently with these definitions, mesh sizes are reported for $i = 2, \dots, 5$, while the largest mesh side h_1 is included in the label. Results are reported for two different values of excitation index, $n = 5$ and $n = 80$.

(a) Sensitivity results for $n = 5$ ($h_1 = 1.08$).

h	$\Delta\varepsilon_n$	Δr_{Out}	Δf_{Out}	Δr_{inn}	Δv_{inn}
0.91	$-1.28\cdot10^{-6}$	$1.48\cdot10^{-4}$	$-1.58\cdot10^{-6}$	$-5.84\cdot10^{-4}$	$-1.76\cdot10^{-6}$
0.78	$-8.15\cdot10^{-7}$	$-6.84\cdot10^{-5}$	$-1.03\cdot10^{-6}$	$1.75\cdot10^{-3}$	$-1.49\cdot10^{-6}$
0.65	$-6.90\cdot10^{-7}$	$3.42\cdot10^{-5}$	$-9.50\cdot10^{-7}$	$-4.38\cdot10^{-4}$	$-1.17\cdot10^{-7}$
0.56	$-3.90\cdot10^{-7}$	$2.28\cdot10^{-5}$	$-5.77\cdot10^{-7}$	$-5.84\cdot10^{-4}$	$-8.10\cdot10^{-8}$

(b) Sensitivity results for $n = 80$ ($h_1 = 123$).

h	$\Delta\varepsilon_n$	Δr_{Out}	Δf_{Out}	Δr_{inn}	Δv_{inn}
107	$-7.32\cdot10^{-5}$	$1.95\cdot10^{-5}$	$-9.28\cdot10^{-5}$	$-4.94\cdot10^{-3}$	$-7.13\cdot10^{-5}$
90	$-6.27\cdot10^{-5}$	$6.82\cdot10^{-5}$	$-8.02\cdot10^{-5}$	$9.88\cdot10^{-3}$	$-2.10\cdot10^{-4}$
82	$-2.74\cdot10^{-5}$	$5.85\cdot10^{-5}$	$-3.52\cdot10^{-5}$	$-1.73\cdot10^{-2}$	$4.75\cdot10^{-5}$
74	$-2.49\cdot10^{-5}$	$2.92\cdot10^{-5}$	$-3.20\cdot10^{-5}$	$1.23\cdot10^{-2}$	$-4.66\cdot10^{-5}$

3.3 Comparison with WKB approximation

The stationary SP problem (3.2) is a nonlinear Schrödinger equation, with the nonlinearity arising from the coupling with the Poisson equation. This property makes the problem rather difficult to handle, so that its solutions are estimated numerically, but an exact analytical expression is not currently available. In such cases, it is natural to look for approximations, based on wise ansätze. A relevant tool in this framework is the well-known WKB method, independently developed by Wentzel [144], Kramers [86] and Brillouin [30]. The original method refers to the linear Schrödinger equation for particles of mass m subjected to an external potential $U(x)$. The typical unidimensional problem, presented for example by Fermi and Schluter [48] and describing stationary states of the Schrödinger equation in the form $e^{i\bar{E}t}u(x)$, is expressed as:

$$u'' + \frac{2m}{\hbar^2}(E - U(x))u = 0. \tag{3.11}$$

Problem (3.11) has a formal similarity with the Choquard equation (3.2a), from which it differs in the form of the potential, that is external in the former case and depending on the unknown function in the latter. Based on this similarity, one could be tempted to apply the same type of tools. However, a thorough adaptation of the method would be subtle to handle, due to the difficulties arising from the nonlinearity. Thus, we just consider a formal analogy, assuming the eigenpotential $\phi_n(r)$ and the eigenvalue ε_n as known and using their numerical values to approximate the eigenfunction $f_n(r)$. Although far from exhaustive, this partial analysis gives an interesting insight on the relation between eigenfunction, eigenpotential and eigenvelocity, showing how the transition between the oscillating region and the final monotonic decay in the eigenfunction occurs when a specific relation between eigenvalue and eigenpotential is satisfied. In addition, the comparison with the numerically simulated eigenstates suggests that the WKB method tightly approximates the actual function, with deviation just in the small region around the transition point. Thus, the formal analogy with the linear case seems to be fruitful even in the nonlinear case, suggesting a promising research line for future work.

In this section we adopt the same notation used in [48], highlighting in the final part how to connect to our stationary SP problem (3.2).

WKB approximation in the linear case

Starting from equation (3.11), Fermi and Schluter proceed as follows. First, the coefficient of u is collected in a function $g(x)$, whose physical interpretation is related to the kinetic energy. In fact, recall that the difference between total and potential energy $E - U(x)$ can be interpreted as the kinetic energy $\frac{1}{2}mV(x)^2$, with $V(x)$ denoting the classical velocity.

$$u'' + g(x)u = 0\,, \qquad\qquad g(x) \equiv \frac{2m}{\hbar^2}(E - U(x)) = \frac{m^2V(x)^2}{\hbar^2}\,. \tag{3.12}$$

At this point, a distinction is introduced on the sign of the function $g(x)$ and two cases are analyzed separately. For each case, an approximate solution is derived. Being (3.11) a second order equation, each approximate solution will be obtained by combining two approximate sub-solutions, which in turn are derived based on suitable selected guessed.

Let us first assume $g(x) > 0$. Without loss of generality, the function $u(x)$ can be written either in the form $u = e^{iy(x)}$ or in the form $u = e^{-iy(x)}$. We consider the former first, and then apply an analogous procedure for the latter. Substituting the expression for u into the equation (3.12) recasts the problem in the form:

$$(y')^2 - iy'' = g(x)\,.$$

We consider an approximate relation between $y(x)$ and $g(x)$:

$$y' \approx \sqrt{g}\,.$$

Calculating $y'' \approx \frac{g'(x)}{s\sqrt{g(x)}}$, substituting into the equation for $y(x)$ and dividing by $g(x)$ results in the approximate equation:

$$1 - i\frac{g'(x)}{2g(x)^{\frac{3}{2}}} = 1\,,$$

suggesting that the approximation is fair when:

$$\left|\frac{g'}{g}\right| \ll 2g^{1/2}\,.$$

This informal consideration helps in setting a more formal guess. Without loss of generality, we define $\varepsilon(x)$ as:

$$y' = \sqrt{g} + \varepsilon\,. \tag{3.13}$$

We compute $y'' = \frac{g'(x)}{s\sqrt{g(x)}} + \varepsilon'(x)$ and substitute in the equation for $y(x)$ to obtain:

$$g + \varepsilon^2 - 2\varepsilon\sqrt{g} - i\frac{g'}{2\sqrt{g}} - i\varepsilon' = g\,.$$

We then introduce the actual approximation, by assuming a small ($\varepsilon \ll 1$) and slowly varying ($\varepsilon' \ll 1$) deviation. Neglecting the ε^2 and ε' terms, we find:

$$g + 2\varepsilon\sqrt{g} - i\frac{g'}{2\sqrt{g}} = g \quad \Rightarrow \quad \varepsilon = \frac{ig'(x)}{4g(x)}\,.$$

The resulting approximate expression can be substituted back into the equation (3.13) relating y' and g. We integrate it and obtain:

$$y \approx \int \left(\sqrt{g(x)} + \frac{ig'(x)}{4g(x)}\right) dx = \int \sqrt{g(x)}dx + \frac{i}{4}\ln g(x)\,,$$

which can finally be substituted back to obtain an approximation for the original variable:

$$u(x) = e^{iy(x)} \approx \frac{1}{g(x)^{1/4}} e^{i\int\sqrt{g(s)}ds}\,.$$

Analogous considerations can be set starting from the alternative form $u(x) = e^{-iy(x)}$, resulting in the approximated expression:

$$u(x) = e^{-iy(x)} \approx \frac{1}{g(x)^{1/4}} e^{-i\int\sqrt{g(s)}ds}\,.$$

Combining the two approximate sub-solutions we derive an approximation of the complete solution:

$$u(x) \approx \frac{1}{g(x)^{1/4}} \sin\left(\int \sqrt{g(s)}ds + \text{const}\right)\,. \tag{3.14}$$

An analogous procedure can be applied in the alternative case $g(x) < 0$. Based on the intuitive guess $y'(x) \approx \sqrt{-g(x)}$, we obtain the two solutions:

$$u \approx \frac{1}{-g(x)^{1/4}} e^{\pm i\int\sqrt{-g(s)}ds}\,. \tag{3.15}$$

Comparison with stationary states of SP

Consider now the stationary states of the SP system (3.2), $\{f_n(r), \phi_n(r)\}_{n=0}^{\infty}$. Assuming $\phi_n(r)$ is known, the function $rf_n(r)$ satisfies problem (3.12) with $g(r) = -(\varepsilon_n + 2\phi_n(r))$. Based on the known properties of $\phi_n(r)$, considerations can be made about the sign of $g(r)$ in different region of the domain, so to apply approximations (3.14) and (3.15). In particular:

$$g(r) > 0 \Rightarrow \phi(r) < -\frac{\varepsilon_n}{2} \qquad \text{and} \qquad g(r) < 0 \Rightarrow \phi(r) > -\frac{\varepsilon_n}{2}$$

Observe that in our definition $\varepsilon_n > 0$ and recall that the potential is a negative function, monotonically decaying to zero at $r > 0$. This behavior suggests that $g(r) > 0$ will occur for small radial positions $r < R$ and $g(r) < 0$ for large radial positions $r > R$, with R defined by $\phi_n(R) = \frac{\varepsilon_n}{2}$. If the approximation is fair, WKB would suggest for $rf_n(r)$ – and therefore for $f_n(r)$ – a short-range oscillatory behavior and a large-range exponential decay. This is precisely the situation observed in numerical simulations.

Thus, it is natural to make a comparison between numerically simulated functions $rf_n(r)$ and the corresponding predictions from the WKB approximation. The predictions, given by equations (3.14) and (3.15) with $g(r) = -(\varepsilon_n + 2\phi_n(r))$, are estimated from the numerical values found for the eigenvalue ε_n and the eigenpotential $\phi_n(r)$. Observe that such approximations are defined up to a multiplicative factor, which can be adjusted by hand when setting the comparison. An example with $n = 24$ is shown in figure 3.2. The matching between the WKB prediction and the numerical curve is quite tight, exception made for a very small region around the critical value R, showing that the approximation is fair. The comparison for large $r > R$, better appreciated in log-scale, is deteriorated just in the very last part of the domain, where the numerical necessity of enforcing a finite domain in computing the eigenstates results in a faster truncation of the function.

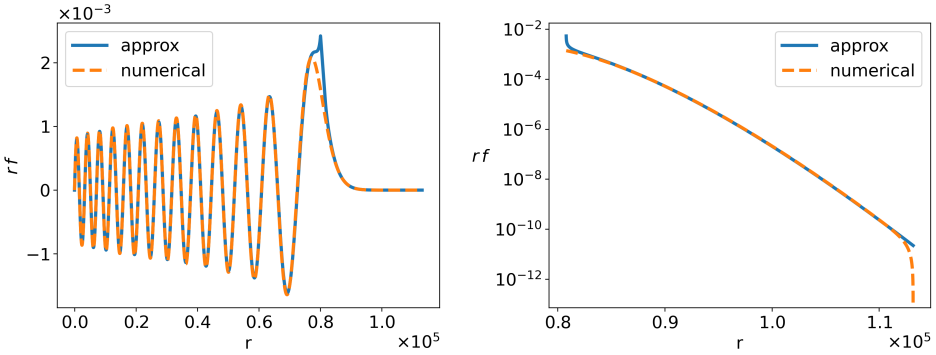

(a) $rf_n(r)$. (b) $rf_n(r)$, log scale and zoomed.

Figure 3.2: Comparison between numerically computed $rf_n(r)$ function and WKB approximations, for $n = 24$. The left panel plots the complete behavior, while the right panel shows the same graph in log scale, zoomed in the large range region $r > R$.

3.4 Conclusions

This Chapter focuses on the excited stationary states of the SP problem. Through numerical implementation, we analyzed the main features characterizing the eigenstates and derived heuristic laws to describe their dependence on the excitation index n.

The heuristic laws are accurate and capture well the behavior displayed by numerical computations, as can be appreciated from the figures in Section **??**. Key characteristics of the eigenfunctions include: the effective support, which exhibits a parabolic dependence on the excitation index; the distances between adjacent nodes, whose pattern varies regularly with n; and the oscillation amplitude, which follows a power law with an exponent approaching -1 for large n. The characterization of the associated eigenpotential focuses on the central value and on two distinct decay regions, the first of logarithmic type and the second described by a power law. Finally, the eigenvelocities exhibit a mid-range oscillatory region with an average linear trend, whose slope approaches zero in the large n limit; and they are characterized by heuristic scaling relationships with the excitation index n, revealing an intrinsic universal behavior.

This characterization offers a double advantage. On the one hand, it may support future analytical studies, which may provide a rigorous derivation of the heuristic laws derived here. On the other hand, it may facilitate the application of the SP system to model experimental data, as exemplified in Chapter 4 for galactic rotation curves.

Concerning the analytical derivation of the heuristic laws, an interesting approach could consist in further developing the parallelism with the WKB-like approximation, as outlined in Section 3.3. While the comments reported in this thesis are only formal, since they consider eigenvalues and eigenpotentials as fixed and use numerical results to approximate the eigenfunctions, the remarkable agreement between the approximation and its computational counterpart suggests that this approach may lead to interesting results. This research line is rather challenging, since the problem is nonlinear, which introduces considerable difficulties in defining a rigorous technique. For these reasons, although we do not treat the problem more thoroughly in this thesis, we consider this topic highly worth further investigation.

Regarding the application of the heuristic laws to the experimental data, let us highlight the relevance of the study of the SP stationary states in the presence of external sources. The results

reported in Section **??** suggest that the presence of a constant additional source in the Poisson equation has a limited impact on the shape of the eigenstates, which are roughly stretched or contracted but are not subjected to strong local deformations. Although this thesis is limited to a graphical representation of these behaviors, we believe that an heuristic characterization of the eigenstates would be possible even in the presence of external sources. The features analyzed in this Chapter are still well defined, and the heuristic laws defined in Section **??** could be computed even in this case, checking how their parameters vary with the profile of the external source. This would be an interesting direction for future developments, which would shed more light into the inner structure of the stationary SP problem.

Chapter 4

Fitting Rotation Curves

4.1 Introduction

In the previous Chapter 3 we thoroughly studied the properties of the excited Schrödinger-Poisson eigenstates and derived a comprehensive set of heuristic laws describing their structure. We now wish to fit these stationary states to experimental data. Such comparison represents the natural step for testing a model's predictive abilities: experimental data are selected, fits are performed to estimate optimal parameter values, and prediction quality is evaluated through appropriate metrics.

In the Schrödinger-Poisson case, setting a fit is a delicate problem. Indeed, due to the instability of the excited eigenstates, their role in modeling galactic dark matter distributions has been reconsidered, and their direct application is currently judged physically questionable. In this work, we include the fitting analysis to complete our model study, demonstrating how our mathematical description can reduce computational costs in the fitting procedure. Our focus is thus on the technical advantages of our mathematical approach rather than on the physical interpretation of the fitting results, which we leave as an open question.

This Chapter demonstrates how the heuristic laws derived in Chapter 3 can be used to set a comparison with experimental data, namely the rotation curves. The main limitation to performing a fit lies in the fact that the eigenstates of the Schrödinger-Poisson model are defined in an implicit form, so that solving system (3.2) is required whenever a prediction for a given set of free parameters must be computed. This represents a major computational disadvantage compared to models that provide explicit predictions, where a simple expression evaluation suffices – a much less expensive operation. This problem is elegantly overcome exploiting the mathematical description we presented in Chapter 3: the heuristic laws we derived can be used to explicitly express some reference features, which can then be compared with their experimental counterparts without solving the complete implicit problem. This comparison between heuristic law approximations and experimental data allows us to evaluate a priori the feasibility of each candidate set of free parameter values, enabling a substantial pre-selection. Only for the selected parameter sets – dramatically reduced in number – do we solve the implicit problem and calculate predicted curves. This approach enormously reduces computational cost while achieving good fits through a fully automated and computationally affordable procedure.

In the remainder of this introduction, Section 4.1.1 presents the typical reference experimental data – rotation curves – providing a brief description of the data structure and explaining how they are generally used to derive information about dark matter distributions. We also present SPARC, the reference database in this field, highlighting the specific characteristics of the collected data and the uncertainties affecting them. Section 4.1.2, instead, reviews the relevant literature on rotation curves, presenting recent works and focusing in particular on fitting techniques.

The other Sections of the Chapter detail the construction process for fitting experimental data. Section 4.2 reports our analysis of the experimental data, illustrating how we derive the effective density distributions for galactic luminous components to account for their presence as external gravitational potential sources in our model.

Section 4.3 describes the fitting procedure itself. We first express the Schrödinger-Poisson model in terms of physical quantities, and we introduce the rescalings that are needed to rewrite it in the dimensionless form we studied in Chapter 3. Through this procedure, the free parameters of the Schrödinger-Poisson model emerge, and their physical interpretation and their role in the model are highlighted. We then present the fitting procedure steps: identifying reference elements in the experimental data, establishing analytical correspondence between experimental elements and their

predicted counterparts, obtaining a priori estimates of the model's free parameters, and describing the metric for evaluating fit quality. The complete procedure is schematized at the end of the Section, which also reports the implementation setting.

Finally, Section 4.4 presents fitting results for two sample galaxies: UGC02953, with bulge; and NGC5055, without bulge. The results include optimal predictions with associated free parameter sets and a parameter study in which individual parameters are varied around optimal values to observe their effects on the predicted curves and on the metric quantifying the quality of the fit.

4.1.1 Rotation curves

Rotation curves $V(R)$ represent the reference experimental data for dark matter halos in galaxies and are commonly used as a benchmark to test the quality of predictive models. The typical rotation curve consists of a sample $\{R_j, (V_{Tot}^{Exp})_j \pm \sigma_j\}_{j=1}^{K}$ of K points measuring the radial distance R_j from the center of the galaxy and the associated velocity $(V_{Tot}^{Exp})_j$ of a test mass orbiting around the galaxy, with σ_j the experimental error. As anticipated in Chapter 1, fundamental physics suggests that the velocity V_{Tot} of a test object orbiting around the galaxy depends only on the radial distance R from the center of the galaxy and on the total amount of matter $M_{Tot}(R)$ encompassed in a ball B_R of radius R, which provides the gravitational attraction necessary to maintain the test object in circular motion. Expressing the matter distribution in terms of density $P_{Tot}(X)$, the test object velocity at a radius R reads:

$$V_{Tot}(R) = \sqrt{\frac{GM_{Tot}(R)}{R}} = \sqrt{\frac{G\int_{B_R} P_{Tot}(X)\,\mathrm{d}^3X}{R}}\,. \tag{4.1}$$

The total amount of matter $M_{Tot}(R)$ in a galaxy includes contributions from four different sources: the stellar bulge, highly dense and concentrated at the center of the galaxy; the stellar disk, less dense and spreading for a wider distance; a gas component, aggregated around the stellar part; and a dark matter halo. Denoting by $P_D(X)$, $P_B(X)$, $P_G(X)$, $P_{DM}(X)$ the mass density distributions of the disk, bulge, gas, and dark matter components, the total density distribution $P_{Tot}(X)$ of matter in the galaxy is obtained simply by superposition:

$$P_{Tot}(X) = P_D(X) + P_B(X) + P_G(X) + P_{DM}(X)\,.$$

With this decomposition, the velocity of a test object orbiting around the galaxy can be written as:

$$V_{Tot}(R) = \sqrt{\frac{G\int_{B_R}(P_D(X) + P_B(X) + P_G(X) + P_{DM}(X))\,\mathrm{d}^3X}{R}} \tag{4.2}$$

$$= \sqrt{V_D^2(R) + V_B^2(R) + V_G^2(R) + V_{DM}^2(R)}\,, \tag{4.3}$$

where the velocity contribution of each single source is defined in analogy to (4.1):

$$V_J(R) = \sqrt{\frac{G\int_{B_R} P_J(X)\,\mathrm{d}^3X}{R}}\,, \qquad J \in \{D, B, G, DM\}\,. \tag{4.4}$$

The first three matter components – stellar disk, stellar bulge, and gas – are of luminous nature, and can be observed via brightness measures, which allow reconstructing the respective contributions to the velocity curve: $V_D(R)$ for the disk, $V_B(R)$ for the bulge, and $V_G(R)$ for the gas. Once the luminous components are known, equation (4.3) can be inverted to get an experimental estimate of the dark matter component of velocity $V_{DM}^{Exp}(R)$, to be compared with the predicted counterpart V_{DM}^{Pred} estimated from the model under analysis.

The reconstruction of velocity contributions from luminous sources is based on experimental surface brightness profiles $\Sigma(R)$, which describe the luminosity per unit surface of each stellar component in a galaxy (disk, bulge, gas) as a function of the distance R from the galaxy center. Luminosity distributions coincide approximately with mass distributions up to a proportionality constant Υ, the mass-to-light ratio. This ratio, which is different for each luminous component, is usually assumed to be $\Upsilon_G = 1\,M_\odot/L_\odot$ for the gas, while its value for the disk Υ_D and for the bulge Υ_B is still unknown. However, this proportionality constant is considered rather consistent over a broad range of galaxy masses and morphologies, in particular for measures collected in a luminosity band of 3.6 μm,

which is therefore the preferred setting for the collection of photometric data [94]. Moreover, Stellar Population Synthesis (SPS) models suggest a relationship between the two constants: $\Upsilon_B = 1.4\Upsilon_D$, and fiducial values are available [107, 95]:

$$\Upsilon_D^{fid} = 0.5 M_\odot/L_\odot\,, \qquad \Upsilon_B^{fid} = 0.7 M_\odot/L_\odot\,.$$

The remaining uncertainty is usually accounted for by defining a free parameter Q, representing the deviation factor from the fiducial values [111]:

$$\Upsilon_D = Q\Upsilon_D^{fid}\,, \qquad \Upsilon_B = Q\,\Upsilon_B^{fid}\,. \tag{4.5}$$

Up to this factor Q, surface brightness profiles can therefore be converted to surface mass profiles.

Once surface mass profiles are known up to factors $\Upsilon_D(Q)$ and $\Upsilon_B(Q)$, volumetric mass distributions $P_D(X)$, $P_B(X)$, $P_G(X)$ are reconstructed. This is performed through careful methods, such as that presented in Casertano [35], which need to account for the axial symmetry of the galactic components. Since these methods elaborate on surface brightness profiles, they estimate volumetric luminosity densities $P_D^{(L)}(X)$, $P_B^{(L)}(X)$, $P_G^{(L)}(X)$, while the corresponding volumetric mass densities are defined up to the usual mass-to-light ratios:

$$P_D(X) = \Upsilon_D\, P_D^{(L)}(X)\,, \qquad P_B(X) = \Upsilon_B\, P_B^{(L)}(X)\,, \qquad P_G(X) = \Upsilon_G\, P_G^{(L)}(X)\,. \tag{4.6}$$

Once these mass densities are known, they can be used to compute the corresponding velocity components $V_D(R)$, $V_B(R)$, $V_G(R)$, as in (4.4). A standard choice in tabulating the data consists of reporting the velocity components $V_D^{(L)}$, $V_B^{(L)}$, $V_G^{(L)}$ computed assuming $\Upsilon_D = \Upsilon_B = \Upsilon_G = 1\,M_\odot/L_\odot$. In this way, once a reliable assumption is made on the value of the mass-to-light ratios Υ_D, Υ_B ($\Upsilon_G = 1\,M_\odot/L_\odot$), the actual velocities contribution V_D, V_B, V_G can easily be obtained from the tabulated values:

$$V_D = \sqrt{\Upsilon_D} V_D^{(L)}\,, \qquad V_B = \sqrt{\Upsilon_B} V_B^{(L)}\,, \qquad V_G = \sqrt{\Upsilon_G} V_G^{(L)}\,. \tag{4.7}$$

The SPARC database

SPARC [94] (Spitzer Photometry & Accurate Rotation Curves) is a publicly available sample of 175 nearby galaxies with two types of data: surface photometry at 3.6 μm and high-quality rotation curves collected from previous studies. It spans a broad range of luminosity, surface brightness, rotation velocity, and Hubble type, forming a representative sample for testing galaxy formation models in the nearby Universe.

Surface photometry data include surface brightness profiles for the two stellar components of each galaxy – the stellar disk and the stellar bulge, if present – while no photometric data are reported for the gas component. The typical surface brightness profile consists of a sample $\{R_j, (\Sigma_I)_j\}_{j=1}^K$ of K points measuring the radial distance R_j from the center of the galaxy and the associated surface brightness $(\Sigma_I)_j$ for the disk ($I = D$) and the bulge ($I = B$). The data are collected at 3.6 μm, so that the mass-to-light ratios are approximately constant across the galaxies.

Surface brightness profiles are used to reconstruct velocity contributions $\{R_j, (V_I^{(L)})_j\}_{j=1}^K$ for the disk ($I = D$) and the bulge component ($I = B$), using the method presented in Lelli et al. [94]. Concerning the gas component, for which no surface brightness profiles are available, the velocity contribution is calculated using the method presented by Casertano [35], which solves the Poisson equation for a disk with finite thickness and arbitrary density distribution, accounting for the axial symmetry of the problem. Observe that with this reconstruction $V_G(R)$ can sometimes be negative in the innermost regions: this occurs when the gas distribution has a significant central depression and the material in the outer regions exerts a stronger gravitational force than that in the inner parts [94]. To account for this fact, SPARC adapts the expression for rotation curves decomposition (4.3), so as to preserve the information on the sign:

$$|V_{Tot}|V_{Tot} = |V_D|V_D + |V_B|V_B + |V_G|V_G + |V_{DM}|V_{DM}\,, \tag{4.8}$$

where the radial dependence has been omitted to lighten the notation.

On this basis, the SPARC database tabulates the velocity contributions $V_D^{(L)}$, $V_B^{(L)}$, $V_G^{(L)}$, computing them with $\Upsilon_D = \Upsilon_B = 1\,M_\odot/L_\odot$ so that the actual contributions V_D, V_B, V_G can be recovered as in (4.7) once the mass-to-light ratios are estimated.

The second type of data in SPARC – the high quality rotation curves – include sets of K datapoints $\{R_j, (V_{Tot}^{Exp})_j \pm \sigma_j\}_{j=1}^{K}$, with R_j the same radial distances from the center tabulated in the surface brightness profiles, $(V_{Tot}^{Exp})_j$ the corresponding rotation velocity measured for a test object orbiting around a galaxy, and σ_j the measure error.

In addition to the measure error, the measured radial positions and velocities are affected by the uncertainties in the inclination angle i of the galaxy and in the galaxy distance D, which are involved in the definition of the experimental velocity curves $\{R_j, (V_{Tot}^{Exp})_j \pm \sigma_j\}_{j=1}^{K}$ [99]. The values of i and D used to compute the tabulated rotation curves are reported alongside the other information of each galaxy, and if different values i', D' are deemed more reliable, the SPARC documentation provides formulas to correct radial positions and velocities accordingly:

$$(V_{Tot}^{Exp})'_j = (V_{Tot}^{Exp})_j \frac{\sin(i)}{\sin(i')}\,, \qquad \sigma'_j = \sigma_j \frac{\sin(i)}{\sin(i')}\,, \qquad R'_j = R_j \frac{D'}{D}\,, \qquad (V_I)'_j = (V_I)_j \sqrt{\frac{D'}{D}}\,,$$

with $I \in \{D, B, G\}$ as usual. Based on this, the inclination angle i and the galaxy distance D are sometimes treated as free parameters, and their value is decided along with that of the other free parameters during the fit ([99, 98, 81]). Such uncertainties are relevant in analyzing specific relationships, such as the radial acceleration relation or RAR [99], but may generally be neglected in favor of a reduced number of fitting parameters. Adopting this approach, we assume that the tabulated values of i and D are reliable, and we use the corresponding rotation curves without introducing further corrections.

Other cautions in using the data concern the quality of the curves. Some of them are commonly rejected from the analysis for the following reasons:

1. poor quality, as reported in the database itself, namely "the rotation curve does not trace the equilibrium gravitational potential" [106, 96, 81]. We perform the same selection;
2. insufficient number of data points, for example, fewer points than the number of free parameters [81] or fewer points than fixed threshold (7 in [41], 5 in [80]). We adopt a threshold of 8;
3. lack of radial profiles for gas distribution [111]. We do not adopt this criterion;
4. inclination angle $i < 30°$, causing too large uncertainties in V_{obs} as discussed above [80, 106, 96]. We perform the same rejection.

4.1.2 Literature on Rotation Curves and their Fit

Since the earliest studies on dark matter, experimental data on rotation curves have served as a fundamental tool for testing the quality and predictive ability of models. As increasingly numerous and accurate experimental data have been collected, particularly with the publication of the SPARC database, systematic fitting has become possible, making comparison with rotation curves increasingly significant.

Currently, extensive literature exists on models for rotation curves, based on slightly different assumptions and tested with excellent results against experimental data (see Matos et al. [105] for an excellent review). The main aim is to construct a model that describes the average distribution of dark matter in galaxies. Such models approximate the complicated behavior emerging from numerical simulations – where dark matter distributions oscillate and continuously evolve – to effectively predict corresponding rotation curves. The first attempts at effective distributions were constructed either on an empirical basis, such as the Burkert profile [98, 81], or following N-body numerical simulations, such as the popular Navarro-Frenk-White (NFW) profile [80, 98, 81].These early proposals focus on reproducing oscillating behavior that dampens at large radii, resulting in a wide variety of profiles (see Matos et al. [105] for a more complete list).

Among the most recent models, a frequent choice involves adopting a "soliton+halo" scheme [24, 19], in which the density distribution comprises two components: the ground state of the Schrödinger-Poisson system ("soliton") is used in the central region, while different profiles, such as the NFW, are adopted in the outer regions ("halo").

Following studies on the numerical instability of excited Schrödinger-Poisson eigenstates [66, 67], other potentially more stable variants have been considered. Models of this type include, for example, rotation effects [64, 70], thermal noise [122], or self-interaction [41]. An interesting recently proposed line of research involves assuming that dark matter is organized in a superposition of excited states (multistate model) [140, 122, 24, 3]. Finally, rotation curves are sometimes predicted without assuming the existence of dark matter, but instead by assuming specific modifications to Newton's law of gravity (modified Newtonian dynamics, MOND) [111].

Determining rotation curve fits serves both to find the optimal values of a given theory [41, 70, 111], and to compare alternative models by quantifying their ability to reproduce experimental data [24, 98, 81]. The most widely used approach for this purpose is the Bayesian method [80, 24, 81], which estimates the posterior probability density of the model parameters based on prior knowledge of these parameters and the observed experimental data. Let $\mathcal{M}$ denote the model, θ its free parameters, and d the experimental data. Let $\pi(\theta, \mathcal{M})$ represent the prior probability density, namely the density distribution assumed a priori for the parameters θ. Let $P(d|\theta, \mathcal{M})$ be the likelihood of the data, namely the probability of observing the data d given model $\mathcal{M}$ and fixed parameter values θ. Finally, let $P(d|\mathcal{M})$ be the evidence, obtained by marginalizing the likelihood with respect to the parameters $P(d|\mathcal{M}) = \int P(d|\theta, \mathcal{M})\pi(\theta, \mathcal{M})\mathrm{d}\theta$. This represents the probability of observing the data d given the model $\mathcal{M}$, averaged over all possible parameter values according to the prior. Bayes' theorem defines the posterior probability density of the model parameters $P(\theta|d, \mathcal{M})$, namely the probability of having the parameters θ given model $\mathcal{M}$ and observed data d, as:

$$P(\theta|d, \mathcal{M}) = \frac{P(d|\theta, \mathcal{M})\,\pi(\theta, \mathcal{M})}{P(d|\mathcal{M})} = \frac{P(d|\theta, \mathcal{M})\,\pi(\theta, \mathcal{M})}{\int P(d|\theta, \mathcal{M})\pi(\theta, \mathcal{M})\mathrm{d}\theta}\,, \tag{4.9}$$

The likelihood probability density, which models the errors introduced during measurement, is usually assumed to have Gaussian form:

$$P(d|\theta, \mathcal{M}) = \prod_j \frac{1}{\sqrt{2\pi}\sigma_j} \exp\left(-\frac{\left(V_j^{Exp} - V^{Pred}(r_j;\,\theta, \mathcal{M})\right)^2}{2\sigma_j^2}\right)\,, \tag{4.10}$$

where V_j^{Exp} is the observed rotational velocity at radius r_j, σ_j is the uncertainty in its determination, and $V^{Pred}(r_j;\,\theta, \mathcal{M})$ is the rotational velocity predicted by model $\mathcal{M}$ with parameters θ at the radial position r_j. The prior $\pi(\theta, \mathcal{M})$ is selected according to the assumed prior knowledge for each parameter. Once the likelihood and priors are defined, the parameter values are selected to maximize the posterior.

Regarding the definition of the priors, when there is a priori knowledge of a parameter's expected value and there are no asymmetries, a Gaussian prior is generally chosen. This applies, for example, to the mass-to-light ratios Υ_D and Υ_B, for which fiducial values are typically adopted as the expectation with a standard deviation of 0.1 dex [98]; or to the inclination angle i and the galactic distance D, for which the expectation is set equal to tabulated values [98]. When no prior information is available, maximally wide uniform priors are preferred, requiring minimal assumptions [80, 98, 81].

Once priors are chosen, various standard algorithms are available to compute the posterior (4.9), such as the popular Markov Chain Monte Carlo (MCMC) method [80, 99, 98, 24], or dynamic nested sampling [81]. These algorithms provide not only an estimate of the optimal parameter values θ, but also an estimate of their entire posterior probability distribution. This approach therefore yields highly informative results and enables both fitting the free parameters of a model and comparing different models by analyzing the obtained posteriors to evaluate which model has the highest probability of explaining the data.

The fundamental advantage of the Bayesian approach is that it exploits prior knowledge of the problem. When no prior knowledge is assumed, it may be more convenient to use direct methods that estimate optimal parameter values without necessarily calculating the entire posterior distribution. A widespread method involves defining a metric for the deviation of predictions from experimental data and searching for parameter values that optimize this metric. The most standard choice [99, 24, 41, 111] involves minimizing the χ-squared statistics:

$$\chi^2 = \frac{1}{K-k}\sum_{j=1}^{K}\frac{(V_j^{Exp} - V_j^{Pred})^2}{\sigma_j^2}$$

which involves the squared differences between observed values V_j^{Exp} and predicted values V_j^{Pred}, normalized by the squared error on observed data σ_j^2 when available, or by predicted values if errors are not available [70]. Normalizing by the number of degrees of freedom, computed as the difference between the number of data points K and the number of model parameters k, results in the so called reduced χ-square.

During the minimization process, additional requirements can be enforced. In the case of rotation curves, for example, it is possible to establish ranges for free parameters [41], or to impose particular physical constraints, such as monotonic behavior for certain functions [41] or the positivity of specific

values [99]. Subsequently, the fit quality metric is optimized using standard algorithms, such as the nonlinear least-squares (NLLS) method [70], or genetic algorithms [41] and the optimal values of the free parameters are computed.

Applying the statistical tools we just described – particularly the Bayesian approach – is considerably facilitated by the availability of explicit expressions for model predictions $V^{Pred}(r_j;\,\theta,\mathcal{M})$. Indeed, the vast majority of tested models falls into this category [24, 98, 41, 70, 81, 111]. In the absence of such explicit expressions, executing these algorithms – particularly the MCMC method – remains possible, but becomes much more difficult to implement due to excessive computational costs.

In comparing our model with experimental data, we must therefore handle the difficulty of having predictions in implicit form, which require solving a system of equations for calculation. Given this limitation, we adopt a non-Bayesian approach based on minimizing a metric rather than calculating the entire posterior probability distribution. Furthermore, to reduce computational effort, we employ a strategy based on a priori estimation of parameter validity, allowing upstream selection of parameter sets to be tested. This strategy, based on the heuristic laws obtained in Chapter 3, is described in detail in Section 4.3.

4.2 Effective density distributions from the SPARC database

Based on the experimental data in the SPARC database, we wish to reconstruct volumetric mass densities for disk $\Upsilon_D P_D^{(L)}$, bulge $\Upsilon_B P_B^{(L)}$ and gas $\Upsilon_G P_G^{(L)}$ ($\Upsilon_G = 1\,M_\odot/L_\odot$). These densities are not directly available in the database, but we need to estimate them to allow our model to account for external sources of gravitational potential. Consistent with the symmetry assumptions we made for the Schrödinger-Poisson eigenstates, we would like to estimate effective spherically symmetric densities, neglecting the actual axially symmetric geometry of the distributions to focus on their overall effect on dark matter.

One option for defining these densities would be to start from the photometric data, adopting the same procedure used by Lelli et al. [94] to define the rotation curves. However, this approach requires careful geometric considerations both in reconstructing the actual axisymmetric distribution [35, 19] and in defining the reshaping to spherically symmetry. The latter issue is particularly subtle, being rather arbitrary. A naive approach to this reshaping would be to assume that at every radius R the spherical distribution contains the same mass as the axisymmetric distribution with larger characteristic dimension equal to R (overspreading the actual mass). Alternatively, we could assume that at every radius R the spherical distribution contains the same mass as the axisymmetric distribution with smaller characteristic dimension equal to R (shrinking the actual mass). Finally, any intermediate option trading off between these two assumptions could improve reliability, but no a priori guideline is available for defining this procedure, which is therefore subject to considerable arbitrariness. In addition, such surface density distributions are reported only for disk and bulge, while gas data are not directly reported in the database [19, 111]. This makes direct use of experimental surface densities a hardly viable option.

The second option for defining effective external densities is based on rotation curves. The SPARC database reports, for every galaxy, estimated velocity contributions for each luminous component, $V_D^{(L)}$, $V_B^{(L)}$ and $V_G^{(L)}$. Such contributions to rotation curves incorporate, in some sense, the effective description of mass density we wish to retrieve. The most straightforward way to define each luminous density distribution $P_I^{(L)}(R)$, with $I \in D, B, G$, is to write the definition of rotation curve originating from a spherically symmetric density:

$$V_I^{(L)}(R) = \sqrt{\frac{4\pi G}{R}\int_0^R P_I^{(L)}(S) S^2\,\mathrm{d}S}\,,$$

and to invert it, finding a definition for the effective spherically symmetric luminosity density:

$$P_I^{(L)}(R) \equiv \frac{1}{R^2}\frac{\mathrm{d}}{\mathrm{d}R}\left(\frac{\left(V_I^{(L)}\right)^2 R}{4\pi G}\right) = \frac{1}{4\pi G}\left(\frac{\left(V_I^{(L)}\right)^2}{R^2} + 2\frac{V_I^{(L)}}{R}\frac{\mathrm{d}V_I^{(L)}}{\mathrm{d}R}\right).$$

Observe that since the rotation curves $V_I^{(L)}(R)$ are known at a set of K sample points $\{R_j, (V_I^{(L)})_j\}_{j=1}^K$, the corresponding densities will be calculated at the same radial positions, $\{R_j, (P_I^{(L)})_j\}_{j=1}^K$. In addition, velocities are expressed in km/s and radial positions in kpc, so we select the units for the

physical constant G to express the luminosity densities in $10^9 L_\odot/kpc^3$ (see Section 4.3.2 for more details on the adopted physical units). The data points we obtain are approximately compatible with exponentially decaying functions:

$$P_I^{(L)}(R) = A_I e^{-\frac{R}{R_{0,I}}} . \tag{4.11}$$

where the characteristic density A_I and the characteristic length $R_{0,I}$ are estimated by standard fitting techniques.

Two examples of fitted densities are reported in figure 4.1 for galaxies UGC02953 and NGC5055, which are used later in this Chapter to test the fitting procedure. The figure reports both the log plots of the effective densities $\{R_j, (P_I^{(L)})_j\}_{j=1}^K$ on which fits are performed, and the rotation curves $\{R_j, (V_I^{(L)})_j\}_{j=1}^K$, comparing the experimental data and the velocity profiles reconstructed from the exponential fitted densities. The plots confirm that the exponential density profiles are rather effective in reproducing the rotation curves, even though, especially for the gas component, they do not capture exactly the oscillations of the experimental data points.

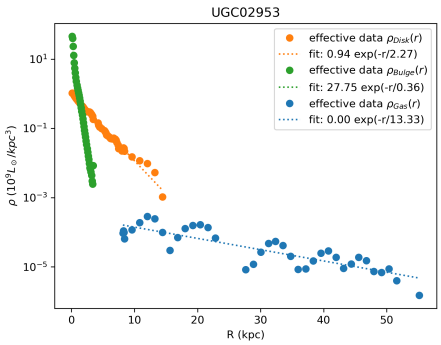

(a) UCG02953, experimental and effective densities.

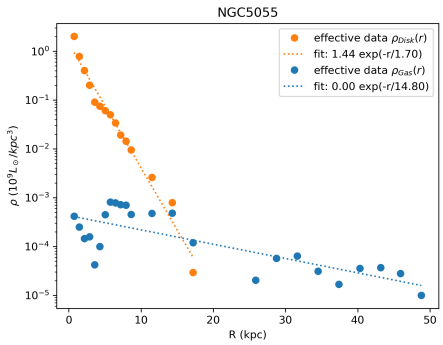

(b) NGC5055, experimental and effective densities.

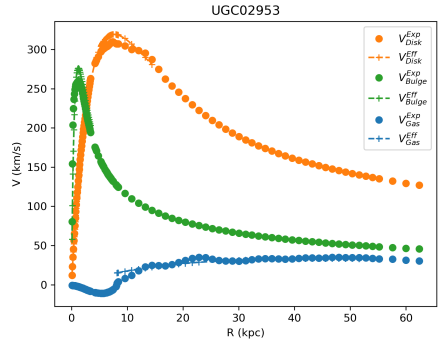

(c) UCG02953, experimental and effective rotation curves.

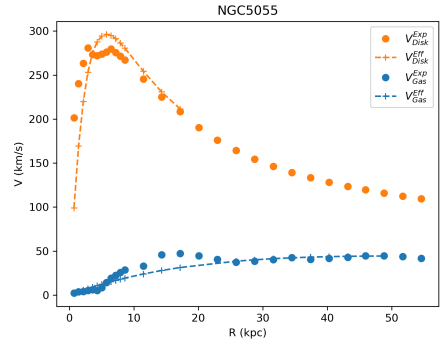

(d) NGC5055, experimental and effective rotation curves.

Figure 4.1: Top panels: fit of effective densities for two sample galaxies, UCG02953 (left) and NGC5055 (right), in log scale. Bottom panes: experimental velocity profiles are compared with rotation curves resulting from the effective exponential densities.

Once the mass densities $\Upsilon_I P_I^{(L)}(R)$ are estimated from experimental data up to the free parameter Q, they can be used in the model as external sources of gravitational potential, after convenient rescalings to express them in non-dimensional form (see Section 4.3.2).

In addition, it is also possible to calculate the total luminous mass M_L, which will be used as a reference quantity in the fitting procedure. We perform the computation based on the exponential

form of the densities (4.11):

$$M_L(R) \equiv 4\pi \int_0^\infty \Upsilon_D P_D^{(L)}(S) S^2 \,\mathrm{d}S + 4\pi \int_0^\infty \Upsilon_B P_B^{(L)}(S) S^2 \,\mathrm{d}S + 4\pi \int_0^\infty P_G^{(L)}(S) S^2 \,\mathrm{d}S$$
$$= 8\pi \left(\Upsilon_D A_D R_{0,D}^3 + \Upsilon_B A_B R_{0,B}^3 + A_G R_{0,G}^3 \right) . \tag{4.12}$$

4.3 The fitting procedure

We now present the procedure we use to fit the excited eigenstates of the Schrödinger-Poisson model to the experimental rotation curves from the SPARC database. First, the Schrödinger-Poisson system is expressed using physical quantities and conveniently rescaled to its dimensionless form (Section 4.3.1). Then, after selecting suitable units for such rescalings (Section 4.3.2), we describe the fitting procedure itself, detailing how we define and enforce a priori estimates of the free parameters of the model (Section 4.3.3).

4.3.1 From physical to non-dimensional quantities

We report here the construction of conversion factors from physical quantities, denoted with capital letters, to non-dimensional quantities, denoted with lowercase letters. The physical Schrödinger-Poisson system, together with matter field normalization, reads:

$$\begin{cases} i\hbar\, \partial_T \Psi = \left(-\frac{\hbar^2}{2m} \Delta_X + m\Phi \right) \Psi \\ \Delta_X \Phi = 4\pi G m |\Psi|^2 + 4\pi G P \\ \int |\Psi|^2 \,\mathrm{d}^3 X = \frac{M_{DM}}{m} \equiv N \end{cases} , \tag{4.13}$$

with Δ_X denoting the Laplacian in the physical space coordinates X, ∂_T the time derivative, $\hbar$ the reduced Planck constant, G the gravitational constant, m the mass of each dark matter particle, M_{DM} the mass of the whole dak matter cluster, and $N \equiv M_{DM}/m$ the number of particles in the cluster. The aim is to scale space X, time T, matter field $\Psi(T, X)$, gravitational potential $\Phi(T, X)$ and external density $P(X)$ in order to express them as non-dimensional quantities x, t, $\psi(t, x)$, $\phi(t, x)$, $\rho(t, x)$, so that the Schrödinger-Poisson system (4.13) reduces to our usual (1.3), without any physical constants and parameters. We report it here for ease of reference:

$$\begin{cases} i\partial_t \psi(t,x) = (-\Delta + 2\phi(t,x))\psi(t,x) \\ \Delta\phi(t,x) = |\psi|^2(t,x) + \rho(x) \\ \int |\psi|^2(t,x) \,\mathrm{d}^3 x = 1 \end{cases} . \tag{4.14}$$

To obtain this non-dimensional system, we set a generic change of variables:

$$X = [x]x, \quad T = [t]t, \quad \Psi = [\psi]\psi, \quad \Phi = [\phi]\phi, \quad P = [\rho]\rho$$

and we choose the scales $[x]$, $[t]$, $[\psi]$, $[\phi]$,$[\rho]$ to progressively adjust the equations in (4.13). Rearranging the matter field normalization as in (4.14) sets the matter field scale to $[\psi]^2 = N[x]^{-3}$; writing the Poisson equation as in (4.14) sets the density scale to $[\rho] = m[\psi]^2 = mN[x]^{-3}$ and the gravitational potential scale to $[\phi][x]^{-2} = 4\pi G m[\psi]^2$, namely $[\phi] = 4\pi G m N[x]^{-1}$; while to obtain the Schrödinger equation in (4.14), we substitute the scalings:

$$i\hbar[t]^{-1}\partial_t\psi = \left[-\frac{\hbar^2}{2m}\frac{1}{[x]^2}\Delta + m[\phi]\phi \right] \psi,$$
$$i\partial_t\psi = \left[-\frac{[t]\hbar}{2m}\frac{1}{[x]^2}\Delta + \frac{[t]m}{\hbar}\frac{4\pi G m N}{[x]}\phi \right] \psi$$

and we adjust the two factors on the right-hand side, setting $[t]\hbar(2m[x]^2)^{-1} \stackrel{!}{=} 1$, which fixes the time scale to $[t] = 2m[x]^2\hbar^{-1}$, and $[t]4\pi G m^2 N(\hbar[x])^{-1} = 2[x]4\pi G m^3 N\hbar^{-2} \stackrel{!}{=} 2$, which fixes the space scale to $[x] = \hbar^2(4\pi G m^3 N)^{-1}$.

Interestingly, the resulting scaling factors can be written as functions of the Planck scale ℓ_P, t_P and m_P giving the dimensionality, of the mass parameter m appearing in powers of the mass ratio

$m_P m^{-1}$, and of the number of particles N. Overall, the scalings read:

$$X = [x]\, x, \qquad [x] = \frac{1}{4\pi} \left(\frac{m_P}{m}\right)^3 N^{-1}\, \ell_P\,, \tag{4.15a}$$

$$T = [t]\, t, \qquad [t] = \frac{2}{(4\pi)^2} \left(\frac{m_P}{m}\right)^5 N^{-2}\, t_P\,, \tag{4.15b}$$

$$\Psi = [\psi]\, \psi, \qquad [\psi] = (4\pi)^{\frac{3}{2}} \left(\frac{m_P}{m}\right)^{-\frac{9}{2}} N^2 \ \ell_P^{-\frac{3}{2}}\,, \tag{4.15c}$$

$$\Phi = [\phi]\phi, \qquad [\phi] = (4\pi)^2 \left(\frac{m_P}{m}\right)^{-4} N^2 \ \frac{G m_P}{\ell_P}, \tag{4.15d}$$

$$P = [\rho]\rho, \qquad [\rho] = (4\pi)^3 \left(\frac{m_P}{m}\right)^{-10} N^4 \ \frac{m_P}{\ell_P^3}\,, \tag{4.15e}$$

where we recall:

$$\ell_P \equiv \sqrt{\frac{\hbar G}{c^3}}\,, \qquad t_P \equiv \sqrt{\frac{\hbar G}{c^5}}\,, \qquad m_P \equiv \sqrt{\frac{\hbar c}{G}}\,. \tag{4.16}$$

Analogously, a velocity scale is required to convert the non-dimensional prediction $v_n(r)$ defined in (3.3) to the corresponding quantity in physical units, $V_{DM}(R)$:

$$V_{DM}(R) = \sqrt{\frac{G\, m\, 4\pi \int_0^R |\Psi|^2 S^2 \,\mathrm{d}S}{R}}\,, \tag{4.17}$$

where we accounted for the 4π factor from angular integration that we omitted in (3.3). The unit conversion scale for velocity is set by combining its definition with the known scalings for space and matter field, yielding a scaling $[v] = \sqrt{G\, m\, 4\pi}[\psi][x]$. Consistently with the other quantities, the result can be expressed in terms of a power of the mass ratio $m_P m^{-1}$, of N and of a standard physical constant giving the dimensionality:

$$V = [v]v, \qquad [v] = 4\pi \left(\frac{m_P}{m}\right)^{-2} N\, c\,. \tag{4.18}$$

4.3.2 Selecting units

We now focus on the quantities that are explicitly involved in the comparison with experimental data: velocities, radii, and volumetric mass densities. In order to work with more interpretable variables, we define the ratio ξ between the total dark matter mass $M_{DM} \equiv mN$ and the total luminous mass M_L accounting for all visible components in a galaxy:

$$\xi \equiv \frac{M_{DM}}{M_L} = \frac{mN}{M_L}\,.$$

We use this ratio instead of N as a free parameter of the model, which is considerably easier to interpret. In terms of ξ, and adjusting the expressions to let the parameter m appear only in mass ratios for ease of interpretation, the scalings for the relevant quantities are:

$$X = [x]\, x, \qquad [x] = \frac{1}{4\pi} \left(\frac{m_P}{m}\right)^2 \left(\frac{m_P}{M_L}\right) \frac{1}{\xi}\, \ell_P\,, \tag{4.19a}$$

$$P = [\rho]\rho, \qquad [\rho] = (4\pi)^3 \left(\frac{m_P}{m}\right)^{-6} \left(\frac{M_L}{m_P}\right)^4 \xi^4 \frac{m_P}{\ell_P^3}\,, \tag{4.19b}$$

$$V = [v]v, \qquad [v] = 4\pi \left(\frac{m_P}{m}\right)^{-1} \left(\frac{M_L}{m_P}\right) \xi \quad c\,. \tag{4.19c}$$

Once we have defined the unit conversion scales in terms of known physical constants and parameters, we must express them in convenient physical units. On galactic scales, the radial positions are naturally expressed in kpc, the velocities in km/s, and the volumetric densities in $10^9 M_\odot/kpc^3$. Moreover, the natural units for the total luminous mass M_L is $10^9\, M_\odot$, while we express the dark matter particle mass m in units of $10^{-56}\, g$.

To handle such units, let us first report the numerical values for the main physical constants in cgs, together with some relevant units conversions from astrophysical units to cgs:

$$\begin{aligned} G &= C_G \;\; 10^{-8}\, g^{-1} cm^3 s^{-2}\,, & C_G &= 6,67\,, \\ \ell_P &= C_{LP}\, 10^{-33}\, cm\,, & C_{LP} &= 1.62\,, \\ m_P &= C_{MP}\, 10^{-5}\, g\,, & C_{MP} &= 2.18\,, \\ kpc &= C_{PC}\, 10^{21}\, cm\,, & C_{PC} &= 3.09\,, \\ M_\odot &= C_{MS}\, 10^{33}\, g\,, & C_{MS} &= 1.99\,. \end{aligned}$$

In the physical units suited for our problem, the relevant physical constants read:

$$\begin{aligned} G &= \frac{C_G C_{MS}}{C_{PC}}\, 10^3 \left[\frac{1}{10^9 M_\odot}\frac{km^2}{s^2} kpc\right], & G_{astro} &\equiv \frac{C_G C_{MS}}{C_{PC}}\,, \\ \ell_P &= \frac{C_{LP}}{C_{PC}} \;\; 10^{-54}\,[kpc]\,, & \ell_{kpc} &\equiv \frac{C_{LP}}{C_{PC}}\,, \\ m_P &= C_{MP} \;\; 10^{51}\,[10^{-56}\, g]\,, & m_{56g} &\equiv C_{MP}\,, \\ m_P &= \frac{10\, C_{MP}}{C_{MS}} \;\; 10^{-48}\,[10^9 M_\odot]\,, & m_{9\odot} &\equiv \frac{10\, C_{MP}}{C_{MS}}\,, \end{aligned}$$

where the units for G are suitable for connecting velocities and densities in their respective natural units, while the two expressions for the Planck mass m_P allow us to compare it both with the dark matter particle mass m and with the total luminous mass M_L, so to construct the required ratios. The unit conversion scales (4.19) for radial positions, densities, and velocities thus read:

$$[x] = x_{sc}\frac{1}{m^2\xi}, \qquad x_{sc} = \frac{1}{4\pi} \;\; \frac{m_{56g}^2 m_{9\odot}\ell_{kpc}}{M_L} \;\; [kpc]\,, \tag{4.20a}$$

$$[\rho] = \rho_{sc}\, m^6 \xi^4, \qquad \rho_{sc} = (4\pi)^3 \frac{M_L^4}{m_{56g}^6 m_{9\odot}^3 \ell_{kpc}^3} \left[\frac{10^9 M_\odot}{kpc^3}\right], \tag{4.20b}$$

$$[v] = v_{sc}\, m\xi, \qquad v_{sc} = \sqrt{4\pi}\, \frac{10^2\sqrt{4\pi}\, c_c M_L}{m_{56g} m_{9\odot}} \left[\frac{km}{s}\right], \tag{4.20c}$$

where the dependence on the free parameters m, ξ has been isolated in view of the fitting procedure.

4.3.3 Fitting procedure

Our model includes four free parameters: the parameter Q arising from the experimental data, the excitation index n selecting the state to be used for predictions and the physical parameters ξ and m involved in the conversion from physical to non-dimensional units. We need to define a convenient procedure to obtain optimal values for these parameters, where optimality means that the prediction for the total velocity $V_{Tot}^{Pred}(R)$ should be as close as possible to the experimental curve $V_{Tot}^{Exp}(R)$ according to a suitable metric, while the computational effort should not be too large.

As anticipated in the introduction to this Chapter, the main difficulty we need to face compared to other literature works consists of the lack of explicit expressions for the predicted dark matter velocity component $V_{DM}^{Pred}(R)$, which prevents us from using standard approaches, such as the popular MCMC method. Our prediction is defined implicitly by the stationary Schrödinger-Poisson problem (**??**) and we need to solve it for every candidate set of free parameters to get a prediction. This constraint is rather demanding in terms of computational effort. Simply testing a uniform grid of values for the free parameters without assuming any prior knowledge is not an efficient choice, since many combinations would result in bad predictions that do not match the experimental scales. In order to save computational effort, we need a way to estimate a priori the rough behavior of our predictions, so to reject in advance unviable combinations of parameters. An efficient tool to perform this task is represented by the heuristic laws we derived in Chapter 3, which bridge the gap between having an implicit model and needing explicit predictions.

The core idea is to select some features of the eigenvelocities that are described by heuristic laws and to constrain them to match their experimental counterparts, so as to get a priori estimates of the free parameters. The available features include: the innermost local maximum $(\tilde{r}_0(n), \tilde{v}_0(n))$; the slope and intercept of the averaged mid-range region $\sigma(n)$, $q(n)$; the outermost local maximum $(\tilde{r}_{2n}(n), \tilde{v}_{2n}(n))$. Each of these features could be rescaled to physical units with conversion factors

(4.20) involving the free parameters Q, ξ, m, and the resulting value could be constrained to match its experimental counterpart. These features are not equally suitable for this task. For example, the eigenvelocities associated with excited Schrödinger-Poisson eigenstates only result in positive mid-range slopes, whereas experimental data admit even vanishing or negative slopes, preventing a consistent analytical comparison. Thus, for the sake of generality, we focus on the other features. The experimental counterpart of the innermost local extremum can be detected and enforced in the model, fixing the value of two of the free parameters. The experimental counterpart of the outermost local extremum, instead, is in general not detected by the measurements, which stop before the onset of the final Keplerian decline. We can thus assume that the experimental counterpart of the outermost local maximum occurs beyond the last measured point (R_{last}, V_{last}), namely at a larger radius and velocity. This results in two other constraints on the free parameters, not fixing their values but helping in rejecting unfeasible combinations of parameters.

In the following, we detail how the required reference features are detected in the experimental data, describe how to enforce them to obtain estimates and constraints on the free parameters, and select a convenient metric to test the quality of the fits.

Detecting reference features

We start by analyzing the experimental data to detect the required reference features. The first step consists of subtracting from the total velocity $V_{Tot}^{Exp}(R)$ the contributions $V_D(R)$, $V_B(R)$, $V_G(R)$ due to luminous sources, thus getting an experimental estimate of the velocity contribution $V_{DM}^{Exp}(R)$ due to dark matter. This is performed by computing:

$$|V_{DM}^{Exp}|V_{DM}^{Exp}(R) = |V_{Tot}^{Exp}|V_{Tot}^{Exp} - (|V_D|V_D + |V_B|V_B + |V_G|V_G) \tag{4.21}$$

where the absolute value follows the sign conventions described in [94]. Recall that, as explained in Section 4.2, contributions $V_D(R)$, $V_B(R)$ are proportional to tabulated curves $V_D^{(L)}(R)$, $V_B^{(L)}(R)$ through the factors $\Upsilon_D(Q)$, $\Upsilon_B(Q)$ that depend on the free parameter Q. Thus, the estimate of the dark matter contribution $V_{DM}^{Exp}(R)$ from the experimental data can be computed only for a given value of the parameter Q. For simplicity, we select a uniform range of values for Q and run through them, performing the rest of the procedure for each given value of Q and applying our constraints on the other free parameters n, ξ, and m.

Once the dark matter contribution $V_{DM}^{Exp}(R)$ is estimated from the experimental data, we can analyze it to detect our reference features. The last measured point (R_{last}, V_{last}) is obtained without any ambiguity. On the other hand, the definition of the point $(\tilde{R}_0, \tilde{V}_0)$ representing the experimental counterpart of the innermost local maximum $(\tilde{r}_0, \tilde{v}_0)$ requires more caution, since the experimental curve $V_{DM}^{Exp}(R)$ might not present a clear local maximum. We thus define the point $(\tilde{R}_0, \tilde{V}_0)$ as the onset of the mid-range region in the following sense. We perform a linear fit $V = CR + D$ in the central part of the curve $V_{DM}^{Exp}(R)$, using an arbitrary portion of the domain $[0.2R_{last}, 0.9R_{last}]$; we define $\tilde{R}_0$ as the innermost radius at which the curve $V_{DM}^{Exp}(R)$ grows larger than the linear fit, $V_{DM}^{Exp}(\tilde{R}_0) \geq C\tilde{R}_0 + D$; and we define $\tilde{V}_0$ as the corresponding velocity in the linear fit, $\tilde{V}_0 = C\tilde{R}_0 + D$.

Observe that with this strategy, the definition of the reference inner point $(\tilde{R}_0, \tilde{V}_0)$ accounts for the average behavior of the entire curve, which encompasses more information than the simple detection of a local maximum. An example of the detected reference points for the two galaxies UGC02953 and NGC5055 is reported in figure 4.2, showing the effectiveness of our definitions.

Enforcing the constraints

Once the reference points $(\tilde{R}_0, \tilde{V}_0)$ and (R_{last}, V_{last}) are detected, we can enforce a match with the corresponding predicted points $(\tilde{r}_0, \tilde{v}_0)$ and $(\tilde{r}_{2n}, \tilde{v}_{2n})$. Recall that the scales $[r]$, $[v]$ converting from non-dimensional to physical units depend on the free parameters ξ, m as in (4.20), with Q assumed to be fixed in performing this procedure; while the non-dimensional quantities $\tilde{r}_0$, $\tilde{v}_0$, $\tilde{r}_{2n}$, $\tilde{v}_{2n}$ depend only on n, as expressed by the heuristic laws derived in Chapter 3 and reported here:

$$\begin{aligned}
&\tilde{r}_0(n) = m_0\, n + q_0\,, && m_0 = 40.1\,, \quad q_0 = 124\,,\\
&\tilde{v}_0(n) = \beta_0\, \tilde{r}_0(n)^{\alpha_0}\,, && \beta_0 = 1.94\,, \quad \alpha_0 = -1.14\,,\\
&\tilde{r}_{2n}(n) = a_{2n}\, n^2 + b_{2n}\, n + c_{2n}\,, && a_{2n} = 133\,, \quad b_{2n} = 245\,, \quad c_{2n} = -185\,,\\
&\tilde{v}_{2n}(n) = \beta_{2n}\, \tilde{r}_{2n}(n)^{\alpha_{2n}}\,, && \beta_{2n} = 0.27\,, \quad \alpha_{2n} = -0.5\,.
\end{aligned}$$

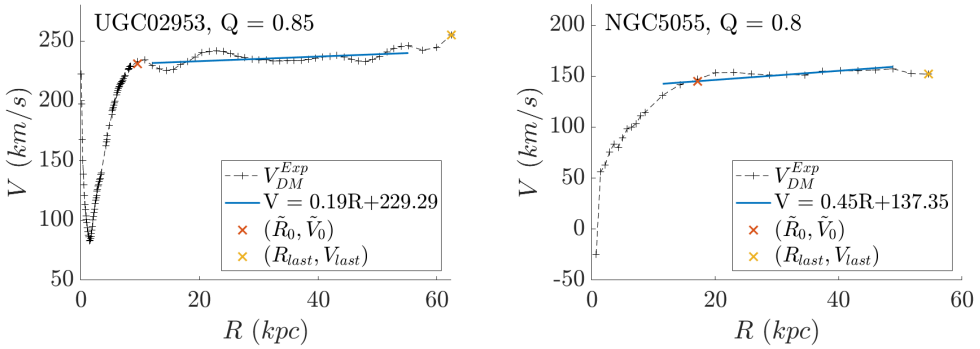

(a) Galaxy UGC02953, $Q = 0.85$.

(b) Galaxy NGC5055, $Q = 0.8$.

Figure 4.2: Dark matter velocity contribution $V_{DM}^{Exp}(R)$ for two sample galaxies, defined according to (4.21) for given values of Q. The plots report the linear fit $V = CR + D$ performed on an arbitrary central part $[0.2R_{last}, 0.9R_{last}]$ of the domain, the radius $\tilde{R}_0$ at which the curve $V_{DM}^{Exp}(R)$ first grows larger than the linear fit, and the corresponding velocity $\tilde{V}_0 = C\tilde{R}_0 + D$, together with the last measured point (R_{last}, V_{last}).

Based on this, we define the constraints, forcing exact matches for the inner point and inequalities for the outer point:

$$\begin{cases} \tilde{R}_0 &= [r]\,\tilde{r}_0 &= r_{sc}\frac{1}{m^2\xi} \quad (m_0 n + q_0) \\ \tilde{V}_0 &= [v]\tilde{v}_0 &= v_{sc}\,\xi m\,\beta_0 (m_0 n + q_0)^{\alpha_0} \\ R_{last} &\leq [r]\,\tilde{r}_{2n} &= r_{sc}\frac{1}{m^2\xi} \quad (a_{2n}n^2 + b_{2n}n + c_{2n}) \\ V_{last} &\leq [v]\tilde{v}_{2n} &= v_{sc}\,\xi m\,\beta_{2n}(a_{2n}n^2 + b_{2n}n + c_{2n})^{\alpha_{2n}} \end{cases}.$$

The two equations can be arranged to express the parameters ξ and m as functions of the excitation index n, while the two inequalities are rephrased as constraints on the value of n:

$$\begin{cases} m = \frac{r_{sc}}{\tilde{R}_0}\frac{v_{sc}}{\tilde{V}_0}\beta_0(m_0 n + q_o)^{\alpha_0+1} \\ \xi = \frac{r_{sc}}{\tilde{R}_0}\left(\frac{v_{sc}}{\tilde{V}_0}\right)^2 \frac{1}{\beta_0^2 (m_0 n + q_o)^{2\alpha_0+1}} \\ \frac{a_{2n}n^2 + b_{2n}n + c_{2n}}{m_0 n + q_0} \geq \frac{R_{last}}{\tilde{R}_0} \\ \frac{\beta_{2n}}{\beta_0}\frac{(a_{2n}n^2 + b_{2n}n + c_{2n})^{\alpha_{2n}}}{(m_0 n + q_0)^{\alpha_0}} \geq \frac{V_{last}}{\tilde{V}_0} \end{cases} \tag{4.22}$$

Observe that in the approximation $\alpha_0 \sim -1$, the exponent $\alpha_0 + 1$ in the expression for m would vanish. This suggests that the parameter m depends rather mildly on the excitation index n and that its value is mainly determined by the experimental data $\tilde{R}_0$, $\tilde{V}_0$ and by the free parameter Q, which is involved in the scales r_{sc}, v_{sc} through the total mass $M_L = M_L(Q)$ (4.12).

Together with these requirements, representing the core of our fitting procedure, we also set a maximum value ξ_{max} on the parameter ξ, arbitrarily modeling the physical intuition that the total amount of dark matter in a galaxy should not be exceedingly larger than the total amount of luminous matter.

Enforcing the match between experimental and predicted features provides an estimate for the free parameters ξ, m – with a threshold check on ξ – and two constraints on n. Observe that these estimates are rough, both due to the intrinsic ambiguity in the definition of the experimental reference points and due to the fact that the heuristic laws were derived in the absence of external source, while we are now computing the excited eigenstates in the presence of luminous sources. Thus, we use the estimates of ξ, m as reference values and include small variations in defining the parameter sets to be tested.

Predictions and optimality

The constraints we defined allow us to select feasible combinations of parameters a priori. Once the selection is performed, the combinations are tested, computing in each case the eigenstate $(f_n(r), \phi_n(r), v_n(r))$ in the presence of non-dimensional external sources. The eigenvelocity is expressed in physical units to obtain the predicted dark matter contribution $V_{DM} \equiv [v]v_n$ and the

latter is then combined with the velocity contributions from the luminous components to get the total predicted rotation curve $V_{Tot}^{Pred}(R)$:

$$|V_{Tot}^{Pred}|V_{Tot}^{Pred} = |V_D|V_D + |V_B|V_B + |V_G|V_G + |V_{DM}|V_{DM} \,. \tag{4.23}$$

Thus, we get a whole set of predictions, each derived from a different feasible combination of parameters, and we need to define a metric to measure the quality of each fit, deciding which are the optimal predictions and the optimal set of values for the free parameters. Consistent with a common choice in the literature, we rely on the χ^2-metric, a standard global metric that accounts for the quality of the fit at all points [99, 41, 111]. Let $\{R_j, (V_{Tot}^{Exp})_j \pm \sigma_j\}_{i=1}^K$ be the set of data points defining an experimental rotation curve, with R_j the radial position, $(V_{Tot}^{Exp})_j$ the corresponding rotation velocity of a test object, and σ_j the experimental error, and let $\{R_j, (V_{Tot}^{Pred})_j\}_{j=1}^K$ be the corresponding prediction from the Schrödinger-Poisson model, computed at the measured radial positions. Then the χ^2 metric evaluating the quality of the fit is defined by:

$$\chi^2 \equiv \frac{1}{K-k}\sum_{j=1}^{K}\frac{[(V_{Tot}^{Exp})_j - (V_{Tot}^{Pred})_j]^2}{\sigma_j^2} \,, \tag{4.24}$$

where K is the number of data points and $k = 4$ is the number of free parameters in the theory. The χ^2-metric measures the global deviation of the prediction from the experimental data, so the optimal fits are those with minimum χ^2 value.

Implementation scheme and parameters

The fitting procedure described above is implemented in `MATLAB`, resulting in an automated procedure that can be run for every galaxy in the SPARC database. Before presenting the results we obtained for two sample galaxies, UGC02953 and NGC5055, we collect here the parameters we adopted in the analysis, summarizing schematically the implemented fitting procedure.

First, a set of test values is fixed for the free parameter Q. In our fit examples, we use:

$$Q \in \{0.75, 0.8, 0.85, 0.9, 1.0, 1.1, 1.25\} \,.$$

For every value of Q, the following quantities are computed: the mass-to-light ratios Υ_D, Υ_B (4.5); the velocity components $V_D(R)$, $V_B(R)$ (4.7); the total luminous mass M_L (4.12); the experimental dark matter curve $V_{DM}^{Exp}(R)$ (4.21); and its reference points $(\tilde{R}_0, \tilde{V}_0)$ and (R_{last}, V_{last}).

Second, we fix a set of test values for n. In our case, we use:

$$n \in \{2, 3, 4, \ldots, 12\} \,.$$

For every couple (Q, n), the inequalities in (4.22) are evaluated, and the couple is accepted or rejected.

Third, for every accepted couple (Q, n), the equations in 4.22 yield estimated values ξ_{est} and m_{est} for the free parameters ξ and m, and a small set of values close to these estimates is tested. In our example, ξ is rounded up and down to an integer number and we test the neighbor values:

$$\xi \in \{\lfloor \xi_{est} \rfloor - 1, \lfloor \xi_{est} \rfloor, \lceil \xi_{est} \rceil, \lceil \xi_{est} \rceil + 1\} \,,$$

checking that these values are below the threshold $\xi \leq \xi_{max}$, set to $\xi_{max} = 100$; while m is rounded to the second digit, and some neighbor values are tested:

$$m \in \left\{ \frac{\lfloor 100 m_{est} \rfloor}{100} - 0.01, \frac{\lfloor 100 m_{est} \rfloor}{100}, \frac{\lceil 100 m_{est} \rceil}{100}, \frac{\lceil 100 m_{est} \rceil}{100} + 0.01 \right\} \,.$$

For each accepted combination (Q, n, ξ, m), the following quantities are computed: the unit conversion factors (4.20); the non-dimensional parameters defining the external sources $\rho_D(r)$, $\rho_B(r)$, $\rho_G(r)$, obtained by rescaling the corresponding physical quantities defined in (**??**); the n-th eigenstate $(f_n(r), \phi_n(r), v_n(r))$, accounting for the presence of the external sources; the dark matter velocity contribution in physical units $V_{DM}(R)$ (4.18); the total predicted rotation curve $V_{Tot}^{Pred}(R)$ (4.23); and the χ^2 metric (4.24).

With this procedure, a large set of viable combinations of parameters is tested and the resulting predicted curves are ordered according to the standard global metric χ^2. The optimal results for the two sample galaxies we use as a test are reported in the following Section.

4.4 Results

We report here the results obtained by fitting our model to the rotation curves of two sample galaxies: UGC02953, with bulge; and NGC5055, without bulge. The results, obtained with the implementation setting described in Section 4.3.3, are as follows.

Figure 4.3 compares for each galaxy the experimental rotation curve $V_{Tot}^{Exp}(R)$ with the five optimal predictions $V_{Tot}^{Pred}(R)$, where optimality is defined according to the χ^2 metric (4.24). The corresponding optimal sets of free parameters and the value of the χ^2 metric are also reported. In addition, the disk, bulge (if present), gas, and dark matter contributions to velocity are detailed for the optimal combination to appreciate their relative impact.

In both galaxies, the optimal parameter combinations favor a value of $Q \sim 0.8$, with slightly higher values for the UCG02953 galaxy, and slightly lower values for the NGC5055 galaxy. This value would result in mass-to-light ratios of $\Upsilon_D = 0.4\, M_\odot/L_\odot$ and $\Upsilon_B = 0.56\, M_\odot/L_\odot$, consistent with the literature values [107]. The optimal values for the excitation index n are slightly different for the two galaxies, but they are in an intermediate range $4 \lesssim n \lesssim 9$, while lower values $\{2, 3\}$ and higher values $\{10, 11, 12\}$ seem to be disfavored. Consistently, the values for the mass ratio ξ are in the range $[35, 55]$ for the UCG02953 galaxy and $[20, 35]$ for the NGC5055 galaxy, suggesting that the content of dark matter is rather large compared to luminous matter. Finally, the values favored for the dark matter particle mass m, expressed in units of 10^{-56} g, are constant across the five best predictions in the UGC02953 galaxy, $m = 0.12 \cdot 10^{-56}$ g, while they are slightly lower and spread more for the NGC5055 galaxy, $m \sim [0.09, 0.11] \cdot 10^{-56}$ g.

Concerning the optimal prediction, the visual comparison between the different velocity contributions suggests that they are comparable, that is, their density is similar in the central regions of the galaxy, while only at larger radial distances dark matter persists while the other components become negligible.

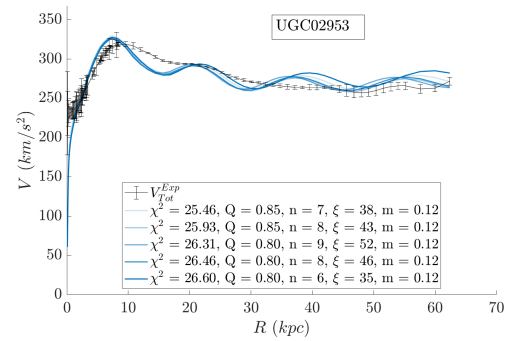

(a) UCG02953, total velocities.

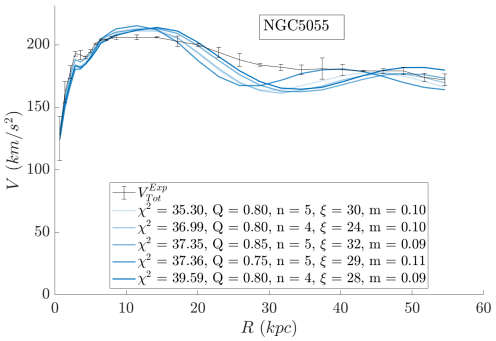

(b) NGC5055, total velocities.

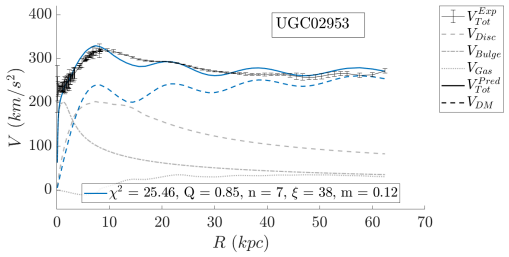

(c) UCG02953, velocity components.

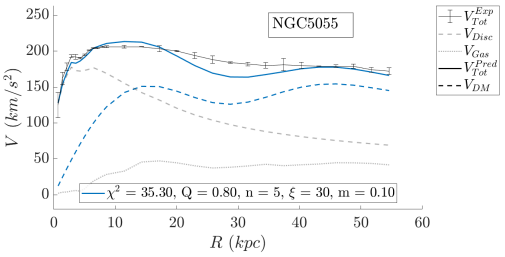

(d) NGC5055, velocity components.

Figure 4.3: Best fits obtained for the UCG02953 galaxy (left) and the NGC5055 galaxy (right). Top panels show the total rotation curves in the experimental data and in the five best predictions, sorted by increasing χ^2 value. The corresponding estimated parameters (Q, n, ξ, m) and the resulting χ^2 values are reported in the plots. Bottom panels focus on the optimal fit, detailing the experimental velocity contributions from the luminous sources (disk, bulge, gas) and the predicted dark matter velocity contribution.

In order to study the effect of each free parameter on the resulting predicted rotation curve, figures 4.4 and 4.5 let them vary one by one, while the other free parameters are kept fixed at their optimal

values. The overall results show that the non-dimensional eigenstate is very little affected by the luminous sources, which, with the tested values of free parameters, become negligible once scaled to non-dimensional units. On the other hand, their contribution to the rotation curve is clearly visible, and we can visually appreciate the difference in the predicted curve $V_{Tot}^{Pred}(R)$ as the parameters vary.

The last Figure 4.6 completes the study on the effect of each single free parameter by plotting the value of the χ^2 metric in six different panels, each constructed by letting two of the four free parameters vary and keeping the other two fixed at their optimal value. The construction of this plot involved testing a uniform grid of parameters around the optimal values, which required computing additional predictions, since the combinations analyzed with our fitting procedure did not cover systematically a uniform neighborhood of the optimal values, as required by this type of graph. This representation allows to appreciate how optimal regions generally favor intermediate values of the free parameters, confirming the results reported in the initial part of our analysis.

4.5 Conclusions

In this Chapter, we fit the stationary states of the SP problem to some sample experimental rotation curves from the SPARC database. This task is rather challenging due to the implicit form in which the SP eigenstates are defined, which causes parameter space exploration to be computationally very expensive. Instead of introducing approximations to express our predictions in explicit form, we reduce computational cost by exploiting the heuristic laws derived for the eigenvelocities to guide the parameter space exploration. Indeed, by comparing reference features of the experimental curves to their prediction according to the heuristic laws, we are able to recognize in advance viable combinations of parameter values, so to restrict the number of computations to be run. This represents a great computational advantage compared to testing all uniform combinations of parameters, which would be the natural choice in absence of heuristic laws: in that case, a large number of computations would fail to match even the roughest scales of experimental curves, resulting in an unnecessary computational effort.

On the other side, observe that more complete collections of data would improve even more the computational efficiency through the applications of the heuristic laws: if the experimental measures were spanning the whole extent of dark matter halos and the outermost peak were detected, then two further equalities could be written instead of the inequalities in constraint (4.22), and all four free parameters could be estimated a priori, minimizing the computational effort in performing the fit. Since this is not the case, there is still a certain arbitrariness in defining the optimal set of fitting parameters, which requires further physical considerations to be fixed. This, however, is out of the scope of this thesis, which is limited to showing the potential of heuristic laws in physical and numerical applications.

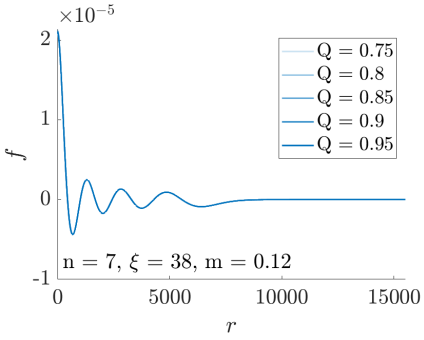

(a) $f_n(r)$, varying Q.

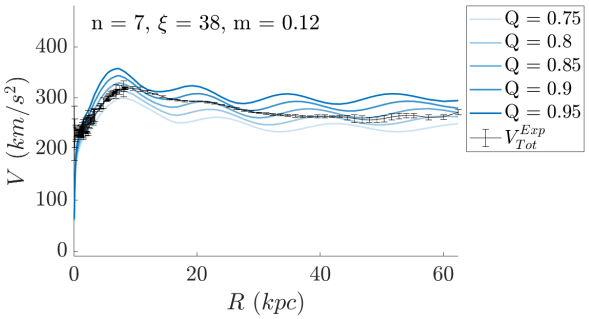

(b) $V_{Tot}(R)$, varying Q.

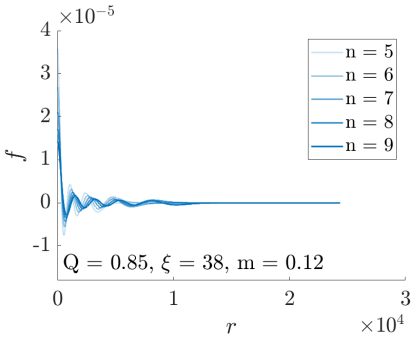

(c) $f_n(r)$, varying n.

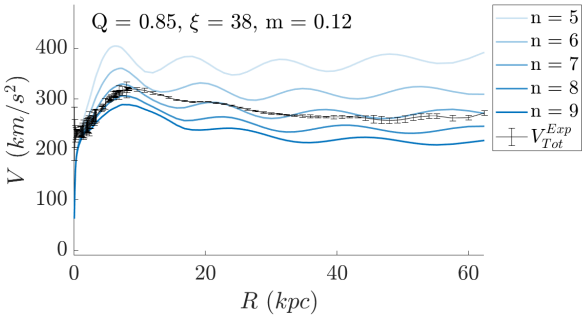

(d) $V_{Tot}(R)$, varying n.

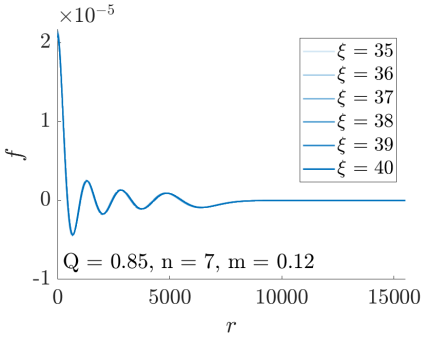

(e) $f_n(r)$, varying ξ.

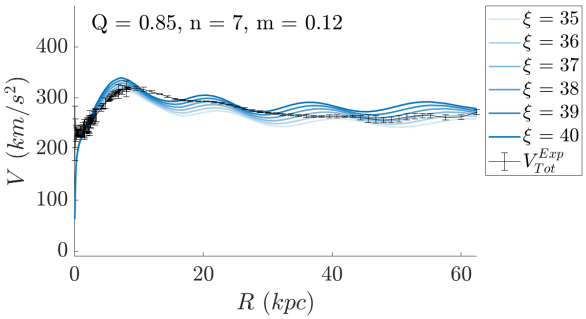

(f) $V_{Tot}(R)$, varying ξ.

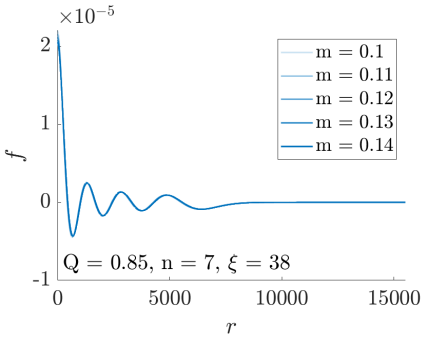

(g) $f_n(r)$, varying m.

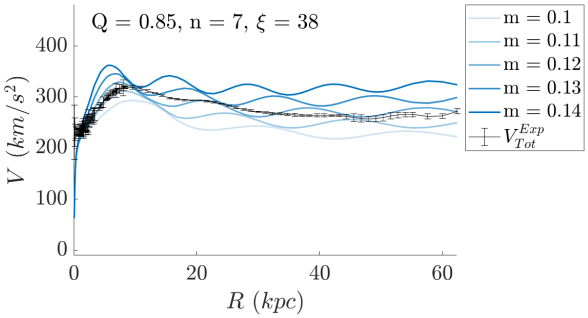

(h) $V_{Tot}(R)$, varying m.

Figure 4.4: Galaxy UGC02953. Panels report eigenfunctions $f_n(r)$ (left) and total rotation curves $V_{Tot}^{Pred}(R)$ (right) for one-by-one variations of each parameter: Q, n, x, m (from top to bottom). The optimal combination $\{Q = 0.85,\ n = 7,\ \xi = 38,\ m = 0.12\}$ is used as a reference.

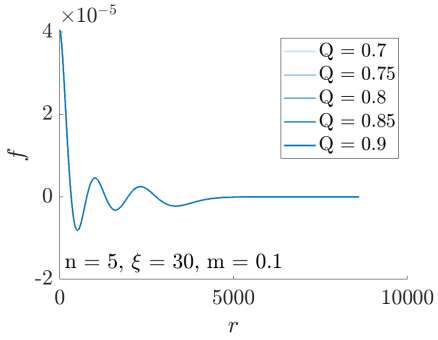

(a) $f_n(r)$, varying Q.

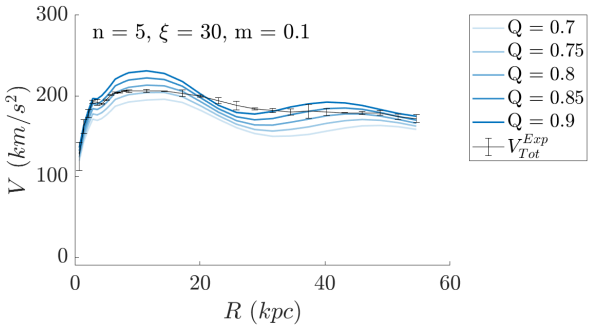

(b) $V_{Tot}(R)$, varying Q.

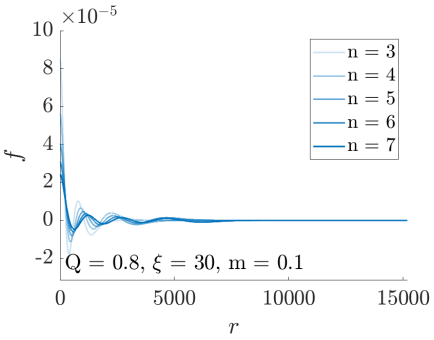

(c) $f_n(r)$, varying n.

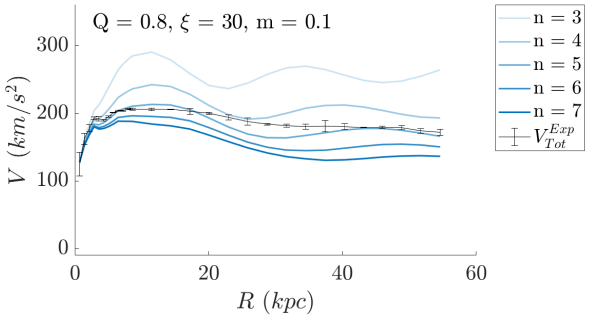

(d) $V_{Tot}(R)$, varying n.

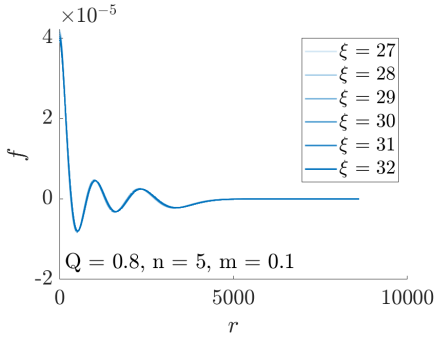

(e) $f_n(r)$, varying ξ.

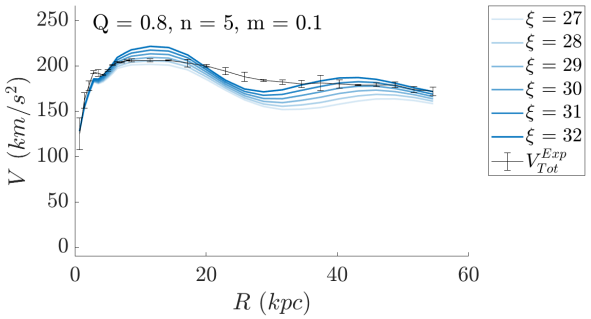

(f) $V_{Tot}(R)$, varying ξ.

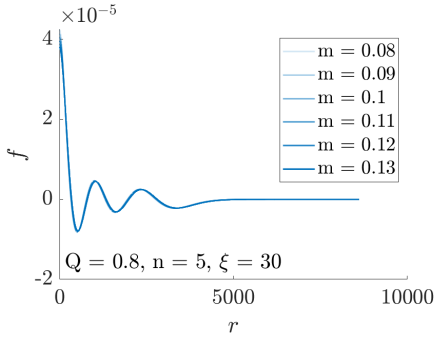

(g) $f_n(r)$, varying m.

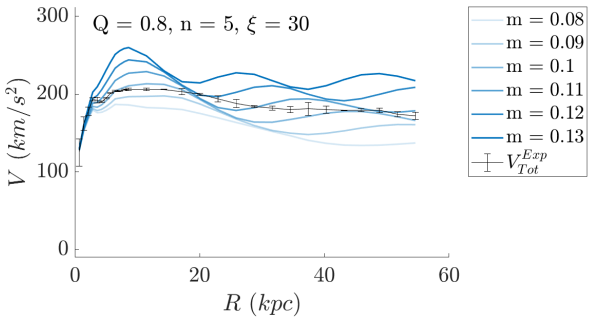

(h) $V_{Tot}(R)$, varying m.

Figure 4.5: Galaxy NGC5055. Panels report eigenfunctions $f_n(r)$ (left) and total rotation curves $V_{Tot}^{Pred}(R)$ (right) for one-by-one variations of each parameter: Q, n, x, m (from top to bottom). The optimal combination $\{Q = 0.8,\ n = 5,\ \xi = 30,\ m = 0.1\}$ is used as a reference.

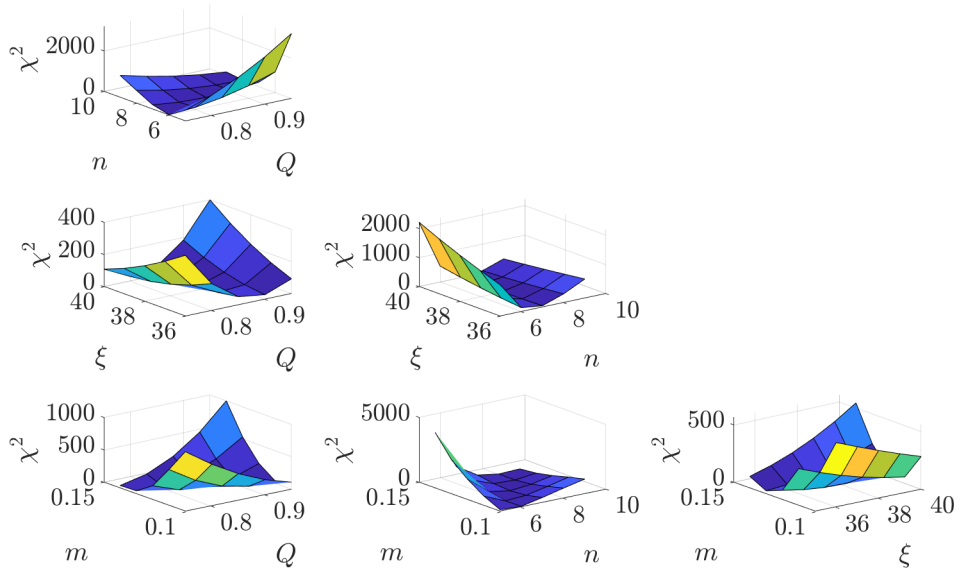

(a) UCG02953

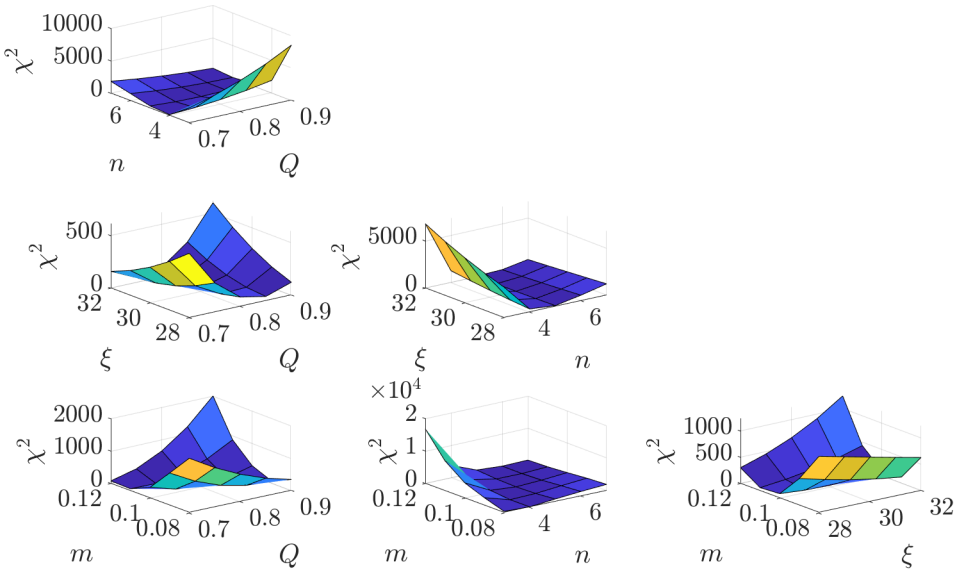

(b) NGC5055

Figure 4.6: Values of the χ^2 metric for slices of the tested parameter space. Plots are reported for the UCG02953 galaxy (top) and the NGC5055 galaxy (left).

Chapter 5

A Relativistic Extension: the Klein-Gordon-Wave Model

5.1 Introduction

The Schrödinger-Poisson system analyzed in this thesis is not Lorentz invariant. As described in Chapter 2, it is obtained in the weak field and low energy limit from the Einstein-Klein-Gordon system, and the structure that characterizes it is not compatible with a relativistic formalism, lacking even Lorentz covariance. In this Chapter, we consider alternative models to Schrödinger-Poisson that share the same basic idea – a simple mathematical structure for an effective description of a system of self-gravitating particles – but that present a semi-relativistic or relativistic structure, positioned halfway between the fundamental Einstein-Klein-Gordon system and the effective Schrödinger-Poisson approximation.

In the past decades, wide research efforts have been dedicated to the definition and the analysis of classical semi-relativistic or non-relativistic approximations of the Einstein-Klein-Gordon equations. The emerging systems, among which Schrödinger-Poisson, share the same common intuition: modeling the evolution of a scalar matter field and a scalar gravitational potential field, coupled through a Yukawa interaction. The differences lie in the specific assumptions made for the two fields, such as the inclusion of a massive term for the gravitational field or the adoption of a Lorentz covariant structure for the two evolution equations. Different assumptions may result in extremely different dynamical properties, including the existence and uniqueness of the solutions of the associated initial value problems, the stability near the equilibria or the number of conservation laws. Most of these systems share an underlying Hamiltonian structure, which enables the application of Hamiltonian-specific tools to explore their connection. A valuable example is the construction of Hamiltonian normal forms through which a Hamiltonian system can be expressed in a simpler, more controllable way and can be approximated at a given order, neglecting the higher-order remainder to obtain a new system displaying the most relevant properties of the dynamics.

In this Chapter, we refer to two of these systems, which complement Schrödinger-Poisson. The first is a Klein-Gordon–Wave (KGW) model, which assumes a Klein-Gordon dynamics for the massive field $u(t,x)$ and a wave dynamics for the massless gravitational field $\phi(t,x)$:

$$\begin{cases} \Box u = \mu^2 u + 2\phi u \\ \Box \phi = u^2 \end{cases} , \quad \Box \equiv \Delta - \partial_t^2 \,, \tag{5.1}$$

with $\mu^2 \in \mathbb{R}_0^+$ a parameter of the model. This model has the distinctive feature of being Lorentz covariant, that is, having a structure compatible with a special relativity framework. Among systems with this characteristic, it is as similar as possible to Schrödinger-Poisson, having a Hamiltonian formulation and presenting the same coupling between the matter field and the gravitational field. Unlike Schrödinger-Poisson, however, the Klein-Gordon-Wave dynamics does not preserve the $L^2(\mathbb{R}^3)$-norm of the matter field, which represents the amount of mass in the system.

The second model we consider is a Schrödinger-Wave (SW) model. This system, with intermediate properties between Schrödinger-Poisson and Klein-Gordon-Wave, assumes a Schrödinger dynamics for

the matter field $\psi(t,x)$ and a wave dynamics for the gravitational potential $\phi(t,x)$:

$$\begin{cases} i\partial_t\psi = -\frac{1}{2}\Delta\psi + \phi\psi \\ \Box_\varepsilon\phi = |\psi|^2 \end{cases} \quad , \quad \Box_\varepsilon \equiv \Delta - \varepsilon\partial_t^2 \tag{5.2}$$

with ε a parameter of the model, often set to $\varepsilon = 1$. The SW system (5.2) is semi-relativistic, assuming Lorentz covariance for the gravitational field but not for the matter field. Thanks to this structure, its dynamics preserves the $L^2(\mathbb{R}^3)$-norm of the matter field, as happens in Schrödinger-Poisson, while having a Hamiltonian structure that is closer to that of the KGW problem.

Our research investigates the relationship between these three models, based on their Hamiltonian formulation and the above-mentioned normal form techniques. In particular, we derive the second-order Hamiltonian normal form of the Klein-Gordon-Wave system and we show that its first-order truncation results in the Schrödinger-Wave model, which further reduces to the Schrödinger-Poisson system in the singular limit of a vanishing perturbative parameter. Our constructive technique offers a new point of view on how these systems relate to each other, clarifying how Lorentz covariance is gradually lost and a conservation law is gained in the approximation process.

From a normal form perspective, the approach we use for the Klein-Gordon-Wave problem is nontrivial. Unlike other standard problems with bounded unperturbed flow – such as the Birkhoff-Gustavson problem, which describes a set of harmonic oscillators with higher-order couplings – the unperturbed flow of the Klein-Gordon-Wave system includes an unbounded contribution of free-particle type. This prevents the direct application of standard averaging procedures in the definition of normal form. To address this issue, we construct the normal form only with respect to the unperturbed contribution with bounded flow, a restriction that reflects in a non-trivial modification of the standard computations. The resulting procedure is, at present, still formal, but its versatility, together with the understanding it provides on the connection between well-studied physical systems, attests its validity in supporting research on physically relevant dynamical systems.

In the remainder of this preamble, in Section 5.1.1 we briefly present the KGW and SW models, illustrating the contexts from which they emerge and describing the most relevant literature work on them. In the same Section, we summarize the main results of our research on this topic and place them within the broad literature on normal forms of Hamiltonian systems.

In Section 5.2, we give a more thorough description of the KGW model, highlighting its Lagrangian and Hamiltonian formulations and the symmetries and conservation laws that characterize it. We also illustrate its construction from physical assumptions, highlighting the connections with the heuristic presented in Chapter 2 and the interpretation that emerges for the μ^2 parameter. We observe how the latter has a governing role, determining two regimes in which the KGW model can operate. In the first regime, when $\mu^2 = \mathcal{O}(1)$, the system admits stationary states, and these formally coincide with the stationary states of the Schrödinger-Poisson system. In the second regime, when $\mu^2 \gg 1$, stationary states are not admitted, but it is possible to approximate the system with Hamiltonian perturbative normal form techniques. We briefly illustrate the physical meaning of the two regimes, showing the physical situations with which they are compatible and clarifying the physical interpretation of the governing parameter μ^2. Finally, we introduce some preliminary notions for the normal form study of the models.

In Section 5.3, we present in detail the results of our analysis, showing the normal form obtained for the KGW Hamiltonian and illustrating the systems that emerge from its truncation at the first and second order (Sections 5.3.1, 5.3.2), with a specific focus on the limit recovering the SP system (Section 5.3.1). A discussion of the interpretation of the KGW system as a set of harmonic oscillators and free particles with higher-order coupling is also included (Section 5.3.3).

Section 5.4 is dedicated to explicit computation of the first- and second-order normal form, each step being first performed in algebraic form and then specialized to the KGW problem. Remarks on the extension of the procedure to higher orders are also included (Section 5.4.5).

5.1.1 Comparison with previous works and main results

The KGW system (5.1) we analyze in this Chapter emerges as a particular case of a class of problems introduced by LeFloch and Ma [91] and Ionescu and Pausader [74] as a simplified version of the Einstein–Klein–Gordon equations of general relativity, with the aim of studying their global nonlinear

stability. Problems in this class take the form:

$$\begin{cases} (-\Box + 1)u = \phi B^{\alpha\beta}\partial_\alpha\partial_\beta u + E\phi u \\ -\Box\phi = A^{\alpha\beta}\partial_\alpha u\,\partial_\beta u + Du^2 \end{cases},$$

with u representing the massive scalar field, ϕ replacing the deviation of the Lorentzian metric from the Minkowski metric, and $A^{\alpha\beta}, B^{\alpha\beta}, D, E$ real constants. This system is obtained by expressing the Einstein–Klein–Gordon equations of general relativity in harmonic gauge, and by retaining only, schematically, quadratic interactions that involve the massive scalar field [74]. In this work, we specialize to $A^{\alpha\beta} = B^{\alpha\beta} = 0$ and adjust the remaining constants to obtain the KGW system (5.1).

This class of problems has attracted considerable interest, initiating a series of sophisticated mathematical works that have studied their global nonlinear stability. The latter was first proved in the case of small, smooth and compactly supported perturbations using the hyperboloidal foliation method [91, 93] (see also [90] for a detailed description of the method) and then extended with different techniques to relax the compact support hypothesis [74, 76]. Later studies focused on specific configurations of this class of problems [44, 116]. This series of works provided a solid foundation for analyzing the same results for the more general Einstein-Klein-Gordon system [92, 75, 76, 143].

In the $\mu^2 \gg 1$ regime, the KGW system (5.1) can be approximated to the leading order, as detailed below, by the Schrödinger-Wave system (5.2). This system, mostly studied in the literature for $\varepsilon = 1$, is a particular case of the more general Schrödinger-Klein-Gordon (SKG) model, which assumes the gravitational field $\phi(t, x)$ to be massive:

$$\begin{cases} i\partial_t\psi = -\frac{1}{2}\Delta\psi + \phi\psi \\ (\Box + m)\phi = |\psi|^2 \end{cases}.$$

The analytical properties of the Schrödinger-Klein-Gordon system have been thoroughly analyzed. The global well-posedness of the associated Cauchy problem was first established by Fukuda and Tsutsumi [51] on a bounded domain; then it was extended by Baillon and Chadam [10] to the case $x \in \mathbb{R}^3$ (see also [72]); while Bachelot [8] relaxed the smallness assumption on the initial data and addressed a larger class of couplings, overcoming the limitations of standard fixed-point techniques by exploiting the $L^2(\mathbb{R}^3)$-norm conservation of the matter field rather than the energy conservation. More recent results by Colliander et al. [39], Pecher [118] (see also [1]) extended the global well-posedness to solutions with different regularity. Ginibre and Velo [54] specialized to the SW system (5.2) with a massless gravitational field to prove the existence of wave solutions and study their asymptotic behavior in time, while Ohta [115] first focused on the orbital stability of the ground standing wave solution, a result that was then thoroughly discussed in a series of works for the massive gravitational field case [84, 85, 83].

The wide interest in the Schrödinger-Klein-Gordon and Schrödinger-Wave models is motivated by their connection with the Nelson model, a consistent quantum field theory constructed by Nelson [114] that describes the Yukawa-like interaction of a non-relativistic nucleon field with a relativistic meson field. Ever since the introduction of the Nelson model, the SKG system is considered the classical limit of this theory, a result later proved by Ammari and Falconi [5]. Based on preliminary studies [47, 4], the latter authors manipulate the classical Schrödinger-Klein-Gordon system through Hamiltonian normal form techniques: using the flow of a suitably defined generating Hamiltonians as change of variables, they rewrite the system in a form that is suitable for quantization, avoiding – even in infinite-dimensional spaces – the incurrence of divergences and thus the necessity of cutoffs.

The technique we use in our work to show that the SW system (5.2) approximates the KGW system (5.1) in the $\mu^2 \gg 1$ limit is based on Hamiltonian perturbation theory. More precisely, we rely on normal forms, which express dynamical systems – not necessarily Hamiltonian – highlighting their underlying hierarchical structure and facilitating their qualitative and quantitative understanding [6, 52, 37]. Through normal forms, the functionals defining the problem – such as the Hamiltonian, or the vector fields for generic PDEs and ODEs – are first expressed as series of terms, each representing a higher-order correction to the order zero, and then manipulated to shift the corrections to higher orders. This structure is often interpreted in terms of perturbations, with a perturbative parameter – either naturally present in the problem or manually added as an auxiliary bookmark – discriminating the order of the corrections. The zero-order term is referred to as the unperturbed term. In the final form, low-order contributions that cannot be removed have the special property of being preserved by the flow of the unperturbed term. Once in normal form, approximations of the

system can be constructed by truncating higher-order residual terms, that are small in the perturbative parameter. Thus, systems with different mathematical properties can be connected, interpreting one as an approximation of the other at a given order, with explicit estimates on the higher-order corrections. In our case, we construct the normal form of the KGW Hamiltonian to the second order in $\varepsilon = \mu^{-2}$ and show that its first-order truncation results in the SW Hamiltonian.

The construction of normal forms is based on the iterative application of near-identity variable transformations, each bringing the functional, in our case the Hamiltonian, to a successive order of the normal form. According to the Poincaré procedure [52], the transformations are often expressed as a conveniently selected series expansion with unknown coefficients, which are determined by requiring the transformation to map the problem into normal form.

For Hamiltonian systems, such a transformation does not ensure canonicity and could modify the symplectic structure of the problem. A more convenient choice, known as the Lie transform method [14], consists of defining the variable transformations as flows of auxiliary generating Hamiltonians to be determined, ensuring canonicity. The unknown Hamiltonians are found by requiring the transformation to map the problem into normal form. This step reduces to solving a homological equation at each order, which has as unknowns the new normal form correction term and the generating Hamiltonian. The homological equations can be solved either through appropriate series expansions with unknown coefficients or via the so called averaging principle [53], a procedure that consists of appropriately averaging the homological equations to derive the unknowns without any assumption on their specific form. The advantage of the latter procedure, which is purely algebraic, lies in its independence from the choice of coordinates, which facilitates the interpretation of the results.

The averaging principle is based on the hypothesis that the unperturbed flow is bounded, which is necessary to construct well-defined time averages along the unperturbed flow. This condition is satisfied for integrable systems and in particular for Birkhoff systems (Birkhoff-Gustavson problem [27, 63]), consisting of perturbations of N harmonic oscillators with frequencies $\{\omega_k\}_{k=1}^N$, whose unperturbed dynamics preserves the actions I_k and evolves the angles on a torus, $\dot{\theta} = \omega_k$, with Hamiltonian $\sum_{k=1}^N \omega_k I_k$ [22]. A simple but meaningful extension of the Birkhoff problem consists of adding M free particles to the system, decoupled from the oscillators in the unperturbed problem. The resulting Hamiltonian reads:

$$K_0 = \sum_{k=1}^{N} \omega_k I_k + \sum_{k=1}^{M} \frac{p_k^2}{2} \tag{5.3}$$

and the associated Hamiltonian dynamics $\dot{\theta} = \omega_k$, $\dot{q_k} = p_k$ is bounded in the angles but not in the free particle coordinates, which undergo a linear unbounded growth. This unboundedness prevents the computation of the time averages along the unperturbed flow, that would be necessary to compute the Hamiltonian normal form according to the standard techniques [53].

Indeed, the unperturbed Hamiltonian of the KGW system (5.1) is an infinite-dimensional version of the Hamiltonian (5.3) (see Sec. 5.3.3 for a detailed description) and our study extends the Hamiltonian normal form construction to any problem where the unperturbed flow has two decoupled components, one with bounded flow and one with unbounded flow. In particular, we address this issue by computing time averages only along the bounded component of the unperturbed flow while keeping the free particle component fixed, a modification that reflects in a nontrivial way in the computations. Although our system is completely resonant ($\omega_k = 1$ for all k), the same procedure can also be applied in the presence of resonant frequencies, with due caution in treating possible small divisors.

A major problem in Hamiltonian perturbation theory consists of controlling the remainders: they should be estimated to verify their smallness, and in neglecting them, the difference between the solutions of the original system and those of the truncated system should be controlled. These controls are extremely delicate even when dealing with finite-dimensional systems. Notable work in this regard can be found in [142, 77, 148, 149, 134, 127, 32]. The extension to the infinite-dimensional case is even more delicate as it requires controlling possible divergences on an additional level. Remarkable examples in this direction can be found in [87, 61, 79, 16, 17, 13, 15, 18, 12]. In the case addressed in this work, we limit ourselves to giving a formal definition of normal form for the Klein-Gordon-Wave problem, deferring the careful analysis of its well-posedness to a more technical work. The focus of this study is on showing how standard procedures can be adapted to include unperturbed flows with an unbounded component and on demonstrating, in our specific case, how they can relate dynamical systems of physical relevance.

5.2 Model

In this Section we give a thorough presentation of the KGW system, intended as the relativistic generalization of the SP system analyzed in the previous Chapters. We first detail its mathematical structure, showing its Lagrangian and Hamiltonian formulations and presenting its symmetries. Then, we show its heuristic derivation from physical principles, describing the scalings needed to write it in non-dimensional form and elucidating the physical meaning of the governing parameter μ^2. Based on its value, we identify the two main regimes in which the system operates, showing which physical situations they are compatible with.

5.2.1 Mathematical Structure of the KGW system

The KGW system (5.1) describes the coupled evolution of a real massive field u, satisfying a Klein-Gordon equation, and of a real massless field ϕ, satisfying a wave equation. As usual, the square of the massive field u^2 represents the number density distribution of a cluster of particles, while the massless field ϕ models the gravitational potential generated by the particle distribution and acting on the particles themselves. Their coupling is compatible with a Lagrangian and a Hamiltonian formalism.

Lagrangian Formulation

The KGW system (5.1) admits a Lagrangian formulation. Let $u_t \equiv \partial_t u$ and $u_{x_j} \equiv \partial_{x_j} u$ for $j = 1, 2, 3$ denote the partial derivatives of the matter field u with respect to time t and space coordinates $x \equiv (x_1, x_2, x_3) \in \mathbb{R}^3$. A similar notation is adopted for the gravitational field ϕ, namely $\phi_t \equiv \partial_t \phi$ and $\phi_{x_j} \equiv \partial_{x_j} \phi$ for $j = 1, 2, 3$. The appropriate Lagrangian density is the following functional of the fields u, ϕ and their partial derivatives:

$$\mathscr{L} \equiv \frac{u_t^2 - \mu^4 u^2 - |\nabla u|^2}{2} + \frac{\phi_t^2 - |\nabla \phi|^2}{2} - u^2 \phi \, . \tag{5.4}$$

The associated action functional is $S = \int \mathscr{L} \, \mathrm{d}^3x \, dt$. To derive the equations of motion, we apply the principle of stationary action $\delta S = 0$, namely we look for the functions u, ϕ which let the differential of the action δS vanish for any increment δu and $\delta \phi$. These critical points of the action are characterized as the solutions of the following Euler-Lagrange equations:

$$\begin{aligned} \frac{\partial \mathscr{L}}{\partial u} - \sum_{j=1}^{3} \frac{\partial}{\partial x_j} \frac{\partial \mathscr{L}}{\partial u_{x_j}} - \frac{\partial}{\partial t} \frac{\partial \mathscr{L}}{\partial u_t} = 0 \, , \\ \frac{\partial \mathscr{L}}{\partial \phi} - \sum_{j=1}^{3} \frac{\partial}{\partial x_j} \frac{\partial \mathscr{L}}{\partial \phi_{x_j}} - \frac{\partial}{\partial t} \frac{\partial \mathscr{L}}{\partial \phi_t} = 0 \, , \end{aligned}$$

which coincide exactly with the KGW system (5.1).

Symmetries and Conservation Laws

The KGW system (5.1) exhibits three fundamental symmetries. Indeed, there are three transformations involving space and time coordinates that leave its Lagrangian density (5.4) invariant: time translation $t \to t + s$, for any $s \in \mathbb{R}$; space translation $x \to x + y$ for any $y \in \mathbb{R}^3$; and space rotation $x \to Ax$, for any $A \in SO(3)$.

According to Noether's theorem, each symmetry corresponds to a conservation law. The KGW dynamics thus preserves the following quantities: the energy functional, associated with time translation

$$H = \int \left(\frac{u_t^2 + \mu^4 u^2 + |\nabla u|^2}{2} + \frac{\phi_t^2 + |\nabla \phi|^2}{2} + u^2 \phi \right) \mathrm{d}^3x \, , \tag{5.5}$$

the total momentum, associated with space translation

$$\mathbf{P} = \int (u_t \nabla u + \phi_t \nabla \phi) \, \mathrm{d}^3x \, ,$$

the angular momentum, associated with space rotation

$$\mathbf{L} = \int x \wedge (u_t \nabla u + \phi_t \nabla \phi) \, \mathrm{d}^3x \, .$$

Unlike the SP problem, the KGW problem is not invariant under any gauge transformation of the matter field. As a consequence, the particle number $\int u^2(t,x)\,\mathrm{d}^3x$, namely the $L^2(\mathbb{R}^3)$-norm of the matter field, is not preserved by the dynamics.

A slight difference with respect to the SP case occurs also for the scaling:

$$\tilde{x} = N^{-1}x\,, \qquad \tilde{t} = N^{-1}t\,, \qquad \tilde{u} = N^2 u\,, \qquad \tilde{\phi} = N^2\phi\,, \qquad \tilde{\mu}^2 = N^2\mu^2\,, \tag{5.6}$$

which is the analogue of the SP transformation (1.6). While in the SP case the scaling preserved the equations while modifying the Lagrangian, resulting in a family of solutions with different constant of motions, the scaling (5.6) of the KGW problem also involves the governing parameter μ^2, which was not present in the SP problem. Thus, selecting a given value of μ^2 already uniquely identifies the solutions u, ϕ, avoiding the degeneracy that occurred in the SP case.

Hamiltonian Formulation

The KGW system (5.1) also admits a Hamiltonian formulation. Let $(u, p_u \equiv \partial_t u)$ and $(\phi, p_\phi \equiv \partial_t\phi)$ be the canonical conjugate variables, with the Poisson bracket:

$$\{F,G\} \equiv \int \left(\frac{\delta F}{\delta u}\frac{\delta G}{\delta p_u} - \frac{\delta F}{\delta p_u}\frac{\delta G}{\delta u}\right)\mathrm{d}^3x + \int \left(\frac{\delta F}{\delta \phi}\frac{\delta G}{\delta p_\phi} - \frac{\delta F}{\delta p_\phi}\frac{\delta G}{\delta \phi}\right)\mathrm{d}^3x\,,$$

equivalently expressed by the non-vanishing Poisson brackets on the fundamental variables:

$$\{u(x), p_u(y)\} = \delta(x-y) \quad , \quad \{\phi(x), p_\phi(x)\} = \delta(x-y)\,.$$

The Hamiltonian functional $H = \int \mathscr{H}\,\mathrm{d}^3x$ coincides with the conserved energy (5.5) derived from the time translation symmetry, expressed in terms of the conjugated variables:

$$H = \int \mathscr{H}\,\mathrm{d}^3x = \int \left[\frac{p_u^2 + \mu^2 u^2 + |\nabla u|^2}{2} + \frac{p_\phi^2 + |\nabla\phi|^2}{2} + \phi u^2\right],$$

where, with a convention that we adopt throughout the Chapter, we omit the d^3x symbol for space integration.

The resulting Hamilton equations

$$\begin{cases} \partial_t u &= \frac{\delta\mathscr{H}}{\delta p_u} = p_u \\ \partial_t p_u &= -\frac{\delta\mathscr{H}}{\delta u} = -\mu^2 u + \Delta u - 2\phi \\ \partial_t \phi &= \frac{\delta\mathscr{H}}{\delta p_\phi} = p_\phi \\ \partial_t p_\phi &= -\frac{\delta\mathscr{H}}{\delta \phi} = \Delta\phi - u^2 \end{cases}$$

coincide exactly with the Klein-Gordon-Wave system (5.1).

The integrals of motion derived with the Lagrangian formulation can be expressed in canonical variables, and their Poisson bracket against the Hamiltonian density $\mathscr{H}$ vanishes denoting preservation along the flow. Conversely, the Poisson bracket $\{\int u^2, H\}$ does not vanish, since the L^2-norm of the massive field is not a conserved quantity.

5.2.2 Physical derivation and scaling to non-dimensional formulation

The KGW system in physical units can be defined through few heuristic assumptions, which naturally lead to a Lorentz covariant formalism. Denote with U, Φ the massive and massless fields in physical units and with T, X the physical time and space variables. The construction of the system consists in considering a relativistic dispersion relation for both fields, massive for U and massless for Φ, and in first-quantizing the energy and momentum, $E = i\hbar\partial_T$ and $p = -i\hbar\nabla$:

$$\begin{aligned} &E^2 = p^2c^2 + m^2c^4 \quad &\Rightarrow \quad &-\hbar^2\partial_T^2(\cdot) = -\hbar^2c^2\Delta(\cdot) + m^2c^4(\cdot) \quad &\Rightarrow \quad &\partial_T^2 U = c^2\Delta U - \frac{m^2c^4}{\hbar^2}U \\ &E^2 = p^2c^2 \quad &\Rightarrow \quad &-\hbar^2\partial_T^2(\cdot) = -\hbar^2c^2\Delta(\cdot) \quad &\Rightarrow \quad &\partial_T^2\Phi = c^2\Delta\Phi \end{aligned}$$

The resulting Klein-Gordon and wave equations are then coupled through a minimal Yukawa interaction, with prefactors adjusted to preserve the underlying Hamiltonian formulation. This results in the KGW system, expressed in physical units:

$$\begin{cases} \Box U &= \frac{m^2c^2}{\hbar^2}U + 2\frac{m^2}{\hbar^2}\Phi U \\ \Box\Phi &= GmU^2 \end{cases}, \qquad \Box \equiv \Delta - c^{-2}\partial_T^2\,. \tag{5.7}$$

In addition, recall that the squared massive field $U^2(T,X)$ physically represents the number density distribution of the particles, and that the total number of particles $\int U^2(T,X)\,\mathrm{d}^3X$ is not preserved by the dynamics. We can still fix a time $t=0$ and use the total number of particles at that moment as a physical reference parameter, to keep the analogy with the SP problem:

$$N \equiv \int U^2(T,X)\,\big|_{T=0}\,\mathrm{d}^3X \ .$$

To cast the problem in non-dimensional units, we can proceed as we did in Chapter 4 (Sec. 4.3.1) for the SP system, defining generic transformations for all quantities:

$$X=[x]x, \quad T=[t]t, \quad U=[u]u, \quad \Phi=[\phi]\phi$$

and choosing the scales $[x]$, $[t]$, $[u]$, $[\phi]$ to progressively remove all physical parameters and constants from the equations (5.7). The time scale $[t]=c^{-1}[x]$ removes the constant c from the D'Alembert operator; the matter field scale $[U]=\sqrt{N}[x]^{-3/2}$ ensures a non-dimensional unitary normalization condition; the gravitational field scale $[\phi]\equiv GNm[x]^{-1}$ adjusts the wave equation; while the space scale $[x]\equiv\hbar^2(m^3GN)^{-1}$ removes the physical constants from the interaction term in the Klein-Gordon equations. The linear term in the Klein-Gordon equation is naturally non-dimensional, with the remaining physical constants and parameters collected in a single, non-dimensional governing parameter $\mu^2\equiv[x]^2m^2c^2\hbar^{-2}=\hbar^2c^2G^{-2}m^{-4}N^{-2}$. The physical system (5.7) thus reduces to the non-dimensional system (5.1).

Some remarks on these scalings are in order. Their definition, expressed purely in terms of the Planck constants $\ell_P\equiv\sqrt{\hbar Gc^{-3}}$, $t_P\equiv\sqrt{\hbar Gc^{-5}}$, $m_P\equiv\sqrt{\hbar cG^{-1}}$, of the mass ratio m_Pm^{-1} and of the initial number of particles N, reads:

$$X=[x]\,x, \qquad [x]=\left(\frac{m_P}{m}\right)^3 \quad N^{-1}\,\ell_P\,, \tag{5.8a}$$

$$T=[t]\,t, \qquad [t]=\left(\frac{m_P}{m}\right)^3 \quad N^{-1}\,t_P\,, \tag{5.8b}$$

$$U=[u]\,u, \qquad [u]=\left(\frac{m_P}{m}\right)^{-\frac{9}{2}} N^2 \quad \ell_P^{-\frac{3}{2}}\,, \tag{5.8c}$$

$$\Phi=[\phi]\phi, \qquad [\phi]=\left(\frac{m_P}{m}\right)^{-4} N^2 \quad \frac{Gm_P}{\ell_P}\,. \tag{5.8d}$$

First, we notice that the scalings for space $[x]$, matter field $[u]$ and gravitational field $[\phi]$ are the same (4.15) we derived in Section 4.3.1 for the SP problem[1]. The only different scaling is that on time $[t]$, which is now in line with the relativistic formalism we are adopting.

Second, as in the SP case, the space scale $[x]$ coincides with the characteristic length R (2.40) we derived in Chapter 2 (Sec. 2.5.2) for a virialized, completely condensed cluster of bosonic self-gravitating particles. This highlights the physical meaning underlying the KGW system: it encodes these heuristic assumptions and represents a virialized bosonic gas in complete Bose-Einstein condensation, whose characteristic extension depends only on the mass of the particles and on their number at a given instant of time. At the same time it displays a Lorentz covariant formalism that was lacking in the SP case, offering a generalization to that popular system.

Third, we derived a physical definition for the parameter μ^2 involved in the Klein-Gordon equation. Analogously to the typical scales, it depends solely on the mass ratio m_Pm^{-1} and on the initial number of particles N:

$$\mu^2\equiv\frac{1}{N^2}\left(\frac{m_p}{m}\right)^4 . \tag{5.9}$$

Similarly to the characteristic length R, its role is strictly related to the heuristic description of the system as a virialized, completely condensed bosonic gas, deeply influencing the interpretation of its dynamic behavior.

5.2.3 Two regimes of the KGW system

The parameter μ^2 defined in (5.9) has a fundamental role in determining the regimes in which the KGW system operates. To understand this point, consider again the heuristic study of Chapter 2 (Sec.

[1]Exception made for the 4π factors, that we included in the physical SP problem (4.13) in view of the comparison with the experimental data and that we omitted in the KGW model to simplify the notation.

2.5.2) for a virialized and completely condensed bosonic gas, and recall the parameter $\varepsilon = p^2(mc)^{-2}$ we derived there (2.41). This parameter was defined as the square of the ratio between two energies: the relativistic kinetic energy pc and the rest mass energy mc^2 of the system. Its value defined the energetic regime of the system: for high values of ε, the system exhibited relativistic behavior, while for low values the energy was sufficiently reduced to allow for a non-relativistic treatment. Our heuristic analysis showed that this parameter could be expressed in terms of the number of particles N and of their mass m (2.41).

The expression (5.9) we just derived for the KGW parameter μ^2 coincides exactly with the inverse of that parameter, $\mu^2 = \varepsilon^{-1}$. Its role in the KGW framework is therefore analogous: $\mu \sim mcp^{-1}$ represents the ratio between rest energy and momentum energy of the clustered matter, and its square μ^2 serves as a ruling parameter, with a non-relativistic regime when $\mu^2 \gg 1$ and a relativistic regime otherwise, $\mu^2 = \mathcal{O}(1)$.

The dependence of the parameter μ^2 on the number of particles N in the cluster and their mass m suggests that the amount of mass in a system is closely linked to the energetic regime in which it operates. Lighter masses m characterize low-energy systems, and for a given mass m – whose influence if greater than that of N due to the higher power – it is a low number of particles that favors a non-relativistic system.

Relativistic regime $\mu^2 = \mathcal{O}(1)$: stationary states

We consider the case $\mu^2 = \mathcal{O}(1)$, where the dimensionless parameter μ^2 assumes values of order unity or smaller. In this case, the system is in the relativistic regime, and the dynamics cannot be further simplified. In this regime, it is possible to investigate the presence of stationary states.

In the absence of gauge invariance, stationary states are time-independent solutions of the KGW system, $(u(x), \phi(x))$, denoted for convenience with the same symbols as their time-dependent counterparts. Moreover, by construction of the rescaling to non-dimensional quantities (5.8), the $L^2(\mathbb{R}^3)$-norm of the matter field u is unitary at time $t = 0$, and by stationarity this condition is preserved for all times. The stationary KGW problem therefore becomes:

$$\begin{cases} \Delta u = \mu^2 u + 2\phi u \\ \Delta \phi = u^2 \\ \int u^2(x)\,\mathrm{d}^3x = 1 \end{cases} . \tag{5.10}$$

This system is formally identical to the stationary SP problem (1.8) introduced in Chapter 1. All known results from the literature and the observations of Chapter (3) are therefore valid for KGW stationary states as well. In particular, the system (5.10) can be written by explicitly solving the equation for the gravitational field and substituting the result into the equation for the matter field, which assumes the known form of the Choquard equation:

$$\begin{cases} \Delta u + \dfrac{1}{2\pi}\left(\displaystyle\int_{\mathbb{R}^3} \frac{u^2(y)}{|x-y|}\,\mathrm{d}^3y\right) u = \mu^2 u & \text{(5.11a)} \\ \phi = -\dfrac{1}{4\pi}\displaystyle\int_{\mathbb{R}^3} \frac{u^2(y)}{|x-y|}\,\mathrm{d}^3y & \text{(5.11b)} \\ \displaystyle\int_{\mathbb{R}^3} u^2(x)\,\mathrm{d}^3x = 1 & \text{(5.11c)} \end{cases} .$$

The Choquard equation (5.11a) is still a nonlinear eigenvalue problem, with the matter field as eigenfunction and μ^2 as eigenvalue. Unlike the SP case, the latter now has a well-defined physical meaning, being linked to the number of particles N and their mass m through (5.9). Let us examine the consequences of this change.

When restricting to the spherically symmetric case, there exists an infinite discrete family of stationary states $\{\mu_n^2, u_n(r), \phi_n(r)\}_{n=0}^{\infty}$ whose eigenvalues μ_n^2 are positive and decrease monotonically to zero for growing n [101]. Given the physical interpretation of μ^2 in the KGW case, this means that stationary states are realized only for specific amounts of mass in the system, i.e., the values of N and m must be such as to realize one of the eigenvalues, $\mu^2 \in \{\mu_n^2\}_{n=0}^{\infty}$. Given the monotonicity of these eigenvalues, the ground state eigenvalue μ_0^2 represents a threshold: for values of $\mu^2 > \mu_0^2$, it is impossible to realize stationary states. This condition is consistent with the definition of regimes we have given, specifying that only in the relativistic regime $\mu^2 = \mathcal{O}(1)$ is it possible to realize stationary states.

It is interesting to ask whether this regime is compatible with physically observed systems. On this point, we limit ourselves to speculation, without advancing concrete physical proposals. We consider, for example, the case of primordial black holes, which are aggregates formed in the early phases of the universe and surviving to the present day as relics, remnants of an evaporation process. These objects were proposed by Carr and Hawking [34] as candidates for dark matter – a hypothesis that was highly regarded at the time – and were studied extensively. Their characteristic mass is of the order of the Planck mass $m \sim m_P$, so that an aggregate with $N \sim \mathcal{O}(1)$ particles would have a parameter μ^2 compatible with our regime. One can imagine that the evaporation process that led to their formation consisted of mass loss through diffusion, with mechanisms compatible with KGW, and that this process concluded once stationarity was reached, i.e., when the amount of mass was such that $\mu^2 \in \{\mu_n^2\}_{n=0}^{\infty}$. A model like KGW could therefore potentially explain, with an effective approach, cooling processes such as the evaporation of primordial black holes [34] and their stabilization around specific mass values.

Non-relativistic regime $\mu^2 \gg 1$: perturbative setting

We now turn our attention to the second regime, $\mu^2 \gg 1$, in which the kinetic energy of the system is sufficiently low to justify non-relativistic behavior. As illustrated in Chapter 2, this regime is particularly relevant in the study of galactic-scale aggregates, for which the characteristic quantities lead to a value $\mu^2 \sim 10^4 \gg 1$ compatible with this regime. In this case, it is possible to exploit the Hamiltonian structure of the KGW system to derive an approximation, using the inverse of the governing parameter, $\varepsilon \equiv \mu^{-2}$, as a small perturbative parameter. We lay the foundations of this approach here, then we formalize and develope it in detail in the following Sections.

We start our analysis by rewriting the KGW equations (5.1) highlighting time derivatives and performing a time rescaling, namely:

$$\begin{cases} \partial_{t'}^2 u + u = \frac{1}{\mu^2}(\Delta u - 2\phi u) \\ \partial_{t'}^2 \phi = \frac{1}{\mu^2}(\Delta\phi - u^2) \end{cases} \quad , \qquad t' = \mu t \tag{5.12}$$

With this manipulation, the parameter $\varepsilon \equiv \mu^{-2} \ll 1$ (small in the $\mu^2 \gg 1$ regime) appears in both right-hand sides. This endows the KGW equations with a perturbative structure: in the limit $\varepsilon \to 0$ – henceforth referred to as the unperturbed limit – the Klein-Gordon equation reduces to the harmonic oscillator equation $\partial_{t'}^2 u + u = 0$, while the wave equation becomes the free-particle equation $\partial_{t'}^2 \phi = 0$. The Laplacian terms and the interaction terms appear as corrections of order ε. The time rescaling preserves the Hamiltonian structure, which is now realized with conjugate variables $(u, p'_u \equiv \partial_{t'} u)$ and $(\phi, p'_\phi \equiv \partial_{t'}\phi)$. From now on, we work with this set of variables and neglect the superscript of time and momenta to simplify the notation. The Hamiltonian now reads:

$$H_\varepsilon = \underbrace{\int \frac{p_u^2 + u^2 + p_\phi^2}{2}}_{H_0} + \varepsilon \underbrace{\int \frac{|\nabla u|^2}{2} + \frac{|\nabla\phi|^2}{2} + \phi u^2}_{H_1} \quad , \quad \varepsilon \equiv \frac{1}{\mu^2}\,, \tag{5.13}$$

where we highlighted the unpertubed Hamiltonian H_0 and the first-order perturbation H_1. Observe that the unperturbed component H_0 includes two decoupled contributions: a harmonic oscillator Hamiltonian h in the massive field coordinates and a free particle Hamiltonian k in the massless field coordinates:

$$H_0 = h + k\,, \qquad h \equiv \int \frac{p_u^2 + u^2}{2}\,, \qquad k \equiv \int \frac{p_\phi^2}{2}\,, \qquad \{h, k\} = 0\,. \tag{5.14}$$

The first-order correction H_1 has a polynomial structure. It involves a contribution $Q_1(u)$ which scales quadratically with the massive field, a contribution $Q_2(\phi)$ which scales quadratically with the massless field, and an interaction contribution $C(u, \phi)$ which is cubic in the variables, depending quadratically on the massive field u and linearly on the massless field ϕ:

$$H_1 = Q_1(u) + Q_2(\phi) + C(u, \phi)\,,$$
$$Q_1(u) \equiv \int \frac{|\nabla u|^2}{2}\,, \quad Q_2(\phi) \equiv \int \frac{|\nabla\phi|^2}{2}\,, \quad C(u, \phi) \equiv \int \phi u^2\,.$$

We now perform a further change of variables on the massive field coordinates, which is suited for harmonic oscillators. Observe that, while convenient for computations, this change of variables is

not strictly necessary since the whole normal form construction is actually coordinate-free. The only assumptions, explained in detail in Section 5.3, concern the underlying structure of the unperturbed Hamiltonian H_0, described in (5.14) and independent of the specific choice of coordinates. We thus introduce the complex fields:

$$\psi = \frac{u + ip_u}{\sqrt{2}}\,, \qquad \psi^* = \frac{u - ip_u}{\sqrt{2}}\,, \tag{5.15}$$

which are an infinite-dimensional analogue of the complex Birkhoff coordinates for the harmonic oscillator [27]. The Hamiltonial in the new variables – still denoted by H_ε with abuse of notation – reads:

$$H_\varepsilon = \underbrace{\int \left[|\psi|^2 + \frac{p_\phi^2}{2} \right]}_{H_0} + \varepsilon \underbrace{\int \left[\frac{|\nabla\psi + \nabla\psi^*|^2}{4} + \frac{|\nabla\phi|^2}{2} + \frac{\phi(\psi+\psi^*)^2}{2} \right]}_{H_1}, \tag{5.16}$$

where now $h = \int |\psi|^2$ and $k = \int \frac{p_\phi^2}{2}$. Observe that the change of variables is non-canonical, so the Poisson brackets need to be updated:

$$\{\psi(x), \psi^*(y)\} = -i\delta(x-y)\,, \qquad \{\phi(x), p_\phi(x)\} = \delta(x-y)\,. \tag{5.17}$$

These coordinates are suitable for studying the flow of the unperturbed system, which is fundamental in the application of the averaging principle discussed below. The unperturbed equations are:

$$\begin{cases} i\partial_t\psi &= \psi \\ -i\partial_t\psi^* &= \psi^* \\ \partial_t\phi &= p_\phi \\ \partial_t p_\phi &= 0 \end{cases} \tag{5.18}$$

and the associated flows are easily obtained:

$$\begin{aligned} \Phi_h^s(\psi, \psi^*, \phi, p_\phi) &= (e^{-is}\psi,\, e^{is}\psi^*, \phi, p_\phi)\,, \\ \Phi_k^s(\psi, \psi^*, \phi, p_\phi) &= (\psi, \psi^*, \phi + p_\phi s,\, p_\phi)\,, \end{aligned} \tag{5.19}$$

and the flow along the unperturbed Hamiltonian H_0 is the composition of the flows along the two commuting components h and k: $\Phi_{H_0}^s = \Phi_{h+k}^s = \Phi_h^s \circ \Phi_k^s$.

Observe that the unperturbed flow Φ_h^s of the harmonic oscillator Hamiltonian h is bounded, since it involves only phase shiftings. In contrast, the flow Φ_k^s of the free particle Hamiltonian k is unbounded, growing linearly with time. The presence of an unbounded component in the flow of the unperturbed Hamiltonian represents the main difference with respect to the ordinary Birkhoff problem, and the main obstacle to the application of the standard averaging principle technique.

5.2.4 Preliminaries to the Normal Form Result

Before stating our main result on the perturbative regime, let us report some standard definitions and properties that are common in Hamiltonian normal form techniques and that will be used in the following.

Definition 5.1 (Lie derivative operator)**.** Let K be an Hamiltonian, with X_K the associate Hamiltonian vector field. The Lie derivative L_K of a functional F along the vector field X_K is defined by [6]:

$$L_K F \equiv \{F, K\} = X_K \cdot \nabla F\,.$$

Observe that with this definition, the operator L_K inherits all the properties of the Poisson brackets, such as linearity ($L_{K_1+K_2} = L_{K_1} + L_{K_2}$) and antisymmetry ($L_{K_1}K_2 = -L_{K_2}K_1$). In addition, if two Hamiltonians commute, $\{K_1, K_2\} = 0$, then the corresponding Lie derivative operators commute: $L_{K_1}L_{K_2} = L_{K_2}L_{K_1}$.

Lemma 1 (Flow composition)**.** *The composition of a functional F with the flow Φ_K^s of the Hamiltonian K can be expressed as:*

$$F \circ \Phi_K^s = e^{sL_K} F = (1 + L_K + \frac{1}{2}L_K^2 + \dots)\,, \tag{5.20}$$

where the exponential form of the flow composition allows for a formal Taylor expansion.

Definition 5.2 (Time average along the flow)**.** The time average of a functional F along the flow Φ_K^s of the Hamiltonian K is defined as

$$\overline{F}^K \equiv \lim_{t\to\infty} \frac{1}{t}\int_0^t F\circ\Phi_K^s \,\mathrm{d}s = \lim_{t\to\infty}\frac{1}{t}\int_0^t e^{sL_K}F\,\mathrm{d}s\,.$$

For periodic flows Φ_K^s with fundamental period T, the definition is equivalent to averaging on the period:

$$\overline{F}^K = \frac{1}{T}\int_0^T e^{sL_K}F\,\mathrm{d}s\,.$$

Observe that in this study we will need to compute only time averages along the 2π-periodic flow of the unperturbed Hamiltonian component h defined in (5.14). To simplify the notation, we will omit the superscript h, denoting only by $\overline{F}$ the time average along the flow Φ_h^s:

$$\overline{F} = \overline{F}^h = \frac{1}{2\pi}\int_0^{2\pi} e^{sL_h}F\,\mathrm{d}s\,.$$

Definition 5.3 (Deviation from the average)**.** Let h be the Hamiltonian defined (5.14). The difference of a functional F with respect to its time average along the flow Φ_h^s is denoted by:

$$\delta F \equiv F - \overline{F} \tag{5.21}$$

Lemma 2. *Let h be the Hamiltonian defined in* (5.14) *and $L_h = \{\cdot, h\}$ its Lie derivative. For any functional F, the solution of the equation:*

$$L_h G = \delta F$$

is given by:

$$G = \mathcal{G} + L_h^{-1}\delta F = \mathcal{G} + \frac{1}{2\pi}\int_0^{2\pi} s e^{sL_h}\delta F\,, \tag{5.22}$$

where $\mathcal{G}$ is an arbitrary element of $\ker L_h$*, i.e. any function satisfying $\{\mathcal{G}, h\} = 0$.*

The proof of this Lemma can be found in [53].

5.3 Main Result

In this section we state the main result of this part of our research, namely the construction of the first- and second-order Hamiltonian normal forms for the KGW problem, and we study the Hamiltonian equations obtained by truncating the higher-orders.

As mentioned in Section 5.2, the novelty of our problem lies in the presence of an unbounded component Φ_k^s in the unperturbed flow $\Phi_{H_0}^s$. To handle this new feature, we first adapt the standard concept of normal form to define it only with respect to the component h of the unperturbed Hamiltonian. In other words, we only require all corrections to commute with h, rather than with H_0.

Definition 5.4 (Normal Form)**.** Let $H_0 = h + k$ be an Hamiltonian with two decoupled components, $\{h, k\} = 0$, both integrable, with bounded flow for h and unbounded flow for k. A Hamiltonian H_ε is said to be in normal form to order n with respect to h if it is in the form

$$H_\varepsilon = H_0 + \sum_{j=1}^{n}\varepsilon^j Z_j + \mathcal{R}_{n+1}$$

where $\{Z_j, h\} = 0$ for any $j = 1, \ldots, n$, and $\mathcal{R}_{n+1}$ is of order ε^{n+1}.

Observe that $\{H_0, h\} = 0$ as well, due to the decoupling $\{h, k\} = 0$, so that the commuting property characterizing the normal form holds even at order zero.

The definition 5.4 of normal form has a relevant consequence: the condition $\{Z_j, h\} = 0$ implies that all the truncated normal form Hamiltonians obtained by neglecting the remainder $\mathcal{R}_{n+1}$ will commute with h. As a consequence, h is preserved along the flow of the truncated normal form Hamiltonian. In our case, since $h = \int |\psi|^2$, this means that the $L^2(\mathbb{R}^3)$-norm of the massive field ψ is an integral of motion for the approximated dynamics to any order.

We can now state the following theorem.

Theorem 3 (Normal Form for KGW)**.** *There exist two generating Hamiltonians G_1, G_2 and a canonical transformation*

$$\mathcal{C}^{-1} \equiv \Phi^{\varepsilon}_{G_1} \circ \Phi^{\varepsilon^2}_{G_2}$$

mapping the Hamiltonian H_ε of the KGW problem, defined in (5.16)*, into a new Hamiltonian:*

$$\widetilde{H}_\varepsilon = H_\varepsilon \circ \mathcal{C}^{-1} = H_0 + \varepsilon Z_1 + \varepsilon^2 Z_2 + \mathcal{R}_3 \tag{5.23}$$

which is in normal form to order 2 with respect to h, according to Definition 5.4. Its components are defined by:

$$Z_1 \equiv \overline{H_1}\,, \quad Z_2 \equiv \overline{F_2}\,, \quad F_2 \equiv L_{G_1} H_1 + \frac{1}{2} L^2_{G_1} H_0\,, \tag{5.24}$$

with explicit expressions:

$$\begin{aligned} Z_1 &= \int \left[\frac{|\nabla\phi|^2}{2} + \frac{|\nabla\psi|^2}{2} + \phi|\psi|^2 \right], \\ Z_2 &= -\frac{1}{8}\int |\Delta\psi|^2 + \frac{1}{4}\int \phi\left(\psi^*\Delta\psi + \psi\Delta\psi^*\right) + \\ &\quad + \frac{i}{16}\int p_\phi\left[\psi^*\Delta\psi - \psi\Delta\psi^*\right] - \frac{1}{2}\int \phi^2|\psi|^2 + \frac{1}{16}\int |\psi|^4\,. \end{aligned}$$

The generating Hamiltonians are defined by:

$$G_1 \equiv (1 + L_h^{-1}L_k)^{-1} L_h^{-1}\,\delta H_1\,, \qquad \delta H_1 \equiv H_1 - \overline{H_1}\,, \tag{5.25}$$

$$G_2 \equiv (1 + L_h^{-1}L_k)^{-1} L_h^{-1}\,\delta F_2\,, \qquad \delta F_2 \equiv F_2 - \overline{F_2}\,, \tag{5.26}$$

with explicit expression for G_1:

$$G_1 = \int \left[\frac{i}{8}((\nabla\psi)^2 - (\nabla\psi^*)^2) + \frac{i}{4}\phi(\psi^2 - \psi^{*2}) + \frac{1}{8}p_\phi(\psi^2 + \psi^{*2}) \right].$$

An explicit expression for G_2 is reported in Section 5.4. Notice that G_2 is not involved in the explicit computation of Z_2, its expression becoming necessary only at higher orders. The proof of the theorem is given in Section 5.4.

5.3.1 First Order Hamilton Equations

We now truncate the normal form Hamiltonian (5.23) at first-order, neglecting all contributions of order ε^2. We get:

$$\widetilde{H}_{(1)} \equiv H_0 + \varepsilon Z_1 = \left[\int |\psi|^2 + \int \frac{p_\phi^2}{2} \right] + \varepsilon \left[\int \frac{|\nabla\phi|^2}{2} + \frac{|\nabla\psi|^2}{2} + \phi|\psi|^2 \right].$$

The associated Hamilton equations read:

$$\begin{cases} i\partial_t\psi = \ \ \frac{\delta\widetilde{H}_{(1)}}{\delta\psi^*} = \psi + \varepsilon\left[\frac{1}{2}(-\Delta\psi) + \phi\psi\right] \\ i\partial_t\psi^* = -\frac{\delta\widetilde{H}_{(1)}}{\delta\psi} = \psi^* + \varepsilon\left[\frac{1}{2}(-\Delta\psi^*) + \phi\psi^*\right] \\ \partial_t\phi \ = \ \ \frac{\delta\widetilde{H}_{(1)}}{\delta p_\phi} = p_\phi \\ \partial_t p_\phi = -\frac{\delta\widetilde{H}_{(1)}}{\delta\phi} = \varepsilon\left[\Delta\phi - |\psi|^2\right] \end{cases}.$$

The second equation is just the complex conjugate of the first equation, so we omit it. The ψ term in the first equation is removed by the gauge transformation $\psi \to e^{-it}\psi$, and the equations on ϕ and p_ϕ are combined into one second-order-in-time equation, to obtain:

$$\begin{cases} i\partial_t\psi = \varepsilon\left[-\frac{1}{2}\Delta\psi + \phi\psi\right] \\ \partial_t^2\phi \ = \varepsilon\left[\Delta\phi - |\psi|^2\right] \end{cases}.$$

We can perform a final time scaling, similar the one we applied at the very beginning, $t'' = \varepsilon t$ (overall, we performed $t' = \mu t$, with $\varepsilon = \mu^{-2}$ (see (5.12)) and then $t'' = \varepsilon t' = \mu^{-1} t$). Thus, the equations read:

$$\begin{cases} i\partial_{t''}\psi = -\frac{1}{2}\Delta\psi + \phi\psi \\ \varepsilon\partial^2_{t''}\phi \ = \Delta\phi - |\psi|^2 \end{cases} . \tag{5.27}$$

Here, we recognize the SW system (5.2). As mentioned in the introduction 5.1, in the singular limit $\varepsilon \to 0$ the SW system (5.2) reduces to the SP system (1.2). This intuition is refined by solving the second equation in (5.27) by Fourier transform:

$$\begin{aligned} -\varepsilon\omega^2\hat{\phi} &= -|k|^2\hat{\phi} - \widehat{|\psi|^2}\,, \\ \hat{\phi} &= -\frac{1}{|k|^2}\frac{1}{1-\varepsilon\frac{\omega^2}{|k|^2}}\widehat{|\psi|^2} = -\frac{1}{|k|^2}\left(1 + \varepsilon\frac{\omega^2}{|k|^2} + \varepsilon^2\frac{\omega^4}{|k|^4} + \dots\right)\widehat{|\psi|^2}\,. \end{aligned}$$

This expression for the solution, which can be mapped back to ϕ with an inverse Fourier transform, highlights its hierarchical structure. The factor $|k|^{-2}$ represents in the Fourier transform the inverse Δ^{-1} of the Laplace operator, so that, at order zero, we recognize the solution of the Poisson equation. Higher-order corrections involve the parameter ω^2 and its powers, representing time derivatives in the Fourier transform. To preserve the perturbative structure in ε, the parameter ω should be $\mathcal{O}(\varepsilon^0)$, or equivalently, the field ψ should avoid strong oscillations in time. In this case, we could safely take the $\varepsilon \to 0$ limit, approximating the wave equation with a Poisson equation.

5.3.2 Second Order Hamilton Equations

We now truncate the normal form Hamiltonian (5.23) at second-order, thus getting:

$$\begin{aligned} \widetilde{H}_{(2)} =& H_0 + \varepsilon Z_1 + \varepsilon^2 Z_2 \\ =& \left[\int |\psi|^2 + \int \frac{p_\phi^2}{2}\right] + \varepsilon\left[\int \frac{|\nabla\phi|^2}{2} + \frac{|\nabla\psi|^2}{2} + \phi|\psi|^2\right] + \\ &+ \varepsilon^2\left[-\frac{1}{8}\int |\Delta\psi|^2 + \frac{1}{4}\int \phi\left(\psi^*\Delta\psi + \psi\Delta\psi^*\right) + \right. \\ &\left. + \frac{i}{16}\int p_\phi\left[\psi^*\Delta\psi - \psi\Delta\psi^*\right] - \frac{1}{2}\int \phi^2|\psi|^2 + \frac{1}{16}\int |\psi|^4\right]. \end{aligned}$$

The associated Hamilton equations read:

$$\begin{cases} i\partial_t\psi = & \frac{\delta\widetilde{H}_{(2)}}{\delta\psi^*} = \psi + \varepsilon\left[\frac{1}{2}(-\Delta\psi) + \phi\psi\right] + \\ & \qquad + \varepsilon^2\left[-\frac{1}{8}\Delta(\Delta\psi) + \frac{1}{4}\left(\phi(\Delta\psi) + \Delta(\phi\psi)\right) + \right. \\ & \qquad \left. + \frac{i}{16}\left(p_\phi(\Delta\psi) - \Delta(p_\phi\psi)\right) - \frac{1}{2}\phi^2\psi + \frac{2}{16}\psi^2\psi^*\right] \\ \partial_t\phi \ = & \frac{\delta\widetilde{H}_{(2)}}{\delta p_\phi} = p_\phi + \varepsilon^2\left[\frac{i}{16}(\psi^*\Delta\psi - \psi\Delta\psi^*)\right] \\ \partial_t p_\phi = & -\frac{\delta\widetilde{H}_{(2)}}{\delta\phi} = \varepsilon\left[\Delta\phi - |\psi|^2\right] + \varepsilon^2\left[-\frac{1}{4}(\psi^*\Delta\psi + \psi\Delta\psi^*) + \phi|\psi|^2\right] \end{cases} .$$

As in the first-order analysis, the ψ term in the first equation is removed by the gauge transformation $\psi \to e^{-it}\psi$ and the time can be rescaled to $t'' = \varepsilon t$:

$$\begin{cases} i\partial_{t''}\psi = \left[-\frac{\Delta\psi}{2} + \phi\psi\right] + \varepsilon\left[-\frac{\Delta(\Delta\psi)}{8} + \frac{\phi(\Delta\psi)+\Delta(\phi\psi)}{4} + \frac{i(p_\phi(\Delta\psi)-\Delta(p_\phi\psi))}{16} - \frac{\phi^2\psi}{2} + \frac{|\psi|^2\psi}{8}\right] \\ \varepsilon\partial_{t''}\phi \ = p_\phi + \varepsilon^2\left[\frac{i(\psi^*\Delta\psi - \psi\Delta\psi^*)}{16}\right] \\ \partial_{t''}p_\phi = \left[\Delta\phi - |\psi|^2\right] + \varepsilon\left[-\frac{\psi^*\Delta\psi + \psi\Delta\psi^*}{4} + \phi|\psi|^2\right] \end{cases} .$$

The equations on ϕ and p_ϕ can be combined into one second-order-in-time equation. This is performed by computing the time derivative of the equation for ϕ: on the right-hand side we get a $\partial_{t''}p_\phi$ contribution, as in the first-order, and a new contribution, that could be explicitly computed by plugging it into the equation for ψ. This second contribution is of order ε^2, so we can simply write:

$$\begin{cases} i\partial_{t''}\psi = \left[-\frac{\Delta\psi}{2} + \phi\psi\right] + \varepsilon\left[-\frac{\Delta(\Delta\psi)}{8} + \frac{\phi(\Delta\psi)+\Delta(\phi\psi)}{4} + \frac{i(p_\phi(\Delta\psi)-\Delta(p_\phi\psi))}{16} - \frac{\phi^2\psi}{2} + \frac{|\psi|^2\psi}{8}\right] \\ \varepsilon\partial^2_{t''}\phi \ = \left[\Delta\phi - |\psi|^2\right] + \varepsilon\left[-\frac{\psi^*\Delta\psi + \psi\Delta\psi^*}{4} + \phi|\psi|^2\right] \end{cases} ,$$

where the remainder $\mathcal{O}(\varepsilon^2)$ has been omitted by consistency.

5.3.3 Harmonic oscillators and free particles

In describing the KGW model in Section 5.2 we remarked that the unperturbed Hamiltonian H_0 is composed of a harmonic oscillator Hamiltonian h and a free particle Hamiltonian k. To further clarify this statement, let us write the fields ψ, ψ^* and ϕ, p_ϕ as linear combinations of a given orthonormal basis $\{\varphi_k\}_{k=1}^{\infty}$:

$$\psi(t,x) = \sum_{k=1}^{\infty} \sqrt{I_k(t)} e^{-i\theta_k(t)} \varphi_k(x)\,, \quad \phi(t,x) = \sum_{k=1}^{\infty} q_k(t)\varphi_k(x)\,, \quad p_\phi(t,x) = \sum_{k=1}^{\infty} p_k(t)\varphi_k(x) \tag{5.28}$$

where the Fourier expansion in action-angle variables has been used for the complex field ψ and for its complex conjugate ψ^*, not reported for simplicity. In these variables, the unperturbed Hamiltonian – still denoted H_0 with a slight abuse of notation – reads:

$$H_0 = \sum_{k=1}^{\infty} I_k + \sum_{k=1}^{\infty} \frac{p_k^2}{2}\,.$$

With this notation, we can interpret the KGW Hamiltonian $H_\varepsilon = H_0 + \varepsilon H_1(\theta, I, q)$ as defining an infinite set of harmonic oscillators, described by variables $\{\theta_k, I_k\}_{k=1}^{\infty}$, and of free particles, described by variables $\{q_k, p_k\}_{k=1}^{\infty}$, coupled at higher orders in the perturbative parameter ε. In our case, all harmonic oscillators share the same frequency $\omega_k = 1$ and all the free particles share the same mass $m_k = 1$. By relaxing this condition, the unperturbed KGW Hamiltonian can be generalized to:

$$K_0 = \sum_{k=1}^{\infty} \omega_k I_k + \sum_{k=1}^{\infty} \frac{p_k^2}{2m_k}\,.$$

Adding higher-order perturbations to this unperturbed Hamiltonian, $K = K_0 + K_1(\theta, I, q, p)$, we can define a more general Hamiltonian dynamics, that can be analyzed with the same techniques we developed in this work. We highlight that in this extension small divisors issues may arise when specific conditions on the frequencies $\{\omega_k\}_{k=1}^{\infty}$ are met (see e.g. [146] for more details on the topic).

In this work we derive the normal form for the KGW in a formal way. A more detailed study would include a check on the analytical details of the computation, such as the existence of the flow of the generating Hamiltonians or the explicit dependence on ε of the remainder $\mathcal{R}_3$. To check these properties, the most convenient way exploits again the expanded notation (5.28): choosing a convenient basis, it is possible to introduce a cutoff, neglecting the contributions with index k higher of a given threshold N, then to study the desired properties in the resulting finite-dimensional space, and finally to recover the original problem by letting $N \to \infty$. This procedure, presented for example by Bambusi [13], is extremely delicate, and its application to the present problem is postponed to future works.

5.4 Normal Form Computation

As prescribed by the standard averaging principle, computing the normal form to second-order requires looking for a canonical transformation in the form:

$$\mathcal{C}^{-1} = \Phi_{G_1}^{\varepsilon} \circ \Phi_{G_2}^{\varepsilon^2}\,, \tag{5.29}$$

with G_1, G_2 two generating Hamiltonians and with times ε, ε^2 of different order in ε. This canonical transformation maps the original Hamiltonian H_ε into a new Hamiltonian in the form:

$$\begin{aligned} H_\varepsilon \circ \mathcal{C}^{-1} &= e^{\varepsilon^2 L_{G_2}} e^{\varepsilon L_{G_1}} (H_0 + \varepsilon H_1) \\ &= (1 + \varepsilon^2 L_{G_2} + \mathcal{O}(\varepsilon^4))(1 + \varepsilon L_{G_1} + \frac{\varepsilon^2}{2} L_{G_1}^2 + \mathcal{O}(\varepsilon^3))(H_0 + \varepsilon H_1) \\ &= H_0 + \varepsilon \underbrace{(L_{G_1} H_0 + H_1)}_{Z_1} + \varepsilon^2 \underbrace{(L_{G_2} H_0 + L_{G_1} H_1 + \frac{1}{2} L_{G_1}^2 H_0)}_{Z_2} + \mathcal{O}(\varepsilon^3)\,, \end{aligned} \tag{5.30}$$

where we use Lemma 1 to write the flow composition in algebraic form, expand the transformed Hamiltonian and collect the contributions based on the perturbative parameter ε. We can thus

denote by Z_1, Z_2 the first- and second-order terms in the transformed Hamiltonian. Recalling the antisymmetry of the Poisson brackets, which implies $L_{G_n} H_0 = -L_{H_0} G_n$, we set the so called first- and second-order homological equations:

$$-L_{H_0} G_1 + H_1 = Z_1 \,, \tag{5.31}$$

$$-L_{H_0} G_2 + F_2 = Z_2 \,, \qquad F_2 \equiv L_{G_1} H_1 + \frac{1}{2} L^2_{G_1} H_0 \,, \tag{5.32}$$

having the generating Hamiltonians G_1, G_2 and the first- and second-order corrections Z_1, Z_2 as the unknowns.

Observe that the generating Hamiltonians G_1, G_2 enter the equations only through the action of the L_{H_0} operator. This means that they are defined up to terms in the kernel of $L_{H_0} = \{\cdot, H_0\}$. Thus, for example, we are free to add terms depending only on $|\psi|^2$, due to the gauge invariance of the unperturbed equations. This freedom can be used to require that G_1, G_2 satisfy specific properties, such as having zero average with respect to the flow of h, i.e. $\overline{G_1} = 0$ and $\overline{G_2} = 0$.

Computing the normal form thus reduces to solving the two homological equations (5.31) and (5.32). Observe that due to the distinct time orders ε, ε^2 in the canonical transformation (5.29) the two homological equations are hierarchically decoupled: the first-order homological equation (5.31) sets G_1, Z_1, and once they are known, the second-order homological equation (5.32) allows to compute G_2, Z_2. We can therefore focus on the two homological equations separately, adapting the standard averaging principle to our case to derive the desired unknowns.

5.4.1 First order correction Z_1

In order to find the first unknown Z_1, we compute the average of the first-order homological equation (5.31) along the flow of h. This allows to impose the definition 5.4 of normal form: we require $\{Z_1, h\} = 0$, which implies that Z_1 is invariant with respect to the average flow of h, i.e. $\overline{Z_1} = Z_1$. We thus have:

$$-\overline{L_{H_0} G_1} + \overline{H_1} = Z_1 \,. \tag{5.33}$$

Then, we elaborate on the first term of the left-hand side to show that it vanishes. We write explicitly the definition of time average, recalling that the unperturbed flow of h is periodic of period $T = 2\pi$. We use the identity $L_{H_0} = L_h + L_k$ and we recall that the operators L_h, L_k commute. The Poisson bracket L_k is independent from the time s of the flow of h, so it can be brought outside the integral:

$$\overline{L_{H_0} G_1} = \frac{1}{2\pi} \int_0^{2\pi} e^{sL_h} L_{H_0} G_1 \, \mathrm{d}s = \frac{1}{2\pi} \int_0^{2\pi} e^{sL_h} L_h G_1 \, \mathrm{d}s + \frac{L_k}{2\pi} \int_0^{2\pi} e^{sL_h} G_1 \, \mathrm{d}s \,. \tag{5.34}$$

In the last integral we recognize the average of G_1 along the flow of h. We exploit the freedom we have in defining G_1 to require it has vanishing average: $\overline{G_1} = 0$. The last integral is therefore zero. As for the first integral, observe that we can reconstruct a total derivative in the integrand and trivially solve the integral, which vanishes by periodicity:

$$\frac{1}{2\pi} \int_0^{2\pi} e^{sL_h} L_h G_1 \, \mathrm{d}s = \frac{1}{2\pi} \int_0^{2\pi} \frac{\mathrm{d}}{\mathrm{d}s} \left(e^{sL_h} G_1 \right) \mathrm{d}s = \frac{1}{2\pi} \left[e^{sL_h} G_1 \right]_0^{2\pi} = 0 \,. \tag{5.35}$$

The homological equation, averaged on the flow of h, thus reduces to:

$$Z_1 = \overline{H_1} \,, \tag{5.36}$$

a result which is analogous to the standard averaging principle, but involves only the average on the flow of h rather than on that of the complete H_0. The first-order normal form correction Z_1 is thus equal to the original first-order term H_1 averaged along the flow Φ_h^s of the h contribution in the unperturbed Hamiltonian.

Explicit computations in the KGW case

To perform the explicit computation of $Z_1 = \overline{H_1}$ we use coordinates $(\psi, \psi^*, \phi, p_\phi)$. Recall that this choice is arbitrary, since the normal form procedure is independent from the specific coordinates used for computations. In our case, the result is straightforward: it is sufficient to recall that the flow Φ_h^s acts only on ψ, ψ^* by shifting the phase and that the only non vanishing terms in the integration are

those invariant under phase shifting, which remain unchanged. As a result, recalling the definition of H_1 and denoting $(\nabla\psi)^2 \equiv \nabla\psi \cdot \nabla\psi$, we have:

$$\begin{aligned} H_1 :&= \int \left(\frac{|\nabla\phi|^2}{2} + \frac{|\nabla\psi + \nabla\psi^*|^2}{4} + \frac{\phi}{2}(\psi + \psi^*)^2 \right) \\ &= \int \left(\frac{|\nabla\phi|^2}{2} + \frac{|\nabla\psi|^2}{2} + \phi|\psi|^2 \right) + \int \left(\frac{(\nabla\psi)^2 + (\nabla\psi^*)^2}{4} + \frac{\phi}{2}(\psi^2 + {\psi^*}^2) \right), \end{aligned}$$

from which it is immediate to derive:

$$Z_1 = \overline{H_1} = \int \frac{|\nabla\phi|^2}{2} + \frac{|\nabla\psi|^2}{2} + \phi|\psi|^2 .$$

This gives the first-order correction in the Hamiltonian normal form 5.4 and defines one of the two unknowns of the first-order homological equation (5.31).

5.4.2 First order generating Hamiltonian G_1

To find the second unknown of the first-order homological equation (5.31), we substitute in it the result (5.36) obtained for Z_1 and we reconstruct the deviation of H_1 from its average along the flow of h:

$$L_{H_0} G_1 = H_1 - Z_1 = H_1 - \overline{H_1} =: \delta H_1 .$$

In order to solve for G_1, we need to invert the L_{H_0} operator. Let us first proceed formally, in analogy to what observed in the standard averaging principle procedure. In order to exploit the structure of our problem, we use $L_{H_0} = L_h + L_k$ and collect the L_k contribution, before formally inverting to solve for G_1:

$$\begin{aligned} L_h(1 + L_h^{-1} L_k) G_1 &= \delta H_1 , \\ G_1 &= (1 + L_h^{-1} L_k)^{-1} L_h^{-1} \delta H_1 . \end{aligned} \tag{5.37}$$

Observe that from Lemma 2 we already have a definition for the L_h^{-1} operator. Thus, in order to compute G_1 we need to understand how to describe the action of the operator $(1 + L_h^{-1} L_k)^{-1}$. To this aim, let us proceed by formally expanding it in series:

$$(1 + L_h^{-1} L_k)^{-1} = 1 - L_h^{-1} L_k + (L_h^{-1} L_k)^2 + \dots \tag{5.38}$$

In this way, the problem reduces to compute successive (potentially infinite) applications of the operators L_k and L_h^{-1}, which are already defined.

Explicit computations in the KGW case

In order to perform explicit computations, let us focus again on coordinates $(\psi, \psi^*, \phi, p_\phi)$. Using the definition of H_1 and the computed average $\overline{H_1}$ it is immediate to obtain:

$$\delta H_1 = H_1 - \overline{H}_1 = \int \frac{(\nabla\psi)^2 + (\nabla\psi^*)^2}{4} + \frac{\phi(\psi^2 + {\psi^*}^2)}{2} .$$

As a next step, we need to understand how to describe the action of the L_h^{-1} and L_k operators, to be iteratively applied to δH_1.

Action of L_h^{-1}. Consider first the L_h^{-1} operator, which is a time average along the periodic flow $\Phi_h^s = (e^{-is}\psi_0, e^{is}{\psi^*}_0)$ weighted by time s, as described in Lemma 2. Observe that the composition with this flow modifies only the coordinates ψ, ψ^*. Thus, if a given functional F is polynomial in these coordinates, each term in $e^{sh}F = F \circ \Phi_h^s$ will depend on s only through a phase $e^{i(-n_\psi + n_{\psi^*})s} =: e^{\pm ins}$, with exponents n_ψ, n_{ψ^*} denoting the degree of ψ, ψ^* in that term, and $n \equiv |n_\psi - n_{\psi^*}|$. The integration

in time s will therefore focus on the weighted phases $se^{\pm ins}$ only. For example, for $F = \delta H_1$:

$$\begin{aligned} L_h^{-1}\delta H_1 &= \frac{1}{2\pi}\int_0^{2\pi} se^{sL_h}\left[\int \frac{(\nabla\psi)^2}{4} + \frac{(\nabla\psi^*)^2}{4} + \frac{\phi\psi^2}{2} + \frac{\phi{\psi^*}^2}{2}\right] \mathrm{d}s \\ &= \frac{1}{2\pi}\int_0^{2\pi}\left[\int se^{-i2s}\frac{(\nabla\psi_0)^2}{4} + se^{+i2s}\frac{(\nabla{\psi^*}_0)^2}{4} + se^{-i2s}\frac{\phi\psi_0^2}{2} + se^{+i2s}\frac{\phi{\psi^*}_0^2}{2}\right]\mathrm{d}s \\ &= \int\left[\left(\frac{1}{2\pi}\int_0^{2\pi} se^{-i2s}\,\mathrm{d}s\right)\frac{(\nabla\psi_0)^2}{4} + \left(\frac{1}{2\pi}\int_0^{2\pi} se^{+i2s}\,\mathrm{d}s\right)\frac{(\nabla{\psi^*}_0)^2}{4}\right. \\ &\quad \left. + \left(\frac{1}{2\pi}\int_0^{2\pi} se^{-i2s}\,\mathrm{d}s\right)\frac{\phi\psi_0^2}{2} + \left(\frac{1}{2\pi}\int_0^{2\pi} se^{+i2s}\,\mathrm{d}s\right)\frac{\phi{\psi^*}_0^2}{2}\right]. \end{aligned}$$

Integration in time s thus involves only terms in the form:

$$\begin{aligned} &\frac{1}{2\pi}\int_0^{2\pi} se^{\pm ins}\,\mathrm{d}s = \frac{1}{2\pi}\left[s\frac{e^{\pm ins}}{\pm in}\right]_0^{2\pi} - \frac{1}{2\pi}\int_0^{2\pi}\frac{e^{\pm ins}}{\pm in}ds = \mp\frac{i}{n} && \text{for } n \neq 0\,, \\ &\frac{1}{2\pi}\int_0^{2\pi} se^{\pm ins}\,\mathrm{d}s = \frac{1}{2\pi}\int_0^{2\pi} s\,\mathrm{d}s = \frac{1}{2\pi}\left[\frac{s^2}{2}\right]_0^{2\pi} = \pi && \text{for } n = 0\,, \end{aligned}$$

which is easily solved through integration by parts in the case $n \neq 0$. Thus, the operator L_h^{-1} acts on a functional F that is polynomial in (ψ, ψ^*) by adding a proportionality factor to each term: π for terms invariant under phase shifting ($n = 0$), and $\pm in^{-1}$ to other terms, where the exponent $n = |n_\psi + n_{\psi^*}|$ accounts for the degrees n_ψ, n_{ψ^*} of ψ, ψ^* in that term. Note that in our case the operator L_h^{-1} is always applied to deviations from averages, which by definition have vanishing average with respect to the flow of h. Thus, the case $n = 0$ never occurs. Schematically, in our case we only need:

- for terms proportional to ψ^{n_ψ}, the integrand has a phase $e^{-in_\psi s}$ and integration yields a proportionality constant $+i/n_\psi$;
- for terms proportional to ${\psi^*}^{n_{\psi^*}}$, the integrand has a phase $e^{in_{\psi^*}s}$ and integration yields a proportionality constant $-i/n_\psi$.

To conclude our example, the application $L_h^{-1}\delta H_1$ yields:

$$\begin{aligned} L_h^{-1}\delta H_1 &= -\frac{1}{2i}\int\frac{(\nabla\psi)^2}{4} + \frac{1}{2i}\int\frac{(\nabla\psi^*)^2}{4} - \frac{1}{2i}\int\frac{\phi\psi^2}{2} + \frac{1}{2i}\int\frac{\phi{\psi^*}^2}{2} \\ &= \int\frac{i}{8}((\nabla\psi)^2 - (\nabla\psi^*)^2) + \frac{i}{4}\int\phi(\psi^2 - {\psi^*}^2)\,, \end{aligned}$$

where the subscript 0 for the initial conditions has been omitted for simplicity. We adopt the same notation in the following.

Action of L_k. Consider now the L_k operator. Its action on a generic functional $F(\psi, \psi^*, \phi, p_\phi)$ is:

$$L_k F \equiv \left\{F, \int\frac{p_\phi^2}{2}\right\}.$$

Observe that, since L_k involves only p_ϕ, the only non-vanishing contributions in F are those depending on ϕ. In our case we just need:

$$\left\{\int\phi^n, \int\frac{p_\phi^2}{2}\right\} = \int n\phi^{n-1}p_\phi\,,$$

which lowers the degree of ϕ and raises that of p_ϕ. Observe that if F is a polynomial of degree n in ϕ, only n applications of L_k will give a non-vanishing result. Thus, in this case, only a finite number of contributions will actually matter in the series (5.38) representing the $(1 + L_h^{-1}L_k)^{-1}$ operator.

With this information, we can actually compute the first-order generating Hamiltonian G_1 by successive applications of the operators L_h^{-1}, L_k:

$$\begin{aligned} L_h^{-1}\delta H_1 &= \int \frac{i}{8}((\nabla\psi)^2 - (\nabla\psi^*)^2) + \frac{i}{4}\phi(\psi^2 - \psi^{*2})\,, \\ L_k\ L_h^{-1}\delta H_1 &= \int \frac{i}{4}p_\phi(\psi^2 - \psi^{*2})\,, \\ L_h^{-1}L_k\ L_h^{-1}\delta H_1 &= -\int \frac{1}{8}p_\phi(\psi^2 + \psi^{*2})\,, \\ L_k\ L_h^{-1}L_k\ L_h^{-1}\delta H_1 &= 0\,. \end{aligned}$$

Therefore, we conclude the computation of the first-order generating Hamiltonian:

$$\begin{aligned} G_1 &= (1 + L_h^{-1}L_k)^{-1}L_h^{-1}\delta H_1 \\ &= (1 - L_h^{-1}L_k) \quad L_h^{-1}\delta H_1 \\ &= \int \left[\frac{i}{8}((\nabla\psi)^2 - (\nabla\psi^*)^2) + \frac{i}{4}\phi(\psi^2 - \psi^{*2}) + \frac{1}{8}p_\phi(\psi^2 + \psi^{*2})\right]. \end{aligned}$$

5.4.3 Second order correction Z_2

Similarly to the first-order, we average the second-order homological equation (5.32) along the flow Φ_h^s of the harmonic unperturbed Hamiltonian h. The computation is exactly as in the first-order, and the $\overline{L_{H_0}G_2}$ term vanishes by requiring G_2 to have zero mean along the flow of h. Thus, we have:

$$Z_2 = \overline{F_2}\,.$$

To simplify the computation of $\overline{F_2}$, let us first manipulate its definition, by plugging in the first-order homological equation:

$$\begin{aligned} L_{G_1}^2 H_0 = L_{G_1}(L_{G_1}H_0) = L_{G_1}(\overline{H_1} - H_1)\,, \\ F_2 \equiv L_{G_1}H_1 + \frac{1}{2}L_{G_1}^2 H_0 = \frac{1}{2}L_{G_1}H_1 + \frac{1}{2}L_{G_1}\overline{H_1}\,. \end{aligned}$$

When averaging, the last term vanishes, since we required G_1 to have zero average along the flow of h:

$$\overline{L_{G_1}\overline{H_1}} = \overline{\{\overline{H_1}, G_1\}} = \{\overline{H_1}, \overline{G_1}\} = \{\overline{H_1}, 0\} = 0\,,$$

and we can use the same trick in the remaining term, by adding and subtracting the average $\overline{H_1}$ to reconstruct $\delta H_1 \equiv H_1 - \overline{H_1}$:

$$\begin{aligned} \overline{F_2} &= \frac{1}{2}\overline{L_{G_1}H_1} \\ &= \frac{1}{2}\overline{\{H_1 - \overline{H_1}, G_1\}} + \frac{1}{2}\overline{\{\overline{H_1}, G_1\}} \\ &= \frac{1}{2}\overline{\{\delta H_1, G_1\}}\,. \end{aligned}$$

Calculating this is usually simpler than computing F_2. However, the latter is still necessary if we want to compute the generating Hamiltonian G_2 as well. Thus, in this work, we proceed by computing F_2 and averaging along h.

Explicit computations in the KGW case

To obtain F_2,it is necessary to compute the Poisson bracket $L_{G_1}(H_1 + \overline{H_1}) = \{H_1 + \overline{H_1}, G_1\}$. The required calculations are postponed to a dedicated Section 5.4.6 at the end of this Chapter and the

final result reads:

$$\begin{aligned}
F_2 =&\frac{1}{2}L_{G_1}(H_1+\overline{H_1})\\
=&-\frac{1}{8}\int|\Delta\psi|^2+\frac{1}{4}\int\phi\left(\psi^*\Delta\psi+\psi\Delta\psi^*\right)+\frac{i}{16}\int p_\phi\left[\psi^*\Delta\psi-\psi\Delta\psi^*\right]+\\
&-\frac{1}{2}\int\phi^2|\psi|^2+\frac{1}{16}\int|\psi|^4+\\
&-\frac{1}{8}\int\left((\Delta\psi)^2+(\Delta\psi^*)^2\right)+\frac{1}{8}\int|\psi|^2(\psi^2+\psi^{*2})+\frac{1}{2\cdot16}\int(\psi^4+\psi^{*4})+\\
&-\frac{1}{8}\int(\Delta\phi)(\psi^2+\psi^{*2})+\frac{1}{2}\int\phi\left(\psi\Delta\psi+\psi^*\Delta\psi^*\right)-\frac{1}{2}\int\phi^2(\psi^2+\psi^{*2})+\\
&-\frac{i}{8}\int p_\phi(\psi\Delta\psi-\psi^*\Delta\psi^*)+\frac{i}{4}\int\phi p_\phi(\psi^2-\psi^{*2})\,.
\end{aligned}$$

The second-order correction Z_2 is finally computed by averaging along the flow of h, which – we recall – acts only on ψ,ψ^* by shifting the phase, so that through integration it lets all terms vanish except for those invariant under phase shifting, which remain unchanged:

$$\begin{aligned}
Z_2\equiv\overline{F_2}=&-\frac{1}{8}\int|\Delta\psi|^2+\frac{1}{4}\int\phi\left(\psi^*\Delta\psi+\psi\Delta\psi^*\right)+\frac{i}{16}\int p_\phi\left[\psi^*\Delta\psi-\psi\Delta\psi^*\right]+\\
&-\frac{1}{2}\int\phi^2|\psi|^2+\frac{1}{16}\int|\psi|^4\,.
\end{aligned}$$

5.4.4 Second order generating Hamiltonian G_2

Let us finally compute the second-order generating Hamiltonian G_2. To this aim, we proceed as for the first-order, by inverting the homological equation and expanding in series the operator:

$$G_2=(1-(L_h^{-1}L_k)+(L_h^{-1}L_k)^2+\ldots)L_h^{-1}\delta F_2\,.$$

We can proceed directly with the explicit computations.

Explicit computations in the KGW case

Let us first write the difference $\delta F_2\equiv F_2-\overline{F_2}$:

$$\begin{aligned}
\delta F_2 =&F_2-\overline{F_2}\\
=&-\frac{1}{8}\int\left((\Delta\psi)^2+(\Delta\psi^*)^2\right)+\frac{1}{8}\int|\psi|^2(\psi^2+\psi^{*2})+\frac{1}{32}\int(\psi^4+\psi^{*4})+\\
&-\frac{1}{8}\int(\Delta\phi)(\psi^2+\psi^{*2})+\frac{1}{2}\int\phi(\psi\Delta\psi+\psi^*\Delta\psi^*)-\frac{1}{2}\int\phi^2(\psi^2+\psi^{*2})+\\
&-\frac{i}{8}\int p_\phi(\psi\Delta\psi-\psi^*\Delta\psi^*)+\frac{i}{4}\int\phi p_\phi(\psi^2-\psi^{*2})\,.
\end{aligned}$$

The remaining computation now consists in successive applications of the operators L_h^{-1} and L_k, whose action has already been described in the first-order analysis. In this case, observe that δF_2 has at most a quadratic dependence on the ϕ coordinate, meaning that three successive applications of the L_k operator will let all contributions vanish. The only relevant contributions are computed as

follows:

$$\begin{aligned}
L_h^{-1}\delta F_2 =& -\frac{i}{16}\int\left((\Delta\psi)^2-(\Delta\psi^*)^2\right)+\frac{i}{16}\int|\psi|^2(\psi^2-\psi^{*2})+\frac{i}{4\cdot 32}\int(\psi^4-\psi^{*4})+\\
&-\frac{i}{16}\int(\Delta\phi)(\psi^2-\psi^{*2})+\frac{i}{4}\int\phi\left(\psi\Delta\psi-\psi^*\Delta\psi^*\right)-\frac{i}{4}\int\phi^2(\psi^2-\psi^{*2})+\\
&+\frac{1}{16}\int p_\phi(\psi\Delta\psi+\psi^*\Delta\psi^*)-\frac{1}{8}\int\phi p_\phi(\psi^2+\psi^{*2})\,,\\
L_kL_h^{-1}\delta F_2 =& \frac{i}{4}\int p_\phi(\psi\Delta\psi-\psi^*\Delta\psi^*)-\frac{i}{4}\int 2\phi p_\phi(\psi^2-\psi^{*2})-\frac{1}{8}\int p_\phi^2(\psi^2+\psi^{*2})+\\
&-\frac{i}{16}\int(\psi^2-\psi^{*2})\Delta p_\phi\,,\\
L_h^{-1}L_kL_h^{-1}\delta F_2 =& -\frac{1}{8}\int p_\phi(\psi\Delta\psi+\psi^*\Delta\psi^*)+\frac{1}{4}\int\ \phi p_\phi(\psi^2+\psi^{*2})+\\
&-\frac{i}{16}\int p_\phi^2(\psi^2-\psi^{*2})+\frac{1}{32}\int(\Delta p_\phi)(\psi^2+\psi^{*2})\,,\\
L_kL_h^{-1}L_kL_h^{-1}\delta F_2 =& \frac{1}{4}\int p_\phi^2(\psi^2+\psi^{*2})\,,\\
(L_h^{-1}L_k)^2L_h^{-1}\delta F_2 =& \frac{i}{8}\int p_\phi^2(\psi^2-\psi^{*2})\,.
\end{aligned}$$

The second-order generating Hamiltonian thus reads:

$$\begin{aligned}
G_2 =&(1+L_h^{-1}L_k)^{-1}L_h^{-1}\delta F_2\\
=&(1-L_h^{-1}L_k+(L_h^{-1}L_k)^2)L_h^{-1}\delta F_2\\
=&-\frac{i}{16}\int\left((\Delta\psi)^2-(\Delta\psi^*)^2\right)+\frac{i}{16}\int|\psi|^2(\psi^2-\psi^{*2})+\frac{i}{4\cdot 32}\int(\psi^4-\psi^{*4})+\\
&-\frac{i}{16}\int(\Delta\phi)(\psi^2-\psi^{*2})+\frac{i}{4}\int\phi(\psi\Delta\psi-\psi^*\Delta\psi^*)-\frac{i}{4}\int\phi^2(\psi^2-\psi^{*2})+\\
&+\frac{3}{16}\int p_\phi(\psi\Delta\psi+\psi^*\Delta\psi^*)-\frac{3}{8}\int\phi p_\phi(\psi^2+\psi^{*2})\\
&+\frac{3i}{16}\int p_\phi^2(\psi^2-\psi^{*2})-\frac{1}{32}\int(\Delta p_\phi)(\psi^2+\psi^{*2})\,.
\end{aligned}$$

5.4.5 Remark on Higher Orders

Observe that the construction suggested in this work can be extended to compute the normal form to higher orders. By composing the $(n-1)$-th order canonical transformation with a new flow $\Phi_{G_n}^{\varepsilon^n}$, the transformed Hamiltonian can be studied to construct the n-th order normal form. This is done by setting n-th homological equation:

$$-L_{H_0}G_n+F_n=Z_n\,, \tag{5.39}$$

with unknowns G_n, Z_n and with the term F_n depending only on known previous-orders contributions. In analogy with the computations performed in this work, the n-th order correction Z_n can be obtained by averaging the n-th order homological equation (5.39), resulting in:

$$Z_n=\overline{F_n}\,,$$

while the generating Hamiltonian G_n is defined by substituting this result in the n-th order homological equation (5.39), reconstructing the difference δF_n and solving for G_n:

$$G_n=(1+L_h^{-1}L_k)^{-1}L_h^{-1}\delta F_n\,,\qquad \delta F_n\equiv F_n-\overline{F_n}\,.$$

Analogously to the first- and second-order, the explicit computation of the inverse operator $(1+L_h^{-1}L_k)^{-1}$ can be performed with the algebraic expansion:

$$(1+L_h^{-1}L_k)^{-1}=1-L_h^{-1}L_k+(L_h^{-1}L_k)^2+\dots$$

involving the iterated application of the L_h^{-1}, L_k operators described in this work. As already observed, when applying this operator to a functional δF_n with a polynomial dependence on ϕ only a finite list of terms will result in a non-vanishing contribution. The series defining the inverse operator would thus reduce to a finite number of terms, allowing for an explicit computation of G_n.

5.4.6 Computing F_2

We report here the calculations needed to compute:

$$F_2 = \frac{1}{2} L_{G_1}(H_1 + \overline{H_1})\,.$$

To begin with, let us report here the definitions we have from the first-order:

$$\begin{aligned}
H_1 &= \int \frac{(\nabla\phi)^2}{2} + \frac{|\nabla\psi|^2}{2} + \phi|\psi|^2 + \int \frac{(\nabla\psi)^2 + (\nabla\psi^*)^2}{4} + \frac{\phi}{2}(\psi^2 + \psi^{*2}) \\
\overline{H_1} &= \int \frac{(\nabla\phi)^2}{2} + \frac{|\nabla\psi|^2}{2} + \phi|\psi|^2 \\
H_1 + \overline{H_1} &= \int (\nabla\phi)^2 + |\nabla\psi|^2 + 2\phi|\psi|^2 + \int \frac{(\nabla\psi)^2 + (\nabla\psi^*)^2}{4} + \frac{\phi}{2}(\psi^2 + \psi^{*2}) \\
G_1 &= \int \frac{i}{8}\left((\nabla\psi)^2 - (\nabla\psi^*)^2\right) + \frac{i}{4}\phi(\psi^2 - \psi^{*2}) + \int \frac{p_\phi}{8}(\psi^2 + \psi^{*2})
\end{aligned}$$

We are now ready to compute the required Poisson brackets. We obtain:

$$\begin{aligned}
&L_{G_1}(H_1 + \overline{H_1}) = \\
&= \quad \{H_1 + \overline{H_1}, G_1\} \\
&= \quad \left\{\int (\nabla\phi)^2, \frac{1}{8}\int p_\phi(\psi^2 + \psi^{*2})\right\} + \\
&\quad + \left\{\int |\nabla\psi|^2, \frac{i}{8}\int \left((\nabla\psi)^2 - (\nabla\psi^*)^2\right) + \frac{i}{4}\int \phi(\psi^2 - \psi^{*2}) + \int \frac{p_\phi}{8}(\psi^2 + \psi^{*2})\right\} + \\
&\quad + \left\{2\int \phi|\psi|^2, \frac{i}{8}\int \left((\nabla\psi)^2 - (\nabla\psi^*)^2\right) + \frac{i}{4}\int \phi(\psi^2 - \psi^{*2}) + \int \frac{p_\phi}{8}(\psi^2 + \psi^{*2})\right\} + \\
&\quad + \left\{\frac{1}{4}\int (\nabla\psi)^2, -\frac{i}{8}\int (\nabla\psi^*)^2 - \frac{i}{4}\int \phi\psi^{*2} + \int \frac{p_\phi}{8}\psi^{*2}\right\} + \\
&\quad + \left\{\frac{1}{4}\int (\nabla\psi^*)^2, \frac{i}{8}\int (\nabla\psi)^2 + \frac{i}{4}\int \phi\psi^2 + \int \frac{p_\phi}{8}\psi^2\right\} + \\
&\quad + \left\{\frac{1}{2}\int \phi\psi^2, \frac{i}{8}\int \left((\nabla\psi)^2 - (\nabla\psi^*)^2\right) + \frac{i}{4}\int \phi(\psi^2 - \psi^{*2}) + \int \frac{p_\phi}{8}(\psi^2 + \psi^{*2})\right\} + \\
&\quad + \left\{\frac{1}{2}\int \phi\psi^{*2}, \frac{i}{8}\int \left((\nabla\psi)^2 - (\nabla\psi^*)^2\right) + \frac{i}{4}\int \phi(\psi^2 - \psi^{*2}) + \int \frac{p_\phi}{8}(\psi^2 + \psi^{*2})\right\}
\end{aligned}$$

$$\begin{aligned}
&L_{G_1}(H_1 + \overline{H_1}) = \\
&= \quad \frac{1}{8}\int (-2\Delta\phi)(\psi^2 + \psi^{*2}) + \\
&\quad + (-i)\left[\frac{i}{8}\int \left[-(\Delta\psi^*)(2\Delta\psi^*) - (\Delta\psi)(2\Delta\psi)\right] + \right. \\
&\quad \left. + \frac{i}{4}\int \phi\left[(\Delta\psi^*)(2\psi^*) + (\Delta\psi)(2\psi)\right] + \frac{1}{8}\int p_\phi\left[-(\Delta\psi^*)(2\psi^*) + (\Delta\psi)(2\psi)\right]\right] + \\
&\quad + (-i)\left[\frac{2i}{8}\int \phi\left[\psi^*(2\Delta\psi^*) + \psi(2\Delta\psi)\right] + \frac{2i}{4}\int \phi^2\left[-\psi^*(2\psi^*) - \psi(2\psi)\right] + \right. \\
&\quad \left. + \frac{2}{8}\int \phi p_\phi\left[\psi^*(2\psi^*) - \psi(2\psi)\right]\right] + \frac{2}{8}\int |\psi|^2(\psi^2 + \psi^{*2}) + \\
&\quad + (-i)\left[-\frac{i\cdot 2}{4\cdot 8}\int (2\Delta\psi)(2\Delta\psi^*) - \frac{i}{4\cdot 4}\int \phi\left[-(2\Delta\psi)(2\psi^*) - (2\Delta\psi^*)(2\psi)\right]\right. \\
&\quad \left. + \frac{1}{4\cdot 8}\int p_\phi\left[-(2\Delta\psi)(2\psi^*) + (2\Delta\psi^*)(2\psi)\right]\right] + \\
&\quad + (-i)\left[\frac{i}{2\cdot 8}\int \phi\left[(2\psi)(2\Delta\psi^*) + (2\psi^*)(2\Delta\psi)\right] + \frac{i\cdot 2}{2\cdot 4}\int \left[-\phi^2(2\psi)(2\psi^*)\right] + \right.
\end{aligned}$$

$$+\frac{1\cdot 0}{2\cdot 8}\int \phi p_\phi(2\psi)(2\psi^*)\Big]+\Big[\frac{1}{2\cdot 8}\int \psi^2(\psi^2+\psi^{*2})+\frac{1}{2\cdot 8}\int \psi^{*2}(\psi^2+\psi^{*2})\Big]$$

$$\begin{aligned}
&L_{G_1}(H_1+\overline{H_1})=\\
&=-\frac{1}{4}\int(\Delta\phi)(\psi^2+\psi^{*2})+\\
&-\frac{1}{4}\int\left((\Delta\psi)^2+(\Delta\psi^*)^2\right)+\frac{1}{2}\int\phi\left(\psi\Delta\psi+\psi^*\Delta\psi^*\right)-\frac{i}{4}\int p_\phi\left(\psi\Delta\psi-\psi^*\Delta\psi^*\right)+\\
&+\frac{1}{2}\int\phi(\psi\Delta\psi+\psi^*\Delta\psi^*)-\int\phi^2(\psi^2+\psi^{*2})+\frac{i}{2}\int\phi p_\phi(\psi^2-\psi^{*2})+\\
&+\frac{1}{4}\int|\psi|^2(\psi^2+\psi^{*2})-\frac{1}{4}\int|\Delta\psi|^2+\frac{1}{2}\int\phi\left[\psi^*\Delta\psi+\psi\Delta\psi^*\right]+\\
&+\frac{i}{8}\int p_\phi\left[\psi^*\Delta\psi-\psi\Delta\psi^*\right]-\int\phi^2|\psi|^2+\frac{1}{16}\int(\psi^2+\psi^{*2})^2\,.
\end{aligned}$$

Thus, collecting first the terms invariant under phase shifting, F_2 reads:

$$\begin{aligned}
F_2=&\frac{1}{2}L_{G_1}(H_1+\overline{H_1})\\
=&-\frac{1}{8}\int|\Delta\psi|^2+\frac{1}{4}\int\phi\left(\psi^*\Delta\psi+\psi\Delta\psi^*\right)+\frac{i}{16}\int p_\phi\left[\psi^*\Delta\psi-\psi\Delta\psi^*\right]+\\
&-\frac{1}{2}\int\phi^2|\psi|^2+\frac{1}{16}\int|\psi|^4+\\
&-\frac{1}{8}\int\left((\Delta\psi)^2+(\Delta\psi^*)^2\right)+\frac{1}{8}\int|\psi|^2(\psi^2+\psi^{*2})+\frac{1}{2\cdot 16}\int(\psi^4+\psi^{*4})+\\
&-\frac{1}{8}\int(\Delta\phi)(\psi^2+\psi^{*2})+\frac{1}{2}\int\phi\left(\psi\Delta\psi+\psi^*\Delta\psi^*\right)-\frac{1}{2}\int\phi^2(\psi^2+\psi^{*2})+\\
&-\frac{i}{8}\int p_\phi(\psi\Delta\psi-\psi^*\Delta\psi^*)+\frac{i}{4}\int\phi p_\phi(\psi^2-\psi^{*2})\,.
\end{aligned}$$

5.5 Conclusions

In this Chapter, we derive the Hamiltonian normal form for the KGW problem (5.1), to second order, in a regime where the parameter μ^2 (5.9) is large. We write the Hamilton equations obtained by neglecting the remainders and analyze the first- and second-order approximations of the KGW system in a normal form sense. We observe that a SW system emerges as a first-order approximation, which can be further approximated by a SP equation in the limit $\varepsilon=\mu^{-2}\to 0$, provided that the time oscillations of the complex massive field (Ψ) are not too large. We also provide the explicit second-order corrections to the SW system. Our constructive procedure - a modification of the standard averaging principle that admits a component with unbounded flow in the unperturbed Hamiltonian - could be iteratively applied to compute higher-order approximations.

The perturbative scheme used here preserves, by construction, the L^2 norm of the complex massive field to all orders. Such a result is obviously relevant from a physical point of view. For example, in the dark matter problem, it corresponds to the conservation of the total dark mass in the system to any perturbative order. In turn, this means that, with respect to the original KGW dynamics, the total mass is approximately conserved over long time scales ($1/\varepsilon^n$ to order n), even when the original dynamics and the approximating one are far apart from each other (which typically occurs on the time scale $1/\varepsilon$). Another important point concerns the possibility of explaining the cooling mechanism of dark matter, i.e. why, starting with a relativistic dynamics, particles of extremely small mass that interact gravitationally move according to approximate, non relativistic equations (as the SW and the SP equations).

We observe that interpreting the KGW system as a set of coupled harmonic oscillators and free particles proves useful when studying the analytical details of the normal form procedure. Moreover, such an idea could be applied to physical systems having nothing to do with those considered here, but that can be reduced - from a mathematical point of view - to normal modes coupled with free particles.

Chapter 6

Stability Analysis

6.1 Introduction

One of the most challenging aspects of the Schrödinger-Poisson system is the analysis of stability for its stationary states. This problem is particularly complex due to its infinite-dimensional and nonlinear nature, which has led numerical approaches to become the dominant methods for its investigation.

Pioneering work in this area was developed by Guzman, who conducted a series of studies focused on the radial case, examining the system in its original form [66] and in the presence of self-interaction [67]. As described in Chapter 3, his results demonstrate that dynamics starting near excited states leads to mass radiation, and the remaining matter collapses to the ground state – a phenomenon termed gravitational cooling. In parallel work, Harrison et al. [71] obtained similar results, examining even stationary states with axial symmetry rather than spherical symmetry. His findings also revealed the collapse of excited states toward the ground state. These initial works were followed by much more sophisticated and computationally intensive simulations that investigated the full three-dimensional dynamics without symmetry restrictions. These studies revealed that the evolution continues without reaching a clear equilibrium, and that radial profiles resembling stationary states can only be recovered when averaged over time and space.

Analytical studies remain scarce due to the inherent complexity of this infinite-dimensional, nonlinear problem. Notable analytical work includes that of Ohta [115], who focused not on the Schrödinger-Poisson system but rather on the Schrödinger-Wave system and its Schrödinger-Klein-Gordon variant. We cite this work because it remains relevant to this thesis, given the connections between the KGW, SW, and SP systems outlined in Chapter 5. Ohta's analysis centers on the ground state and proves that the energy attains a strict minimum at this configuration. This result guarantees the existence of a neighborhood around the ground state where the energy level sets are compact, ensuring that dynamics starting sufficiently close remain confined near the ground state. The proof relies on both energy conservation and conservation of the $L^2(\mathbb{R}^3)$-norm of the matter field, and applies only to the ground state. Subsequent interesting developments have extended these ideas to the Schrödinger-Klein-Gordon system [84, 85, 83].

Given the difficulties inherent in treating excited states for the Schrödinger-Poisson system, researchers often study restricted cases that can first be developed analytically and then complemented with numerical solutions. The simplest such problem studies radial perturbations of spherically symmetric stationary states, often linearized to examine first-order contributions. This spectral analysis provides insight into the existence of stable or unstable characteristic modes – directions along which perturbations oscillate, decay, or grow over time. However, this approach is limited by the linearization itself. While in finite-dimensional systems linearized dynamics can provide good approximations to the full problem under appropriate conditions, as guaranteed by the Großman-Hartman theorem, the infinite-dimensional case is far more complex. The relationship between linearized and complete dynamics becomes much harder to establish, and a linearized problem exhibiting certain stability properties might correspond to a complete nonlinear system with entirely opposite behavior.

This Chapter aims to collect observations on the stability of stationary states in the Klein-Gordon-Wave problem, for which, to our knowledge, no specific results yet exist. Given the complexity of the problem, we present only a preliminary study rather than attempting a complete and exhaustive analysis, which would require dedicated independent research.

In Section 6.2, we develop analytical considerations regarding the stability problem, demonstrating why standard strategies based on the compactness of level sets of first integrals fail to apply. Through

counterexamples, we show that stationary states do not serve as energy minima but rather behave like saddle points. Moreover, the application of standard approaches like Ohta's method is further complicated by the absence of $L^2(\mathbb{R}^3)$-norm conservation for the matter field, which reduces the number of available first integrals and thus limits the possibility of establishing confinement results for the dynamics.

In Section 6.3, we focus on linearized perturbations around Klein-Gordon-Wave stationary states, restricting our analysis to the first-order contributions. We begin with analytical considerations on unstable modes, which suggest the existence of unstable directions along which perturbations can grow over time. By exploiting known properties of the problem's stationary states, which serve as background configurations for the perturbation dynamics, we lay the foundations for a complete proof of this result.

We complement this analytical work with numerical studies restricted to radial perturbations. Focusing on the unstable modes, we find numerical confirmation of our theoretical insights. All spherically symmetric stationary states of the KGW system – both ground and excited states – possess directions along which perturbations grow. For a stationary state with excitation index n, we identify $n+1$ unstable modes. Our numerical calculations not only allow us to study the problem's spectrum but also to examine the profiles of the associated eigenfunctions, which we compare with the examples derived from our analytical study.

The work presented here represents only the initial stage of what could become much more extensive research on stability. While our analysis of the linearized perturbation problem does not provide information about stability in the full nonlinear case, we hope this study will strengthen intuition about the problem and provide a foundation for future systematic and comprehensive investigations.

6.2 Analytical Considerations on stability

Intuitively, investigating the stability of a system around a stationary state $f_n(x)$ means considering initial conditions $f(t=0,x) \equiv f(x)$ which are close in some norm to the stationary state $f_n(x)$, and checking if the distance between the associated flow $f(t,x)$ and $f_n(x)$ – computed in the same norm – remains finite as long as the flow exists. Formally, this intuitive notion can be formulated in different definitions of stability, depending on the selected norm and on the domain of existence of the flow. In our study on the stability of the KGW system, we start by reviewing the structure of equations with the goal of defining the domain of its dynamical variables. This suggests a natural norm for the state of the system, which we use to formulate a definition of stability. Based on this notion of stability, we recall the most commonly used method to prove it, which relies on studying the level sets of the first integrals of the problem, and we show how this is not applicable in the case of stationary states of the KGW problem. These observations are a typical feature of the KGW problem, and distinguish it from other systems where the characterization of level sets of first integrals is more accessible. We emphasize that what we adopt is only one of the possible approaches, and that different notions of stability, for example associated with a different choice of norm, could highlight different behaviors from those we present.

To define an appropriate norm for the KGW system, we consider the mathematical structure of the problem, and formulate reasonable assumptions for the domain of the fields that describe it. We recall from Chapter 5.2 that the KGW problem is of Hamiltonian type, with conjugate variables $(u, p_u \equiv \partial_t u)$ for the matter field and $(\phi, p_\phi \equiv \partial_t \phi)$ for the gravitational potential, which we denote globally as $f \equiv (u, \phi, p_u, p_\phi)$. We report the system Hamiltonian for convenience:

$$H = \int \left[\frac{p_u^2 + \mu^2 u^2 + |\nabla u|^2}{2} + \frac{p_\phi^2 + |\nabla \phi|^2}{2} + \phi u^2 \right] . \tag{6.1}$$

In order for the Hamiltonian to be well defined, momenta p_u and p_ϕ need to be in $L^2(\mathbb{R}^3)$, the field u in $H^1(\mathbb{R}^3)$ and the potential ϕ be such that $\nabla\phi \in L^2(\mathbb{R}^3)$, even though ϕ itself may not be in $L^2(\mathbb{R}^3)$. We assume ϕ to be in $L^6(\mathbb{R}^3)$, overall resulting in:

$$f \equiv (u, \phi, p_u, p_\phi) \in \mathcal{X} \qquad \mathcal{X} \equiv H^1(\mathbb{R}^3) \times \{\phi \,|\, \phi \in L^6(\mathbb{R}^3), \nabla\phi \in L^2(\mathbb{R}^3)\} \times L^2(\mathbb{R}^3) \times L^2(\mathbb{R}^3) \,.$$

While the domains for u, p_u and p_ϕ are standard Banach spaces with associated natural norms, the domain for the ϕ component is taken as the intersection of two Banach spaces: $L^6(\mathbb{R}^3)$ with natural norm $\|\cdot\|_6$ and $\{\phi \,|\, \nabla\phi \in L^2(\mathbb{R}^3)\}$ with natural norm $\|\nabla \cdot\|_2$. The intersection of two Banach spaces

is still a Banach space, with natural norm defined as the maximum of the two natural norms. In the present case, the Gagliardo-Nirenberg inequality can be applied to control the $L^6(\mathbb{R}^3)$-norm of the function with the $L^2(\mathbb{R}^3)$-norm of its grandient: $\|\phi\|_6 \leq C_{GN}\|\nabla\phi\|_2$, with optimal Gagliardo-Nirenberg constant $C_{GN} \equiv 4^{1/3}/(3^{1/2}\pi^{2/3}) < 1$ [42]. In particular $\max(\|\phi\|_6, \|\nabla\phi\|_2) = \|\nabla\phi\|_2$ is the natural norm for ϕ, so that we can define:

$$\|f\|^2_{\mathcal{X}} \equiv \|u\|^2_{H^1} + \|\nabla\phi\|^2_2 + \|p_u\|^2_2 + \|p_\phi\|^2_2 \,. \tag{6.2}$$

The $\|\cdot\|_{\mathcal{X}}$ norm is therefore a natural choice for the KGW problem. Denote with $f_n(x) \equiv (u_n(r), \phi_n(r), p_u(r) = 0, p_\phi(r) = 0)$ the n-th excited spherically symmetric stationary state and consider the KGW dynamics (5.1) with $\mu^2 = \mu_n^2$. Assuming existence and uniqueness of the KGW flow in $[0, T]$, we consider the following definition of stability:

Definition 6.1 (Stability)**.** The KGW problem (5.1) is stable around its stationary solution f_n if:

$$\forall\varepsilon > 0\ \exists\delta > 0 \text{ s.t.: } f \text{ solves (5.1) with } \|f(0,\cdot) - f_n\|_{\mathcal{X}} < \delta \Rightarrow \|f(t,\cdot) - f_n\|_{\mathcal{X}} < \varepsilon, \quad \forall t \in [0,T]\,.$$

A common strategy to prove stability consists in analyzing the structure of the constants of motion, in this case the energy functional H (6.1). If its level sets are compact, at least in a neighborhood of f_n, then all the flows starting from that neighborhood will remain confined for all times, since they are constrained in the level set selected by the initial condition. A typical way of proving compactness of energy level sets consists in showing that the energy functional is either a strictly growing or a strictly decreasing function of the distance from f_n. This is typically achieved by checking the variations of the energy functional. Let $\delta f \equiv f - f_n$ be the difference between a generic $f \in \mathcal{X}$ and the n-th stationary state f_n, and denote by $\Delta H_n(\delta f) \equiv H(f_n + \delta f) - H(f_n)$ the difference of the corresponding energies. The latter can be computed using a Taylor expansion around f_n, which, being $H(f)$ polynomial, involves only terms up to the third order:

$$\begin{aligned}
\Delta H_n(\delta f) &\equiv H(f_n + \delta f) - H(f_n) \\
&= H'(f_n)\delta f + H''(f_n)\delta f^2 + H'''(f_n)\delta f^3 \\
&= \frac{1}{2}\int_{\mathbb{R}^3} \left((\delta p_u)^2 + (\delta p_\phi)^2\right) \mathrm{d}^3x + \frac{1}{2}\int_{\mathbb{R}^3} \left(|\nabla\delta u|^2 + |\nabla\delta\phi|^2\right) \mathrm{d}^3x + \frac{\mu_n^2}{2}\int_{\mathbb{R}^3} (\delta u)^2 \,\mathrm{d}^3x + \\
&\quad + \int_{\mathbb{R}^3} 2u_n\,\delta u\delta\phi \;\mathrm{d}^3x + \int_{\mathbb{R}^3} \phi_n(\delta u)^2 \;\mathrm{d}^3x + \int_{\mathbb{R}^3} \delta\phi(\delta u)^2 \;\mathrm{d}^3x \,.
\end{aligned} \tag{6.3}$$

Observe that the first order variation of the energy is zero in correspondence of a stationary state, $H'(f_n) = 0$. Among the non-vanishing integrals in expansion (6.3), the first three are non-negative for every variation δf, whereas the last three – originating from the second and third order variations of the interaction part $\int \phi u^2$ – may have both positive and negative sign.

Given the energy difference (6.3), a sufficient condition to prove stability 6.1 is given by:

$$\exists C_1, C_2 > 0 \text{ s.t.: } \quad \forall\varepsilon > 0, \quad 0 < \|\delta f\|_{\mathcal{X}} < \varepsilon \;\Rightarrow\; C_1\|\delta f\|^2_{\mathcal{X}} \leq |\Delta H_n(\delta f)| \leq C_2\|\delta f\|^2_{\mathcal{X}} \tag{6.4}$$

Condition (6.4) ensures that variations of the energy functional in a neighborhood of f_n are either strictly positive or strictly negative, with the lower bound preventing the case of null energy difference along some directions δf. This would imply the existence of compact level sets of the energy near the stationary state, and thus stability in the sense of Def. 6.1.

Unfortunately, condition (6.4) does not hold in the KGW case, as can be seen through appropriate counterexamples:

Lemma 4. *The KGW problem does not satisfy condition* (6.4)*. In particular:*

(1) $\forall\varepsilon > 0 \quad \exists\delta f_*, \quad 0 < \|\delta f_*\|_{\mathcal{X}} < \varepsilon, \quad$ *s.t.:* $\quad \Delta H_n(\delta f_*) = 0,$

(2) $\forall\varepsilon > 0 \quad \exists\delta f_+, \delta f_-, \quad 0 < \|\delta f_+\|_{\mathcal{X}} < \varepsilon, \quad 0 < \|\delta f_-\|_{\mathcal{X}} < \varepsilon, \quad$ *s.t.:* $\quad \Delta H_n(\delta f_+) > 0,$
$\Delta H_n(\delta f_-) < 0\,.$

In particular, the first property of Lemma 4 ensures the existence of a direction δf_* along which the energy functional vanishes. This prevents us from writing the lower bound in condition (6.4), more explicitly:

$$\forall C_1 > 0, \quad C_1 \|\delta f_*\|^2_{\mathcal{X}} > \Delta H_n(\delta f)\,.$$

Moreover, the second property of Lemma 4 ensures the existence, in the same neighborhood of f_n, of two directions δf_+ and δf_- yielding positive and negative energy differences, respectively. This suggests that the stationary states behave as saddle points for the energy functional H (6.1).

Proof of Lemma 4. Let us first define δf_* such that the energy difference is equal to zero. A simple choice consists in choosing a matter field component proportional to the matter field u_n of the stationary state f_n, while all other components are zero :

$$\delta f_* \equiv (\varepsilon_* u_n, 0, 0, 0).$$

Its norm is strictly positive, and there always exists a choice of ε_* so to satisfy the hypothesis:

$$\|\delta f_*\|^2_{\mathcal{X}} = \varepsilon_*^2 \| u_n\|^2_{H^1}, \qquad 0 < \|\delta f_*\|_{\mathcal{X}} < \varepsilon \qquad \text{provided that: } \varepsilon_* < \frac{\varepsilon}{\| u_n\|_{H^1}},$$

where the existence of such ε_* is guaranteed by the fact that, being $f_n \in \mathcal{X}$, the norm $\| u_n\|_{H^1}$ is finite. The energy difference associated to such δf_* is equal to zero, ending the first proof:

$$\begin{aligned}\Delta H_n(\delta f_*) &= \varepsilon_*^2 \left[\frac{1}{2}\int_{\mathbb{R}^3} \left(|\nabla u_n|^2\right) \mathrm{d}^3x + \frac{\mu_n^2}{2}\int_{\mathbb{R}^3} u_n^2 \,\mathrm{d}^3x + \int_{\mathbb{R}^3} u_n^2\phi_n \,\mathrm{d}^3x\right] \\ &= \varepsilon_*^2 \left[\frac{1}{2}\int_{\mathbb{R}^3} \left(|\nabla u_n|^2 + \mu_n^2 u_n^2 + 2u_n^2\phi_n\right) \mathrm{d}^3x\right] = 0\,.\end{aligned}$$

where the last equality is guaranteed by the stationary Klein-Gordon equation in the definition (5.10) of stationary state.

Let us now define δf_- such that the energy difference is negative. A simple choice, obtained as a modification of the previous counterexample, is:

$$\delta f_- \equiv (\varepsilon_* u_n, \varepsilon_* \phi_n, 0, 0).$$

With considerations analogous to the previous counterexample, one can prove that its norm is strictly positive, and there always exists a choice of ε_* so to satisfy the hypothesis:

$$\|\delta f_-\|^2_{\mathcal{X}} = \varepsilon_*^2(\| u_n\|^2_{H^1} + \| \nabla\phi_n\|^2_2), \qquad 0 < \|\delta f_-\|_{\mathcal{X}} < \varepsilon \qquad \text{provided that: } \varepsilon_*^2 < \frac{\varepsilon^2}{\| u_n\|^2_{H^1} + \| \nabla\phi_n\|^2_2},$$

When computing the energy difference, the terms which are common to the previous counterexample still give a null contribution, whereas the new terms contribute negatively:

$$\begin{aligned}\Delta H_n(\delta f_-) &= \frac{\varepsilon_*^2}{2}\int_{\mathbb{R}^3} \left(|\nabla\phi_n|^2\right) \mathrm{d}^3x + 2\varepsilon_*^2 \int_{\mathbb{R}^3} u_n^2\phi_n \,\mathrm{d}^3x + \varepsilon_*^3 \int_{\mathbb{R}^3} u_n^2\phi_n \,\mathrm{d}^3x \\ &= \left(\frac{3}{2}\varepsilon_*^2 + \varepsilon_*^3\right)\int_{\mathbb{R}^3} u_n^2\phi_n \,\mathrm{d}^3x < 0\,.\end{aligned}$$

where the stationary wave equation in the definition (5.10) of stationary state has been used, and where the sign is determined by the fact that stationary states have strictly negative potential $\phi_n < 0$.

Finally, the case of positive energy difference can be set by considering a potential with strictly positive sign:

$$\delta f_+ \equiv (\varepsilon_* u_n, -\varepsilon_* \phi_n, 0, 0)\,.$$

The norm is the same as for the δf_+ case, and analogous computations prove that energy difference is positive. □

The counterexamples presented in the proof of Lemma 4 suggest that in the neighborhood of f_n, defined according to the $\mathcal{X}$-norm, the energy difference $\Delta H_n(\delta f)$ may assume both positive and negative values, depending on the choice of δf. Observe that the terms in $\Delta H_n(\delta f)$ which are responsible for sign determination are not restricted to third order terms. The presence of possibly negative second order terms suggests that instabilities may emerge even at the first order approximation of the system, when considering its linearized form.

6.3 Linear perturbations in KGW

A standard approach to the stability of dynamical problems consists of studying the perturbation problem, that is, to consider small variations of the eigenstates of the system and to check how they evolve over time. When non-linearity is involved, this problem is often linearized, focusing on first order contributions to detect stable and unstable directions along which the perturbations may oscillate, collapse or diverge. This type of analysis is known as linear or spectral stability.

In the finite-dimensional case, the stability or instability of the linear problem often reflects the behavior of the complete system in the neighborhood of the equilibrium: the Hartman-Großman theorem ensures that the behavior of a dynamical system in a domain near a hyperbolic equilibrium point is qualitatively the same as the behaviour of its linearization near this equilibrium point, where hyperbolicity means that no eigenvalue of the linearization has real part equal to zero.

In the infinite-dimensional case the problem is more difficult to treat, since the results obtained for the linearized problem in the neighborhood of an equilibrium may differ considerably from their nonlinear counterparts. Nevertheless, given the difficulty of studying the stability for the complete KGW problem, we restrict to studying the stability of the linearized perturbation problem. This problem is interesting by itself and if future works were to shed more light on the stability properties of the complete KGW problem, then a comparison with our results would clarify the role of the nonlinear contribution, isolating it from the effects of the linear part.

Let us consider the usual KGW problem, reported here for ease of reference:

$$\begin{cases} \Box\, u = (\mu^2 + 2\phi)\, u \\ \Box\, \phi = u^2 \end{cases} . \tag{6.5}$$

In order to study the spectral stability of the problem, consider small variations of the n-th stationary solution (μ_n^2, u_n, ϕ_n):

$$\begin{cases} u(t,x) \equiv u_n(x) + \delta u(t,x) \\ \phi(t,x) \equiv \phi_n(x) + \delta\phi(t,x) \end{cases}$$

and plug these expressions in the KGW system (6.5) with $\mu^2 = \mu_n^2$. Recalling the definition of stationary states, that lets all terms without perturbations $(\delta u, \delta\phi)$ vanish, we get:

$$\begin{cases} \triangle\,(\delta u) - \partial_t^2\,(\delta u) = \mu_n^2(\delta u) + 2\phi_n(\delta u) + 2u_n(\delta\phi) + 2(\delta u)(\delta\phi) \\ \triangle\,(\delta\phi) - \partial_t^2\,(\delta\phi) = 2u_n(\delta u) + (\delta u)^2 \end{cases} ,$$

which expresses the KGW problem (6.5) in terms of the variations $\delta u(t,x)$, $\delta\phi(t,x)$, while $u_n(r)$, $\phi_n(r)$ play the role of background functions. At this point, let us approximate the problem, by neglecting higher order terms in the variations. The linearized KGW perturbation problem reads:

$$\begin{cases} \triangle\,(\delta u) - \partial_t^2\,(\delta u) = \mu_n^2(\delta u) + 2\phi_n(\delta u) + 2u_n(\delta\phi) \\ \triangle\,(\delta\phi) - \partial_t^2\,(\delta\phi) = 2u_n(\delta u) \end{cases} . \tag{6.6}$$

Due to the second-order temporal character of the Klein-Gordon equation, we consider perturbations in the harmonic form:

$$\delta u(t,x) \equiv U(x)e^{i\omega t}\,, \qquad \delta\phi(t,x) \equiv \Phi(x)e^{i\omega t}\,, \tag{6.7}$$

where the spatial functions $U(x)$ and $\Phi(x)$ can be chosen to be real without loss of generality. The system becomes:

$$\begin{cases} \triangle\, U + \omega^2\, U = \mu_n^2 U + 2\phi_n U + 2u_n \Phi \\ \triangle\, \Phi + \omega^2\, \Phi = 2u_n U \end{cases}$$

or, in matrix form:

$$\begin{bmatrix} -\triangle + \mu_n^2 + 2\phi_n & 2u_n \\ 2u_n & -\triangle \end{bmatrix} \begin{pmatrix} U \\ \Phi \end{pmatrix} = \omega^2 \begin{pmatrix} U \\ \Phi \end{pmatrix} . \tag{6.8}$$

For fixed μ_n^2, (u_n, ϕ_n), system (6.8) is a linear eigenvalue problem in the form $Av = \omega^2 v$. The operator A is real and symmetric – observe that it involves the Δ operator, that is also symmetric – resulting in real eigenfunctions U, Φ and real eigenvalues $\omega^2 \in \mathbb{R}$. In particular, the sign of the eigenvalue determines the nature of the frequency parameter ω: if $\omega^2 \geq 0$ the frequency ω is real, $\omega \in \mathbb{R}$; otherwise, if $\omega^2 < 0$, the frequency is purely imaginary, $i\omega \in \mathbb{R}$.

This distinction determines the behavior of the linearized perturbation problem: if $\omega^2 \geq 0$ and thus $\omega \in \mathbb{R}$, then the variations $\delta u(t,x)$, $\delta\phi(t,x)$ defined in (6.7) would oscillate in time and their norm would remain confined, neither diverging nor collapsing; if $\omega^2 < 0$ and $i\omega \in \mathbb{R}$, then the variations $\delta u(t,x)$, $\delta\phi(t,x)$ would collapse to zero along $i\omega < 0$ directions (absolute spectral stability), or diverge to infinity along $i\omega > 0$ directions (spectral instability).

In the following, we study the sign of the eigenvalue ω^2 of the linear perturbation problem (6.8) in order to investigate the existence of unstable modes $\omega^2 < 0$. First, we address the problem from an analytical point of view, characterizing the eigenvalues ω^2 through an appropriate functional and proving it admits negative values along specific directions. This suggest that all stationary states of the KGW problem – ground included – admit unstable perturbations. Then, we complement the study with a numerical computation of the negative part of spectrum, restricted to the radial perturbation case. The numerical results confirm and refine the analytical considerations, specifying that the n-th stationary state of the KGW problem admits $n+1$ unstable eigenmodes, along which the linearized perturbations diverge. The numerical approach also offers the possibility of visualizing the eigenmodes profiles, and to appreciate the similarity with the example suggested by the analytical study.

6.3.1 Analytical approach to the linear perturbation problem

Adopting an analytical approach, we study the sign of ω^2 through considerations on the weak form of the linearized problem (6.8). Starting from the problem in matrix form, we left multiply both sides by the row vector $[U, \Phi]$, integrate and apply integration by parts to obtain an equivalence in the form $\langle v, Av\rangle = \omega^2 \langle v, v\rangle$:

$$\int \left(|\nabla U|^2 + |\nabla\Phi|^2 + \mu_n^2 U^2 + 2\phi_n U^2 + 4u_n U\Phi\right) \mathrm{d}^3x = \omega^2 \int \left(U^2 + \Phi^2\right) \mathrm{d}^3x\,. \tag{6.9}$$

Based on this weak form of the eigenvalue problem, and extending to generic, possibly complex-valued functions U, Φ, let us define the functional:

$$Q[U,\Phi] = \frac{N[U,\Phi]}{D[U,\Phi]} \equiv \frac{\int \left(|\nabla U|^2 + |\nabla\Phi|^2 + \mu_n^2|U|^2 + 2\phi_n|U|^2 + 2u_n(\overline{U}\Phi + U\overline{\Phi})\right) \mathrm{d}^3x}{\int (|U|^2 + |\Phi|^2)\, \mathrm{d}^3x}\,, \tag{6.10}$$

where the $\int 4u_n U\Phi\, \mathrm{d}^3x$ term in (6.9) has been substituted by $\int 2u_n(\overline{U}\Phi + U\overline{\Phi})\, \mathrm{d}^3x$ to account for the eventual complexity of U, Φ. This functional provides a natural rephrasing of the eigenproblem (6.8) in its weak form, characterizing the solutions (U,Φ) associated with a given ω^2 as the functions satisfying:

$$Q[U,\Phi] = \omega^2\,, \tag{6.11}$$

Using this formulation of the problem, we aim to prove the existence of a negative eigenvalue $\omega_*^2 < 0$ and of functions U_*, Φ_* solving problem (6.11) with $\omega^2 = \omega_*^2$. According to the considerations described above, this would imply spectral instability, with perturbations $\delta u(t,y) = U_*(y)e^{i\omega_* t}$, $\delta\phi(t,y) = \Phi_*(y)e^{i\omega_* t}$ diverging with a characteristic time ω_*^{-1}.

In order to prove the existence of a negative eigenvalue, we may demonstrate that the functional $Q[\delta u, \delta\phi]$ is lower bounded and coercive, which ensures the existence of a minimum [46]. Then, we may prove that there exists a specific choice of functions (U,Φ) for which the functional $Q[U,\Phi]$ is negative valued. This implies that the minimum is also negative valued, and we would prove our thesis. In this work, we limit ourselves to prove the lower boundedness of the functional and the existence of negative values $Q[U,\Phi] < 0$. This is not sufficient to complete the proof, but supports the intuition on the nature of the problem. We conclude by corroborating these analytical considerations with a numerical study, that confirm the existence of negative eigenvalues $\omega^2 < 0$ for all stationary states of the KGW problem, ground included.

Lower bound

Let us start by proving that the functional $Q[U,\Phi]$ defined in (6.10) is lower bounded. In the numerator, the bound on square contributions is easily set, recalling that $\mu_n^2 > 0$:

$$\int (|\nabla U|^2 + |\nabla\Phi|^2 + \mu_n^2|U|^2)\,\mathrm{d}^3x \geq 0\,,$$

while the term involving the eigenpotential ϕ_n can be estimated by recalling that $\phi_n(y) < 0$ is negative valued and that $\phi_n \in L^\infty$ [100]:

$$\int 2\phi_n|U|^2\,\mathrm{d}^3x = -2\int |\phi_n|\,|U|^2\,\mathrm{d}^3x \geq -2\sup_{x\in\mathbb{R}^3}|\phi_n(x)|\int |U|^2\,\mathrm{d}^3x = -2\|\phi_n\|_{L^\infty}\|U\|_{L^2}^2\,.$$

The last term in the numerator of the functional (6.10) is bounded using $u_n \in L^\infty$ together with the Cauchy-Schwarz (CS) and the Young (Y) inequality:

$$\begin{aligned}\int 2u_n(\overline{U}\Phi + U\overline{\Phi})\,\mathrm{d}^3x &\geq -4\int |u_n|\,|U\Phi|\,\mathrm{d}^3x \geq -4\|u_n\|_{L^\infty}\int |U\Phi|\,\mathrm{d}^3x \\ &\overset{CS}{\geq} -4\|u_n\|_{L^\infty}\|U\|_{L^2}\|\Phi\|_{L^2} \overset{Y}{\geq} -2\|u_n\|_{L^\infty}(\|U\|_{L^2}^2 + \|\Phi\|_{L^2}^2)\end{aligned}$$

Overall, the lower bound on the functional (6.10) reads:

$$\begin{aligned}Q[U,\Phi] &\geq \frac{-2\|\phi_n\|_{L^\infty}\|U\|_{L^2}^2 - 2\|u_n\|_{L^\infty}(\|U\|_{L^2}^2 + \|\Phi\|_{L^2}^2)}{\|U\|_{L^2}^2 + \|\Phi\|_{L^2}^2} \\ &\geq -2\|\phi_n\|_{L^\infty}\frac{\|U\|_{L^2}^2}{\|U\|_{L^2}^2 + \|\Phi\|_{L^2}^2} - 2\|u_n\|_{L^\infty} \\ &\geq -2\|\phi_n\|_{L^\infty} - 2\|u_n\|_{L^\infty}\end{aligned}$$

where in the last inequality we used $\|\Phi\|_{L^2}^2 \geq 0$ to let the fraction simplify.

These inequalities are not sharp and might be improved to get a reliable estimate of the characteristic instability time $\tau = (i\omega_*)^{-1}$. Nevertheless, they are sufficient to prove the lower boundedness required for our purposes.

Existence of negative value

We now prove that there exists a specific choice of functions U, Φ for which the functional $Q[U,\Phi]$ is negative valued. As a preliminary observation, notice that the numerator in (6.10) has some similarities with the energy variations $\Delta H_n(\delta f)$ we studied in Section 6.2, suggesting that the construction we need here might be similar to the counterexamples we set there. In particular, the choice $U = u_n$, $\Phi = 0$ still allows one to recover the definition of eigenfunction u_n in the numerator, thus letting the functional vanish:

$$Q[u_n, 0] = \frac{\int \left(\Delta u_n + \mu_n^2 u_n + 2\phi_n u_n\right) u_n\,\mathrm{d}^3x}{\int u_n^2\,\mathrm{d}^3x} = 0$$

This result is not surprising. When applied to the original eigenstate (μ_n^2, u_n, ϕ_n), the perturbation we consider does not affect the eigenpotential and modifies the eigenfunction only by a proportionality factor. Thus, the perturbed state still solves the stationary KGW problem (6.5), although with a different normalization, meaning that it is still a fixed point of the KGW dynamics. Thus, the perturbation is preserved, and naturally solves the (linearized) perturbation problem with $\omega^2 = 0$.

Following the same intuition, we maintain a perturbation $U = u_n$ on the eigenfunction and we tune Φ to yield $Q[u_n,\Phi] < 0$. A natural choice, consistent with the counterexamples of Section 6.2, would be to set $\Phi = \phi_n$ and use the stationary Poisson equation, which would lead to a negative valued numerator in (6.10):

$$N[u_n,\phi_n] = \int \left(\left(\Delta u_n + \mu_n^2 u_n + 2\phi_n u_n\right) u_n + (-\Delta\phi_n + 4u_n^2)\phi_n\right)\mathrm{d}^3x = -3\int u_n^2|\phi_n|\,\mathrm{d}^3x < 0$$

However, this choice is not viable, since the perturbation Φ needs to be in $L^2(\mathbb{R}^3)$ in order for the denominator of (6.10) to be well defined, and the eigenpotential ϕ_n does not satisfy this requirement. We therefore introduce a regularization, and define the family of functions:

$$\phi_n^\varepsilon(x) = -\frac{1}{4\pi}\int \frac{e^{-\varepsilon|x-y|}}{|x-y|} u_n^2(y)\,\mathrm{d}^3y$$

which solve the following equation:

$$(\Delta - \varepsilon^2)\phi_n^\varepsilon = u_n^2 \tag{6.12}$$

and have the required regularity $\phi_n^\varepsilon \in L^2(\mathbb{R}^3)$, while reducing to the stationary state potential $\phi_n(r)$ in the limit $\varepsilon \to 0$. By choosing $U = u_n$, $\Phi = \phi_n^\varepsilon$ and by using the regularized equation (6.12) instead of the Poisson equation to simplify the numerator, we get:

$$N[u_n, \phi_n^\varepsilon] = -3\int |\nabla\phi_n^\varepsilon|^2\,\mathrm{d}^3x - 4\varepsilon^2\int (\phi_n^\varepsilon)^2\,\mathrm{d}^3x < 0\,,$$

which is negative valued. Due to the improved regularity $\phi_n^\varepsilon \in L^2(\mathbb{R}^3)$, the denominator $D[u_n, \phi_n^\varepsilon]$ is also well defined, and we can state the desired result:

$$Q[u_n, \phi_n^\varepsilon] = \frac{-3\int |\nabla\phi_n^\varepsilon|^2\,\mathrm{d}^3x - 4\varepsilon^2\int (\phi_n^\varepsilon)^2\,\mathrm{d}^3x}{\int (|U|^2 + |\Phi|^2)\,\mathrm{d}^3x} < 0\,.$$

6.3.2 Numerical approach to the radial linear perturbation problem

A standard option for studying the spectral properties of the system consists of numerically solving system (6.8). As a preliminary study, we restrict to the radial case: we assume spherically symmetric initial conditions and this symmetry is preserved by the dynamics, so we can write $U(r) = U(x)$, $\Phi(r) = \Phi(x)$. Recalling that the Laplace operator acts on a radial function $f(r)$ as $\Delta f = r^{-1}\partial_r^2(rf)$, let us define a convenient change of variables:

$$V(r) \equiv rU(r), \qquad W(r) \equiv r\Phi(r)\,.$$

The linear perturbation problem (6.8) can then be restated considering only the radial part:

$$\begin{bmatrix} -\partial_r^2 + \mu_n^2 + 2\phi_n & 2u_n \\ 2u_n & -\partial_r^2 \end{bmatrix} \begin{pmatrix} V \\ W \end{pmatrix} = \omega^2 \begin{pmatrix} V \\ W \end{pmatrix}\,. \tag{6.13}$$

As for the boundary conditions, we assume perturbations to share the same regularity properties of the stationary states. At $r = 0$, both $U(r)$ and $\Phi(r)$ have finite values, implying $V(0) = W(0) = 0$. Instead, their asymptotic behavior with r is different. While $U(r)$ decays superlinearly, causing $V(r) \to 0$ as $r \to \infty$, the eigenmode $\Phi(r)$ associated with the gravitational potential admits an approximately linear decay, $\Phi(r) \sim 1/r$ as $r \to \infty$, which would imply a non-vanishing counterpart $W(r) = \mathcal{O}(1)$. More specifically, in the asymptotic limit of large r the equation for $\Phi(r)$ in (6.13) simplifies, due to the vanishing of the coupling $V(r) \approx 0$, and reduces to:

$$\partial_r^2 W(r) + \omega^2 W(r) = 0 \qquad \text{for large } r\,.$$

The asymptotic solution thus depends on the sign of the eigenvalue ω^2:

$$\begin{aligned} &W(r) \approx A\cos(|\omega|r) + B\sin(|\omega|r) && \text{for } \omega^2 > 0, \\ &W(r) \approx Ce^{-|\omega|r} && \text{for } \omega^2 < 0, \end{aligned}$$

where the additional term $De^{+|\omega|r}$ is not included in the last equation since is would result in a non-physical non-vanishing behavior for $\Phi(r)$. This suggests that eigenmodes $W(r)$ with positive eigenvalue $\omega^2 > 0$, namely those associated with oscillatory behavior in time, have a non-vanishing sinusoidal behavior for large r. On the other side, eigenmodes with negative eigenvalue $\omega^2 < 0$, namely those admitting spectral instability, vanish exponentially for large r.

In our numerical study, aiming to test the existence of unstable eigenmodes, we focus on the latter case $\omega^2 < 0$ and we write $W(r) \to 0$ as $r \to \infty$ as the last boundary condition. We thus need to solve (6.13) with:

$$\begin{cases} V(0) = W(0) = 0 \\ V(\infty) = W(\infty) = 0 \end{cases} \tag{6.14}$$

Implementation

In order to solve the problem numerically, we choose a range $[0, L]$ for r, regarding $r = L$ as being at infinity for the purpose of setting boundary conditions. We set the outer boundary L equal to the numerical domain of the background functions $u_n(r)$, $\phi_n(r)$, additionally testing larger values to ensure the robustness of the implementation. We consider a uniform discretization of $[0, L]$ into N-points $\{r_i\}_{i=0}^N$, with $h \equiv L/N$ the mesh size. The background functions $u_n(r), \phi_n(r)$ are evaluated on the grid, forming the vectors $\mathbf{u}_n \equiv \{u_n(r_i)\}_{i=0}^N$, $\boldsymbol{\phi}_n \equiv \{\phi_n(r_i)\}_{i=0}^N$ and the eigenfunctions $V(r)$, $W(r)$ are also approximated by their evaluation points, $\mathbf{v} \equiv \{v_i = V(r_i)\}_{i=0}^N$, $\mathbf{w} \equiv \{w_i = W(r_i)\}_{i=0}^N$. We approximate the second order derivative with a centered difference scheme, $\partial_r^2 f(r_i) = h^{-2}(f(r_{i+1}) - 2f(r_i) + f(r_{i-1}))$. The discretized system (6.13) reads

$$\begin{bmatrix} -D_2 + \mu_n^2 \mathbb{I} + 2\mathbb{I}\boldsymbol{\phi}_n & 2\mathbb{I}\mathbf{u}_n \\ 2\mathbb{I}\mathbf{u}_n & -D_2 \end{bmatrix} \begin{pmatrix} \mathbf{v} \\ \mathbf{w} \end{pmatrix} = \omega^2 \begin{pmatrix} \mathbf{v} \\ \mathbf{w} \end{pmatrix}, \tag{6.15}$$

with D_2 a tridiagonal matrix

$$D_2 = \frac{1}{h^2} \begin{bmatrix} -2 & 1 & & & \mathbb{0} \\ 1 & -2 & 1 & & \\ & \ddots & \ddots & \ddots & \\ & & 1 & -2 & 1 \\ \mathbb{0} & & & 1 & -2 \end{bmatrix}$$

and with $\mathbb{I}$ the identity matrix, so that $\mu_n^2\mathbb{I}$ is a diagonal matrix with non-vanishing entries μ_n^2, and $\mathbb{I}\mathbf{u}_n$, $\mathbb{I}\boldsymbol{\phi}_n$ are diagonal matrices with non vanishing entries $\{u_n(r_i)\}_{i=0}^N$ and $\{\phi_n(r_i)\}_{i=0}^N$ respectively.

The Dirichlet boundary conditions for both $\mathbf{v}$ and $\mathbf{w}$ are set simply by excluding the boundary points from the system. More explicitly, we delete the corresponding rows and columns in the matrix and the entries in the eigenvectors, and we solve the system on the interior points, setting a posteriori $v_0 = v_N = 0$ and $w_0 = w_N = 0$.

The problem is implemented in `MATLAB` and solved with the built-in function `eig()`. The resulting eigenvectors are normalized to one, their $L^2(\mathbb{R})$-norm being computed on the evaluation points and using the mesh size h as the local weight, $\mathrm{d}r \sim h$. The resulting eigenvalues are then classified as stable, unstable, or zero depending on their sign, with a tolerance tol$= 10^{-10}$ to detect possible zero eigenvalues. Only unstable eigenvalues and their eigenmodes are considered, as the boundary condition (6.14) are not appropriate for stables ones. The number of computed eigenmodes coincides with the rank of the matrix, $2N - 4$. They may include points of the discrete spectrum, samples of the discretized continuum spectrum and possibly spurious modes. In order to identify the reliable physical information, we perform the analysis with different refinements $N \in \{1000, 1050, \ldots, 1500\}$ and check the convergence of the results.

Results

We tested perturbations around the ground state and excited stationary states up to $n = 30$, which could be further extended by allowing for larger computation times. The computations are repeated varying the number N of discretization points, $N \in \{1000 + 50j\}_{j=0}^{10}$, to check the quality and reliability of the results.

The spectrum of the radial linear perturbation problem (6.13) includes $n+1$ negative eigenvalues $\{\omega_k^2\}_{k=0}^n$ for each n-th background stationary solution, belonging to the discrete spectrum and conventionally sorted in descending order. Examples for $n \in \{20, 22, \ldots, 30\}$ are reported in figure 6.1. Each set $\{\omega_k^2\}_{k=0}^n$ displays a smooth dependence on k, with a moderate growth for higher eigenvalues and a steeper growth for more negative eigenvalues. However, fits with the most common functions (exponential law, logarithmic law, power law, parabolic law, and cubic law) do not provide a good match. Smooth behavior is also observed for increasing n, with higher eigenvalues for more excited background states. Thus, the most negative eigenvalue is obtained for $n = 0$, for which $\omega_0^2 \simeq -0.0013$.

Figure 6.2 tests the convergence of the spectrum as the mesh is progressively refined, to verify the robustness of the method. It includes a low excitation example $n = 3$ and a higher excitation example $n = 30$. In each case, the left panel reports the negative part of the spectrum for an increasing number of discretization points N, corroborating its discrete nature. Denoting with $\omega_k^2(N_j)$ the eigenvalue obtained for the j-th value of N, we compute and plot in the right panels the differences between

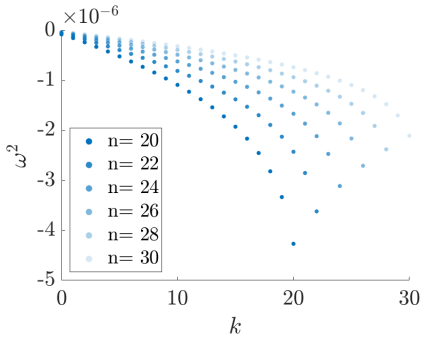

Figure 6.1: Negative eigenvalues $\{\omega_k^2\}_{k=0}^n$ of the radial linear perturbation problem (6.13), sorted in descending order and plotted for different excitations n of the background stationary state $\{\mu_n^2, u_n(r), \phi_n(r)\}$.

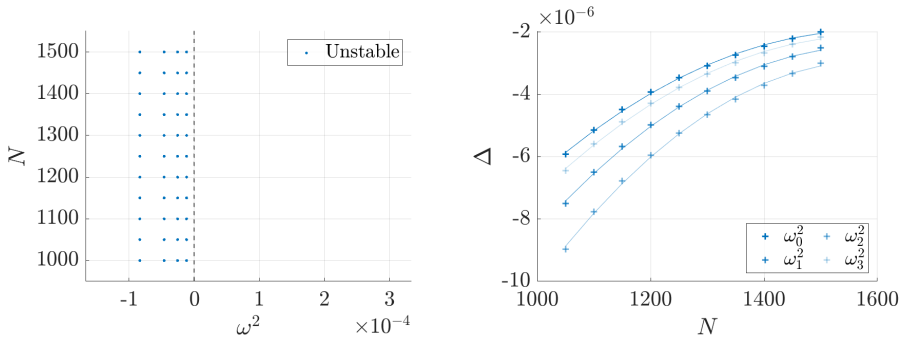

(a) Spectrum as N varies, $n = 3$.

(b) Relative differences, $n = 3$.

(c) Spectrum as N varies, $n = 30$.

(d) Relative differences, $n = 30$.

Figure 6.2: Convergence of the negative part of the spectrum for the radial linear perturbation problem (6.13) as the number N of discretization points varies. Top and bottom panels are relative to the $n = 3$ and the $n = 30$ background stationary states, respectively. Left panels show the spectrum, while right panels plot the corresponding eigenvalue differences between successive refinements relative to the coarsest eigenvalue $\omega^2(N_0)$, as defined in (6.16). For visual simplicity, the differences in the $n = 30$ case are reported only for the last (i.e. with most negative eigevalue) eigenmodes $k = 24, \ldots, 31$.

successive refinements, relative to the coarsest eigenvalue $\omega^2(N_0)$:

$$\Delta_k(N_j) = \frac{\omega_k^2(N_j) - \omega_k^2(N_{j-1})}{\omega_k^2(N_0)}\,. \tag{6.16}$$

We further fit the computed differences $\Delta_k(N)$, finding that for every fixed k they decay parabolically as N increases. The resulting fits are also plotted in the right panels of figure 6.2.

Figure 6.3 focuses on the eigenmodes $\{V_k(r), W_k(r)\}_{k=0}^n$ of the radial linear perturbation problem (6.13) computed for the n-th background stationary state $\{\mu_n^2, u_n(r), \phi_n(r)\}$. It includes a low excitation example $n = 3$ and a higher excitation example $n = 30$.

The eigenmodes $V_k(r)$ associated with matter field perturbations, plotted in the left panels, display a considerable similarity with the function $r\,u_n(r)$ defined for the matter field $u_n(r)$. They share the

same oscillatory behavior and the same number of nodes. This similarity is consistent with the observations of Section 6.3.1, that showed how the matter field $u_n(r)$ is a natural choice to construct an unstable eigenmode. To have a visual comparison, both $V_k(r)$ and the corresponding $r\,u_n(r)$ are plotted, rescaling the latter to match the last local oscillation. In all cases, a slight mismatch is detected, suggesting that the eigenmodes $V_k(r)$ are very similar to but do not coincide with $r\,u_n(r)$. In addition, the first eigenmodes $V_k(r)$ computed for $n = 3$ (top left panel) are very similar to the first eigenmodes $V_k(r)$ computed for $n = 30$ (central left panel), exception made for a different scale factor. This might be due to the fact that the corresponding eigenvalues ω_k^2 computed for $n = 3$ and $n = 30$ are rather similar for low values of k (see figure 6.1).

The eigenmodes $W_k(r)$ associated with gravitational perturbations, plotted in the right panels, do not display any similarity with the functions associated with the n-th stationary state of the KGW problem. They display an oscillating behavior, but nodal patterns and amplitude modulations are more difficult to guess. In addition, differently from the $V_k(r)$ eigenmodes, the first $W_k(r)$ eigenmodes associated with high excitations $n = 30$ are not similar in their shape to the corresponding eigenmodes associated with low excitations $n = 3$. On the contrary, it is the last $W_k(r)$ eigenmodes associated with high excitations $n = 30$ that may share a qualitative "on average" similarity with the $W_k(r)$ eigenmodes of the $n = 3$ case. Nevertheless, the underlying structure is rather difficult to identify and would require a dedicated study.

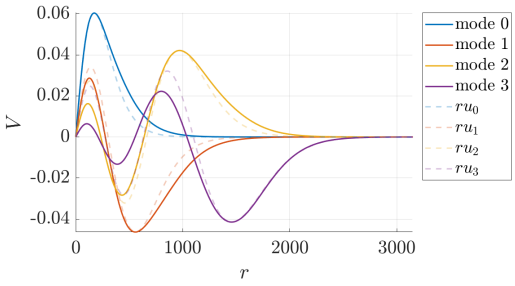

(a) $n = 3$, eigenmodes $V(r) = rU(r)$.

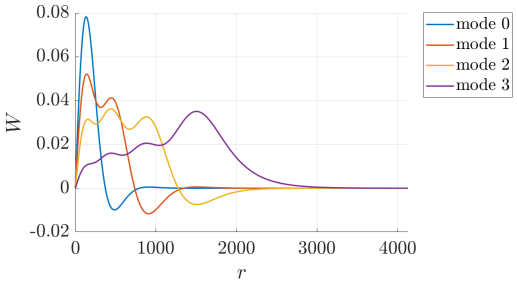

(b) $n = 3$, eigenmodes $W(r) = r\Phi(r)$.

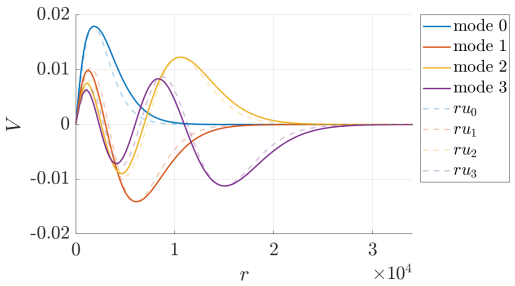

(c) $n = 30$, first eigenmodes $V(r) = rU(r)$.

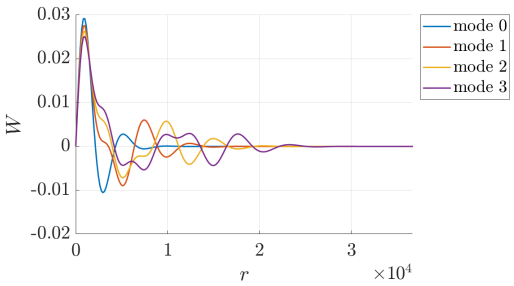

(d) $n = 3$, first eigenmodes $W(r) = r\Phi(r)$.

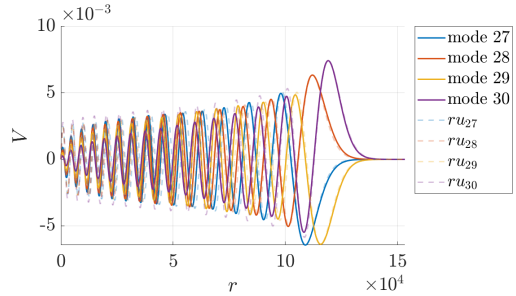

(e) $n = 30$, last eigenmodes $V(r) = rU(r)$.

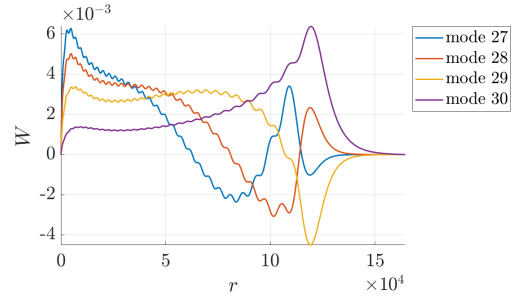

(f) $n = 30$, last eigenmodes $W(r) = r\Phi(r)$.

Figure 6.3: Eigenmodes $V_k(r)$ (left panels) and $W_k(r)$ (right panels) for the radial linear perturbation problem (6.13). Top panels are computed for the $n = 3$ excited background stationary state $\{\mu_3^2, u_3(r), \phi_3(r)\}$ and report all computed eigenmodes, $k = 0, 1, 2, 3$. The remaining panels are computed for the $n = 30$ excited background stationary state $\{\mu_{30}^2, u_{30}(r), \phi_{30}(r)\}$, central panels plotting the first eigenmodes $k = 0, 1, 2, 3$ (with higher eigenvalues) and bottom panels plotting the last eigenmodes $k = 27, 28, 29, 30$ (with more negative eigenvalues).

6.4 Conclusions

In this Chapter, we collect some relevant observations on the stability of the KGW problem. After developing analytical considerations to show how standard strategies fail to apply to our case, we focus on linearized perturbations around Klein-Gordon-Wave stationary states, restricting our analysis to the first-order contributions. Our analytical insights on the problem suggest the existence of unstable modes for each background state, while a complementary computational analysis – restricted to the radial case – confirms this result and provides quantitative support to the analytical study.

The work presented in this Chapter is a preliminary study and may be further developed to gain more solid understanding of this difficult problem. On the computational side, the research could be extended to the stable modes, completing the overview of the linearized radial problem, and could be gradually generalized to relax the simplifying hypotheses, e.g. by considering the angular part of the problem or the higher orders of the perturbations. Of course, these approaches would be very challenging even from the computational point of view, due to the complexity of the non-linear problem under consideration, and would require a careful design of the solver to maintain an affordable computational cost. Computational studies of this type would provide relevant quantitative insight into the stability problem, which could effectively support more rigorous and thorough analytical studies.

Conclusions

The content of this thesis is highly varied in contents and approaches. Motivated by the physical problem of describing the dynamics of galactic dark matter halos, we have explored several features of the Schrödinger-Poisson model, the system most widely employed in the physics community.

Through a broad overview of the physical foundations of the Schrödinger-Poisson system, we have illustrated its connection to General Relativity and Quantum Mechanics, showing its derivation in the Newtonian limit and highlighting the different interpretative nuances that the problem acquires depending on whether one adopts a quantum gravity or semiclassical gravity framework. The presented discussion aims to emphasize how delicate and subtle the physical interpretation of this system and its related results can be. Acknowledging this complexity, we have sought to support the technical aspects of the problem by developing its mathematical study and providing results that are transversal and independent of the chosen interpretation, which we leave open.

We then examined the foundational assumptions underlying the system, showing how a few heuristic principles allow one to derive its essential characteristics. Considering the dark matter cluster as a virialized and fully condensed gas of bosonic particles, we demonstrated how its characteristic length scale and its energy regime depend solely on the amount of mass in the system, particularly on the number of particles and the mass of each individual particle. We then showed how these assumptions apply to galactic dark matter halos by discussing the orders of magnitude of the involved quantities. We also applied the same assumptions to the Schrödinger-Poisson many-body problem, providing a justification to the rescaling of the potential by the number of particles. An interesting aspect of this analysis is that it is carried out independently of any specific choice of dynamics. Although based on an order-of-magnitude approach – more intuitive than rigorous – it yields the most essential relations among the physical quantities involved. These same relations are later reflected in both the Schrödinger-Poisson and Klein-Gordon–Wave dynamics, providing in both cases the rescalings needed to write the system in dimensionless form and assign physical meaning to the parameters governing the dynamics. In this sense, our approach proves particularly effective in capturing the physical content of the problem, condensing it into a few dominant parameters and isolating it from the mathematical structure, which can then be studied independently.

In a subsequent part of the research, we numerically studied the highly excited spherically symmetric stationary states of the Schrödinger-Poisson problem. By separately focusing on eigenfunctions, eigenpotentials, and eigenvelocities, we identified their dominant features and explored their dependence on the excitation index, aiming to compensate for the lack of explicit expressions for these states. The analysis is both complete and accurate, and reveals an underlying highly regular structure which could be further investigated using analytical tools, based on the numerical results we have presented. Moreover, the heuristic laws we identify seem to reflect features considered desirable in a galactic dark matter model: the support of the matter distribution exhibits parabolic growth with the excitation index, characteristic of Keplerian systems; the amplitude of the oscillations in the eigenfunctions decreases following a power law with an exponent asymptotically approaching -1; correspondingly, the mid-range region of the eigenvelocity is on average linear, with a slope that tends asymptotically to zero, reproducing the behavior of many observed rotation curves; finally, through appropriate rescalings, we find that the excited states share a universal character.

We included in the analysis of excited eigenstates a comparison based on a WKB approach. This study is preliminary in nature and limited to constructing an analogy with the linear Schrödinger case – analytically treatable via the WKB method – by assuming known eigenvalues and eigenpotentials to formulate a prediction for the eigenfunctions. Although partial, the result is very encouraging, showing how the analogy with the WKB method in the linear case can yield numerically accurate outcomes. This observation invites further investigation by applying the WKB method, suitably adapted, to the analysis of the full nonlinear problem. This direction, both promising and challenging, remains open as a future line of research.

We finally extended the numerical study of excited eigenstates to the case of stationary external sources contributing to the gravitational potential. By testing various types of sources and systematically varying the parameters that define their profile, we showed that the eigenstates vary in a rather regular fashion, again suggesting that an analytical study of the problem might not be out of reach. This part of the research has been developed in view of fitting experimental data, although further advancement is possible. As a future direction, one could numerically quantify how the heuristic laws we derived change as the profile of the external source is varied. As in the source-free case, such studies could serve as a foundation for further analytical developments concerning the explicit form of stationary states in the Schrödinger-Poisson system.

Once the heuristic laws characterizing the excited eigenstates were identified, we applied them to fit the model to experimental rotation curves. Although the study was performed in the most realistic way possible, using available information from the SPARC database and processing it for our purposes, we stress that our goal was not to extract reliable physical information, since the direct use of excited eigenstates as a model for galactic dark matter is largely disfavored due to their instability. Rather, we aim to demonstrate the usefulness of having explicit heuristic laws when dealing with a fitting problem for an implicitly defined model. The study is intended to show how such auxiliary laws allow one to predict the viability of a certain combination of free parameters without solving the full model. One can thus perform a preliminary exploration of the parameter space, significantly reducing the portion to investigate and thereby lowering the computational cost. In this sense, the problem we address is a particular case of a broader class of problems, consisting in optimizing, as efficiently as possible, a model defined implicitly. In this thesis, we have investigated one possible approach, but the space for exploration remains vast, making further research in this open problem entirely viable.

We then proposed a possible relativistic extension of the Schrödinger-Poisson model: the Klein-Gordon–Wave system. By illustrating its main features, we showed that it operates in two regimes: a high-energy regime where stationary states can be observed, and a low-energy regime where a non-relativistic approximation of the problem is possible. We treated the latter by employing perturbative techniques typical of Hamiltonian systems. In particular, we wrote the Hamiltonian of the Klein-Gordon–Wave system in second-order normal form and showed that its first-order truncation yields the Hamiltonian of the Schrödinger-Wave system, which further reduces to the Schrödinger-Poisson case in the limit of a vanishing perturbative parameter. This analysis is interesting from two perspectives. Physically, it provides a clear, quantitative, and interpretable account of the connection between different physical systems. Analytically, it proposes a first example of a normal form study in the presence of an unperturbed system whose flow has an unbounded component. We showed how in this case it is possible to slightly modify the definition of the normal form by referring only to the bounded component of the unperturbed flow, and to adapt the classical procedures for computing it in a natural yet non-trivial way. Our study is for now purely formal. Its translation into rigorous terms, and in particular the control of the remainder terms, represents a challenging but promising line of research for the future.

The final part of our work aims to offer a small contribution to a highly complex open problem: the stability of stationary states in the Klein-Gordon–Wave system. Drawing inspiration from analogous studies on the Schrödinger-Poisson case, we analyzed the linearized perturbation problem using both analytical and numerical approaches, showing that each stationary state, including the ground state, exhibits directions of instability. The possibilities for future developments on this topic are vast, given the limited literature on the stability of this specific system. The challenges involved in addressing such studies for a nonlinear problem are well known, and advances of this kind – both numerical and analytical – could generate considerable interest.

The variety of approaches adopted in this thesis reflects our strong belief in interdisciplinarity and in the benefits arising from the merging of different skills and perspectives. In this spirit, we hope that the work carried out, though not exhaustive, may spark interest and stimulate further boundary-crossing research in this challenging and fascinating field.

Bibliography

[1] T. Akahori. Global solutions of the wave-Schrödinger system with rough data. *Communications on Pure and Applied Analysis*, 4(2):209–240, 2005. ISSN 1534-0392. doi: 10.3934/cpaa.2005.4.209. URL https://www.aimsciences.org/article/id/e925f052-c65a-4976-809a-2532e1d823ad.

[2] M. Alcubierre, J. Barranco, A. Bernal, J. C. Degollado, A. Diez-Tejedor, M. Megevand, D. Núñez, and O. Sarbach. Boson stars and their relatives in semiclassical gravity. *Phys. Rev. D*, 107:045017, Feb 2023. doi: 10.1103/PhysRevD.107.045017. URL https://link.aps.org/doi/10.1103/PhysRevD.107.045017.

[3] I. Álvarez-Rios, T. Bernal, P.-H. Chavanis, and F. S. Guzmán. Galactic rotation curves of low surface brightness galaxies using core-halo fuzzy dark matter configurations. *Phys. Rev. D*, 110:063502, Sep 2024. doi: 10.1103/PhysRevD.110.063502. URL https://link.aps.org/doi/10.1103/PhysRevD.110.063502.

[4] Z. Ammari and M. Falconi. Wigner Measures Approach to the Classical Limit of the Nelson Model: Convergence of Dynamics and Ground State Energy. *Journal of Statistical Physics*, 157(2):330–362, Oct 2014. ISSN 1572-9613. doi: 10.1007/s10955-014-1079-7. URL https://doi.org/10.1007/s10955-014-1079-7.

[5] Z. Ammari and M. Falconi. Bohr's Correspondence Principle for the Renormalized Nelson Model. *SIAM Journal on Mathematical Analysis*, 49(6):5031–5095, 2017. doi: 10.1137/17M1117598. URL https://doi.org/10.1137/17M1117598.

[6] V. Arnold. *Mathematical Methods of Classical Mechanics*. Applied Mathematical Sciences. Springer New York, 1978. ISBN 9783540903147. URL https://books.google.it/books?id=_0rvAAAAMAAJ.

[7] A. Ashtekar, A. Magnon, and R. Penrose. Quantum fields in curved space-times. *Proceedings of the Royal Society of London. A. Mathematical and Physical Sciences*, 346(1646):375–394, 1975. doi: 10.1098/rspa.1975.0181. URL https://royalsocietypublishing.org/doi/abs/10.1098/rspa.1975.0181.

[8] A. Bachelot. Problème de Cauchy pour des systèmes hyperboliques semi-linéaires. *Annales de l'I.H.P. Analyse non linéaire*, 1(6):453–478, 1984. URL https://www.numdam.org/item/AIHPC_1984__1_6_453_0/.

[9] M. Bahrami, A. Großardt, S. Donadi, and A. Bassi. The Schrödinger–Newton equation and its foundations. *New Journal of Physics*, 16(11):115007, nov 2014. doi: 10.1088/1367-2630/16/11/115007. URL https://dx.doi.org/10.1088/1367-2630/16/11/115007.

[10] J. Baillon and J. M. Chadam. The Cauchy Problem for the Coupled Schroedinger-Klein-Gordon Equations. In G. M. De La Penha and L. A. J. Medeiros, editors, *Contemporary Developments in Continuum Mechanics and Partial Differential Equations*, volume 30 of *North-Holland Mathematics Studies*, pages 37–44. North-Holland, 1978. doi: https://doi.org/10.1016/S0304-0208(08)70857-0. URL https://www.sciencedirect.com/science/article/pii/S0304020808708570.

[11] M. Baldeschi, G. Gelmini, and R. Ruffini. On massive fermions and bosons in galactic halos. *Physics Letters B*, 122(3):221–224, 1983. ISSN 0370-2693. doi: https://doi.org/10.1016/0370-2693(83)90688-3. URL https://www.sciencedirect.com/science/article/pii/0370269383906883.

[12] P. Baldi and E. Haus. On the Normal Form of the Kirchhoff Equation. *Journal of Dynamics and Differential Equations*, 33(3):1203–1230, Sep 2021. ISSN 1572-9222. doi: 10.1007/s10884-020-09904-w. URL https://doi.org/10.1007/s10884-020-09904-w.

[13] D. Bambusi. Galerkin Averaging Method and Poincaré Normal Form for Some Quasilinear PDEs . *Ann. Scuola Norm. Sup. Pisa Cl. Sci.*, 4(4):669–702, Dec 2005. doi: 10.2422/2036-2145.2005.4.06. URL https://journals.sns.it/index.php/annaliscienze/article/view/84.

[14] D. Bambusi. An introduction to Birkhoff normal form, 2014. URL http://users.mat.unimi.it/users/bambusi/dispense.html.

[15] D. Bambusi and B. Grébert. Birkhoff normal form for partial differential equations with tame modulus. *Duke Mathematical Journal*, 135(3):507 – 567, 2006. doi: 10.1215/S0012-7094-06-13534-2. URL https://doi.org/10.1215/S0012-7094-06-13534-2.

[16] D. Bambusi and N. Nekhoroshev. A property of exponential stability in nonlinear wave equations near the fundamental linear mode. *Physica D: Nonlinear Phenomena*, 122(1):73–104, 1998. ISSN 0167-2789. doi: https://doi.org/10.1016/S0167-2789(98)00169-9. URL https://www.sciencedirect.com/science/article/pii/S0167278998001699.

[17] D. Bambusi and N. N. Nekhoroshev. Long Time Stability in Perturbations of Completely Resonant PDE's. *Acta Applicandae Mathematica*, 70(1):1–22, Jan 2002. ISSN 1572-9036. doi: 10.1023/A:1013943111479. URL https://doi.org/10.1023/A:1013943111479.

[18] D. Bambusi and L. Stolovitch. Convergence to Normal Forms of Integrable PDEs. *Communications in Mathematical Physics*, 376(2):1441–1470, Jun 2020. ISSN 1432-0916. doi: 10.1007/s00220-019-03661-8. URL https://doi.org/10.1007/s00220-019-03661-8.

[19] N. Bar, K. Blum, J. Eby, and R. Sato. Ultralight dark matter in disk galaxies. *Physical Review D*, 99, 5 2019. ISSN 24700029. doi: 10.1103/PhysRevD.99.103020.

[20] C. Bardos, L. Erdös, F. Golse, N. Mauser, and H.-T. Yau. Derivation of the Schrödinger–Poisson equation from the quantum N-body problem. *Comptes Rendus Mathematique*, 334(6):515–520, 2002. ISSN 1631-073X. doi: https://doi.org/10.1016/S1631-073X(02)02253-7. URL https://www.sciencedirect.com/science/article/pii/S1631073X02022537.

[21] R. Bekenstein, R. Schley, M. Mutzafi, C. Rotschild, and M. Segev. Optical simulations of gravitational effects in the Newton–Schrödinger system. *Nature Physics*, 11(10):872–878, oct 2015. doi: 10.1038/nphys3451. URL https://doi.org/10.1038/nphys3451.

[22] G. Benettin and G. Gallavotti. Stability of motions near resonances in quasi-integrable Hamiltonian systems. *Journal of Statistical Physics*, 44(3):293–338, Aug 1986. ISSN 1572-9613. doi: 10.1007/BF01011301. URL https://doi.org/10.1007/BF01011301.

[23] F. Berezin and M. Shubin. *The Schrödinger Equation*. Mathematics and its Applications. Springer Netherlands, 1991. ISBN 9780792312185. URL https://books.google.ie/books?id=ODTRwwEACAAJ.

[24] T. Bernal, L. M. Fernández-Hernández, T. Matos, and M. A. Rodríguez-Meza. Rotation curves of high-resolution LSB and SPARC galaxies with fuzzy and multistate (ultralight boson) scalar field dark matter. *Monthly Notices of the Royal Astronomical Society*, 475:1447–1468, 4 2018. ISSN 13652966. doi: 10.1093/mnras/stx3208.

[25] D. Bernstein, E. Gilardi, and K. Jones. Eigenstates of the gravitational Schrödinger equation. *Modern Physics Letters A*, 13(29):2327–2336, 1998. doi: 10.1142/S0217732398002473. URL https://doi.org/10.1142/S0217732398002473.

[26] J. Binney and S. Tremaine. *Galactic Dynamics: Second Edition*. Princeton Series in Astrophysics. Princeton University Press, 2011. ISBN 9781400828722. URL https://books.google.it/books?id=6mF4CKxlbLsC.

[27] G. Birkhoff. *Dynamical Systems*. American Mathematical Society / Providence, Estados Unidos. American Mathematical Society, 1927. ISBN 9780821810095. URL https://books.google.it/books?id=ygmWAwAAQBAJ.

[28] D. Bohm. A suggested interpretation of the quantum theory in terms of "hidden" variables. i. *Phys. Rev.*, 85:166–179, Jan 1952. doi: 10.1103/PhysRev.85.166. URL https://link.aps.org/doi/10.1103/PhysRev.85.166.

[29] C. G. Böhmer and T. Harko. Can dark matter be a Bose–Einstein condensate? *Journal of Cosmology and Astroparticle Physics*, 2007(06):025, jun 2007. doi: 10.1088/1475-7516/2007/06/025. URL https://dx.doi.org/10.1088/1475-7516/2007/06/025.

[30] L. Brillouin. La mécanique ondulatoire de Schrödinger; une méthode générale de resolution par approximations successives. *Compt. Rend. Hebd. Seances Acad. Sci.*, 183(1):24–26, 1926.

[31] M. Brito, C. Herdeiro, E. Radu, N. Sanchis-Gual, and M. Zilhão. Stability and physical properties of spherical excited scalar boson stars. *Phys. Rev. D*, 107:084022, Apr 2023. doi: 10.1103/PhysRevD.107.084022. URL https://link.aps.org/doi/10.1103/PhysRevD.107.084022.

[32] A. Bruno. Analytical form of differential equations. *Transactions of the Moscow Mathematical Society*, 25:131–288, 01 1971.

[33] D. Burstein and V. C. Rubin. The distribution of mass in spiral galaxies. *Astrophysical Journal*, 297:423–435, Oct. 1985. doi: 10.1086/163541.

[34] B. J. Carr and S. W. Hawking. Black holes in the early Universe. *Monthly Notices of the Royal Astronomical Society*, 168:399–416, Aug. 1974. doi: 10.1093/mnras/168.2.399.

[35] S. Casertano. Rotation curve of the edge-on spiral galaxy NGC 5907 : disc and halo masses. *Monthly Notices of the Royal Astronomical Society*, 203:735–747, may 1983. doi: 10.1093/mnras/203.3.735.

[36] E. Chávez Nambo, A. Diez-Tejedor, A. A. Roque, and O. Sarbach. Linear stability of nonrelativistic self-interacting boson stars. *Phys. Rev. D*, 109:104011, May 2024. doi: 10.1103/PhysRevD.109.104011. URL https://link.aps.org/doi/10.1103/PhysRevD.109.104011.

[37] G. Cicogna and G. Gaeta. Normal forms and nonlinear symmetries. *Journal of Physics A: Mathematical and General*, 27(21):7115, nov 1994. doi: 10.1088/0305-4470/27/21/026. URL https://dx.doi.org/10.1088/0305-4470/27/21/026.

[38] P. Coles and A. Gallagher. Classical Fluid Analogies for Schrödinger-Newton Systems, 2025. URL https://arxiv.org/abs/2507.08583.

[39] J. Colliander, J. Holmer, and N. Tzirakis. Low regularity global well-posedness for the Zakharov and Klein-Gordon-Schrödinger systems. *Trans. Amer. Math. Soc.*, 360(9):4619–4638, 2008. URL https://www.ams.org/journals/tran/2008-360-09/S0002-9947-08-04295-5/home.html.

[40] M. Combescure and D. Robert. *Coherent States and Applications in Mathematical Physics*. Theoretical and Mathematical Physics. Springer Netherlands, 2012. ISBN 9789400701960. URL https://books.google.ie/books?id=mJgh0XAemNIC.

[41] M. Crăciun and T. Harko. Testing Bose–Einstein condensate dark matter models with the SPARC galactic rotation curves data. *European Physical Journal C*, 80, 8 2020. ISSN 14346052. doi: 10.1140/epjc/s10052-020-8272-4.

[42] M. Del Pino and J. Dolbeault. Best constants for Gagliardo–Nirenberg inequalities and applications to nonlinear diffusions. *Journal de Mathématiques Pures et Appliquées*, 81(9): 847–875, 2002. ISSN 0021-7824. doi: https://doi.org/10.1016/S0021-7824(02)01266-7. URL https://www.sciencedirect.com/science/article/pii/S0021782402012667.

[43] L. Diósi. Gravitation and quantum-mechanical localization of macro-objects. *Physics Letters A*, 105(4):199–202, 1984. ISSN 0375-9601. doi: https://doi.org/10.1016/0375-9601(84)90397-9. URL https://www.sciencedirect.com/science/article/pii/0375960184903979.

[44] S. Dong and Z. Wyatt. Stability of a coupled wave-Klein-Gordon system with quadratic nonlinearities. *Journal of Differential Equations*, 269(9):7470–7497, 2020. ISSN 0022-0396. doi: https://doi.org/10.1016/j.jde.2020.05.019. URL https://www.sciencedirect.com/science/article/pii/S002203962030262X.

[45] A. Elgart and B. Schlein. Mean field dynamics of boson stars. *Communications on Pure and Applied Mathematics*, 60(4):500–545, 2007. doi: https://doi.org/10.1002/cpa.20134. URL https://onlinelibrary.wiley.com/doi/abs/10.1002/cpa.20134.

[46] L. Evans. *Partial Differential Equations*. Graduate Studies in Mathematics. American Mathematical Society, 2022. ISBN 9781470469429. URL https://books.google.ie/books?id=Ott1EAAAQBAJ.

[47] M. Falconi. Classical limit of the Nelson model with cutoff. *Journal of Mathematical Physics*, 54(1):012303, 01 2013. ISSN 0022-2488. doi: 10.1063/1.4775716. URL https://doi.org/10.1063/1.4775716.

[48] E. Fermi and R. Schluter. *Notes on Quantum Mechanics*. University of Chicago Press, 1995. ISBN 9780226243818. URL https://books.google.it/books?id=mBP4utLG6i0C.

[49] E. G. M. Ferreira. Ultra-light dark matter. *The Astronomy and Astrophysics Review*, 29, 2021. doi: 10.1007/s00159-021-00135-6. URL https://doi.org/10.1007/s00159-021-00135-6.

[50] H. Foidl, T. Rindler-Daller, and W. Zeilinger. Halo formation and evolution in scalar field dark matter and cold dark matter: New insights from the fluid approach, 2023. URL https://arxiv.org/abs/2305.12982.

[51] I. Fukuda and M. Tsutsumi. On coupled Klein-Gordon-Schrödinger equations, II. *Journal of Mathematical Analysis and Applications*, 66(2):358–378, 1978. ISSN 0022-247X. doi: https://doi.org/10.1016/0022-247X(78)90239-1. URL https://www.sciencedirect.com/science/article/pii/0022247X78902391.

[52] G. Gaeta. Poincaré normal and renormalized forms. *Acta Applicandae Mathematica*, 70(1): 113–131, Jan 2002. ISSN 1572-9036. doi: 10.1023/A:1013974115113. URL https://doi.org/10.1023/A:1013974115113.

[53] M. Gallone and A. Ponno. Hamiltonian Field Theory Close to the Wave Equation: From Fermi-Pasta-Ulam to Water Waves. In V. Georgiev, A. Michelangeli, and R. Scandone, editors, *Qualitative Properties of Dispersive PDEs*, pages 205–244, Singapore, 2022. Springer Nature Singapore. ISBN 978-981-19-6434-3.

[54] J. Ginibre and G. Velo. Long Range Scattering and Modified Wave Operators for the Wave-Schrödinger System. *Annales Henri Poincaré*, 3(3):537–612, Jun 2002. ISSN 1424-0637. doi: 10.1007/s00023-002-8627-4. URL https://doi.org/10.1007/s00023-002-8627-4.

[55] S. Giovanazzi, G. Kurizki, I. E. Mazets, and S. Stringari. Collective excitations of a "gravitationally" self-bound Bose gas. *Europhysics Letters*, 56(1):1, oct 2001. doi: 10.1209/epl/i2001-00478-8. URL https://dx.doi.org/10.1209/epl/i2001-00478-8.

[56] D. Giulini and A. Großardt. The Schrödinger–Newton equation as a non-relativistic limit of self-gravitating Klein–Gordon and Dirac fields. *Classical and Quantum Gravity*, 29(21): 215010, oct 2012. doi: 10.1088/0264-9381/29/21/215010. URL https://dx.doi.org/10.1088/0264-9381/29/21/215010.

[57] D. Giulini, A. Großardt, and P. K. Schwartz. *Coupling Quantum Matter and Gravity*, pages 491–550. Springer International Publishing, Cham, 2023. ISBN 978-3-031-31520-6. doi: 10.1007/978-3-031-31520-6_16. URL https://doi.org/10.1007/978-3-031-31520-6_16.

[58] D. Greiner and G. Wunner. Quantum defect analysis of the eigenvalue spectrum of the Newton-Schrödinger equation. *Phys. Rev. A*, 74:052106, Nov 2006. doi: 10.1103/PhysRevA.74.052106. URL https://link.aps.org/doi/10.1103/PhysRevA.74.052106.

[59] D. Griffiths. *Introduction to Quantum Mechanics*. Cambridge University Press, 2017. ISBN 9781107179868. URL https://books.google.it/books?id=0h-nDAAAQBAJ.

[60] A. Großardt, J. Bateman, H. Ulbricht, and A. Bassi. Optomechanical test of the Schrödinger-Newton equation. *Phys. Rev. D*, 93:096003, May 2016. doi: 10.1103/PhysRevD.93.096003. URL https://link.aps.org/doi/10.1103/PhysRevD.93.096003.

[61] B. Grébert and T. Kappeler. *The Defocusing NLS Equation and Its Normal Form*. EMS Press, 03 2014. ISBN 978-3-03719-131-6. doi: 10.4171/131.

[62] R. L. Guenther. *A Numerical Study of the Time Dependent Schroedinger Equation Coupled with Newtonian Gravity*. PhD thesis, University of Texas, Austin, Jan. 1995.

[63] F. G. Gustavson. On constructing formal integrals of a Hamiltonian system near an equilibrium point. *Astron. J.*, 71:670, Oct. 1966. doi: 10.1086/110172. URL https://ui.adsabs.harvard.edu/abs/1966AJ.....71..670G/abstract.

[64] F. S. Guzmán and F. D. Lora-Clavijo. Rotation curves of ultralight BEC dark matter halos with rotation. *General Relativity and Gravitation*, 47:21, Mar. 2015. doi: 10.1007/s10714-015-1865-9. URL https://link.springer.com/article/10.1007/s10714-015-1865-9.

[65] F. S. Guzmán and L. A. Ureña López. Newtonian collapse of scalar field dark matter. *Phys. Rev. D*, 68:024023, Jul 2003. doi: 10.1103/PhysRevD.68.024023. URL https://link.aps.org/doi/10.1103/PhysRevD.68.024023.

[66] F. S. Guzmán and L. A. Ureña López. Evolution of the Schrödinger-Newton system for a self-gravitating scalar field. *Phys. Rev. D*, 69:124033, Jun 2004. doi: 10.1103/PhysRevD.69.124033. URL https://link.aps.org/doi/10.1103/PhysRevD.69.124033.

[67] F. S. Guzmán and L. A. Ureña López. Gravitational Cooling of Self-gravitating Bose Condensates. *The Astrophysical Journal*, 645(2):814, jul 2006. doi: 10.1086/504508. URL https://dx.doi.org/10.1086/504508.

[68] F. S. Guzmán and L. A. Ureña López. Gravitational atoms: General framework for the construction of multistate axially symmetric solutions of the Schrödinger-Poisson system. *Phys. Rev. D*, 101(8):081302, 2020. doi: 10.1103/PhysRevD.101.081302.

[69] F. S. Guzmán and T. Matos. Scalar fields as dark matter in spiral galaxies. *Classical and Quantum Gravity*, 17(1):L9, jan 2000. doi: 10.1088/0264-9381/17/1/102. URL https://dx.doi.org/10.1088/0264-9381/17/1/102.

[70] T. Harko and E. J. Madarassy. Bose-Einstein Condensate dark matter models in the presence of baryonic matter and random confining potentials. *The European Physical Journal C*, 82, 4 2022. doi: 10.1140/epjc/s10052-022-10344-7. URL http://arxiv.org/abs/2205.00297http://dx.doi.org/10.1140/epjc/s10052-022-10344-7.

[71] R. Harrison, I. Moroz, and K. P. Tod. A numerical study of the Schrödinger-Newton equations. *Nonlinearity*, 16(1):101, nov 2002. doi: 10.1088/0951-7715/16/1/307. URL https://dx.doi.org/10.1088/0951-7715/16/1/307.

[72] N. HAYASHI and W. von WAHL. On the global strong solutions of coupled Klein-Gordon-Schrödinger equations. *Journal of the Mathematical Society of Japan*, 39(3):489 – 497, 1987. doi: 10.2969/jmsj/03930489. URL https://doi.org/10.2969/jmsj/03930489.

[73] L. Hui, J. P. Ostriker, S. Tremaine, and E. Witten. Ultralight scalars as cosmological dark matter. *Phys. Rev. D*, 95:043541, Feb 2017. doi: 10.1103/PhysRevD.95.043541. URL https://link.aps.org/doi/10.1103/PhysRevD.95.043541.

[74] A. D. Ionescu and B. Pausader. On the Global Regularity for a Wave-Klein—Gordon Coupled System. *Acta Mathematica Sinica, English Series*, 35(6):933–986, jun 2019. doi: 10.1007/s10114-019-8413-6. URL https://doi.org/10.1007/s10114-019-8413-6.

[75] A. D. Ionescu and B. Pausader. The Einstein-Klein-Gordon coupled system: global stability of the Minkowski solution. *arXiv preprint arXiv:1911.10652*, 2020.

[76] A. D. Ionescu and B. Pausader. Global regularity of solutions of the Einstein-Klein-Gordon system: A review. *Quart. Appl. Math.*, 78:277–303, 2020. doi: 10.1090/qam/1555. URL https://doi.org/10.1090/qam/1555.

[77] H. Ito. Convergence of Birkhoff normal forms for integrable systems. *Commentarii Mathematici Helvetici*, 64(1):412–461, Dec 1989. ISSN 1420-8946. doi: 10.1007/BF02564686. URL https://doi.org/10.1007/BF02564686.

[78] S. U. Ji and S. J. Sin. Late-time phase transition and the galactic halo as a Bose liquid. II. The effect of visible matter. *Physical Review D*, 50, 1994. doi: 10.1103/PhysRevD.50.3655. URL https://journals.aps.org/prd/abstract/10.1103/PhysRevD.50.3655.

[79] T. Kappeler and J. Pöschel. *KdV & KAM*. Ergebnisse der Mathematik und ihrer Grenzgebiete. 3. Folge / A Series of Modern Surveys in Mathematics. Springer Berlin Heidelberg, 2003. ISBN 9783540022343. URL https://books.google.it/books?id=0gY7TSZbKSoC.

[80] H. Katz, F. Lelli, S. S. McGaugh, A. Di Cintio, C. B. Brook, and J. M. Schombert. Testing feedback-modified dark matter haloes with galaxy rotation curves: estimation of halo parameters and consistency with λcdm scaling relations. *Monthly Notices of the Royal Astronomical Society*, 466(2):1648–1668, 12 2016. ISSN 0035-8711. doi: 10.1093/mnras/stw3101. URL https://doi.org/10.1093/mnras/stw3101.

[81] M. Khelashvili, A. Rudakovskyi, and S. Hossenfelder. Dark matter profiles of SPARC galaxies: a challenge to fuzzy dark matter. *Monthly Notices of the Royal Astronomical Society*, 523:3393–3405, 7 2022. doi: 10.1093/mnras/stad1595. URL http://arxiv.org/abs/2207.14165http://dx.doi.org/10.1093/mnras/stad1595.

[82] M. K. Kiessling. On the asymptotic decay of the Schrödinger-Newton ground state. *Physics Letters A*, 395:127209, 2021. ISSN 0375-9601. doi: https://doi.org/10.1016/j.physleta.2021.127209. URL https://www.sciencedirect.com/science/article/pii/S0375960121000736.

[83] H. Kikuchi. Orbital stability of semitrivial standing waves for the Klein–Gordon–Schrödinger system. *Annales de l'Institut Henri Poincaré C, Analyse non linéaire*, 28(2):315–323, 2011. ISSN 0294-1449. doi: https://doi.org/10.1016/j.anihpc.2011.02.003. URL https://www.sciencedirect.com/science/article/pii/S0294144911000175.

[84] H. KIKUCHI and M. OHTA. Instability of standing waves for the Klein-Gordon-Schrödinger system. *Hokkaido Mathematical Journal*, 37(4):735 – 748, 2008. doi: 10.14492/hokmj/1249046366. URL https://doi.org/10.14492/hokmj/1249046366.

[85] H. Kikuchi and M. Ohta. Stability of standing waves for the Klein–Gordon–Schrödinger system. *Journal of Mathematical Analysis and Applications*, 365(1):109–114, 2010. ISSN 0022-247X. doi: https://doi.org/10.1016/j.jmaa.2009.10.024. URL https://www.sciencedirect.com/science/article/pii/S0022247X09008440.

[86] H. A. Kramers. Wellenmechanik und halbzahlige Quantisierung. *Zeitschrift für Physik*, 39 (10):828–840, Oct 1926. ISSN 0044-3328. doi: 10.1007/BF01451751. URL https://doi.org/10.1007/BF01451751.

[87] S. Kuksin and G. Perelman. Vey theorem in infinite dimensions and its application to KdV. *Discrete and Continuous Dynamical Systems*, 27(1):1–24, 2010. ISSN 1078-0947. doi: 10.3934/dcds.2010.27.1. URL https://www.aimsciences.org/article/id/5b491874-a663-4601-ae34-b8d92105ee84.

[88] J.-W. Lee. Galaxies with fuzzy dark matter. *Journal of the Korean Physical Society*, 78 (10):873–877, May 2021. ISSN 1976-8524. doi: 10.1007/s40042-021-00077-3. URL https://doi.org/10.1007/s40042-021-00077-3.

[89] J.-w. Lee and I.-g. Koh. Galactic halos as boson stars. *Phys. Rev. D*, 53:2236–2239, Feb 1996. doi: 10.1103/PhysRevD.53.2236. URL https://link.aps.org/doi/10.1103/PhysRevD.53.2236.

[90] P. G. LeFloch and Y. Ma. *The hyperboloidal foliation method*, volume 2. World Scientific, 2014.

[91] P. G. LeFloch and Y. Ma. The Global Nonlinear Stability of Minkowski Space for Self-gravitating Massive Fields. *Communications in Mathematical Physics*, 346(2):603–665, sep 2016. doi: 10.1007/s00220-015-2549-8. URL https://doi.org/10.1007/s00220-015-2549-8.

[92] P. G. LeFloch and Y. Ma. *The Global Nonlinear Stability of Minkowski Space for Self-Gravitating Massive Fields*. WORLD SCIENTIFIC, 2017. doi: 10.1142/10730. URL https://www.worldscientific.com/doi/abs/10.1142/10730.

[93] P. G. LeFloch and Y. Ma. Nonlinear stability of self-gravitating massive fields. A wave-Klein–Gordon model. *Classical and Quantum Gravity*, 40(15):154001, jun 2023. doi: 10.1088/1361-6382/acde31. URL https://dx.doi.org/10.1088/1361-6382/acde31.

[94] F. Lelli, S. S. McGaugh, and J. M. Schombert. SPARC: mass models for 175 disk galaxies with Spitzer photometry and accurate rotation curves. *The Astronomical Journal*, 152(6):157, nov 2016. doi: 10.3847/0004-6256/152/6/157. URL https://dx.doi.org/10.3847/0004-6256/152/6/157.

[95] F. Lelli, S. S. McGaugh, and J. M. Schombert. The small scatter of the baryonic Tully-Fisher relation. *The Astrophysical Journal Letters*, 816:L14, 1 2016. ISSN 2041-8205. doi: 10.3847/2041-8205/816/1/l14.

[96] F. Lelli, S. S. McGaugh, J. M. Schombert, and M. S. Pawlowski. One law to rule them all: the radial acceleration relation of galaxies. *The Astrophysical Journal*, 836, 10 2016. doi: 10.3847/1538-4357/836/2/152. URL http://arxiv.org/abs/1610.08981http://dx.doi.org/10.3847/1538-4357/836/2/152.

[97] M. Lewin, P. T. Nam, and N. Rougerie. Derivation of Hartree's theory for generic mean-field Bose systems. *Advances in Mathematics*, 254:570–621, 2014. ISSN 0001-8708. doi: https://doi.org/10.1016/j.aim.2013.12.010. URL https://www.sciencedirect.com/science/article/pii/S0001870813004568.

[98] P. Li, F. Lelli, S. McGaugh, and J. Schombert. A comprehensive catalog of dark matter halo models for SPARC galaxies. *The Astrophysical Journal Supplement Series*, 247:31, 3 2020. ISSN 0067-0049. doi: 10.3847/1538-4365/ab700e. URL https://iopscience.iop.org/article/10.3847/1538-4365/ab700e.

[99] Li, Pengfei, Lelli, Federico, McGaugh, Stacy, and Schombert, James. Fitting the radial acceleration relation to individual SPARC galaxies. *A&A*, 615:A3, 2018. doi: 10.1051/0004-6361/201732547. URL https://doi.org/10.1051/0004-6361/201732547.

[100] E. H. Lieb. Existence and uniqueness of the minimizing solution of Choquard's nonlinear equation. *Studies in Applied Mathematics*, 57(2):93–105, 1977. doi: https://doi.org/10.1002/sapm197757293. URL https://onlinelibrary.wiley.com/doi/abs/10.1002/sapm197757293.

[101] P. Lions. The Choquard equation and related questions. *Nonlinear Analysis: Theory, Methods & Applications*, 4(6):1063–1072, 1980. ISSN 0362-546X. doi: https://doi.org/10.1016/0362-546X(80)90016-4. URL https://www.sciencedirect.com/science/article/pii/0362546X80900164.

[102] G. Marangon, A. Ponno, and L. Zanelli. From Klein-Gordon-Wave to Schrödinger-Wave: a Normal Form Approach. Submitted to Journal of Physics A. URL https://doi.org/10.48550/arXiv.2504.20576.

[103] G. Marangon, A. Ponno, and L. Zanelli. Scaling of highly excited Schrödinger-Poisson eigenstates and universality of their rotation curves. *Physics Letters A*, 555:130761, 2025. ISSN 0375-9601. doi: https://doi.org/10.1016/j.physleta.2025.130761. URL https://www.sciencedirect.com/science/article/pii/S0375960125005419.

[104] G. Marangon, A. Ponno, and L. Zanelli. On the scaling properties of excited stationary states of the schrödinger-poisson model. *Communications in Nonlinear Science and Numerical Simulation*, 152:109486, 2026. ISSN 1007-5704. doi: https://doi.org/10.1016/j.cnsns.2025.109486. URL https://www.sciencedirect.com/science/article/pii/S1007570425008950.

[105] T. Matos, L. A. Ureña-López, and J.-W. Lee. Short review of the main achievements of the scalar field, fuzzy, ultralight, wave, BEC dark matter model. *Frontiers in Astronomy and Space Sciences*, 11, 2024. ISSN 2296-987X. doi: 10.3389/fspas.2024.1347518. URL https://www.frontiersin.org/journals/astronomy-and-space-sciences/articles/10.3389/fspas.2024.1347518.

[106] S. McGaugh, F. Lelli, and J. Schombert. The radial acceleration relation in rotationally supported galaxies. *Physical Review Letters*, 117, 9 2016. doi: 10.1103/PhysRevLett.117.201101. URL http://arxiv.org/abs/1609.05917http://dx.doi.org/10.1103/PhysRevLett.117.201101.

[107] S. S. McGaugh and J. M. Schombert. Color–mass-to-light-ratio relations for disk galaxies. *The Astronomical Journal*, 148(5):77, sep 2014. doi: 10.1088/0004-6256/148/5/77. URL https://dx.doi.org/10.1088/0004-6256/148/5/77.

[108] J. T. Mendonça. Wave-kinetic approach to the Schrödinger–Newton equation. *New Journal of Physics*, 21(2):023004, feb 2019. doi: 10.1088/1367-2630/ab0045. URL https://dx.doi.org/10.1088/1367-2630/ab0045.

[109] A. Michelangeli and B. Schlein. Dynamical collapse of boson stars. *Communications in Mathematical Physics*, 311(3):645–687, May 2012. ISSN 1432-0916. doi: 10.1007/s00220-011-1341-7. URL https://doi.org/10.1007/s00220-011-1341-7.

[110] C. Misner, K. Thorne, J. Wheeler, and D. Kaiser. *Gravitation*. Princeton University Press, 2017. ISBN 9780691177793. URL https://books.google.ie/books?id=SyQzDwAAQBAJ.

[111] T. Mistele, S. McGaugh, and S. Hossenfelder. Galactic mass-to-light ratios with superfluid dark matter. *Extragalactic astronomy*, 664, 1 2022. doi: 10.1051/0004-6361/202243216. URL http://arxiv.org/abs/2201.07282http://dx.doi.org/10.1051/0004-6361/202243216.

[112] I. M. Moroz, R. Penrose, and P. Tod. Spherically-symmetric solutions of the Schrödinger-Newton equations. *Classical and Quantum Gravity*, 15(9):2733, sep 1998. doi: 10.1088/0264-9381/15/9/019. URL https://dx.doi.org/10.1088/0264-9381/15/9/019.

[113] A. Navarrete, A. Paredes, J. R. Salgueiro, and H. Michinel. Spatial solitons in thermo-optical media from the nonlinear Schrödinger-Poisson equation and dark-matter analogs. *Phys. Rev. A*, 95:013844, Jan 2017. doi: 10.1103/PhysRevA.95.013844. URL https://link.aps.org/doi/10.1103/PhysRevA.95.013844.

[114] E. Nelson. Interaction of Nonrelativistic Particles with a Quantized Scalar Field. *Journal of Mathematical Physics*, 5(9):1190–1197, 09 1964. ISSN 0022-2488. doi: 10.1063/1.1704225. URL https://doi.org/10.1063/1.1704225.

[115] M. Ohta. Stability of stationary states for the coupled Klein — Gordon — Schrödinger equations. *Nonlinear Analysis: Theory, Methods & Applications*, 27(4):455–461, 1996. ISSN 0362-546X. doi: https://doi.org/10.1016/0362-546X(95)00017-P. URL https://www.sciencedirect.com/science/article/pii/0362546X9500017P.

[116] Z. Ouyang. Modified wave operators for the Wave-Klein-Gordon system. *Advances in Mathematics*, 423:109042, 2023. ISSN 0001-8708. doi: https://doi.org/10.1016/j.aim.2023.109042. URL https://www.sciencedirect.com/science/article/pii/S0001870823001858.

[117] A. Paredes, D. N. Olivieri, and H. Michinel. From optics to dark matter: A review on nonlinear Schrödinger–Poisson systems. *Physica D: Nonlinear Phenomena*, 403:132301, 2020. ISSN 0167-2789. doi: https://doi.org/10.1016/j.physd.2019.132301. URL https://www.sciencedirect.com/science/article/pii/S0167278919307079.

[118] H. Pecher. Some new well-posedness results for the Klein-Gordon-Schrödinger system. *Differential and Integral Equations*, 25(1/2):117 – 142, 2012. doi: 10.57262/die/1356012829. URL https://doi.org/10.57262/die/1356012829.

[119] R. Penrose. On the gravitization of quantum mechanics 1: Quantum state reduction. *Foundations of Physics*, 44(5):557–575, 2014. doi: 10.1007/s10701-013-9770-0.

[120] R. Penrose and P. Marcer. Quantum computation, entanglement and state reduction [and discussion]. *Philosophical Transactions: Mathematical, Physical and Engineering Sciences*, 356(1743):1927–1939, 1998. ISSN 1364503X. URL http://www.jstor.org/stable/55019.

[121] C. Rampf. Cosmological Vlasov–Poisson equations for dark matter. *Rev. Mod. Plasma Phys.*, 5(1), Dec. 2021. doi: https://doi.org/10.1007/s41614-021-00055-z. URL https://link.springer.com/article/10.1007/s41614-021-00055-z.

[122] V. H. Robles and T. Matos. Exact solution to finite temperature SFDM: natural cores without feedback. *Astrophysical Journal*, 763, 1 2013. ISSN 15384357. doi: 10.1088/0004-637X/763/1/19. URL https://iopscience.iop.org/article/10.1088/0004-637X/763/1/19.

[123] A. A. Roque, E. C. Nambo, and O. Sarbach. Radial linear stability of nonrelativistic ℓ-boson stars. *Phys. Rev. D*, 107:084001, Apr 2023. doi: 10.1103/PhysRevD.107.084001. URL https://link.aps.org/doi/10.1103/PhysRevD.107.084001.

[124] V. C. Rubin, J. Ford, W. K., and N. Thonnard. Rotational properties of 21 SC galaxies with a large range of luminosities and radii, from NGC 4605 (R=4kpc) to UGC 2885 (R=122kpc). *Astrophysical Journal*, 238:471–487, June 1980. doi: 10.1086/158003.

[125] V. C. Rubin, D. Burstein, W. K. Ford, Jr., and N. Thonnard. Rotation velocities of 16 SA galaxies and a comparison of Sa, Sb, and SC rotation properties. *Astrophys. J.*, 289:81, 1985. doi: 10.1086/162866.

[126] R. Ruffini and S. Bonazzola. Systems of self-gravitating particles in general relativity and the concept of an equation of state. *Phys. Rev.*, 187:1767–1783, Nov 1969. doi: 10.1103/PhysRev.187.1767. URL https://link.aps.org/doi/10.1103/PhysRev.187.1767.

[127] H. Rüssmann. Über das Verhalten analytischer Hamiltonscher Differentialgleichungen in der Nähe einer Gleichgewichtslösung. *Mathematische Annalen*, 154(4):285–300, Aug 1964. ISSN 1432-1807. doi: 10.1007/BF01362565. URL https://doi.org/10.1007/BF01362565.

[128] P. Salucci. The distribution of dark matter in galaxies. *The Astronomy and Astrophysics Review*, 27(1):2, Feb. 2019. doi: 10.1007/s00159-018-0113-1.

[129] M. Schaller, C. Becker, O. Ruchayskiy, A. Boyarsky, and M. Shaposhnikov. A new framework for numerical simulations of structure formation. *Monthly Notices of the Royal Astronomical Society*, 442(4):3073–3095, 06 2014. ISSN 0035-8711. doi: 10.1093/mnras/stu1069. URL https://doi.org/10.1093/mnras/stu1069.

[130] H.-Y. Schive, T. Chiueh, and T. Broadhurst. Cosmic structure as the quantum interference of a coherent dark wave. *Nature Physics*, 10, Jul 2014. doi: 10.1038/nphys2996. URL https://doi.org/10.1038/nphys2996.

[131] F. E. Schunck and E. W. Mielke. General relativistic boson stars. *Classical and Quantum Gravity*, 20(20):R301, sep 2003. doi: 10.1088/0264-9381/20/20/201. URL https://dx.doi.org/10.1088/0264-9381/20/20/201.

[132] S.-J. Sin. Late-time phase transition and the galactic halo as a Bose liquid. *Phys. Rev. D*, 50:3650–3654, Sep 1994. doi: 10.1103/PhysRevD.50.3650. URL https://link.aps.org/doi/10.1103/PhysRevD.50.3650.

[133] Y. Sofue. Rotation curve decomposition for size–mass relations of bulge, disk, and dark halo components in spiral galaxies. *Publications of the Astronomical Society of Japan*, 68(1):2, 10 2015. ISSN 0004-6264. doi: 10.1093/pasj/psv103. URL https://doi.org/10.1093/pasj/psv103.

[134] L. Stolovitch. Singular complete integrability. *Publications Mathématiques de l'IHÉS*, 91: 133–210, 2000. URL https://www.numdam.org/item/PMIHES_2000__91__133_0/.

[135] K. Tod. The ground state energy of the Schrödinger-Newton equation. *Physics Letters A*, 280 (4):173–176, 2001. ISSN 0375-9601. doi: https://doi.org/10.1016/S0375-9601(01)00059-7. URL https://www.sciencedirect.com/science/article/pii/S0375960101000597.

[136] P. Tod and I. M. Moroz. An analytical approach to the Schrödinger-Newton equations. *Nonlinearity*, 12(2):201, mar 1999. doi: 10.1088/0951-7715/12/2/002. URL https://dx.doi.org/10.1088/0951-7715/12/2/002.

[137] D. Tong. Lectures on quantum field theory, 2007. URL https://www.damtp.cam.ac.uk/user/tong/qft.html.

[138] D. Tong. Lectures on general relativity, 2019. URL `https://www.damtp.cam.ac.uk/user/tong/gr.html`.

[139] C. Uhlemann, M. Kopp, and T. Haugg. Schrödinger method as N-body double and UV completion of dust. *Phys. Rev. D*, 90:023517, Jul 2014. doi: 10.1103/PhysRevD.90.023517. URL `https://link.aps.org/doi/10.1103/PhysRevD.90.023517`.

[140] L. A. Urena-Lopez and A. Bernal. Bosonic gas as a Galactic Dark Matter Halo. *Phys. Rev. D*, 82:123535, 2010. doi: 10.1103/PhysRevD.82.123535.

[141] L. A. Ureña-López. Brief review on scalar field dark matter models. *Frontiers in Astronomy and Space Sciences*, Volume 6 - 2019, 2019. ISSN 2296-987X. doi: 10.3389/fspas.2019.00047. URL `https://www.frontiersin.org/journals/astronomy-and-space-sciences/articles/10.3389/fspas.2019.00047`.

[142] J. Vey. Sur Certains Systemes Dynamiques Separables. *American Journal of Mathematics*, 100(3):591–614, 1978. ISSN 00029327, 10806377. URL `http://www.jstor.org/stable/2373841`.

[143] Q. Wang. An intrinsic hyperboloid approach for Einstein Klein–Gordon equations. *Journal of Differential Geometry*, 115(1):27 – 109, 2020. doi: 10.4310/jdg/1586224841. URL `https://doi.org/10.4310/jdg/1586224841`.

[144] G. Wentzel. Eine Verallgemeinerung der Quantenbedingungen für die Zwecke der Wellenmechanik. *Zeitschrift für Physik*, 38(6):518–529, Jun 1926. ISSN 0044-3328. doi: 10.1007/BF01397171. URL `https://doi.org/10.1007/BF01397171`.

[145] L. M. Widrow and N. Kaiser. Using the Schrödinger equation to simulate collisionless matter. *Astrophysical Journal Letters*, 416:L71, Oct. 1993. doi: 10.1086/187073.

[146] J.-C. Yoccoz. *An Introduction To Small Divisors Problems*, pages 659–679. Springer Berlin Heidelberg, Berlin, Heidelberg, 1992. ISBN 978-3-662-02838-4. doi: 10.1007/978-3-662-02838-4_14. URL `https://doi.org/10.1007/978-3-662-02838-4_14`.

[147] W. Zhang, D. Feng, and R. Gilmore. Coherent states: Theory and some applications. *Reviews of Modern Physics*, 62(4):867–927, 1990. ISSN 0034-6861. doi: 10.1103/RevModPhys.62.867. Copyright: Copyright 2015 Elsevier B.V., All rights reserved.

[148] N. T. Zung. Convergence versus integrability in Poincare-Dulac normal form. *Mathematical Research Letters*, 9:217–228, 06 2002. doi: 10.4310/MRL.2002.v9.n2.a8.

[149] N. T. Zung. Convergence versus integrability in Birkhoff normal form. *Annals of Mathematics*, 16:141–156, 05 2005. doi: 10.4007/annals.2005.161.141. URL `https://annals.math.princeton.edu/2005/161-1/p04`.

Ringraziamenti (Acknowledgements)

Concludo una tesi, e concludo un percorso per me di grande impatto. E' non solo dovuto, ma voluto, chiuderlo con dei ringraziamenti.

Il primo ringraziamento va ad Antonio, origine e conclusione di questo percorso, che ringrazio profondamente per avermi ispirata, mostrandomi la ricchezza, eleganza e sorpresa che sono proprie di questo mondo, e per avermi insegnato la perseveranza, la lucida analisi e la costante apertura verso comunità diverse. Con lui ringrazio Lorenzo, per la presenza e la dedizione.

Ringrazio poi tutti i ragazzi del 7BC per aver condiviso con me un pezzetto di vita. Sono profondamente grata per questo ambiente di parità, di gentilezza e di familiarità in cui mi sono sentita a casa. Un grazie particolare ad Alessandra, per l'onestà con cui ci siamo conosciute, a Pietro, compagno di mimesi tra i matematici, a Tommaso, che strada facendo vedrai che non sei più da solo, a Martina, che rende argute e dolci le pause caffé, a Francesco, che credo sia stato più forte di me. Grazie ai dottorandi di prima e di poi, che mi fanno sentire parte di una storia che continua. Grazie a Loretta e a Marinella, sulle cui spalle questa storia si posa.

Ringrazio i miei genitori, per il sostegno immancabile, emotivo ed anche materiale, e ringrazio Alba, con cui ci intersechiamo pur correndo parallelamente. Ringrazio Michela e Simone, la Formazione e ilGruppo, per essere la mia famiglia spirituale, e per l'equilibrio, la forza e la cura che con voi continuo a condividere, anche quando gli spazi si dilatano. Ringrazio Giulia e Riccarda, per la profondità e la certezza di esserci sempre, ed Erika e Andrea, per essere rimasti anche al di là del Piovego. Ringrazio Daniele, la sorpresa più bella di questo dottorato. Lo ringrazio altrove, per mille cose, e lo ringrazio qui, per avermi mostrato la leggerezza e lo slancio di cui la ricerca si può vestire, e come si può osare e riuscire, come per gioco.